From shelf dynamics to shelf export: Evidence from sedimentologic and palaeoceanographic slope records

Dissertation zur Erlangung

des Doktorgrades am

Fachbereich Geowissenschaften

der Universität Bremen

vorgelegt von

Vera Barbara Bender

Bremen, 8. Mai 2012.

Gutachter / thesis reviewer:

Prof. Tilo von Dobeneck

Universität Bremen
Fachbereich Geowissenschaften
Fachgebiet Marine Geophysik

Postfach 330 440
28334 Bremen, Germany

Prof. Michel Michaelovitch de Mahiques

Universidade de São Paulo
Instituto Oceanográfico
Departamento de Oceanografia Física

Praça do Oceanográfico, 191
05508-900 São Paulo, SP, Brazil

Weitere Mitglieder der Prüfungskommission/
Further members of the examination board:

Prof. Tobias Mörz
PD Dr. Till J.J. Hanebuth
Dr. Torsten Bickert
Anna Lipke

Tag des öffentlichen Kolloquiums/
Day of public colloquium:

June 29, 2012

Declaration

Name: Vera Barbara Bender
Address: Bei den Drei Pfählen 50, 28205 Bremen

Herewith I declare that

I. This document and the accompanying data has been composed by myself, and describes my own work

II. Material from the published or unpublished work of others, which is referred to in this dissertation, is credited to the author in the text

III. This work has not been submitted for any other degree

Bremen, 08 May 2012

.....
(Signature)

This cumulative doctoral thesis is the outcome of research project III-12b within the International Graduate College EUROPROX - Proxies in Earth History. The studies compiled in this thesis were carried out from October 2008 until April 2012 at the Faculty of Geosciences, University of Bremen; MARUM – Centre for Marine Environmental Sciences, University of Bremen; and Instituto Oceanográfico, Universidade de São Paulo (Brazil).

Table of Contents

Abstract

The continental shelf and slope are among the most dynamic sedimentary and oceanographic environments on Earth, strongly influenced by processes within the terrestrial and marine realm. The shelf break, geographically separating the two areas, marks one of the major physiographic transitions on Earth. The oceanographic and sedimentary processes that lead sediments across this boundary represent the dynamic link between both sedimentary systems. With a multi-proxy approach, this thesis tries to elucidate i) how strong sedimentary and (palae)oceanographic processes modify the primary shelf export signal, ii) if sedimentary records from the slope can be used as reliable archives for reconstructing sedimentary and paleoceanographic shelf dynamics, and iii) how important the local morphology is, in influencing shelf sediment export routes, transport process and/or the creation of depocentres on the slope.

The key study areas of this thesis cover two different continental slope settings, the lower slope region (off Northwest Iberia) and the uppermost slope (off Uruguay).

Off Northwest Iberia, based on high frequency sediment echo-sounding profiles and a large sediment core data set the late Pleistocene sedimentary history of the shelf system, as well as the detailed late Holocene evolution of fluviogenic depocentres on the middle shelf was revealed during the beginning of this thesis. Detailed knowledge of the late Pleistocene shelf sedimentary patterns enables the differentiation of local shelf export signals from over-regional palaeoceanographic signals within the sedimentary patterns at the Northwest Iberian slope. Applying this knowledge, multi-proxy investigation of three slope records off Northwest Iberia reveal the interplay of slope morphology as well as palaeoclimatic effects on shelf - slope sediment dynamics and depositional patterns during the late Quaternary.

At the uppermost slope off Uruguay a small morphologic terrace represents a further type of external archives for the effective and direct recording of shelf sediment export. Contrasting the regional morpho-sedimentary structure of the Southeast South American continental margin, the uppermost slope terrace off Uruguay is not influenced by contouritic sediment transport. Instead, sediment dynamics on the terrace are directly linked to the sedimentary shelf configuration, which is strongly controlled by sea-level rise during the Holocene. Very high sedimentation rates on the terrace (at least approx. 50 cm/kyr) enable the application of these sedimentary sequences for high-resolution palaeoceanographic reconstructions. Holocene latitudinal shifts of the subtropical shelf front across the Southeast South American shelf and uppermost slope were primarily forced by palaeoclimatic variations (northward migration and extension of the Southern Westerlies; middle to late Holocene evolution of the El Niño Southern Oscillation). Moreover, for the most recent 200 years an anthropogenic forcing is suggested.

Overall this thesis makes the attempt to study the complex interplay of palaeoceanographic and sedimentary processes within shelf sediment export and slope sedimentary patterns. It is shown that shelf sedimentary export signals can be recognized as far down-slope as the lower slope. Two different types of slope settings are presented as qualified external records of sedimentary and palaeoceanographic shelf dynamics and export archives. An uppermost slope terrace at the Southeast South American continental margin represents a reliable and direct archive for shelf dynamics, whereas off Northwest Iberia the linkage of middle to lower slope sedimentary patterns with the last deglacial to Holocene history of sediment dynamics on the shelf is more complex. Palaeoceanographic dynamics have little modifying effect on the Holocene shelf export patterns off Southeast South America shelf, off Northwest Iberia deglacial paleoceanographic changes on the outer shelf considerably foster export of shelf sands. Moreover, local margin morphology constitutes a crucial component for shelf – slope linkage as well as in slope

sedimentary patterns: At the uppermost slope, small morphologic steps might act as excellent off-shelf transport archives, whereas slope incisions might act as efficient sediment conduits. At the middle to lower slope, morphologic highs may deflect sediment transporting contour currents, which causes deposition on the stoss-side of these obstacles. The combined findings of this thesis demonstrate that slope records can serve as external archives for shelf sedimentary and palaeoceanographic dynamics, and doing so have great potential for contributing to our integral understanding of sedimentary shelf-slope linkage.

Kurzfassung

Der Kontinentalschelf und –hang sind zwei der dynamischsten sedimentären und ozeanographischen Milieus der Erde, stark beeinflusst von terrestrischen sowie marinen Prozessen. Die Schelfkante, welche diese zwei Gebiete voneinander trennt ist eine der bedeutendsten physiographischen Übergänge auf unserer Erde. Die ozeanographischen und sedimentären Prozesse, welche Sedimente über diese Grenze transportieren, stellen die dynamische Verbindung zwischen beiden sedimentären Systemen dar. Ziele dieser Arbeit sind über eine Multi-Proxy Ansatz zu erläutern i) wie stark sedimentäre und (palä)ozeanographische Prozesse das primäre Schelfexport Signal überprägen, ii) ob und in welcher Weise sedimentäre Ablagerungen vom Kontinentalhang als verlässliche Archive zur Rekonstruktion sedimentärer und ozeanographischer Schelfdynamiken genutzt werden könne, und iii) wie wichtig die Rolle der lokalen Hangmorphologie in Ihrem Einfluss auf Schelfsedimentexport Routen, Transportprozesse und/oder die Anlage von Ablagerungszentren am Kontinentalhang ist.

Die Hauptarbeitsgebiete dieser Studie decken zwei unterschiedliche Kontinentalhangumgebun gen ab, der untere Hang (vor Nordwest Iberien) sowie der oberste Hang (vor Uruguay).

Vor Nordwest Iberien, wurde basierend auf Hochfrequenz Sedimentakustik-Profilen und einer Vielzahl von Sedimentkernen zu Beginn dieser Studie der Spät-Pleistozäne sedimentäre Werdegang des Schelfsystems, sowie die detaillierte Spät-Holozäne Entwicklung fluviogener Ablagerungszentren auf dem mittleren Schelf deutlich. Die detaillierte Kenntnis der Spät-Pleistozänen sedimentären Muster auf dem Schelf erlaubt die Differenzierung lokaler Schelfexport Signale von über-regionalen paläozeanographischen Signalen in den sedimentären Mustern am Hang. Unter Anwendung dieses Wissens enthüllen Multiproxy Untersuchungen dreier Sedimentsequenzen vom Kontinentalhang das Zusammenspiel von Hangmorphologie sowie paläoklimatischer Auswirkungen auf die Schelf - Hang Sedimentdynamik und Ablagerungs-muster während des späten Quatärs.

Am obersten Hang vor Uruguay repräsentiert eine kleine morphologische Terrasse einen weiteren Typus externer Archive zur effektiven und direkten Aufzeichnung von Schelfsediment-export. Im Gegensatz zur regionalen morpho-sedimentären Struktur des Südost südamerikanischen Kontinentalhangs, ist die Terrasse am obersten Hang vor Uruguay nicht von kontouritischem Sedimenttransport beeinflusst. Die Sedimentdynamik auf der Terrasse ist stattdessen direkt mit der sedimentären Schelfkonfiguration verbunden, welche während des Holozäns stark durch den Meeresspiegelanstieg kontrolliert wird. Sehr hohe Sedimentationsraten auf der Terrasse (min. ca. 50 cm/kyr) erlauben die Nutzung dieser Sedimentsequenzen für hochauflösende paläozeanographische Rekonstruktionen. Holozäne latitudinale Verlagerungen der sogenannten subtropischen Schelffront über dem Südost südamerikanischen Schelf und obersten Hang wurden primär durch paläoklimatische Veränderungen (nordwärtige Verlagerung und Ausbreitung der südlichen Westwinde; Mittel- bis Spät-Holozäne Entwicklung der El-Niño-Süd-Oszillation) bestimmt. Darüber hinaus lässt sich für die letzten 200 Jahre ein anthropogen bestimmter Antrieb erkennen.

Insgesamt macht die vorliegende Studie den Versuch das komplexe Zusammenspiel von paläozeanographischen und sedimentären Prozessen innerhalb von Schelfsedimenexport und sedimentären Hangablagerungsmustern zu untersuchen. Es wird gezeigt, dass Schelfexport Signale bis hinunter an den unteren Kontinentalhang erkennbar sind. Zwei unterschiedliche Typen von Hangmilieus werden als adäquate externe Archive für sedimentäre und paläozeanographische Schelfdynamik sowie Schelfexport dargestellt. Am Südost südamerikanischen Kontinentalrand stellt eine Terrasse am obersten Hang ein verlässliches und direktes Archiv der Schelfdynamik dar,

wohingegen vor Nordwest Iberien die sedimentären Ablagerungsmuster am mittlere bis untere Hang unter anderem über paläozeanographische Veränderungen mit der Sedimentdynamik auf dem Schelf verbunden sind. Während paläozeanographische Kräfteverlagerungen wenig Auswirkung auf den holozänen Schelfexport vor Südost Südamerika haben, fördern Deglaziale paläozeanographische Veränderung vor Nordwest Spanien signifikant den Export von Schelfsanden. Darüber hinaus stellt die lokale Morphologie eine kritische Komponente in der Schelf-Hang Verbindung sowie für die sedimentären Muster am Hang dar: Am obersten Hang können kleine morphologische Stufen für die Ablagerung exzellenter Schelf-Export Archive dienen, wohingegen Hangeinschnitte zur effiziente Kanalisierung von Schelfsediment-Export beitragen können. Am mittleren bis unteren Hang können morphologische Erhöhungen Sediment transportierende, hangparallele Strömungen ablenken, was zur Entstehung von Ablagerungszentren an der Luv-Seite dieser Hindernisse führt. Insgesamt demonstrieren die Erkenntnisse dieser Studie, dass Hangablagerungen als externe Archive für sedimentäre und paläozeanographische Schelfdynamik genutzt werden können, und auf diese Weise großes Potential haben zu unserem integralen Verständnis der sedimentären Schelf-Hang Verknüpfung beizutragen.

1. Introduction

The processes transferring sediments across across the shelf break are of special interest, because they represent the dynamic link between the continental shelf and slope. Moreover, the sedimentary material on each side of the shelf break experiences very different fates.

1.1 Shelf sediment dynamics and shelf sediment export through time and space

Shelf sediment export is predefined by the sedimentary and oceanographic dynamics on the shelf, which on millennial to centennial time-scales are forced by a rich diversity of parameters. The most important parameters influencing shelf sediment dynamics are 1) the initial type and quantity of material input, the 2) atmospheric and 3) oceanographic circulation patterns, as well as 3) sea-level variations. Whereas all of these components are externally forced through the climatic system, the latter one is additionally influenced by tectonic processes (Fig. 1.1).

Sediments on the shelf can be of terrigenous or biogenic origin. Terrigenous material is provided primarily via aeolian or fluvial input. Aeolian input appears to be only of importance in areas lacking major rivers (e.g. of NW Africa; deMenocal et al. 2000; Nizou et al. 2011), whereas fluvial input is considered the most dominant source for terrigenous material to the shelf sedimentary systems (globally approx. 85-95% of total particulate matter supply per year; Milliman and Meade 1983; Syvitski et al. 2003). Biogenic input within siliciclastic shelf systems only plays a role in areas with (temporarily) enhanced upwelling (e.g. off NW Spain; Martins et al. 2006). Shoreface erosion and recycling of older shelf sediments are considered as further sources for shelf sedimentary material (e.g. Kennett 1982; Huthnance 1992).

Sediments are transported over the shelf either as bedload or suspension (Curray 1965). Sands and coarser material are principally transported as bedload and remain on the inner shelf, however, they can be by-passed by shore face erosion, enhanced currents or river floods (Swift 1976). Moreover, it has been shown that also strong shelf bottom currents can transport sands towards the outer shelf and further off-shelf (Viana and Faugères 1998). Fine-grained sediments (silt and clay) are mainly contributed by rivers and thus reach the shelf environment as suspension load typically within buoyant plumes (Curray 1965; Hill et al. 2007). Three conceptual mechanisms have been proposed for the transport of suspension load over the shelf 1) diffusion due to storm events, 2) advection by currents, and 3) dense suspension flows driven by gravity (Curray 1965; Swift 1970; McCave 1972; Hill et al. 2007). There are several examples that underline the specific importance of high-energy storm events and bottom currents on resuspension and transport of sediments towards the outer shelf and over the shelf break (e.g. off northern Portugal - Vitorino et al. 2002; off northern California - Fan et al. 2004; off Southeast Brazil - Viana and Faugères 1998). Additionally, off-shelf export of fine sediments is assumed to mainly occur within nepheloid layers, whereby bottom nepheloid layers are the most important type and shelf incisions (such as canyon and gully structures) might serve as efficient export pathways (van Weering et al. 1998; van Weering and McCave 2002). Consequently, considering high-energy storm events and shelf water mass circulation as the main controlling parameters for shelf sediment transport, the steering processes are hosted in the oceanographic (e.g. along shore currents; outer shelf bottom currents, internal tides) and atmospheric (e.g. storm events, wind-induced surface currents) circulation patterns. Thus, adequate records of shelf sediment export might be able to serve as proxy records not only for the reconstruction of sedimentary dynamics on the shelf, but also for the recosntruction of palaeoclimatically induced palaeoceanographic variations.

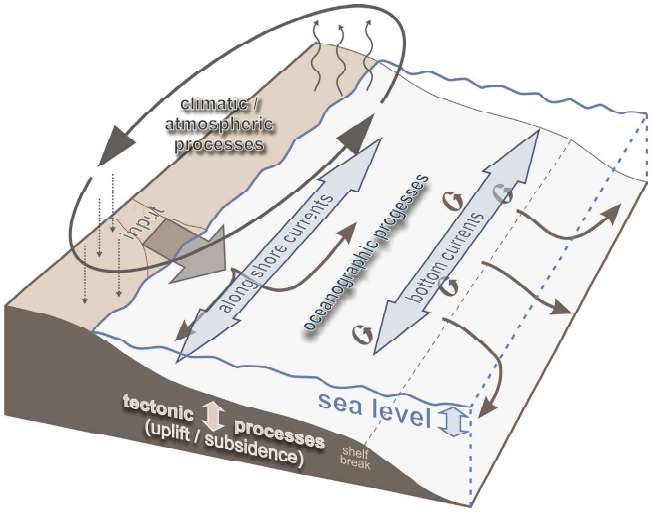

Fig. 1.1: Simplified schematic diagram of the most important components controlling long-term shelf sediment dynamics.

On millennial time-scales sea-level rises and falls are assumed to be the most relevant component in shaping continental shelves and significantly influencing shelf material export, so that slopes switch from direct recipients to relative sediment starvation (Nittrouer et al. 2007). Sea-level fall may foster significant erosion (mainly at the shoreface) and thus may boost sediment export, whereas the increased accommodation space during sea-level rise might lead to ample material accumulation on the shelf and within the estuaries (e.g., Einsele 2000). Eustatic (sea-level movements related to a fixed datum ≈ global validity) and relative (sea-level variations in relation to typically a regional modern coastline ≈ regional validity) sea-level variations are on geologic time-scales forced by climate (volume of the oceans) and tectonic processes (subsidence, uplift, isostacy, and/or shape of the oceans by plate movements; e.g., Warrick 1993; Fleming et al. 1998). For the Late Pleistocene to Holocene eustatic sea-level changes, orbital climate forcing is considered the major impact factor via waxing and waning of the large polar ice sheets (e.g., Imbrie et al. 1992).

Though it is obvious that the sedimentary and (palae)oceanographic systems on the shelf and upper slope are dynamically linked they are still frequently studied separately. To evaluate the linkage between both systems, the key objectives of this thesis are:

> How strong do slope sedimentary and oceanographic processes modify the primary shelf export signal?
>
> Can sedimentary records from the slope be used as external archives for reconstructing palaeoceanographic and sedimentary shelf dynamics via a shelf-slope linkage approach?
>
> How important is the local continental margin morphology in influencing export routes, transport processes, and/or the creation of depocentres?

1.2 Thesis outline

Following a brief summary introducing the two key study areas (Chapter 2), as well as principal methods and proxies (Chapter 3), the central part of this thesis is divided into five chapters, made-up of manuscripts which are published in, or are to be submitted to peer-reviewed scientific journals.

Chapter 4 (*Sedimentary architecture of a low accumulation shelf since the Late Pleistocene (NW Iberia)*) aims at reconstructing the spatio-temporal evolution of the NW Iberian shelf in relation to Late Pleistocene sea-level fluctuations and the resulting depositional patterns. For that purpose about 1900 km of seismic data and 66 sediment cores from the NW Iberian shelf were set into a stratigraphic framework principally supported by 31 radiocarbon dates. The results presented in this study are of key importance for the succeeding chapters 5 and 6, since they enable the regional linkage of deglacial sedimentary patterns on the slope with sea-level

induced sediment redistribution on the shelf. Moreover, the deposition of fine fraction along the middle shelf off NW Iberia as the modern high-stand depocentres is identified in this chapter.

Chapter 5 (*Holocene evolution of mud depocentres on a high-energy, low-accumulation shelf (NW Iberia))* focuses very detailed on the mechanisms of spatial and temporal mud deposition on the NW Iberian shelf during the Holocene. The findings of this chapter contribute to a comprehensive understanding of deglacial sediment dynamics on the NW Iberian shelf.

Chapter 6 (*Control of sediment supply, palaeoceanography and morphology on late Quaternary sediment dynamics at the Galician slope*) aims at unravelling the interplay of the different controlling factors for sedimentation on the slope and within this context links the slope sedimentary patterns with the earlier deciphered sedimentary evolution on the NW Iberian shelf. For this purpose a range of principally sedimentologic and palaeoceanographic proxies have been used on three sediment cores along a contour parallel transect. The findings of this study underline that precise knowledge of the regional morphology and adjoining shelf sedimentary evolution is necessary to differentiate between the interacting contributions of the regional sedimentary and palaeoclimatic - oceanographic system on local sedimentary patterns.

In chapter 7 (*Holocene history of shelf sediment export off Southeast South America*) a small uppermost slope terrace directly below the shelf break at approx. 36°S is presented. In this manuscript the litho- and chronostratigraphic architecture of the terrace sedimentary strata are elucidated within the context of the regional contourite depositional system. With this intention parametric sediment echo-sounding profiles, detailed core descriptions, grain-size distributions and Neodymium isotopic signatures are combined. The results of this study identify the uppermost slope terrace as a reliable, high-resolution archive of Holocene shelf sediment export, controlled by sedimentological and palaeoceanographic dynamics on the shelf.

Chapter 8 (*Palaeoclimatic forcing of Holocene Subtropical Shelf Front shifts off Southeast South America)* employs a high-resolution Holocene sedimentary record from the terrace to reconstruct latitudinal shifts of the Subtropical shelf front. The combination of palaeoceanographic and sediment compositional parameters reveal latitudinal migration patterns of the Subtropical shelf front primarily linked to over-regional palaeoclimatic variations during the Holocene.

Chapter 9 conclusively summarizes the main findings and implications from the presented studies and gives a scientific outlook.

References

Curray JR (1965) Late Quaternary history, continental shelves of the United States. In: Wright Jr. HE, Frey DG (eds) The Quaternary of the United States. Princton University Press, pp 723-745

deMenocal P, Ortiz J, Guilderson T, Adkins J, Sarnthein M, Baker L, Yarusinsky M (2000) Abrupt onset and termination of the African Humid Period: Rapid climate responses to gradual insolation forcing. Quaternary Science Reviews 19:347-361. doi: 10.1016/S0277-3791(99)00081-5

Einsele G (2000) Sedimentary basins: Evolution, facies, and sediment budget. 2nd edn, Springer, Berlin, Heidelberg, 729 p

Fan SJ, Swift DJP, Traykovski P, Bentley S, Borgeld JC, Reed CW, Niedoroda AW (2004) River flooding, storm resuspension, and event stratigraphy on the northern California shelf: Observations compared with simulations. Marine Geology 210:17-41. doi: 10.1016/j.margeo.2004.05.024

Fleming K, Johnston P, Zwartz D, Yokoyama Y, Lambeck K, Chappell J (1998) Refining the eustatic sea-level curve since the Last Glacial Maximum using far- and intermediate-field sites. Earth and Planetary Science Letters 163:327-342. doi: 10.1016/S0012-821X(98)00198-8

Hill PS, Fox JM, Crockett JS, Curran KJ, Friedrichs CT, Rockwell Geyer W, Milligan TG, Ogston AS, Puig P, Scully ME, Traykovski PA, Wheatcroft RA (2007) Sediment delivery to the seabed on continental margins. In: Nittrouer CA, Austin JA, Field ME, Kravitz JH, Syvitski JPM, Wiberg PL (eds) Continental margin sedimentation: From sediment transport to sequence stratigraphy. Blackwell Publishing Ltd., Malden, Oxford, Carlton, pp 49-99

Huthnance JM (1992) Extensive slope currents and the ocean-shelf boundary. Progress in Oceanography 29:161-196. doi: 10.1016/0079-6611(92)90023-s

Imbrie J, Boyle EA, Clemens SC, Duffy A, Howard WR, Kukla G, Kutzbach J, Martinson DG, McIntyre A, Mix AC, Molfino B, Morley JJ,

Peterson LC, Pisias NG, Prell WL, Raymo ME, Shackleton NJ, Toggweiler JR (1992) On the Structure and Origin of Major Glaciation Cycles: 1. Linear Responses to Milankovitch Forcing. Paleoceanography 7:701-738. doi: 10.1029/92pa02253

Kennett JP (1982) Marine Geology. Prentice-Hall, New York, 752 p

Martins V, Jouanneau J-M, Weber O, Rocha F (2006) Tracing the late Holocene evolution of the NW Iberian upwelling system. Marine Micropaleontology 59:35-55. doi: 10.1016/j.marmicro.2005.12.002

McCave IN (1972) Transport and escape of fine-grained sediment from shelf areas. In: Swift DJP, Duane DB, Pilkey OH (eds) Shelf Sediment Transport: Process and Pattern. Dowden, Hutchinson & Ross, Inc., Stroudsburg, Pennsylvania, pp 225-248

Milliman JD, Meade RH (1983) World-Wide Delivery of River Sediment to the Oceans. Journal of Geology 91:1-21

Nittrouer CA, Austin JA, Field ME, Kravitz JH, Syvitski JPM, Wiberg PL (2007) Writing a Rosetta stone: Insights into continental-margin sedimentary processes and strata. In: Nittrouer CA, Austin JA, Field ME, Kravitz JH, Syvitski JPM, Wiberg PL (eds) Continental margin sedimentation: From sediment transport to sequence stratigraphy. Blackwell Publishing Ltd., Malden, Oxford, Carlton, pp 1-48

Nizou J, Hanebuth TJJ, Vogt C (2011) Deciphering signals of late Holocene fluvial and aeolian supply from a shelf sediment depocentre off Senegal (north-west Africa). Journal of Quaternary Science 26:411-421. doi: 10.1002/Jqs.1467

Swift DJP (1970) Quarternary Shelves and Return to Grade. Marine Geology 8:5-30. doi: 10.1016/0025-3227(70)90070-8

Swift DJP (1976) Coastal sedimentation. In: Stanley DJ, Swift DJP (eds) Marine sediment trasport and environmental management. Wiley, New York, pp 255-311

Syvitski JPM, Peckham SD, Hilberman R, Mulder T (2003) Predicting the terrestrial flux of sediment to the global ocean: A planetary perspective. Sedimentary Geology 162:5-24. doi: 10.1016/S0037-0738(03)00232-X

van Weering TCE, McCave IN (2002) Benthic processes and dynamics at the NW Iberian margin: An introduction. Progress in Oceanography 52:123-128. doi: 10.1016/S0079-6611(02)00002-2

van Weering TCE, McCave IN, Hall IR (1998) Ocean Margin Exchange (OMEX I) benthic processes study. Progress in Oceanography 42:1-4. doi: 10.1016/S0079-6611(98)00025-1

Viana AR, Faugères J-C (1998) Upper slope sand deposites: the example of Campos Basin, a latest Pleistocene--Holocene record of the interaction between alongslope and downslope currents. In: Stoker MS, Evans D, Cramp A (eds) Geological Processes on Continental Margins: Sedimentation, Mass-Wasting and Stability. Geological Society, London, Special Publications, pp 287-316

Vitorino J, Oliveira A, Jouanneau JM, Drago T (2002) Winter dynamics on the northern Portuguese shelf. Part 2: Bottom boundary layers and sediment dispersal. Progress in Oceanography 52:155-170. doi: 10.1016/S0079-6611(02)00004-6

Warrick RA (1993) Climate and sea level change: A synthesis. In: Warrick RA, Barrow EM, Wigley TML (eds) Climate and sea level change: Observations, projections, and implications. Cambridge University Press, Cambridge, pp 3-22

2. Study areas

2.1 The Northwest Iberian (Galician) continental margin

The NW Iberian continental margin off Galicia presents a diverse and complex morphology (Fig. 2.1). The mostly crystalline Paleozoic and Precambrian littoral is cut by the deep 'Rías Baixas' which are old Tertiary river valleys drowned during the last sea-level rise (Rey Salgado 1993; Oliveira et al. 2002a). A series of rocky outcrops characterize the inner and outer, generally narrow shelf (max. 40 km width) (Rey Salgado 1993; Dias et al. 2002; Oliveira et al. 2002a). The middle shelf is dominated by fluviogenic, fine-grained depocentres (Fig. 2.1; Dias et al. 2002; Lantzsch et al. 2009a). Inner and outer shelf as well as the shelf break are covered with sandy, partly glauconitic sediments (Dias et al. 2002; Lantzsch et al. 2009b).

The shelf break generally occurs at 160-180 m water depth and leads into a very steep and irregular slope down to about 2000 m water depth (Lallemand et al. 1985; Dias et al. 2002). Several structural highs interrupt the lower slope region before further west the Galicia Bank arises as a marginal flat-topped submarine plateau (<700 m water depth). Between the shelf and Galicia Bank the <3000 m deep and about 50 km wide Galician interior basin is enclosed (Fig. 2.1).

The NW Iberian region experienced substantial tectonic activity since the Early Cretaceous opening of the North Atlantic. During this rifting phase, the Galician continental margin was dissected into a number of tilted blocks, which were partially uplifted during the Eocene Pyrenean orogeny, creating amongst others the Galicia Bank, as well as a series of folds, inverted grabens and reverse faults in the Galician interior basin (Fig, 2.2; Boillot and Malod 1988; Boillot et al. 1989). Frequent occurrence of minor

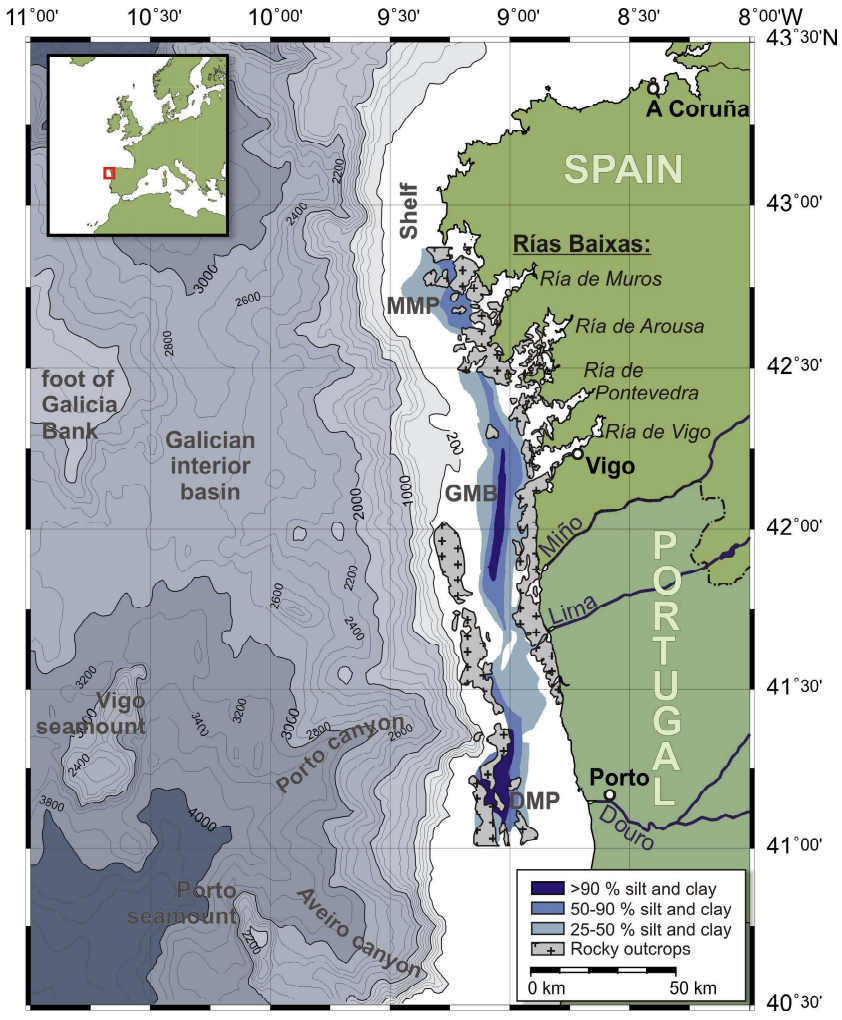

Fig. 2.1: Map of bathymetric and lithologic features on the NW Iberian continental margin. Shelf geology modified from Dias et al. (2002) and Lantzsch et al. (2009b). *MMP* Muros mud patch, *GMB* Galician mud belt, *DMP* Douro mud patch.

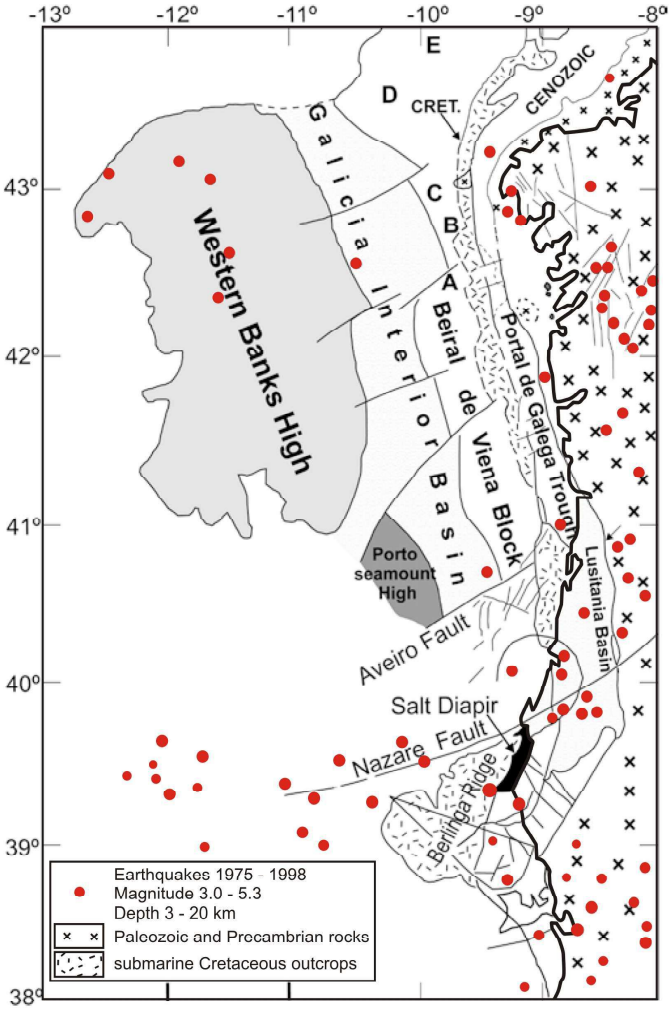

Fig. 2.2: Tectonic map of the NW Iberian continental margin. Uplifted blocks (A – C) and inverted grabens (D, E) along the eastern side of the Galician interior basin were formed during the Pyrenean Orogeny and uplifted during the Baltic Orogeny. Frequent earthquake occurrence signalizes ongoing tectonic activity. (modif. from Muñoz et al. 2003).

earthquakes indicate that the NW Iberian margin is still tectonically active today (Fig. 2.2; Muñoz et al. 2003).

Oceanographic circulation off NW Iberia is very dynamic due to a strong influence of seasonal winds affecting surface and subsurface circulation. Intermediate and deep water circulation is constrained and steered by the complex bathymetry. Water masses bounding the Galician continental margin are the Eastern North Atlantic Central Water of subtropical ($ENACW_{ST}$; <300 m water depth) and subpolar ($ENACW_{SP}$; >450 m water depth) origin, Mediterranean Outflow Water (MW; ~800 to ~1100 m), Deep Intermediate Water (DIW; 1490 ~2150 m water depth, mixed with Labrador Sea Water), Lower North Atlantic Deep Water (LNADW; ~2150 to ~3450 m water depth), and Lower Deep Water (LDW; >~3450 m water depth, containing some fraction of Antarctic Bottom Water, AABW) (Fig. 2.3a, b; Mazé et al., 1997; Varela et al., 2005).

Surface water circulation off NW Iberia is mainly controlled by the North Atlantic sub-tropical gyre and strongly influenced by the seasonally reversing wind regime. As the easternmost branch of the North Atlantic sub-tropical gyre, the Portugal Current (PC), flows equatorward (Varela et al. 2005) (Fig. 2.3a, b). The emergence of an associated coastal current, the Portugal Coastal Current (PCC) carrying cold and nutrient-rich $ENACW_{SP}$ to offshore Galicia, appears to be linked to the NNW summer wind regime (March - August) (Varela et al. 2005). During winter (September - April) SW winds prevail and the PCC practically vanishes (Álvarez-Salgado et al. 2003). A coastal counter current, the Iberian Poleward Current (IPC), flows northwards over the shelf and upper slope transporting mainly ENACWST (Fig. 2.3a, b). Below the two types of ENACW, MW flows northwards with two distinct cores at ~800 m and ~1100 m water depth and an average flow speed of 7 – 10 cm/s (Fig. 2.3b and c; Fiúza et al. 1998; Iorga and Lozier 1999; Varela et al. 2005). The flow direction of the underlying DIW along the NW Iberian margin is variable, but generally in a N-S direction with a stronger tendency towards the North (Fig. 2.3c; Fiúza et al. 1998). CTD data from the World Ocean Circulation Experiment (eWOCE) indicate that the Galician Interior Basin with its less than 3000 m water depth acts as a structural barrier for deeper northern and southern water masses like LNADW and LDW (AABW), respectively (Fig. 2.3a and c).

Present-day sedimentation on the Galician shelf is dominated by fluvial input, whereby the Douro river is the dominant source, supplying approx. 80% of the muddy input (Araújo et al. 2002; Dias et al. 2002). Sediment export from the Galician Rías is considered to be slender and the Rías rather act as sediment traps (Rey Salgado 1993). The main phase of sediment input and transport over the NW Iberian shelf is linked to the winter atmospheric circulation. Fine-grained sediments are frequently resuspended by winter storms and transported in bottom nepheloid layers northward by the IPC (Dias et al. 2002). As a consequence, defined fluviogenic depocentres exist between 100 to 120 m water depth on the NW Iberian shelf, (Fig. 2.1; Dias et al. 2002; Oliveira et al. 2002b). Over the NW Iberian slope sedimentation is dominated by biogenic production in surface nepheloid layers and settling from intermediate nepheloid layers at the level of the ENACW (~450 m; Hall and McCave 2000; McCave and Hall 2002). The presence of intermediate nepheloid layers is strongly linked to the bottom nepheloid layer formation on the Galician shelf and additionally over the upper slope during winter season (Dias et al. 2002; Oliveira et al. 2002b; Vitorino et al. 2002). The uppermost slope and shelf edge are, thus, under modern sediment dynamics regions of non-deposition (Hall et al. 2000; McCave and Hall 2002). Sedimentation on the lower slope is hemi-pelagic (Hall and McCave 2000). Further south at the Portuguese margin, sediment supply through major canyons (e.g. Nazaré Canyon; Milkert et al. 1996) by turbidity currents plays an additional and significant role (Baas et al. 1997). Similar sediment conduits at the Galician continental slope may exist, but have not yet been described in the literature.

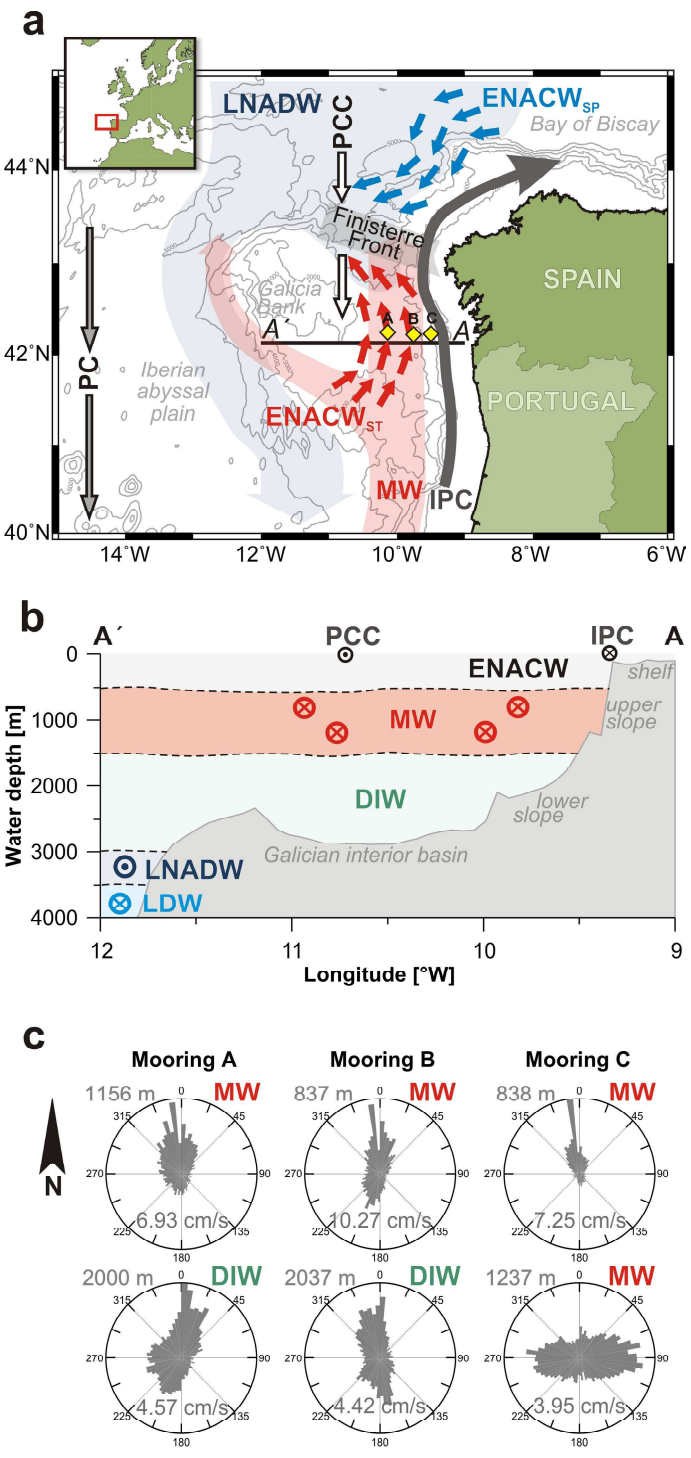

Fig. 2.3: Modern oceanographic circulation off NW Iberia. (**a**) map-view showing geographic distribution of surface circulation (*solid arrows*) and deep-water masses. Yellow diamonds demark mooring locations of data shown in **c**. (**b**) vertical water mass profile of a transect along 42°N. Note that the deep-water masses are not able to pass over the Galician interior basin (**a** and **b**). (**c**) current meter data of moorings A – C, showing the northward flow of MW and diverse N-S flow of DIW. *PC* Portugal Current, *PCC* Portugal Coastal Current, *IPC* Iberian Poleward Current, *MW* Mediterranean Water, *DIW* Deep-Intermediate Water, *LNADW* Lower North Atlantic Deep Water, *LDW* Lower Deep Water.

2.2 The Southeast South American continental margin

Several morpho-structural units border the SE South American continental margin onshore. The most important of those structural units is the Brazilian shield, outcropping along the SE Brazilian and Uruguayan coast (Fig. 2.4; Urien and Ewing 1974). The NW trend of several fracture zones is attributed to extensional stress during an early rifting phase of the Late Jurassic South Atlantic opening initiation (Fig. 2.4; Soto et al. 2011). Offshore, the Brazilian shield is bound by the Pelotas basin, whose NE trend reflects a second rifting stage during the early Cretaceous (Fig. 2.4; Soto et al. 2011).

Shelf width off SE South America largely varies from approx. 300 km off the Buenos Aires region, narrowing to approx. 120 km off Uruguay and SE Brazil (Fig. 2.4). The shelf break occurs between 100 – 180 m water depth, and the bathymetry of the outer shelf and upper slope region is very irregular with several smaller canyons, steps and terraces (Urien and Ewing 1974). The largest and most prominent of those bathymetric features is the Mar del Plata canyon, which appears to follow the Salado fracture zone (Fig. 2.4). Below 500 m water depth, on the middle and lower slope, several morphologic terraces characterize the Argentine continental margin, of which the Ewing terrace constitutes the Northernmost (e.g., Urien and Ewing 1974; Hernández-Molina et al. 2009; Fig. 2.4).

Present-day surface and intermediate water circulation in the western South Atlantic is dominated by the confluence of two large western boundary currents. At ca. 38°S the poleward flowing Brazil current (BC) meets with the northward flowing Malvinas current (MC), forming the Brazil-Malvinas Confluence (BMC) within the level of Antarctic Intermediate Water (AAIW) (Fig. 2.5; Peterson and Stramma 1991; Stramma and England 1999). The BC forms from the bifurcation of the South Equatorial Current at ca. 10°S and carries warm, saline and nutrient-depleted subtropical water masses southward within the levels of Tropical and South Atlantic Central Water (TW and SACW; Fig. 2.5). The cold, relatively fresh and nutrient-rich MC originates as a

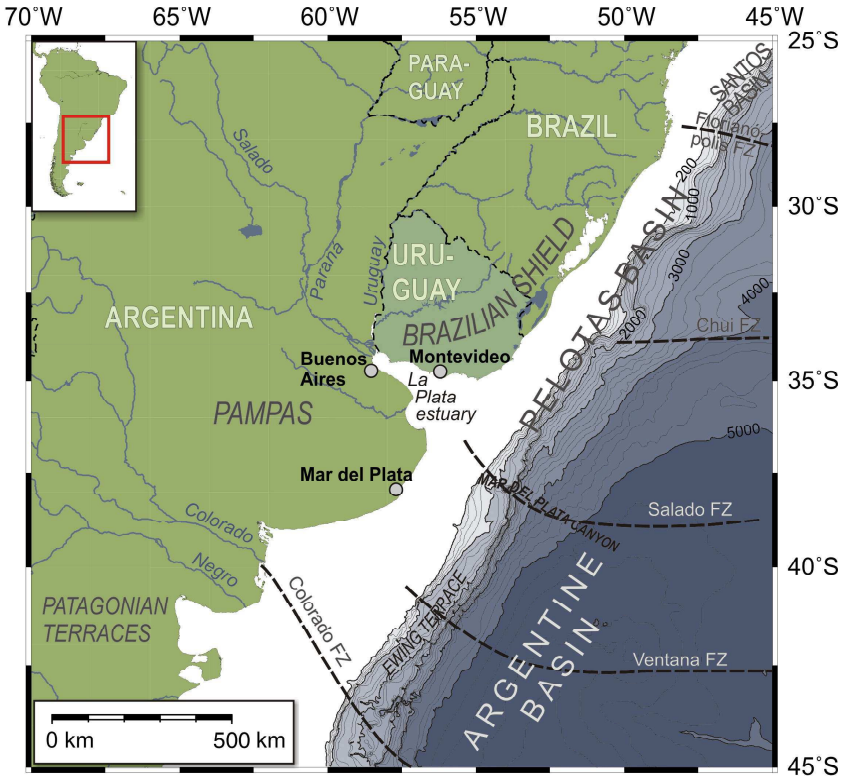

Fig. 2.4: The SE South American continental margin between 25° to 45° South including structural features after Urien and Ewing (1974) and Soto et al. (2011). *FZ* Fracture zone.

branch of the Antarctic Circumpolar Current east of the Drake Passage and carries subantarctic waters over the Argentine shelf and upper slope (Fig. 2.5). Whereas the BC is considered to be a relatively weak boundary current with a strong tendency to meandering flow, the MC is assumed to be a strong western boundary current with significant bottom flow (Peterson et al. 1996). After their confluence BC and MC are deflected southeastward forming the South Atlantic Current (SAC) and contributing to the Antarctic Circumpolar Current (ACC) respectively.

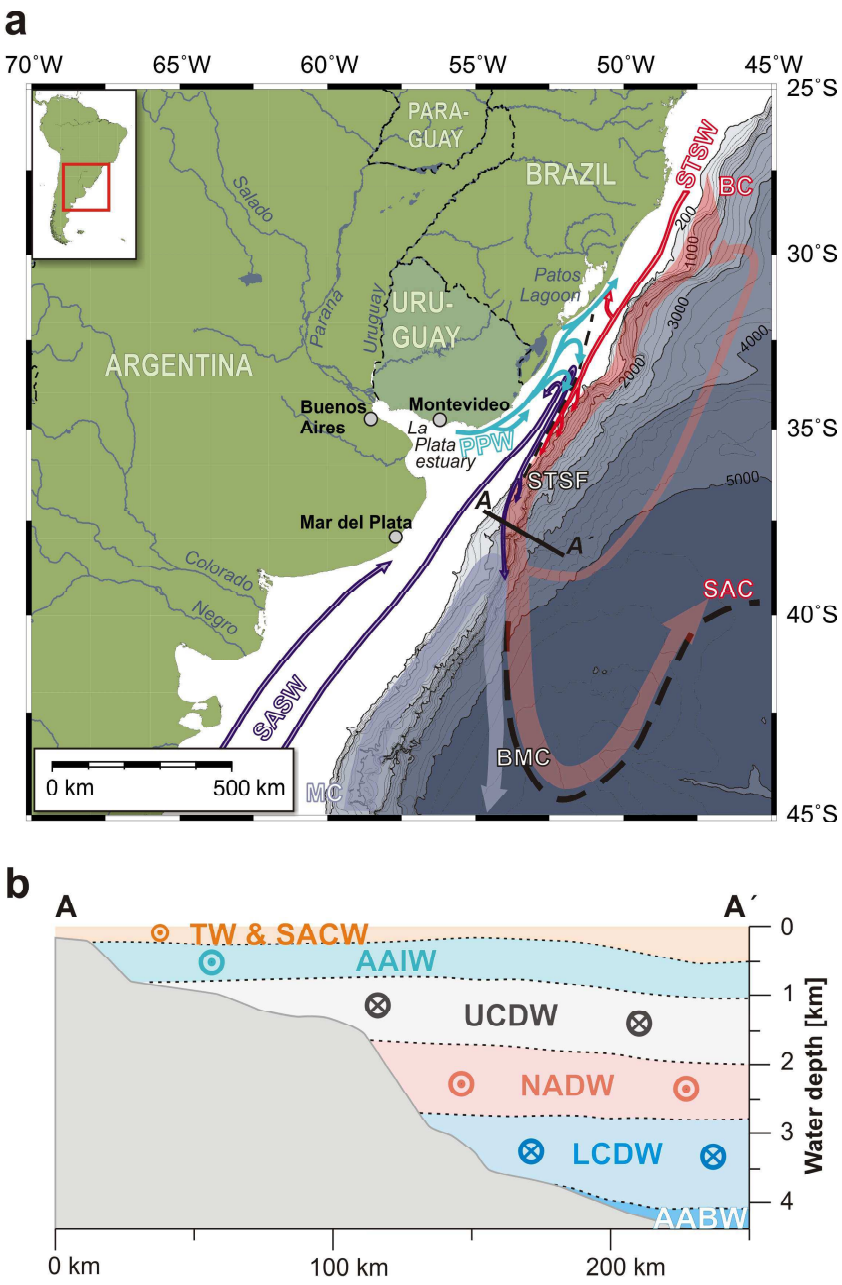

Fig. 2.5: Map of present-day oceanographic features summarizing the mean winter shelf and intermediate water spatial circulation patterns (**a**) and vertical hydrographic section (**b**) off SE South America (after Piola and Matano 2001; Piola et al. 2008). *AABW* Antarctic Bottom Water, *AAIW* Antarctic Intermediate Water, *BC* Brazil Current, *BMC* Brazil-Malvinas Confluence, *LCDW* Lower Circumpolar Deep Water, *MC* Malvinas Current, *NADW* North Atlantic Deep Water, *PPW* Plata Plume Water, *SASW* Subantarctic Shelf Water, *SAC* South Atlantic Current, *SACW* South Atlantic Central Water, *STSF* Subtropical Shelf Front, *STSW* Subtropical Shelf Water, *TW* Tropical Water, *UCDW* Upper Circumpolar Deep Water.

On the shelf this southward versus northward flowing current pattern is pursued by the coalescence of subantarctic shelf water (SASW) and subtropical shelf water (STSW), forming the subtropical shelf front (STSF) (Fig. 2.5; Piola et al. 2000; Piola et al. 2008). The STSF runs southwestward from the 50 m isobath at ca. 32°S towards the shelf break around 36°S (Fig. 2.5) (Piola et al. 2000). The STSF is considered the shelf-ward extension of the BMC and the barotropic pressure gradient enforced by the MC on the shelf circulation is assumed to play a major role in determining the latitudinal STSF location (Palma et al. 2008). Circulation on the inner Argentine shelf is rather uniformly northwards controlled by the northward flow of SASW. In contrast, inner shelf circulation becomes complex off Uruguay and SE Brazil where it is strongly influenced by the La Plata river discharge (~23,000 m^3/s). Together with the Patos Lagoon outflow (~1750 m^3/s), La

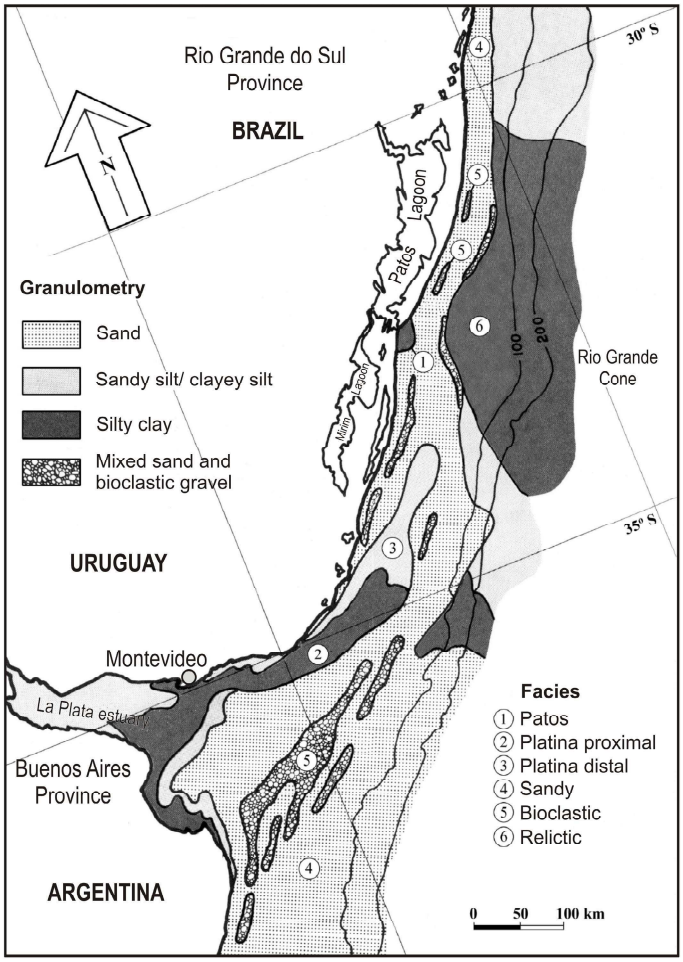

Fig. 2.6: Modern surface lithology on the northern Argentine, Uruguayan to SE Brazilian shelf (modified from Martins et al. 2003).

Plata discharge forms the distinctly buoyant, low-salinity Plata Plume Water (PPW) (Piola et al. 2000; Piola et al. 2008). The PPW is commonly northward directed and recognized as far north as 25°S, however, its maximum northeastward extension is primarily controlled by the regional along shore wind stress (Piola et al. 2005; Möller et al. 2008). Through changes in the interannual wind patterns PPW distribution also responds to El Niño Southern Oscillation (ENSO) variability (Piola et al. 2005). Although positive precipitation anomalies over the drainage basin lead to increased La Plata river outflow during El Niño events, the regional atmospheric circulation (winds from the NE) prevents northeastward extension of PPW and the plume is rather advected offshore (Piola et al. 2005).

The STSF also plays a major role in modern sedimentation on the SE South American continental shelf. Clay-mineralogic analyses between 40° - 27°S suggest that the STSF acts as an effective boundary separating the sandy sediments in the South from the silty – clayey sediments contributed by La Plata discharge and Patos lagoon outflow (Campos et al. 2008). South of ca. 36°S the shelf is widely covered by siliciclastic sands and bioclastic gravels, whereas North of 36°S a silt to silty clay tongue extends out of the La Plata estuary onto the middle shelf (Fig. 2.6.; Martins et al. 2003). The silty clays of the so-called platina facies are genetically linked to the modern circulation of PPW over the shelf, whereas the silty clays on the outer shelf between 31° - 34°S are relictic and assumed to have accumulated during past sea-level lowstands (Fig. 2.6; Martins et al. 2003). Neodymium isotopic (εNd) analyses showed a homogenous younger Andean (Patagonian) volcanic rocks source province for the siliciclastic sands south of approx. 36°S, reflecting the effective sediment redistribution and northward transport within the SASW (de Mahiques et al. 2008). North of 36°S the strong influence of La Plata discharge extending northeastward as PPW is reflected by distinctly lighter εNd signatures of the shelf sediments (de Mahiques et al. 2008).

References

Álvarez-Salgado XA, Figueiras FG, Pérez FF, Groom S, Nogueira E, Borges A, Chou L, Castro CG, Moncoiffé G, Ríos AF, Miller AEJ, Frankignoulle M, Savidge G, Wollast R (2003) The Portugal coastal counter current off NW Spain: New insights on its biogeochemical variability. Progress in Oceanography 56:281-321. doi: 10.1016/S0079-6611(03)00007-7

Araújo MF, Jouanneau JM, Valério P, Barbosa T, Gouveia A, Weber O, Oliveira A, Rodríguez A, Dias JMA (2002) Geochemical tracers of northern Portuguese estuarine sediments on the shelf. Progress in Oceanography 52:277-297. doi: 10.1016/S0079-6611(02)00011-3

Baas JH, Mienert J, Abrantes F, Prins MA (1997) Late Quaternary sedimentation on the Portuguese continental margin: Climate-related processes and products. Palaeogeography Palaeoclimatology Palaeoecology 130:1-23. doi: 10.1016/S0031-0182(96)00135-6

Boillot G, Girardeau J, Kornprobst J (1989) Rifting of the west Galicia continental margin: A review. Bulletin De La Societe Geologique De France 5:393-400

Boillot G, Malod J (1988) The north and north-west Spanish continental margin: A review. Revista de la Sociedad Geológica de España 1:295-316

Campos EJD, Mulkherjee S, Piola AR, de Carvalho FMS (2008) A note on a mineralogical analysis of the sediments associated with the Plata River and Patos Lagoon outflows. Continental Shelf Research 28:1687-1691. doi: 10.1016/j.csr.2008.03.014

de Mahiques MM, Tassinari CCG, Marcolini S, Violante RA, Figueira RCL, da Silveira ICA, Burone L, de Mello e Sousa SH (2008) Nd and Pb isotope signatures on the Southeastern South American upper margin: Implications for sediment transport and source rocks. Marine Geology 250:51-63. doi: 10.1016/j.margeo.2007.11.007

Dias JMA, Gonzalez R, Garcia C, Diaz-del-Rio V (2002) Sediment distribution patterns on the Galicia-Minho continental shelf. Progress in Oceanography 52:215-231. doi: 10.1016/S0079-6611(02)00007-1

Fiúza AFG, Hamann M, Ambar I, Díaz Del Río G, González N, Cabanas JM (1998) Water masses and their circulation off western Iberia during May 1993. Deep Sea Research Part I: Oceanographic Research Papers 45:1127-1160. doi: 10.1016/S0967-0637(98)00008-9

Hall IR, McCave IN (2000) Palaeocurrent reconstruction, sediment and thorium focussing on the Iberian margin over the last 140 ka. Earth and Planetary Science Letters 178:151-164. doi: 10.1016/S0012-821X(00)00068-6

Hall IR, Schmidt S, McCave IN, Reyss JL (2000) Particulate matter distribution and 234Th/238U disequilibrium along the Northern Iberian Margin: Implications for particulate organic carbon export. Deep Sea Research Part I: Oceanographic Research Papers 47:557-582. doi: 10.1016/S0967-0637(99)00065-5

Hernández-Molina FJ, Paterlini M, Violante R, Marshall P, de Isasi M, Somoza L, Rebesco M (2009) Contourite depositional system on the Argentine Slope: An exceptional record of the influence of Antarctic water masses. Geology 37:507-510. doi: 10.1130/g25578a.1

Iorga MC, Lozier MS (1999) Signatures of the Mediterranean outflow from a North Atlantic climatology: 1. Salinity and density fields. Journal of Geophysical Research 104:25985-26009. doi: 10.1029/1999JC900115

Lallemand S, Mazé JP, Monti S, Sibuet JC (1985) New bathymetric map of the northeast Atlantic ocean. Comptes Rendus De L Academie Des Sciences Serie II 300:145-149

Lantzsch H, Hanebuth TJJ, Bender VB (2009a) Holocene evolution of mud depocentres on a high-energy, low-accumulation shelf (NW Iberia). Quaternary Research 72:325-336. doi: 10.1016/j.yqres.2009.07.009

Lantzsch H, Hanebuth TJJ, Bender VB, Krastel-Gudegast S (2009b) Sedimentary architecture of a low accumulation shelf since the Late Pleistocene (NW Iberia). Marine Geology 259:47-58. doi: 10.1016/j.margeo.2008.12.008

Martins LR, Martins IR, Urien CM (2003) Aspectos sedimentares da plataforma continental na área de Influência do Rio de La Plata. Gravel 1:68-80

McCave IN, Hall IR (2002) Turbidity of waters over the northwest Iberian continental margin. Progress in Oceanography 52:299-313. doi: 10.1016/S0079-6611(02)00012-5

Milkert D, Weaver PPE, Liu L (1996) Pleistocene and Pliocene turbidites from the Iberia abyssal plain. In: Whitmarsh RB, Sawyer DS, Klaus A, Masson DG (eds) ODP Proceedings, Scientific Results. Ocean Drilling Program, College Station, Texas, pp 281-294

Möller OO, Piola AR, Freitas AC, Campos EJD (2008) The effects of river discharge and seasonal winds on the shelf off southeastern South America. Continental Shelf Research 28:1607-1624. doi: 10.1016/j.csr.2008.03.012

Muñoz A, Acosta J, Uchupi E (2003) Cenozoic tectonics on the Galicia margin, northwest Spain. Geo-Marine Letters 23:72-80. doi: 10.1007/s00367-003-0126-1

Oliveira A, Rocha F, Rodrigues A, Jouanneau J, Dias A, Weber O, Gomes C (2002a) Clay minerals from the sedimentary cover from the Northwest Iberian shelf. Progress in Oceanography 52:233-247. doi: 10.1016/S0079-6611(02)00008-3

Oliveira A, Vitorino J, Rodrigues A, Jouanneau JM, Dias JA, Weber O (2002b) Nepheloid layer dynamics in the northern Portuguese shelf. Progress in Oceanography 52:195-213. doi: 10.1016/S0079-6611(02)00006-X

Palma ED, Matano RP, Piola AR (2008) A numerical study of the Southwestern Atlantic shelf circulation: Stratified ocean response to local and offshore forcing. Journal of Geophysical Research - Oceans 113:C11010. doi: 10.1029/2007jc004720

Peterson RG, Johnson CS, Krauss W, Davis RE (1996) Lagrangian measurements in the Malvinas Current. In: Wefer G, Berger WH, Siedler G, Webb DJ (eds) The South Atlantic. Springer, Berlin, Heidelberg, pp 239-247

Peterson RG, Stramma L (1991) Upper-level circulation in the South Atlantic ocean. Progress In Oceanography 26:1-73. doi: 10.1016/0079-6611(91)90006-8

Piola AR, Campos EJD, Möller OO, Charo M, Martinez C (2000) Subtropical Shelf Front off eastern South America. Journal of Geophysical Research - Oceans 105:6565-6578

Piola AR, Matano RP, Palma ED, Möller OO, Campos EJD (2005) The influence of the Plata river discharge on the western South Atlantic shelf. Geophysical Research Letters 32:4. doi: 10.1029/2004gl021638

Piola AR, Möller OO, Guerrero RA, Campos EJD (2008) Variability of the subtropical shelf front off eastern South America: Winter 2003 and summer 2004. Continental Shelf Research 28:1639-1648. doi: 10.1016/j.csr.2008.03.013

Rey Salgado J (1993) Relacion morphose dimentaria entre la platforma continental de Galicia y las Rias bajas y su evolucion durante el Cuaternario. Publicaciones Especiales, Instituto Español de Oceanografía 17:1-233

Soto M, Morales E, Veroslavsky G, de Santa Ana H, Ucha N, Rodríguez P (2011) The continental margin of Uruguay: Crustal architecture and segmentation. Marine and Petroleum Geology 28:1676-1689. doi: 10.1016/j.marpetgeo.2011.07.001

Stramma L, England M (1999) On the water masses and mean circulation of the South Atlantic Ocean. Journal of Geophysical Research - Oceans 104:20863-20883

Urien CM, Ewing M (1974) Recent sediments and environments of Southern Brazil, Uruguay, Buenos Aires, and Rio Negro continental shelf. In: Burk CA, Drake CL (eds) The Geology of Continental Margins. Springer, Berlin, Heidelberg, New York, pp 157-177

Varela RA, Rosón G, Herrera JL, Torres-López S, Fernández-Romero A (2005) A general view of the hydrographic and dynamical patterns of the Rías Baixas adjacent sea area. Journal of Marine Systems 54:97-113. doi: 10.1016/j.jmarsys.2004.07.006

Vitorino J, Oliveira A, Jouanneau JM, Drago T (2002) Winter dynamics on the northern Portuguese shelf. Part 2: Bottom boundary layers and sediment dispersal. Progress in Oceanography 52:155-170. doi: 10.1016/S0079-6611(02)00004-6

3. Methods and proxies

The combination of different types of palaeoenvironmental proxies in a multi-proxy approach enables the understanding of past climate dynamics in its full richness. Consequently, a wide suite of methods and proxies were applied to the different sediment cores depending on the site specific objectives within the respective study (Table 3.1). In the following, some specific details about the most important applied methods and proxies are briefly summarized.

The analysis of **grain size distributions** is a widely used sedimentological method, which can give valuable information about sediment sources, transport processes, and depositional mechanisms (e.g. Tucker 2001; Stuut et al. 2007; Frenz et al. 2009; Gyllencreutz et al. 2010). Moreover, in mud-rich deep-sea sediments the weight percentage and mean size of the terrigenous size spectrum 63 to 10 µm (termed sortable silt; McCave et al. 1995b) has been shown a valuable proxy for palaeo-current speed prevailing at the time of deposition (e.g. McCave et al. 1995a; Hall et al. 1998; Bianchi and McCave 1999; Hall et al. 2004; Kissel et al. 2010; Rodrigo-Gamiz et al. 2011). Though Bianchi et al (1999) have shown that the sortable silt proxy works accurately down to approx. 5% sortable silt content of the total <64 µm fraction, it is unclear how applicable the proxy is in sand-rich environments.

Analysis of the parameters **total organic carbon (TOC)** and subsequent calculation of **calcium carbonate ($CaCO_3$) content** is a relatively fast and cheap method for gaining insight into the sedimentary composition of a sample. Particularly in combination with other proxy data they can give valuable palaeoenvironmental information (e.g. Frenz et al. 2003). Carbonate and TOC content have also been discussed as proxies for biogenic production. However, it appears that the relationship is not straight forward and especially carbonate content suffers from dilution and dissolution effects (Wefer et al. 1999). When using carbonate content and/or TOC for biogenic productivity interpretations it is advisable to combine them with an independent productivity proxy.

The quick and non-destructive method of **X-ray fluorescence (XRF) core scanning**, providing quasi-continuous, high resolution (up to 1 mm) bulk-sediment chemistry data, has been proven useful in the various fields of marine research (e.g. Lamy et al. 2001; Zachos et al. 2005; Westerhold and Röhl 2009; Schefuß et al. 2011). However, lithologic inhomogeneity and surface roughness can significantly influence the quality of the measurements and are pronounced in medium to coarse sandy sediments (Richter et al. 2006). When using elemental data from XRF core scanning one has to be aware that due to the measurement principals the output is in relative concentrations. Consequently, it is advised to use elemental ratios instead of single element concentrations (e.g. Croudace et al. 2006; Richter et al. 2006).

The method of **magnetic susceptibility core scanning** is a fast, direct and non-destructive method for gaining quasi-continuous and high-resolution (up to 1 cm) down-core data concerning the relative amount of the terrigenous sedimentary fraction. The applicability of quasi-continuous logged magnetic susceptibility for stratigraphic purposes has already been suggested in 1968 by Radhakrishnamurty et al. (1968) and has since then been extensively employed (e.g. Somayajulu et al. 1975; Gupta et al. 1991; Bloemendal et al. 1995; von Dobeneck and Schmieder 1999; Seltzer et al. 2002; Allen et al. 2011). However, it is clear that magnetic susceptibility needs additional proxy records to give reliable palaeoclimatic implications.

Stable oxygen isotopic composition of foraminiferal calcite is principally determined by isotopic composition and temperature of the ambient sea water during shell calcification (e.g. McCrea 1950; Shackleton 1967; Shackleton and Opdyke 1973; Rohling and Cooke 2003). The

Table 3.1 Reference data and applied methods (down-core sample resolution in cm, if quasi-equidistant; 'x' if sample resolution non-equidistant task specific) of GeoB cores primarily (first-author studies) utilized within this PhD thesis

	Galicia			***Uruguay***					
	GeoB 11035-1	**GeoB 130206-1**	**GeoB 13071-1**	**GeoB 13801-2**	**GeoB 13840-1**	**GeoB 13841-2**	**GeoB 13835-2**	**GeoB 13836-2**	**GeoB 13837-2**
Core reference data									
Expedition	Pos-342	Pos-366/3	Pos-366/3	M78/3a	M78/3a	M78/3a	M78/3a	M78/3a	M78/3a
Coring device	GC-6	GC-6	GC-3	GC-12	GC-12	GC-12	VC-5	VC-5	VC-5
Latitude	42°10.29'N	42°27.51'N	42°48.49'N	36°08.49'S	35°49.21'S	35°49.53'S	35°43.10'S	35°44.72'S	35°46.18'S
Longitude	09°39.47'W	09°37.19'W	09°50.55'W	53°17.96'W	52°54.56'W	52°53.87'W	53°05.13'W	53°03.66'W	53°02.29'W
Water depth	2045 m	1704 m	2274 m	241 m	232 m	285 m	131 m	135 m	140 m
Total recovery	505 cm	485 cm	286 cm	955 cm	387 cm	817 cm	506 cm	507 cm	314 cm
Methods									
Sonic sifter	x	10 cm	10 cm	10 cm	10 cm	X	-	-	-
SediGraph	10 cm	10 cm	10 cm	-	-	-	-	-	-
Coulter Laser Sizer	-	-	-	10 cm	-	20 cm	x	x	x
Sortable silt	10 cm	10 cm	10 cm	10 cm	-	-	-	-	-
TOC, $CaCO_3$	10 cm	10 cm	10 cm	10 cm	-	-	-	-	-
Stable oxygen & carbon isotopes	-	-	-	10 cm	-	-	-	-	-
Neodymium isotopes (εNd)	-	-	-	x	-	-	-	-	-
BF assemblage and indices	-	-	-	x	-	-	-	-	-
XRF core scanning	2 cm	1 cm	1 cm	1 cm	-	-	-	-	-
Magnetic susceptibility	1 cm	1 cm	1 cm	-	-	-	-	-	-
X-Radiographs	continuous	continuous	continuous	continuous	-	continuous	-	-	-
# of radiocarbon datings	6	2	1	9	2	5	1	-	-
Coccolith assemblage	5–10 cm	-	-	-	-	-	-	-	-
N. pachyderma (sin) counts	x	-	-	-	-	-	-	-	-
IRD counts	x	-	-	-	-	-	-	-	-

Abbreviations: GC: Gravity corer (GC-6: 6 m gravity corer, etc.); VC: Vibro corer; Pos: R/V Poseidon; M: R/V Meteor; BF: Benthic foraminifera; XRF: X-ray fluorescence; IRD: Ice-rafted debris

$\delta^{18}O$ of benthic foraminifer tests is a widely used proxy for bottom water temperature (e.g. Arz et al. 1999; Waelbroeck et al. 2002; Malone et al. 2004; Duplessy et al. 2005; Chiessi et al. 2008; Thornalley et al. 2010). However, when applying this proxy it has to be considered that the oxygen isotopic composition of the ambient sea-water can be significantly altered by 1) the ice-volume effect (large ice-sheet formation preferentially removes ^{16}O from the oceanic $^{16/18}O$ reservoir), 2) enhanced fresh water input and precipitation (both enriched in ^{16}O) and 3) evaporation effects (preferentially removing ^{16}O, leaving the residual enriched in ^{18}O) (e.g. Rohling and Cooke 2003).

The use of the **stable carbon isotopic ratio** ($\delta^{13}C$) as a paleoceanographic proxy is even more challenging, since a number of factors influence the carbon isotopic composition of the ambient sea water and the imprint in benthic foraminifer carbonate tests (e.g. review by Rohling and Cooke 2003). Despite this complexity, stable carbon isotopic ratios of benthic foraminifera have, been widely used in paleoceanography as a proxy for palaeoproductivity and deep-ocean water-mass configuration (e.g. Zahn et al. 1986; Curry et al. 1988; Arz et al. 1999; Mackensen et al. 2001; Bickert and Mackensen 2004; Curry and Oppo 2005).

Over the past two decades the **Neodymium isotopic signature** of the bulk terrigenous sediment fraction has been shown a powerful proxy for terrigenous sediment dynamics and provenance (e.g. Vroon et al. 1995; Walter et al. 2000; Gaiero et al. 2007; de Mahiques et al. 2008; Cole et al. 2009; Asahara et al. 2012). The extraction and analysis of the rare earth element Neodymium is very elaborate and time consuming. When applying this proxy on the bulk decarbonated sediment fraction one has to be aware of possible biasing from water mass inhibited Neodymium signatures, potentially transferred to the sediment during authigenic iron oxide formation.

References

Allen CS, Pike J, Pudsey CJ (2011) Last glacial-interglacial sea-ice cover in the SW Atlantic and its potential role in global deglaciation. Quaternary Science Reviews 30:2446-2458. doi:10.1016/j.quascirev.2011.04.002

Arz HW, Pätzold J, Wefer G (1999) The deglacial history of the western tropical Atlantic as inferred from high resolution stable isotope records off northeastern Brazil. Earth and Planetary Science Letters 167:105-117. doi:10.1016/S0012-821X(99)00025-4

Asahara Y, Takeuchi F, Nagashima K, Harada N, Yamamoto K, Oguri K, Tadai O (2012) Provenance of terrigenous detritus of the surface sediments in the Bering and Chukchi Seas as derived from Sr and Nd isotopes: Implications for recent climate change in the Arctic regions. Deep-Sea Research Part II: Topical Studies in Oceanography 61-64:155-171. doi:10.1016/j.dsr2.2011.12.004

Bianchi GG, Hall IR, McCave IN, Joseph L (1999) Measurement of the sortable silt current speed proxy using the Sedigraph 5100 and Coulter Multisizer IIe: Precision and accuracy. Sedimentology 46:1001-1014. doi:10.1046/j.1365-3091.1999.00256.x

Bianchi GG, McCave IN (1999) Holocene periodicity in North Atlantic climate and deep-ocean flow south of Iceland. Nature 397:515-517. doi:10.1038/17362

Bickert T, Mackensen A (2004) Last glacial to Holocene changes in South Atlantic deep water circulation. In: Wefer G, Mulitza S, Ratmeyer V (eds) The South Atlantic in the Late Quaternary. Springer, Berlin, pp 599-620

Bloemendal J, Liu XM, Rolph TC (1995) Correlation of the magnetic susceptibility stratigraphy of Chinese loess and the marine oxygen isotope record: Chronological and palaeoclimatic implications. Earth and Planetary Science Letters 131:371-380. doi:10.1016/0012-821x(95)00016-6

Chiessi CM, Mulitza S, Paul A, Pätzold J, Groeneveld J, Wefer G (2008) South Atlantic interocean exchange as the trigger for the Bølling warm event. Geology 36:919-922. doi:10.1130/g24979a.1

Cole JM, Goldstein SL, deMenocal PB, Hemming SR, Grousset FE (2009) Contrasting compositions of Saharan dust in the eastern Atlantic Ocean during the last deglaciation and African Humid Period. Earth and Planetary Science Letters 278:257-266. doi:10.1016/j.epsl.2008.12.011

Croudace IW, Rindby A, Rothwell RG (2006) ITRAX: Description and evaluation of a new multi-function X-ray core scanner. In: Rothwell RG (ed) New Techniques in Sediment Core Analysis. Geological Society of London, London, pp 51-63

Curry WB, Duplessy JC, Labeyrie LD, Shackleton NJ (1988) Changes in the distribution of $\delta^{13}C$ of deep water $\sum CO_2$ between the Last Glaciation and the Holocene. Paleoceanography 3:317-341. doi:10.1029/PA003i003p00317

Curry WB, Oppo DW (2005) Glacial water mass geometry and the distribution of $\delta^{13}C$ of $\sum CO_2$ in the western Atlantic Ocean. Paleoceanography 20:Pa1017. doi:10.1029/2004pa001021

de Mahiques MM, Tassinari CCG, Marcolini S, Violante RA, Figueira RCL, da Silveira ICA, Burone L, de Mello e Sousa SH (2008) Nd and Pb isotope signatures on the Southeastern South American upper margin: Implications for sediment transport and source rocks. Marine Geology 250:51-63. doi:10.1016/j.margeo.2007.11.007

Duplessy JC, Cortijo E, Ivanova E, Khusid T, Labeyrie L, Levitan M, Murdmaa I, Paterne M (2005) Paleoceanography of the Barents Sea during the Holocene. Paleoceanography 20:Pa4004. doi:10.1029/2004pa001116

Frenz M, Höppner R, Stuut JB, Wagner T, Henrich R (2003) Surface sediment bulk geochemistry and grain size composition related to the oceanic circualtion along the South American continental margin in the Southwest Atlantic. In: Wefer G, Mulitza S, Rat-

meyer V (eds) The South Atlantic in the Late Quaternary: Reconstructions of material budgets and currents systems. Springer, Berlin, Heidelberg, New York, Tokyo, pp 347-373
Frenz M, Wynn RB, Georgiopoulou A, Bender VB, Hough G, Masson DG, Talling PJ, Cronin BT (2009) Provenance and pathways of late Quaternary turbidites in the deep-water Agadir Basin, northwest African margin. International Journal of Earth Sciences 98:721-733. doi:10.1007/s00531-008-0313-4
Gaiero DM, Brunet F, Probst JL, Depetris PJ (2007) A uniform isotopic and chemical signature of dust exported from Patagonia: Rock sources and occurrence in southern environments. Chemical Geology 238:107-120. doi:10.1016/j.chemgeo.2006.11.003
Gupta SK, Sharma P, Juyal N, Agrawal DP (1991) Loess paleosol sequence in Kashmir - Correlation of mineral magnetic stratigraphy with the marine paleoclimatic record. Journal of Quaternary Science 6:3-12. doi:10.1002/jqs.3390060103
Gyllencreutz R, Mahiques MM, Alves DVP, Wainer IKC (2010) Mid- to late-Holocene paleoceanographic changes on the southeastern Brazilian shelf based on grain size records. Holocene 20:863-875. doi:10.1177/0959683610365936
Hall IR, Bianchi GG, Evans JR (2004) Centennial to millennial scale Holocene climate-deep water linkage in the North Atlantic. Quaternary Science Reviews 23:1529-1536. doi:10.1016/j.quascirev.2004.04.004
Hall IR, McCave IN, Chapman MR, Shackleton NJ (1998) Coherent deep flow variation in the Iceland and American basins during the last interglacial. Earth and Planetary Science Letters 164:15-21. doi:10.1016/S0012-821X(98)00209-X
Kissel C, Laj C, Kienast M, Bolliet T, Holbourn A, Hill P, Kuhnt W, Braconnot P (2010) Monsoon variability and deep oceanic circulation in the western equatorial Pacific over the last climatic cycle: Insights from sedimentary magnetic properties and sortable silt. Paleoceanography 25:Pa3215. doi:10.1029/2010pa001980
Lamy F, Hebbeln D, Röhl U, Wefer G (2001) Holocene rainfall variability in southern Chile: A marine record of latitudinal shifts of the Southern Westerlies. Earth and Planetary Science Letters 185:369-382. doi:10.1016/S0012-821X(00)00381-2
Mackensen A, Rudolph M, Kuhn G (2001) Late Pleistocene deep-water circulation in the subantarctic eastern Atlantic. Global and Planetary Change 30:197-229. doi:10.1016/S0921-8181(01)00102-3
Malone MJ, Martin JB, Schönfeld J, Ninnemann US, Nürnburg D, White TS (2004) The oxygen isotopic composition and temperature of Southern Ocean bottom waters during the last glacial maximum. Earth and Planetary Science Letters 222:275-283. doi:10.1016/j.epsl.2004.02.027
McCave IN, Manighetti B, Beveridge NAS (1995a) Circulation in the glacial North Atlantic inferred from grain-size measurements. Nature 374:149-152. doi:10.1038/374149a0
McCave IN, Manighetti B, Robinson SG (1995b) Sortable silt and fine sediment size composition slicing: Parameters for paleocurrent speed and paleoceanography. Paleoceanography 10:593-610. doi:10.1029/94PA03039
McCrea JM (1950) On the isotopic chemistry of carbonates and a paleotemperature scale. Journal of Chemical Physics 18:849-857. doi:10.1063/1.1747785
Radhakrishnamurty C, Likhite SD, Amin BS, Somayajulu BLK (1968) Magnetic susceptibility stratigraphy in ocean sediment cores. Earth and Planetary Science Letters 4:464-468. doi:10.1016/0012-821x(68)90025-3
Richter TO, van der Gaast S, Koster B, Vaars A, Gieles R, de Stigter HC, de Haas H, van Weering TCE (2006) The Avaatech XRF core scanner: Technical description and applications to NE Atlantic sediments. In: Rothwell RG (ed) New Techniques in Sediment Core Analysis. Geological Society of London, London, pp 39-50
Rodrigo-Gamiz M, Martinez-Ruiz F, Jimenez-Espejo FJ, Gallego-Torres D, Nieto-Moreno V, Romero O, Ariztegui D (2011) Impact of climate variability in the western Mediterranean during the last 20,000 years: Oceanic and atmospheric responses. Quaternary Science Reviews 30:2018-2034. doi:10.1016/j.quascirev.2011.05.011
Rohling E, Cooke S (2003) Stable oxygen and carbon isotopes in foraminiferal carbonate shells. In: Sen Gupta B (ed) Modern Foraminifera. Springer Netherlands, pp 239-258
Schefuß E, Kuhlmann H, Mollenhauer G, Prange M, Pätzold J (2011) Forcing of wet phases in southeast Africa over the past 17,000 years. Nature 480:509-512. doi:10.1038/Nature10685
Seltzer GO, Rodbell DT, Baker PA, Fritz SC, Tapia PM, Rowe HD, Dunbar RB (2002) Early warming of tropical South America at the last glacial-interglacial transition. Science 296:1685-1686. doi:10.1126/science.1070136
Shackleton NJ (1967) Oxygen isotope analyses and Pleistocene temperatures re-assessed. Nature 215:15. doi:10.1038/215015a0
Shackleton NJ, Opdyke ND (1973) Oxygen isotope and palaeomagnetic stratigraphy of equatorial Pacific core V28-238: Oxygen isotope temperatures and ice volumes on a 105 year and 106 year scale. Quaternary Research 3:39-55. doi:10.1016/0033-5894(73)90052-5
Somayajulu BLK, Walsh TJ, Radhakrishnamur.C (1975) Magnetic-susceptibility stratigraphy of Pacific Pleistocene sediments. Nature 253:616-617. doi:10.1038/253616a0
Stuut JBW, Kasten S, Lamy F, Hebbeln D (2007) Sources and modes of terrigenous sediment input to the Chilean continental slope. Quaternary International 161:67-76. doi:10.1016/j.quaint.2006.10.041
Thornalley DJR, Elderfield H, McCave IN (2010) Intermediate and deep water paleoceanography of the northern North Atlantic over the past 21,000 years. Paleoceanography 25:Pa1211. doi:10.1029/2009pa001833
Tucker ME (2001) Sedimentary Petrology: An introduction to the origin of sedimentary rocks. 3rd edition, Plackwell Publishing, Malden, Oxford, Carlton, 252 p
von Dobeneck T, Schmieder F (1999) Using rock magnetic proxy reocords for orbital tuning and extended time series analyses into super- and sub-Milankovitch bands. In: Fischer G, Wefer G (eds) Use of proxies in paleoceanography: Examples from the South Atlantic. Springer, Berlin, Heidelberg, pp 601-633
Vroon PZ, Vanbergen MJ, Klaver GJ, White WM (1995) Strontium, neodymium, and lead isotopic and trace-element signatures of the East Indonesian sediments: Provenance and implications for Banda arc magma genesis. Geochimica Et Cosmochimica Acta 59:2573-2598. doi:10.1016/0016-7037(95)00151-4
Waelbroeck C, Labeyrie L, Michel E, Duplessy JC, McManus JF, Lambeck K, Balbon E, Labracherie M (2002) Sea-level and deep water temperature changes derived from benthic foraminifera isotopic records. Quaternary Science Reviews 21:295-305. doi:10.1016/s0277-3791(01)00101-9
Walter HJ, Hegner E, Diekmann B, Kuhn G, van der Loeff MMR (2000) Provenance and transport of terrigenous sediment in the South Atlantic Ocean and their relations to glacial and interglacial cycles: Nd and Sr isotopic evidence. Geochimica Et Cosmochimica Acta 64:3813-3827. doi:10.1016/S0016-7037(00)00476-2
Wefer G, Berger WH, Bijma J, Fischer G (1999) Clues to ocean history: A brief overview of proxies. In: Fischer G, Wefer G (eds) Use of proxies in paleoceanography: Examples from the South Atlantic. Springer, Berlin, Heidelberg, pp 1-68

Westerhold T, Röhl U (2009) High resolution cyclostratigraphy of the early Eocene - new insights into the origin of the Cenozoic cooling trend. Climate of the Past 5:309-327

Zachos JC, Röhl U, Schellenberg SA, Sluijs A, Hodell DA, Kelly DC, Thomas E, Nicolo M, I R, Lourens LJ, McCarren H, Kroon D (2005) Rapid acidification of the ocean during the Paleocene-Eocene thermal maximum. Science 308:1611-1615. doi:10.1126/science.1109004

Zahn R, Winn K, Sarnthein M (1986) Benthic foraminiferal $\delta^{13}C$ and accumulation rates of organic carbon: Uvigerina peregrina group and Cibicidoides wuellerstorfi. Paleoceanography 1:27-42. doi:10.1029/PA001i001p00027

4. Sedimentary architecture of a low accumulation shelf since the Late Pleistocene (NW Iberia)

Hendrik Lantzsch [a], Till J. J. Hanebuth [a], **Vera B. Bender** [a], Sebastian Krastel-Gudegast [a, b]

[a] *MARUM – Center for Marine Environmental Sciences and Faculty of Geosciences, University of Bremen, Klagenfurter Strasse, 28359 Bremen, Germany.*
[b] *Present address: Cluster of Excellence: The Future Ocean, University of Kiel, Leibniz Institute of Marine Sciences (IFM-GEOMAR), Wischhofstrasse 1-3, 24148 Kiel, Germany.*

Marine Geology **259**, 47–58, doi:10.1016/j.margeo.2008.12.008

Marine Geology 259 (2009) 47–58

Contents lists available at ScienceDirect

Marine Geology

journal homepage: www.elsevier.com/locate/margeo

Sedimentary architecture of a low-accumulation shelf since the Late Pleistocene (NW Iberia)

Hendrik Lantzsch *, Till J.J. Hanebuth, Vera B. Bender, Sebastian Krastel [1]

MARUM — Center for Marine Environmental Sciences, and Faculty of Geosciences, University of Bremen, Klagenfurter Strasse, 28359 Bremen, Germany

ARTICLE INFO

Article history:
Received 27 June 2008
Received in revised form 10 December 2008
Accepted 29 December 2008

Keywords:
Late Quaternary
siliciclastic shelves
stratigraphy
Atlantic Ocean
mud belt
sea-level change

ABSTRACT

Continental shelves represent areas of highest economical and ecological importance. Nevertheless, these sedimentary systems remain poorly understood due to a complex interplay of various factors and processes which results in highly individual construction schemes. Previous studies of sedimentary shelf systems have mainly focused on a limited number of cores, retrieved from Holocene fine-grained depocentres. As such, the relation between shelf architecture and sedimentary history remains largely obscure. Here, we present new data from the NW Iberian shelf comprising shallow-seismic profiles, a large number of sediment cores, and an extended set of radiocarbon dates to reveal the Late Quaternary evolution of a low-accumulation shelf system in detail.

On the NW Iberian shelf, three main seismic units are identified. These overly a prominent erosional unconformity on top of the basement. The lowermost Unit 1 is composed of maximal 75-m thick, Late Tertiary to Pleistocene deposits. The youngest sediments of this unit are related to the last glacial sea-level fall. Unit 2 was controlled by the deglacial sea-level rise and shows a maximum thickness of 15 m. Finally, Unit 3 comprises deposits related to the late stage of sea-level rise and the modern sea-level highstand with a thickness of 4 m in mid-shelf position. Two pronounced seismic reflectors separate these main units from each other. Their origin is related to (1) exposure and ravinement processes during lower sea level, and (2) to reworking and re-deposition of coarse sediments during subsequent sea-level rise.

According to the sediment core ground-truthing, sediments of the Late Tertiary to Pleistocene unit predominantly display homogenous fine sands with exceptional occurrences of palaeosols that indicate an ancient exposure surface. Fine sands which were deposited in the run of the last sea-level rise show a time-transgressive retrogradational development. The seismic reflectors, bounding the individual units, appear in the cores as 0.1 to 1-m thick deposits consisting either of shell gravels or siliceous coarse sands with gravels. The modern sea-level highstand stage is characterised by zonal deposition of mud forming a mud belt in mid-shelf position, and sediment starvation on outer shelf zones. Radiocarbon ages indicate that this mud belt was the main depocentre for river-supplied fine material on the NW Iberian shelf at least over the past 5.32 ka BP. The initial onset of this depocentre is proposed to be related to a shift in the balance between rate of sea-level rise and amount of terrigenous sediment supply.

Various other stratigraphical shelf reconstructions reveal analogies in architecture which indicate that timing and shaping of the individual units on low-accumulation shelves is fundamentally controlled by eustatic sea-level changes. Other factors of local importance such as differential elevation of the basement and the presence of morphological barriers formed by rocky outcrops on the seafloor have additionally modifying influence on the sedimentary processes.

1. Introduction

Shelf systems represent a major sink for terrestrial and marine sediments. Nevertheless, the understanding of these environments remains restricted due to the complex interplay of various factors such as changes in sea level, tectonics, morphology and oceanographic conditions. Within this framework, sedimentary processes that control supply, sorting, selective deposition, bypassing, winnowing, and re-mobilization of materials have major influence on the sediment distribution pattern. Tracing the fate of sediments on their paths between land and deep-sea basin helps us to increase the understanding of shelf sediment dynamics in general and provides a better insight into the interaction mechanisms of forcing factors and controlling processes.

During the past decades numerous studies have been carried out regarding the shelf water masses as well as surface sediments off NW Iberia in order to understand the present-day situation (OMEX II; van Weering and McCave, 2002). However, almost no downcore studies

* Corresponding author. Tel.: +49 421 218 65193; fax: +49 421 218 65219.
E-mail address: lantzsch@uni-bremen.de (H. Lantzsch).
[1] Present address: Cluster of Excellence: The Future Ocean, University of Kiel, Leibniz Institute of Marine Sciences (IFM-GEOMAR), Wischhofstr. 1-3, 24148 Kiel, Germany.

0025-3227/$ – see front matter © 2009 Elsevier B.V. All rights reserved.
doi:10.1016/j.margeo.2008.12.008

have been achieved to reveal the Late Quaternary shelf history. For instance, the first four radiocarbon ages from the Galician continental shelf were published by González-Álvarez et al. (2005) and only 14 additional dates were applied by Ferrín (2005), Martins et al. (2007) and Bernárdez et al. (2008). The first major studies concerning the stratigraphy of the NW Iberian shelf were achieved by Rey Salgado (1993) and Ferrín (2005). Nevertheless, their interpretations were mainly restricted to seismic data because core recovery in coarse deposition regimes on low-accumulation shelf systems presents significant challenges. Hence, the majority of shelf studies have focused mainly on muddy depocentres related to the present sea-level highstand, and the Late Quaternary sedimentary evolution remains scarcely known. With consideration of this gap of knowledge, we present new data from the NW Iberian shelf including a grid of shallow-seismic profiles and 18 well-dated sediment cores.

This study (1) reconstructs in a comprehensive manner the spatial and temporal architectural development of a low-accumulation shelf in relation to fluctuations in sea level, (2) describes the resulting depositional pattern, and (3) particularly elucidates the evolution of a major highstand depocentre.

2. Regional settings

2.1. Morphology and geology

The NW Iberian shelf is relatively narrow in the Spanish sector (~30 km), slightly broadening to the north and south with a maximum extension of about 40 km in front of the Minho River mouth (Fig. 1). The shelf break generally occurs in water depths of 160 to 180 m (Dias et al., 2002a). The break is obviously not cut by submarine canyons as is the case for the northern Portuguese continental shelf south of the Cávado River.

Prominent features on the NW Iberian shelf are rocky outcrops on the outer and inner shelf (Fig. 1; Rey Salgado, 1993; Dias et al., 2002a; Oliveira et al., 2002). Outcrops on the outer shelf consist of Mesozoic and Cenozoic rocks. On the inner shelf, rocks are described as plutonic and metamorphic bedrock.

The coastline along the Portuguese and the Spanish sectors shows notable morphological differences. The Spanish coast is comparably rough, characterised by a rocky topography and the four deep Rías Baixas which represent Tertiary river valleys, drowned during the last deglacial sea-level rise (Rey Salgado, 1993; Oliveira et al., 2002). In contrast, the Portuguese coastline in the south of the study area is smoother and characterised by the main estuaries of the Minho, Lima and Cávado River (Fig. 1). The large Douro River is situated 40 km southward of the study area.

2.2. Oceanography and sea-level history

The region of the NW Iberian shelf is characterised by strong seasonal variations in the water column and shows considerable changes in wind regime and oceanography between the winter and summer seasons (Fiuza et al., 1982; Drago et al., 1998). Several authors (Drago et al., 1998; Dias et al., 2002b; Vitorino et al., 2002) pointed out

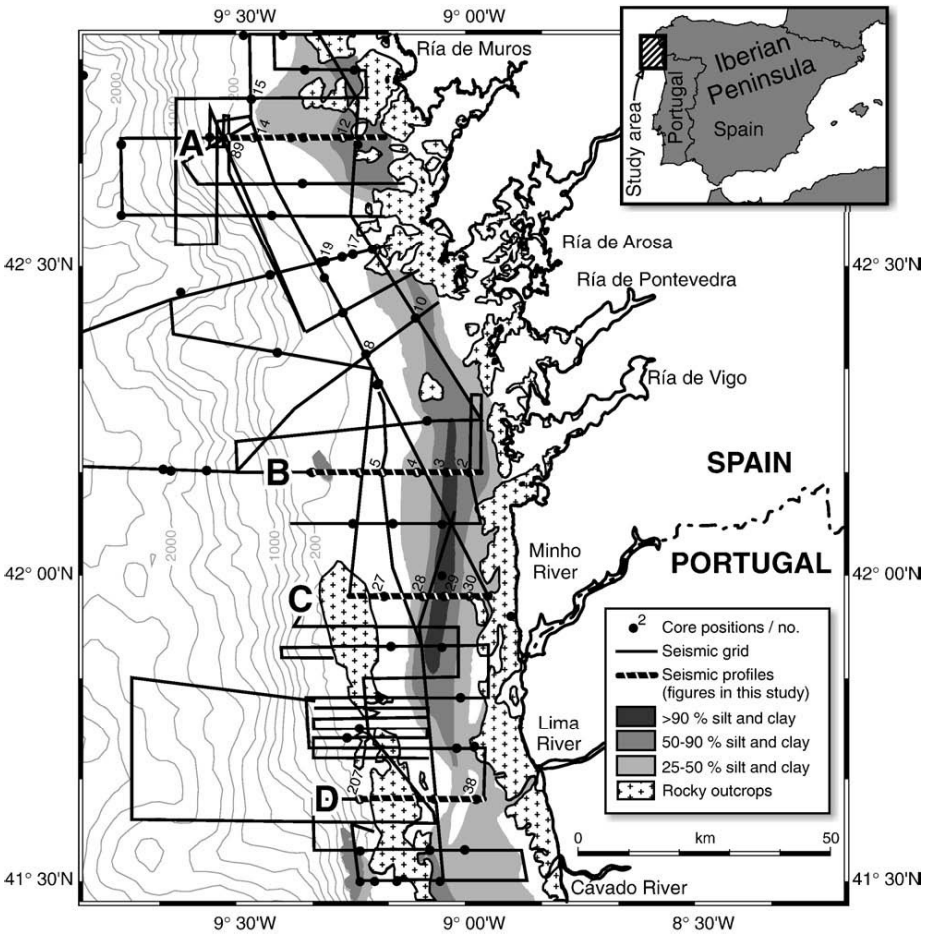

Fig. 1. Map of the study area, core positions and seismic profiles. Surface geology after Dias et al. (2002a). The Galicia Mud Belt is displayed in grey. Core positions of cruises P342 and P366 are marked by black dots. Cores used in this study are labelled in short form with e.g. 11002-3 and 11038-2 being positions 2 and 38 (P342), and 13089-2 and 13207-3 being positions 89 and 207 (P366). Characters A to D represent seismic profiles shown in Figs. 2, 3 and 5.

Table 1
List of the *GALIOMAR* and GALIOMAR II sediment vibrocores of this study

Core no. (GeoB)	Latitude (N)	Longitude (W)	Water depth (m)	Recovery (m)
11002-3	42°10.00	8°59.24	111	4.34
11003-3	42°10.00	9°02.24	129	4.54
11004-2	42°10.00	9°06.17	141	3.78
11005-2	42°10.00	9°10.50	161	3.21
11008-2	42°21.29	9°13.00	157	3.77
11010-2	42°25.00	9°06.28	119	4.10
11012-2	42°42.29	9°16.00	119	4.28
11014-2	42°42.29	9°27.39	153	4.50
11015-2	42°46.11	9°27.58	159	4.94
11017-2	42°31.10	9°14.40	120	4.88
11019-2	42°30.28	9°18.16	149	4.92
11027-2	41°57.59	9°10.34	136	4.54
11028-2	41°57.59	9°05.29	127	4.59
11029-2	41°57.59	9°02.42	114	4.88
11030-2	41°58.00	8°59.24	94	4.60
11038-2	41°38.03	8°58.27	78	4.88
13089-2	42°42.48	9°31.00	190	4.90
130207-3	41°38.01	9°13.70	146	4.94

that the highly energetic regime and prevailing southerly winds during winter season result in (1) a poleward directed current on the mid-shelf, (2) a shelf-wide downwelling cell, and (3) intensified river runoff due to both increased overall precipitation and episodic river floods after storms. These conditions have been suggested to essentially control the modern sediment distribution on the shelf. In contrast, prevailing northerly winds in summer cause an equatorward directed along-shelf current and low-energy conditions, and favour temporal upwelling. These conditions are assumed to be of minor influence on the sedimentation pattern.

For the Late Quaternary time interval, the only available regional sea-level curve for the NW Iberian shelf was constructed by Dias (1985; later in Dias et al., 2000). However, this curve covering the past 20 ka (and frequently cited in the regional literature) does not fulfill the modern criteria of a sea-level curve. The reason is that pioneer-reconstructions from another continent from the 1960s were combined with undated morphological features of the NW Iberian shelf and were supported by only two radiocarbon dates. Therefore, we follow instead the latest eustatic sea-level reconstruction of Peltier and Fairbanks (2006) for a sound interpretation although we are aware that regional effects could have modified this global signal.

2.3. Sediment input, transport and deposition

The fluvial sediment supply to the NW Iberian shelf has been calculated to be approximately $2.25 \cdot 10^6$ t a^{-1} (Oliveira et al., 1982). The Douro River alone is assumed to contribute between 79 and 87% of this supply and is, therefore, the main source of fine sediments (Araújo et al., 2002; Dias et al., 2002a,b). In contrast, the Rías Baixas seem to play a minor role and mostly act as sediment traps (Rey Salgado, 1993).

Although the NW Iberian shelf is generally characterised by a sand cover, well defined areas of mud deposition are developed (Oliveira et al., 2002). Fine-grained fluviogenic sediments are frequently re-suspended by winter storms and transported to the north by the poleward flowing bottom current (Dias et al., 2000, 2002a). This input of fine sediments leads to the development of two confined muddy deposits in 110 to 120 m water depth on the NW Iberian shelf (Dias et al., 2002b).

Of these, the Galicia Mud Patch is a central feature in the study area (Fig. 1) whereas the Douro Mud Patch is situated further southward. Modern-day accumulation rates in these muddy areas range between 0.05 and 0.40 cm ka^{-1}. These rates are comparable to those of the mud

Table 2
Radiocarbon measurements and age calibration

Lab no.	Core no. (GeoB)	Depth in core (cm)	Material	^{14}C ages [a BP]	1σ calibrated [cal a BP][a]	Intercept [cal ka BP]	Stratigraphic position
KIA 33665	11002-3	250	bF	2715±35	2342–2455	2.40±0.06	U3
KIA 33664	11002-3	435	bF, bv pieces, gp	4955±45	5249–5388	5.32±0.07	U3
Poz-24670	11003-3	240	bF	7840±50	8259–8371	8.32±0.06	U3
Poz-22923	11003-3	360	bF	10,770±50	12,101–12,321	12.21±0.11	U3
Poz-24771	11003-3	399	bF	13,080±70	14,814–15,107	14.96±0.15	U2
KIA 33668	11004-2	277	bv piece	14,660±100	16,793–17,297	17.05±0.25	R1
Poz-22944	11005-2	250	*E. crispum*	18,470±100	21,160–21,689	21.42±0.26	R1
Poz-22945	11005-2	300	bF, bv pieces	46,000±3000	48,878–54,952[b]	51.91±3.04	U1
Poz-22946	11010-2	377	*E. crispum*	15,540±80	18,220–18,690	18.46±0.24	R1
Poz-22925	11012-2	100	bF	3995±35	3949–4068	4.01±0.06	U3
Poz-22948	11012-2	320	*E. crispum*	14,820±80	17,073–17,554	17.31±0.24	R1
KIA 33675	11014-2	441	bF, bv pieces	>42,580	uncalibrated	>42.58	U1
KIA 33692	11015-2	430	bF, bv pieces	30,710±670	35,016–36,496[b]	35.76±0.74	U1
KIA 33781	11015-2	448	Plant debris, char coal	49,140±2930	52,154–57,976[b]	55.07±2.91	U1
KIA 33683	11017-2	247	*E. crispum*	28,520±480	32,787–33,860[b]	33.32±0.54	U1
KIA 33684	11017-2	417	*E. crispum*	>42,090	uncalibrated	>42.09	U1
KIA 33685	11017-2	486	bF	>44,990	uncalibrated	>44.99	U1
KIA 33699	11027-2	49	*E. crispum*	17,040±130	19,567–19,900	19.74±0.17	U2
KIA 33700	11027-2	454	*E. crispum*	19,120±160	22,141–22,419	22.28±0.14	U2
Poz-21470	11028-2	140	bF	2555±30	2184–2290	2.24±0.05	U3
Poz-21471	11028-2	416	*E. crispum*	16,780±80	19,444–19,756	19.60±0.16	U2
Poz-22950	11028-2	429	*E. crispum*	17,310±190	19,862–20,243	20.05±0.19	R1
KIA 33687	11029-2	103	bF	850±30	458–503	0.48±0.02	U3
Poz-24772	11029-2	360	bF	2910±35	2669–2737	2.70±0.03	U3
KIA 33689	11029-2	488	Echinoderm pieces	12,740±80	14,082–14,475	14.28±0.20	U2
Poz-21472	11030-2	220	bF	2940±35	2693–2749	2.72±0.03	U3
Poz-21473	11030-2	460	bF, bv	10,740±50	12,035–12,255	12.15±0.11	U2
Poz-22951	11038-2	120	bF	3165±35	2888–3013	2.95±0.06	U3
Poz-22952	11038-2	460	bF, gp	16,880±90	19,501–19,793	19.65±0.15	U2
Poz-26862	13089-2	489	*E. crispum*	17,850±100	20,414–20,742	20.58±0.16	U2
Poz-26864	130207-3	430	bF	18,280±110	20,900–21,338	21.12±0.22	U2

[a] For reservoir correction, the conventional age of 400 years is applied using CALIB 5.0.1. (Stuiver et al., 1998).
[b] Reservoir correction based on the function of Bard et al. (1998).
bF = benthic foraminifers; *E. crispum* = *Elphidium crispum* (monospecific sample); bv = bivalve; gp = gastropod.

centres in the Bay of Biscay and on the Tagus Shelf (Jouanneau et al., 2002). Due to these relatively low accumulation rates and shelf-wide sand draping we consider the NW Iberian shelf as being controlled by a low-accumulation sedimentation regime.

The surface distribution of the Galicia Mud Patch was compiled by Dias et al. (2002a). Fig. 1 displays the present-day extent of this depocentre, defined by a mud content of more than 25%. Here, we introduce the term "Galicia Mud Belt" instead of "Galicia Mud Patch" due to its elongated shape running contour-parallel in mid-shelf position.

3. Materials and methods

3.1. Geophysical methods

Seismic data were collected by means of a Boomer and a high-resolution multichannel system running simultaneously during the *GALIOMAR* (Galician Ocean Margin) cruise in 2006 onboard the German research vessel *Poseidon* (P342). In total, about 1900 km of seismic lines were collected. The frequency band of the Boomer was between 500 Hz and 10 kHz with a main frequency of around 2–3 kHz. The Boomer was shot every second with a two second break every six shots for firing an airgun. The multichannel seismic data were obtained using a Mini-Generator–Injector-Airgun (main frequency ~300 Hz) and a 100-m long 16 channel streamer with a group distance of 6.25 m.

The Boomer data are used in this study to establish the Late Quaternary shelf stratigraphy. Where the penetration depth of the shallow-acoustic Boomer system was insufficient to get the exact position of the basement, the measurements of the high-resolution multichannel system were integrated.

3.2. Coring devices

In total, 66 sediment cores (up to 5-m long) were recovered on the NW Iberian shelf and at the continental slope during the *GALIOMAR* cruise (P342) in 2006 and GALIOMAR II expedition in 2008 (part of PERGAMOM cruise P366; Fig. 1 and Table 1). A vibrocorer was used down

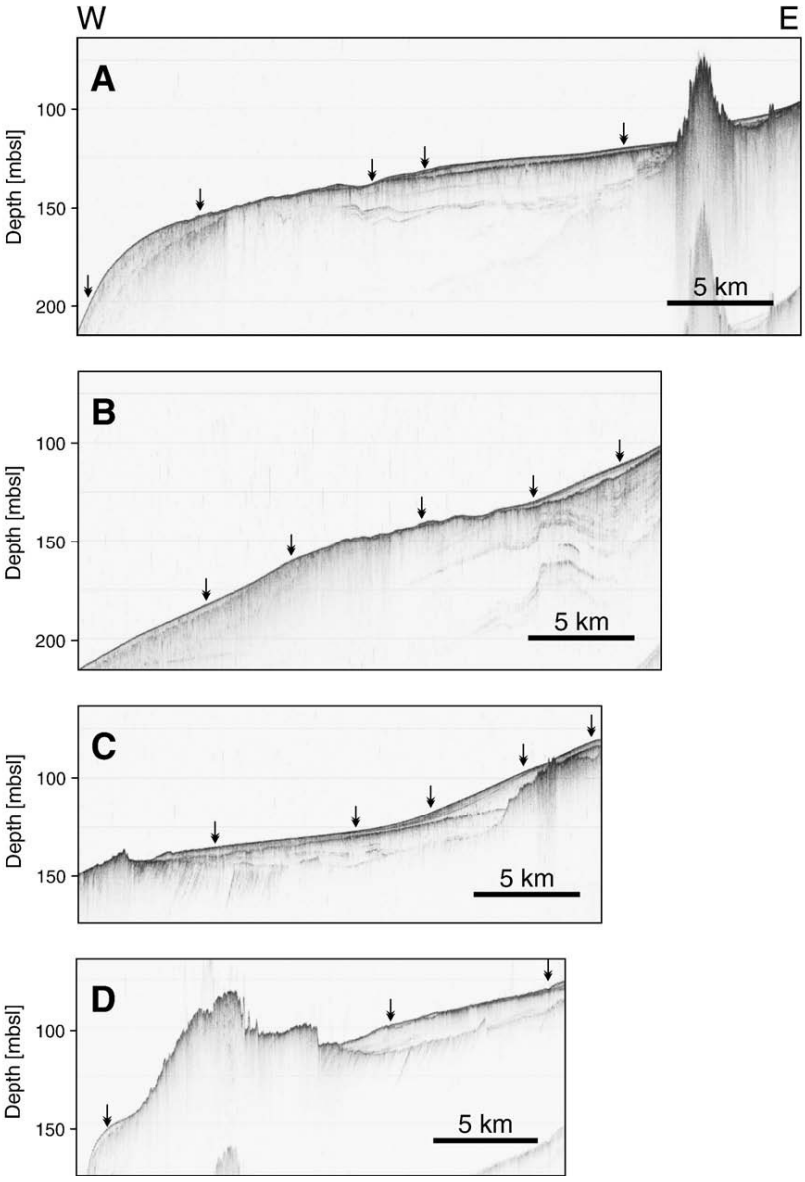

Fig. 2. Boomer profiles of the respective seismic Profiles A to D shown in Fig. 1 and interpreted shelf architecture. B: basement; EU: erosional unconformity; U1, U2, U3: main seismic units; R1, R2: seismic reflectors separating the units. Black arrows indicate sediment core positions. Boxes in the interpretation display magnifications shown in Fig. 3. Depth on *y*-axis is given in metres below modern sea level (mbsl).

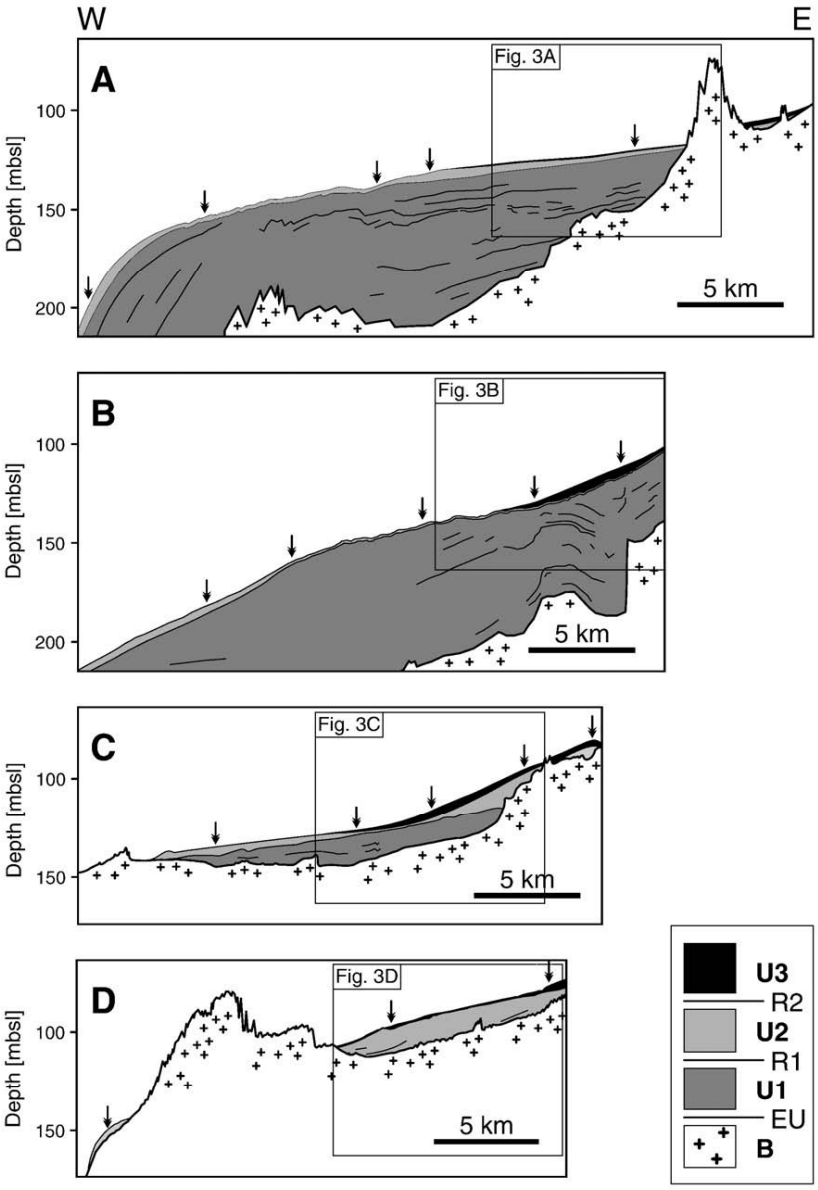

Fig. 2 (*continued*).

to 230 m water depth in places where the sediment was too coarse to retrieve material by gravity coring. Giant box cores were taken at every core location to sample the modern surface. In this study, the sedimentary reconstruction of the shelf architecture is based on the analysis of 18 vibrocores, which represent the range of sediments on the NW Iberian shelf.

3.3. Analyses in the lab

After detailed lithological description and photography, samples were taken at 20-cm intervals. These samples were split into fine and coarse fractions (<63 and >63 μm) by wet sieving. Afterwards, the coarse fraction was sonic-sifted into the grain-size subfractions 63–125 μm, 125–250 μm, 250–500 μm, 500–1000 μm and >1000 μm to obtain the grain-size distribution of the coarse fraction. The classification scheme of Blair and McPherson (1999) was used to determine the different grain-size classes from clay to gravel and the data obtained by grain-size measurement were used to corroborate the visual core description.

The selection of shelf material for radiocarbon dating is a complex issue. Age reversals might occur due to re-deposition of older material. In order to avoid age biasing, only delicate material of fresh preservation was carefully handpicked. Wherever applicable, monospecific samples were selected. However, due to the lack of such a material in some samples, a selection of benthic foraminifers and mollusc shells was necessary. Nevertheless, we found that also such material was of fresh condition and reliable for measurement. As a result, 31 radiocarbon dates on 16 analysed cores are displayed in this study (Table 2). The measurement was carried out by the Leibniz Laboratory in Kiel (Germany), and the Poznań Radiocarbon Laboratory (Poland). All radiocarbon dates are given in calibrated kiloyears before present (ka BP). They are corrected for a standard marine reservoir effect of 400 years and converted into 1-sigma calibrated ages using the program Calib 5.0.1 (Stuiver et al., 1998). Dates with a conventional age >22 ka are calibrated based on the function of Bard et al. (1998). The stratigraphic correlation was applied by combining the interpreted Boomer profiles, lithological facies analysis, and radiocarbon dating.

4. Results

4.1. Shelf architecture

Three main seismic units overly the basement (B) and define the architecture of the NW Iberian shelf (Fig. 2). The basement itself is characterised by a strong tectonic influence (Dias et al., 2002a; Muñoz et al., 2003) as can, for instance, be seen in the western part of Fig. 2C where tilted rocks are exposed on the outer shelf. These rocky outcrops are only present in the southern part of the study area (Fig. 2C, D). In contrast, outcrops on the inner shelf extend parallel to the coastline and are, for example, observed in the eastern parts of the Boomer Profiles A and C (Fig. 2A, C).

A major erosional unconformity surface (EU) separates the tilted basement from the overlying sediments of Units 1 to 3. The lowermost seismic Unit 1 (U1) is characterised by a transparent to semi-transparent seismic facies in the Boomer profiles with minor internal reflections showing an onlap pattern (Fig. 2A, B, C). These internal reflectors are often deformed by folding and follow elevations of tilted basement blocks (see eastern part of Fig. 2B). They appear frequently as local features in the Boomer profiles but also extend, in some cases, across wide parts of the shelf (Fig. 2A). However, the multichannel seismic data suggest that this variation in extension might be due to depth limitations of the Boomer system. The thickness of U1 is highly variable with a maximum thickness of about 75 m in the northernmost part (Fig. 2A) decreasing to the south and being absent south of the Minho River mouth (Fig. 2D).

Seismic Unit 2 (U2) is separated from U1 by a continuous high-amplitude reflector (R1), which can be traced across major parts of the shelf (Fig. 2A, B, C). With increasing water depths, the amplitude of R1 becomes weaker (western part of Fig. 2A, B). U2 is mainly transparent with only scarce internal reflection (Fig. 2D). A maximum thickness of 15 m is observed in the southernmost part of the study area (Fig. 2D). Northern parts of the shelf are characterised by a decreasing sediment thickness, usually to less than 5 m (Fig. 2A, B). However, U2 deposits are not restricted to the mid-shelf but up to 4-m thick deposits are found either beyond (Fig. 2A, B) or directly at the shelf break (Fig. 2D).

The uppermost unit, seismic Unit 3 (U3), is separated from U2 by a weak but continuous reflector (R2; Fig. 2). U3 shows a maximum thickness of about 4 m between the Minho River mouth and the Rías Baixas, representing the central part of this unit (Figs. 1 and 2B, C). A wedge-shaped appearance of U3 and distinct internal stratification are also restricted to this area of maximum thickness (Fig. 2B, C). In contrast, U3 forms a 1-m thin sheet in the northern part of the study area and no internal stratification can be observed within the resolution of the Boomer data, here (Fig. 2A). The latter is also the case for most parts of the southern study area, where the sheet-like U3 reaches a maximum thickness of approximately 3 m (Fig. 2D). Furthermore, U3 displays a gradual thinning in offshore as well as onshore direction. This is most obviously displayed by the lateral pinching out in Profiles B and C, but can also be detected in Profile A (Fig. 2A). The exception to this pattern is visible in the easternmost part of Profile C where sediments between rocky outcrops form an up to 3-m thick sediment

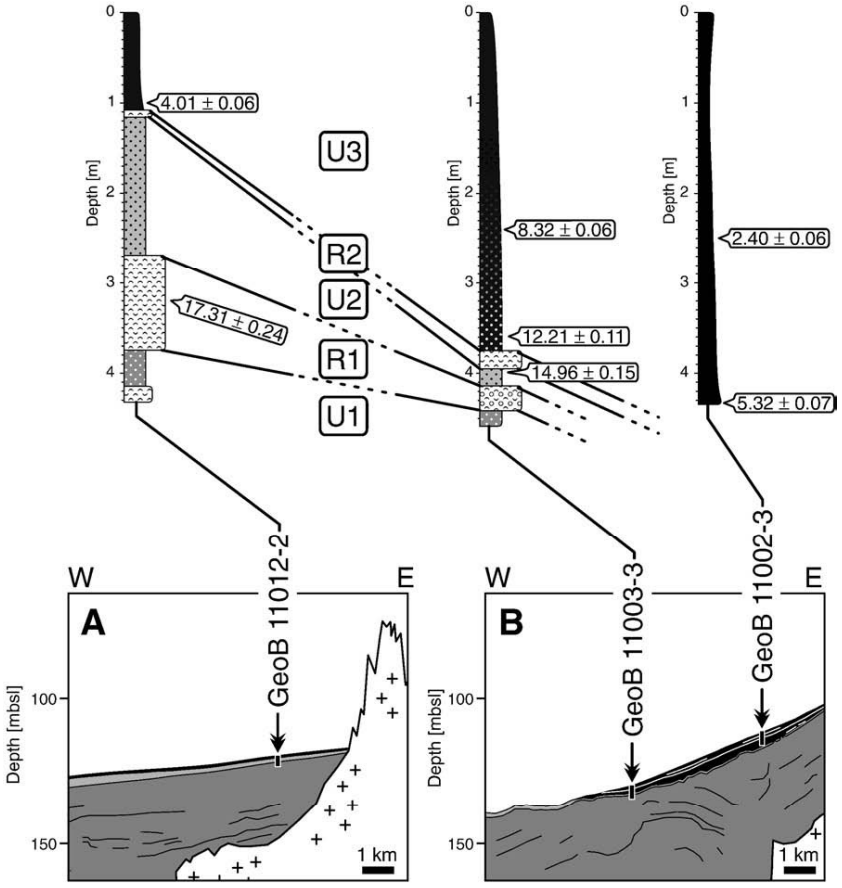

Fig. 3. Interpretations of the Boomer Profiles A to D and respective columns of sediment cores. Boxes display magnifications marked in Fig. 2. Core lithology, grain size and radiocarbon ages are shown in core columns above. All seismic units of the Boomer profiles are found in the sediment cores. U1 and U2 are mainly composed of fine sands and U3 is characterised by mud to muddy fine sands. Reflectors R1 and R2 extend across the shelf as gravel layers. Boomer interpretation, core lithology and radiocarbon measurements enable the correlation between single cores. Position of Profiles A–D is shown in Fig. 1.

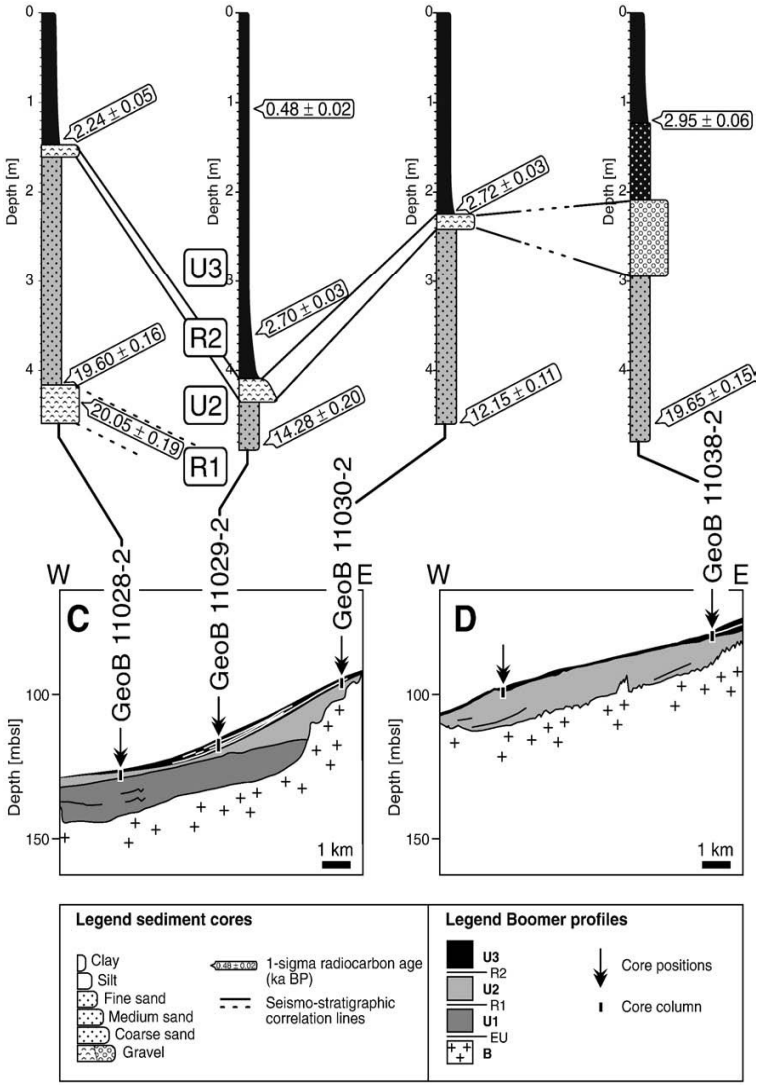

Fig. 3 (*continued*).

body on the inner shelf (Fig. 2C), and in Profile A where a 2-m thick layer deposited next to rocky outcrops in front of the Ría de Muros (Fig. 2A).

4.2. Sedimentary characteristics of the stratigraphical units

Sediment cores were retrieved at selected positions along the Boomer profiles to get insight into the sedimentary characteristics of these individual seismic units (Table 1). The sediments are mainly composed of either homogenous fine sands or homogenous mud, and show only subordinate variations in grain size (Fig. 3). These monotonous deposits are usually several metres thick. However, they are intersected by 0.1 to 1-m thick, coarse-sandy to gravelly beds which are composed of either shell fragments or siliceous gravel. Those drastic grain-size changes are observed in almost all of the cores (Fig. 3). These coarse beds are mirrored in the Boomer profiles by the above mentioned strong reflectors and can be used as stratigraphical marker horizons across the whole shelf. Consequently, the correlation between individual cores is done by combining the sedimentary facies characteristics and the stratigraphical interpretation of the Boomer profiles (Fig. 3). The results are then corroborated by radiocarbon age control (chapter 4.3).

Sediments from all three units overlying the basement were retrieved by coring. U1 is present in a number of cores, for instance in the lower part of Core 11012-2 in Profile A and of Core 11003-3 in Profile B (Fig. 3A, B). The sediments of U1 are mainly composed of grey homogenous fine sands (Fig. 4A) consisting of a mixture of siliciclastic and biogenous material of marine and terrigenous origin. Nevertheless, lateral variations of this facies are found, as documented, for instance, in the lower parts of Cores 11005-2 and 11008-2 (positions 5 and 8 in Fig. 1), where the homogenous fine sands of U1 are dominated by glauconite (Fig. 4B). Another prominent feature of U1 is rigid, yellowish brown to grey sediment with intercalations of clay and mica-rich silt and abundant organic material. These deposits occur in water depths lower than 150 m and a thickness of up to 90 cm was recovered at the bottom of Cores 11015-2 and 11019-2 (15 and 19 in Fig. 1; Fig. 4C).

The bed associated with R1, separating U1 and U2, was retrieved in the lower parts of the selected Cores 11012-2, 11003-3 and 11028-2 (Fig. 3A, B, C). These sediments consist mainly of coarse sands to gravel composed of shell fragments and complete valves (Fig. 4D). Bivalves are very common constituents. To a minor degree, also gastropods, scaphopods, serpulids are present, in complete preservation or fragmented.

U2 is present in all sediment cores of the profiles displayed in Fig. 3 (except for Core 11002-3 in Profile B), and is characterised by homogenous

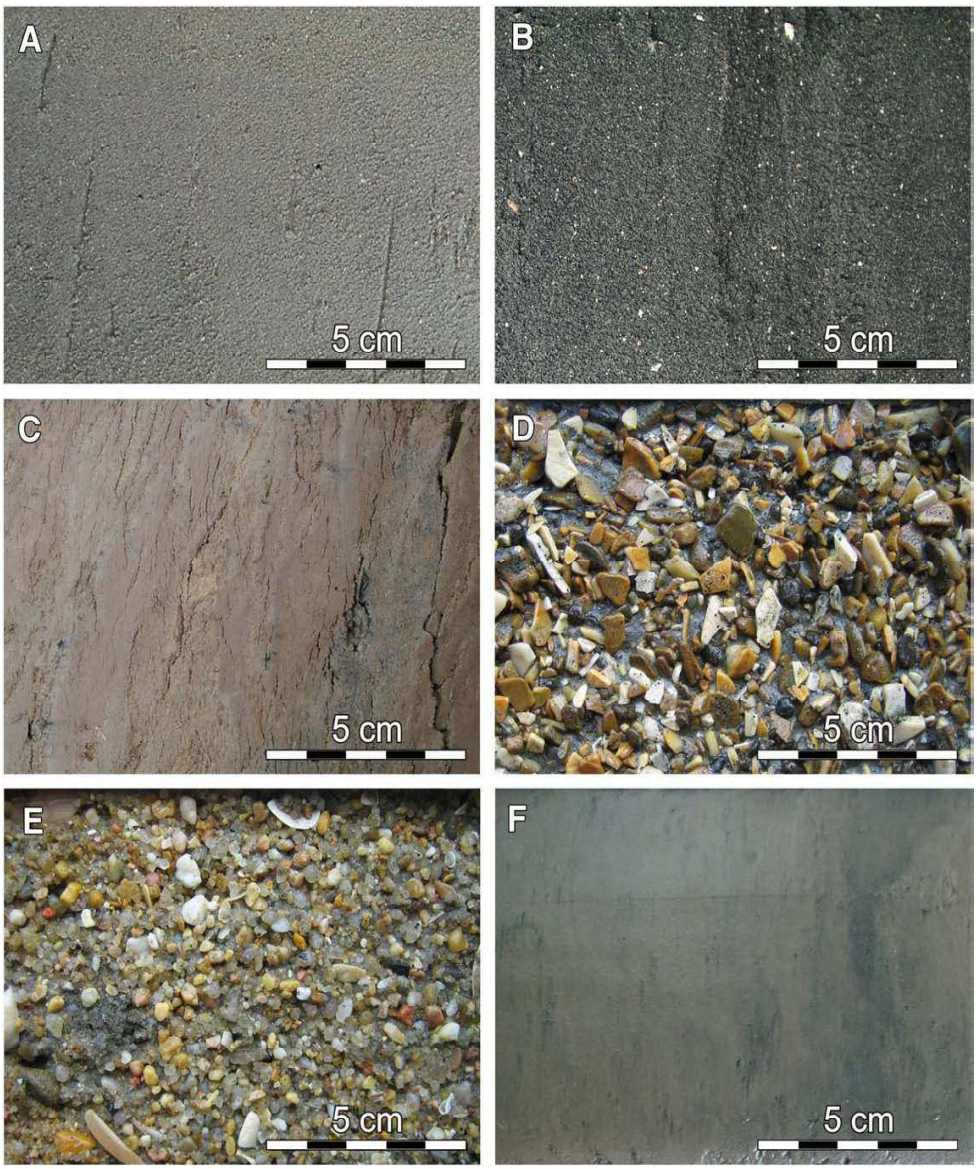

Fig. 4. Core images representing the variety of sediments deposited on the NW Iberian shelf. (A) Homogenous fine sand (exemplarily shown by Core 11027-2; 432–444 cm; U2; interpreted as regressive facies of U1 or transgressive deposits of U2); (B) glauconite-rich fine sand (11008-2; 230–242 cm; U1; outer shelf palimpsest facies); (C) overconsolidated clay (11015-2; 449–461 cm; U1; palaeosol facies); (D) shell fragment gravel (11028-2; 435–447 cm; R1; lag deposit); (E) siliceous gravel (11038-2; 279–291 cm; R2; shoreface deposit); and (F) mud (11029-2; 181–193 cm; U3; mud-belt facies). Core tops are directed to the left, core bottoms to the right.

fine sands that are comparable to the fine sands of U1 in terms of grain size and composition. Grey homogenous sands occur as well as dark greenish fine sands, which are dominated by glauconite (Fig. 4A, B).

A prominent gravel layer separates U2 and U3. These coarse deposits cause the seismic Reflector R2. Again, all sediment cores in the profiles displayed (Fig. 3; except for Core 11002-3) show this abrupt recurrence of a gravel bed, which again consists of shell fragments (Fig. 4D). Quartz is generally a minor component in this bed but can be the dominant constituent. This is the case in Core 11038-2 in the westernmost part of Profile D (Fig. 3D) in which coarse-grained, sub-angular to sub-rounded quartz makes up more than 70% of the bulk sediment (Fig. 4E).

Sediments of U3 are overlying the deposits of R2 in almost all displayed cores (Fig. 3). Only Core 11002-3 is entirely composed of U3 sediments (Fig. 3B). Generally, U3 can be subdivided into two sedimentary units, a lower unit composed of fine sands with less than 10% of fine material ($U3_s$) and an upper unit characterised by a mud content of more than 25% ($U3_m$). The fine-sandy sediments of $U3_s$ were observed in Cores 11003-3 and 11038-2 (Fig. 3B, D), whereas the muddy deposits of $U3_m$ are present in all displayed cores of Fig. 3. Three modes of the initial onset of $U3_m$ were observed: (1) a continuous fining upward from $U3_s$ towards $U3_m$ in Core 11003-3 (Fig. 3B), (2) the deposition of mud above an erosional unconformity, separating $U3_s$ and $U3_m$ in Core 11038-2 (Fig. 3D), and (3) an absence of $U3_s$ and a deposition of $U3_m$ above the coarse sediments of R2 (e.g. Fig. 3C). The spatial distribution of $U3_m$ deposits in the Boomer profiles correlates well with the present-day mud belt as mapped by Dias et al. (2002a; Fig. 1). Hence, sediments of $U3_m$ represent the mud-belt body in depth.

The thickness of this Galicia Mud Belt is highly variable. As demonstrated in Fig. 3, variations in mud-belt thickness are not only visualised in the Boomer profiles but are recorded in the cores. In Profile C (Fig. 3C), for instance, Core 11029-2 was retrieved from the central part of the mud belt and shows an increased thickness of about 4 m, whereas Cores 11028-2 and 11030-2 document marginal

parts of the mud belt, which is described by a decreasing thickness. Moreover, mud-belt sediments show a clear fining-upward trend in lower parts. Additionally, the Galicia Mud Belt shows a slight coarsening to silt or muddy fine sand in offshore as well as onshore directions. These trends are shown in Profile C (Fig. 3C). Core 11029-2 shows muddy sediments and the marginal Cores 11028-2 and 11030-2 consist mainly of silt to muddy fine sands. This coarsening also occurs towards the north and south of the main mud-belt centre, which is displayed by the occurrence of muddy fine sands in Cores 11012-2 and 11038-2 (Fig. 3A, D).

4.3. Age determination of the units

The uppermost part of U1 was dated in seven sediment cores (Table 2). Of these, five radiocarbon ages are older than 42 ka BP, i.e. beyond the measurement limitations of the radiocarbon method (Table 2). The youngest ages of U1 are 35.76±0.74 ka BP and 33.32±0.54 ka BP (Table 2).

The bed representing reflector R1, separating U1 and U2, was retrieved in 15 cores. Within this reflector, five radiocarbon samples were taken and show ages between 21.42±0.26 ka BP and 17.05±0.25 ka BP (Table 2).

U2 was dated in various cores of Profiles C and D (Fig. 3C, D). The radiocarbon ages measured display a range from 22.28±0.14 ka BP to 12.15±0.11 ka BP (Table 2). Thereof, the oldest radiocarbon ages of U2 were measured in outer-shelf cores (positions 27, 89 and 207 in Fig. 1) and the youngest ages were observed in mid-shelf position (3 and 29 in Fig. 1).

In contrast, the bed representing reflector R2, bordering U2 and U3, was not directly dated due to absence of freshly preserved carbonate material. Nevertheless, two radiocarbon dates, taken below and above R2 in Core 11003-3 (Fig. 3B), indicate that the bed formation at this core position must have taken place within the time interval after 14.96±0.15 ka BP and prior to 12.21±0.11 ka BP (Table 2).

The oldest age of U3 was measured within the $U3_s$ sediments of Core 11003-3 (12.21±0.11 ka BP; Fig. 3B) whereas the youngest age in this lower, sandy part of U3 dates at 8.32±0.06 ka BP. A date in Core 11002-3 shows that the transition from the fine-sandy $U3_s$ sediments to deposits of the Galicia Mud Belt ($U3_m$) already took place prior to 5.32±0.07 ka BP (Fig. 3B). Moreover, seven further measurements on the Galicia Mud Belt show a range between 4.01±0.06 ka BP and 0.48±0.02 ka BP (Table 2).

5. Discussion

There are few indications for the age of the basement (B) and for sediments of U1 in literature. Following the work of Rey Salgado (1993) and Dias et al. (2002a) the basement is of Precambrian to Cenozoic age.

U1 overlies the basement over wide parts of the study area. Succeeding internal reflectors within U1 show mainly a progradational to aggradational pattern. The timing and origin of these internal reflectors, however, remains speculative and depends on the stratigraphic interpretation of U1. According to the interpretation of Muñoz et al. (2003) sediments of U1 comprise Late Tertiary to Late Pleistocene sediments and were deformed by mainly normal faulting during the Neogene Betic Orogeny. Ferrín (2005), in contrast, suggested that U1 is composed of Upper Cretaceous to Upper Pliocene deposits. Hence, internal reflectors of U1 are most probably related to prominent sedimentary changes during Tertiary and Pleistocene times. However, these interpretations are almost exclusively based on seismic data and remain speculative. Radiocarbon ages of our study show that the youngest sediments of U1 have been deposited during the last glacial sea-level fall prior to the sea-level lowstand of the Last Glacial Maximum (LGM).

An ancient exposure surface within U1 is indicated by the occurrence of very stiff, yellowish brown to grey intercalations of clay and mica-rich silt in water depths of 150 to 160 m. Following the definition of Rohrlich et al. (1995) these deposits can be considered as overconsolidated and are interpreted as palaeosols. Two alternatives of exposure are conceivable: (1) these soils have developed during the LGM sea-level lowstand, when the eustatic sea-level was located at around 130 m below modern sea level (mbsl; Peltier and Fairbanks, 2006). Consequently, the position of this exposure surface would require an additional local shelf subsidence of about 30 m over the past 20 ka. (2) Alternatively, these palaeosols have originated during low sea levels in earlier Pleistocene times.

Generally, the local thickness of U1 seems to be largely controlled by differential elevation of the basement due to tectonic displacement, and erosion related to sea-level fluctuations. For instance, U1 is absent in the southern part of the study area (Fig. 2D). The local elevation of the basement here might have led to enhanced erosion during succeeding sea-level lowstands. In contrast, the northern part of the study area displays up to 75-m thick deposits of U1 (Fig. 2A, B). The deeper-situated basement surface in this region, thus, has probably caused the preservation of such U1 sediments.

Reflector R1, separating U1 from U2, with ages between 21 and 17 ka BP, is related to the LGM sea-level lowstand and earliest deglacial sea-level rise, respectively (Fig. 5A). The lower boundary of this bed represents, in fact, an erosional surface which probably originated during the last sea-level fall between 33 ka BP, the youngest age of U1, and the LGM. The deposition of coarse R1 sediments was then related to the LGM sea-level lowstand as well as to an early sea-level rise. These data show that the last sea-level lowstand was not only characterised by exposure surfaces and suggested lowstand deposits beyond the shelf break (as stated by Ferrín, 2005). Rather, this interval is documented by sedimentation on the shelf itself. Taking into account the significant deposition of coarse material, as observed in our records, the simplified interpretation as an erosional surface alone, as described by Rodrigues et al. (1991) and Ferrín (2005), is no longer suitable. Furthermore, the age range of R1 between 21 and 17 ka BP indicates that this reflector does not represent a single-event bed but that its formation as lag deposit was largely controlled by a long-lasting development. In this context, sea level and shelf bathymetry have strongly influenced the position of the particular shoreline, which must be considered as the main source of such coarse and shell-rich sediments. Additionally, the re-deposition of coarse material was most probably enhanced by the stronger impact of wave activity in this shallow-water zone.

Other examples of such reflectors, separating deposits of the last sea-level rise from older sediments, have been reported, for instance, from the Mersin Bay shelf, (NE Mediterranean Sea; Ergin et al., 1992; Okyar et al., 2005), the New Jersey continental shelf (Duncan et al., 2000) and the Californian shelf (Slater et al., 2002; Crockett and Nittrouer, 2004; Grossman et al., 2006). These reflectors are usually considered as indicating either a pre-Holocene erosional surface (Ergin et al., 1992; Slater et al., 2002) or a "Late Pleistocene–Early Holocene erosional–depositional surface" (Okyar et al., 2005; Grossman et al., 2006). In contrast, Duncan et al. (2000) suggested for the New Jersey continental shelf that this prominent reflector represents the ravinement surface of the Late Pleistocene regression (120 to 25 ka BP). Our radiocarbon dates of R1 show that the formation of the R1 bed in association with this phase of sea-level fall can be excluded on the NW Iberian shelf. The occurrence of reflectors comparable to R1 on various other shelves might suggest a similar mechanism of formation. It is, however, unlikely that all shelves have experienced changes in oceanography, tectonics, morphology and sedimentary processes in the same way. Therefore, eustatic sea-level fluctuations would be the force of equivalent global effect on the buildup of these extensive reflectors on the different shelves.

The timing of the emplacement of U2 is well documented by radiocarbon dating indicating that the initial onset of this unit had already taken place during the LGM, right after the formation of R1 (Fig. 3C; Table 2). Other radiocarbon ages measured in U2 indicate that

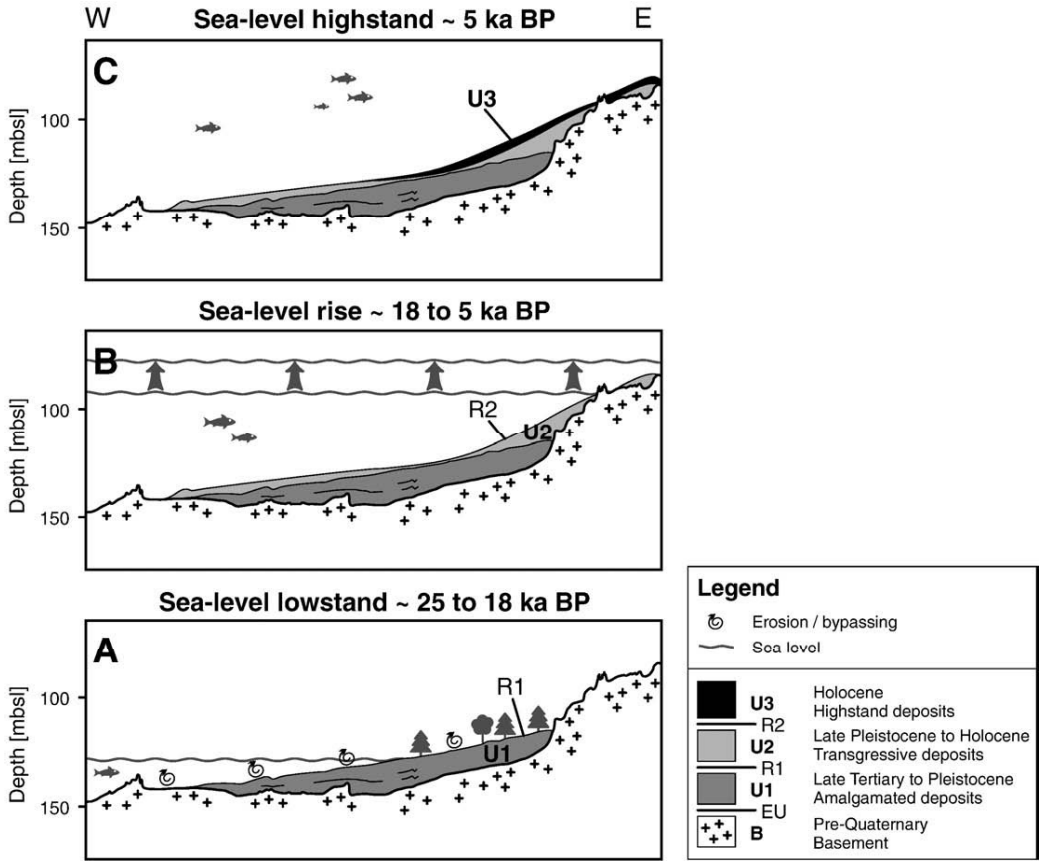

Fig. 5. Scheme of the Late Pleistocene–Holocene shelf evolution related to the superordinated sea-level history along Profile C. The development of seismic reflector R1 during the last sea-level lowstand and early sea-level rise is followed by the deposition of U2 sediments and the formation of reflector R2. (U3) represents the main depocentre during the modern sea-level highstand.

this unit was mainly built up during the time of deglacial sea-level rise (Figs. 3C; 5B). Consequently, a time-transgressive trend can be observed in Profile C with the oldest age occurring on the outer shelf in a water depth of 127 mbsl (19 ka BP) getting younger in landward direction to 14 ka BP in 114 mbsl and to 12 ka BP in 94 mbsl in mid-shelf position (Fig. 3C). This landward shift implies that the development of U2 was largely controlled by the respective position of the sea level (Fig. 5B). However, the irregular thickness distribution of U2 shows that the sea level was not the exclusive factor controlling the architectural development of the sedimentary shelf system. Instead, the increasing thickness of U2 in the southern part of the study area (Fig. 2D) is probably related either to shelf morphology or to sediment input. The pronounced shape of rocky outcrops on the outer shelf has most likely sheltered mid-shelf deposits against stronger wave and current impacts during sea-level rise. An alternative explanation for thicker deposits in the southern sector would be a higher sediment input. Rodrigues et al. (1991) and Dias et al. (2000) proposed a large fluvial palaeo-drainage system south of the Minho River mouth aligned in a SSE–NNW direction. This system could have delivered large amounts of sediments. However, we have to state that not any incision or other remnants of a drowned fluvial system are observed in our study area.

The deposits of U2 predominantly consist of homogenous fine sands that were deposited, respectively re-deposited in the run of the sea-level rise. The coast was retreating landward and the lower wave base during times of lower sea level led to reworking of shelf deposits and winnowing of fines. Additionally, sediment contribution by rivers was probable higher and sandy material was exported to the shelf prior to the flooding of the estuaries during late sea-level rise.

Reflector R2 separates seismic Units 2 and 3 from each other (Fig. 5B). Radiocarbon ages below and above R2 in 129 m water depth define a time span of formation between 14.9 and 12.2 ka BP (Fig. 3B). In contrast, an age of 12.1 ka BP, measured within the underlying U2 in 94 m water depth, indicates again a time-transgressive evolution of R2. Therefore, the time interval between 14.9 and 12.2 ka BP was characterised by both, R2 deposition on the outer part of the shelf, and simultaneous U2 sedimentation on the inner shelf. Necessary transport energy of the coarse R2 deposits suggests a high-energy environment and the time-transgressive trend points again to the rising sea level as driving force. Peltier and Fairbanks (2006) and Hanebuth et al. (2000) described a rapidly rising sea level from 100 mbsl at 15 ka BP to 50 mbsl at 12 ka BP. It is conceivable that the depocentre of coarse material shifted towards the inner shelf during this time.

Erosional surfaces and coarse layers, comparable to R2, were described by several authors e.g. from the New Jersey continental shelf and the Californian shelf (Duncan et al., 2000; Grossman et al., 2006). However, the interpretations vary largely. Grossman et al. (2006) relate a lithological transition from transgressive sands and gravels towards massive silt drape at about 11.5 ka BP to the Melt-Water Pulse 1B event. Duncan et al. (2000) described a seismic reflector between 12.3 and 10.5 ka BP and interpret this feature as a flooding surface internal to a transgressive systems tract. On the NW Iberian continental shelf, Ferrín (2005) proposed a regressive nature of a coarse deposit but without a confirmation by radiocarbon dating. In contrast, González-Álvarez et al. (2005), García-García et al. (2005) and Durán et al. (2007) related a basal coarse layer, respectively an erosional surface to the age interval of the Younger Dryas (11 to 10 ka BP; YD). Our study shows, in contrast, that deposition of R2 material was not confined to the YD time interval. The retrogradational shift of R2, as well as of U2, shows that the occurrence of main sedimentary units on low-accumulation shelves is not necessarily restricted to a certain time interval. Rather, one unit can

record a longer time interval, such as initial deposition during a sea-level lowstand and subsequent sedimentation during a succeeding sea-level rise. Therefore, correlation between a series of cores does not necessarily reveal contemporaneous deposition, but links shifting zones of deposition, which are characterised by a similar genetic background, for instance a formation during the rising sea-level.

Generally, the entire U3 is interpreted to include sediments of both, the late sea-level rise ($U3_s$) and the modern sea-level highstand ($U3_m$; Fig. 5C). However, U3 is not distributed equally over the shelf. On outer parts of the shelf, the deposition of U3 is restricted to low marine background sedimentation (mainly planktonic and benthic foraminifera) on fine-sandy palimpsest deposits, as described by Dias and Nittrouer (1984) for this region. In contrast, the Galicia Mud Belt in mid-shelf position and inner parts of the shelf show a higher thickness of U3 sediments. This is, for instance, the case in the easternmost part of Profile C where sediments are trapped between rocky outcrops on the inner shelf and form an up to 3-m thick sediment body (Fig. 2C). Profile A shows a comparable feature but the sedimentary setting is different. There, a 2-m thick layer is deposited next to rocky outcrops but its increased thickness seems to be related to local sediment input from the Ría de Muros (Fig. 2A). Therefore, the U3 thickness in these inner-shelf areas is controlled by a combination of sediment input and shelf morphology.

The fine-sandy deposits of $U3_s$ document the time interval between R2 deposition and the initial formation of the Galicia Mud Belt ($U3_m$; Fig. 3B). However, in most of the cores either non-deposition or subsequent erosion occurred in this time interval. Depositional remnants of $U3_s$ are only observed in Profiles C and D (Fig. 3C, D).

The oldest measured age of $U3_m$ indicates that the transition from $U3_s$ to $U3_m$ had already taken place in the time interval between 8.3 and 5.3 ka BP (Fig. 3B). Hence, the initial onset of the Galicia Mud Belt is displayed by a gradual development from fine sands towards mud deposition and is presumed to have taken place in the region of Profile B (Fig. 3B).

The sea-level curve of Peltier and Fairbanks (2006) indicates that the modern sea level was established at around 5 ka BP. Radiocarbon dates, taken directly from the base of the Galicia Mud Belt ($U3_m$), mostly record ages between 5.3 and 2.2 ka BP. Therefore, this depocentre has formed during the modern sea-level highstand. Furthermore, radiocarbon ages of our study indicate that the Galicia Mud Belt has been the main depocentre for fluvially supplied fine material on the NW Iberian shelf not only since 2.8 ka BP, as proposed by González-Álvarez et al. (2005), or 4.8 ka, as shown by Martins et al. (2007) and Bernárdez et al. (2008), but at least since 5.3 ka BP.

The initial onset of the Galicia Mud Belt was most probably related to a shift in the balance between sea-level rise and sediment supply. This balance is probably of major influence on the rate of fluvial sediment export towards the shelf. Generally, Long (2001) stated that between 7.8 and 4.4 ka BP the available accommodation space within estuaries was largely filled by very rapid sedimentation due to the early Holocene deceleration in the rate of sea-level rise. This proposed time interval is in agreement with studies of the Gulf of Cadiz (Dabrio et al., 2000) and Tagus River valley (Vis et al., 2008). In addition, Sommerfield and Wheatcroft (2007) proposed a Holocene transition from estuary- to shelf-centred mud accumulation at the northern California shelf. Since the Douro River is considered as the main source for mud-belt sediments, the initiation of the Galicia Mud Belt should be related to the evolution of this river. A change from a continental sedimentary facies towards marine conditions inside the Douro River valley related to the early Holocene flooding of this estuary was observed from 9.8 to about 6 ka BP (Drago et al., 2006). Afterwards, a gradual filling of the estuary and the evolution of a gravel barrier is documented by Drago et al. (2006) and Naughton et al. (2007), indicating a transition from sediment trapping inside the inundated estuary towards sediment export to the shelf. Hence, this transition and the timing of the first onset of the Galicia Mud Belt indicates that the balance between rate of sea-level rise and sediment supply, and the decreasing accommodation space within the estuary were the key factors for initial mud-belt deposition on the NW Iberian shelf. This accumulation of mud was confined to structural lows on the middle shelf (Fig. 3B), that have sheltered these sediments against the erosion by currents and waves.

6. Conclusions

The NW Iberian shelf provides a well-suited example for the stratigraphic construction of a low-accumulation sedimentary shelf system. Three main stratigraphical units are identified on top of a basal unconformity. The lowermost Unit 1 is considered to represent stacked Late Tertiary to Pleistocene deposits, including sediments related to the last glacial sea-level fall. Unit 2 is related to the LGM sea-level lowstand and early deglacial sea-level rise. Unit 3 comprises deposits of the late deglacial sea-level rise and Holocene sea-level highstand. These individual units are separated by strong seismic reflectors that are related to the last glacial sea-level lowstand and late deglacial transgression.

Sediments from all of these units are recovered by coring. Pre-Holocene sediments are predominately composed of homogenous fine sands controlled by the position of sea level and wave base. Also, palaeosols are recovered for the first time on the NW Iberian shelf indicating an ancient exposure of large areas of the shelf. Strong reflectors, bounding the individual units, represent not only erosional surfaces but consist of considerable coarse-grained beds. Sedimentation during the Late Holocene sea-level highstand is mainly restricted to mud deposition in mid-shelf position, forming a mud belt. The Galicia Mud Belt was the main depocentre over at least the past 5.32 ka BP. Its initial formation was related to a shift in the balance between sea-level rise and sediment supply.

This study shows that sea-level changes represent the major force controlling the stratigraphic framework on low-accumulation shelves. Sediment input and other forcing factors such as the morphologic influence of rocky barriers and tectonically induced differences in the elevation of the basement strongly influence the sediment distribution within such a framework. Further work should focus on spatial and temporal variations in sediment composition on local scale to reveal the impact of individual external forces and internal processes on both, sediment distribution pattern as well as material residence times and shelf storage capacities, respectively.

Acknowledgements

Special thanks go to Hannes Riepshoff for his contribution to this project. We also wish to thank Captain Michael Schneider and his complete crew on *RV Poseidon* for their outstanding support, and two anonymous reviewers for constructive comments. We are thankful to Prof. Rüdiger Henrich for providing the laboratory facilities. Furthermore, BSH (Bundesanstalt für Seeschifffahrt und Hydrographie) is acknowledged for providing the Boomer system. This work was funded through DFG-Research Center / Excellence Cluster "The Ocean in the Earth System".

References

Araújo, M.F., Jouanneau, J.M., Valério, P., Barbosa, T., Gouveia, A., Weber, O., Oliveira, A., Rodrigues, A., Dias, J.M.A., 2002. Geochemical tracers of northern Portuguese estuarine sediments on the shelf. Prog. Oceanogr. 52 (2–4), 277–297.

Bard, E., Arnold, M., Hamelin, B., Tisnerat-Laborde, N., Cabioch, G., 1998. Radiocarbon calibration by means of mass spectrometric Th-230/U-234 and C-14 ages of corals: an updated database including samples from Barbados, Mururoa and Tahiti. Radiocarbon 40 (3), 1085–1092.

Bernárdez, P., González-Álvarez, R., Francés, G., Prego, R., Bárcena, M.A., Romero, O.E., 2008. Late Holocene history of the rainfall in the NW Iberian peninsula—evidence from a marine record. J. Mar. Syst. 72 (1–4), 366–382.

Blair, T.C., McPherson, J.G., 1999. Grain-size and textural classification of coarse sedimentary particles. J. Sediment. Res. 69 (1), 6–19.

Crockett, J.S., Nittrouer, C.A., 2004. The sandy inner shelf as a repository for muddy sediment: an example from Northern California. Cont. Shelf Res. 24 (1), 55–73.
Dabrio, C.J., Zazo, C., Goy, J.L., Sierro, F.J., Borja, F., Lario, J., González, J.A., Flores, J.A., 2000. Depositional history of estuarine infill during the last postglacial transgression (Gulf of Cadiz, Southern Spain). Mar. Geol. 162 (2–4), 381–404.
Dias, J.M.A., 1985. Registos da migração da linha de costa nos últimos 18.000 anos na plataforma continental portuguesa setentrional. 1a. Reun. Quat. Ibérico 1, 281–285.
Dias, J.M.A., Nittrouer, C.A., 1984. Continental shelf sediments of northern Portugal. Cont. Shelf Res. 3 (2), 147–165.
Dias, J.M.A., Boski, T., Rodrigues, A., Magalhães, F., 2000. Coast line evolution in Portugal since the Last Glacial Maximum until present—a synthesis. Mar. Geol. 170 (1–2), 177–186.
Dias, J.M.A., Gonzalez, R., Garcia, C., Diaz-del-Rio, V., 2002a. Sediment distribution patterns on the Galicia-Minho continental shelf. Prog. Oceanogr. 52 (2–4), 215–231.
Dias, J.M.A., Jouanneau, J.M., Gonzalez, R., Araújo, M.F., Drago, T., Garcia, C., Oliveira, A., Rodrigues, A., Vitorino, J., Weber, O., 2002b. Present day sedimentary processes on the northern Iberian shelf. Prog. Oceanogr. 52 (2–4), 249–259.
Drago, T., Oliveira, A., Magalhães, F., Cascalho, J., Jouanneau, J.M., Vitorino, J., 1998. Some evidences of northward fine sediment transport in the northern Portuguese continental shelf. Oceanol. Acta 21 (2), 223–231.
Drago, T., Freitas, C., Rocha, F., Moreno, J., Cachao, M., Naughton, F., Fradique, C., Araujo, F., Silveira, T., Oliveira, A., Cascalho, J., Fatela, F., 2006. Paleoenvironmental evolution of estuarine systems during the last 14,000 years—the case of Douro estuary (NW Portugal). J. Coast. Res. 1, 186–192.
Duncan, C.S., Goff, J.A., Austin, J.A., Fulthorpe, C.S., 2000. Tracking the last sea-level cycle: seafloor morphology and shallow stratigraphy of the latest Quaternary New Jersey middle continental shelf. Mar. Geol. 170 (3–4), 395–421.
Durán, R., García-Gil, S., Diez, R., Vilas, F., 2007. Stratigraphic framework of gas accumulations in the Ría de Pontevedra (NW Spain). Geo Mar. Lett. 27 (2–4), 77–88.
Ergin, M., Okyar, M., Timur, K., 1992. Seismic stratigraphy and late quaternary sediments in inner and mid-shelf areas of eastern Mersin Bay, northeastern Mediterranean Sea. Mar. Geol. 104 (1–4), 73–91.
Ferrín, A., 2005. Cenozoic Seismic Stratigraphy of the SW Galician Continental Shelf. Comparative Study With the Canterbury Shelf (SE New Zealand) During the Quaternary. Ph.D. thesis, Facultad de Ciencas del Mar, Departmento de Geociencias Marinas y Ordenación del Territorio, Universidad de Vigo, Spain.
Fiuza, A.F.D., Demacedo, M.E., Guerreiro, M.R., 1982. Climatological space and time variation of the Portuguese coastal upwelling. Oceanol. Acta 5 (1), 31–40.
García-García, A., García-Gil, S., Vilas, F., 2005. Quaternary evolution of the Ría de Vigo, Spain. Mar. Geol. 220 (1–4), 153–179.
González-Álvarez, R., Bernárdez, P., Pena, L.D., Francés, G., Prego, R., Diz, P., Vilas, F., 2005. Paleoclimatic evolution of the Galician continental shelf (NW of Spain) during the last 3000 years: from a storm regime to present conditions. J. Mar. Syst. 54 (1–4), 245–260.
Grossman, E.E., Eittreim, S.L., Field, M.E., Wong, F.L., 2006. Shallow stratigraphy and sedimentation history during high-frequency sea-level changes on the central California shelf. Cont. Shelf Res. 26 (10), 1217–1239.
Hanebuth, T., Stattegger, K., Grootes, P.M., 2000. Rapid flooding of the Sunda Shelf: a late-glacial sea-level record. Science 288 (5468), 1033–1035.
Jouanneau, J.M., Weber, O., Drago, T., Rodrigues, A., Oliveira, A., Dias, J.M.A., Garcia, C., Schmidt, S., Reyss, J.L., 2002. Recent sedimentation and sedimentary budgets on the western Iberian shelf. Prog. Oceanogr. 52 (2–4), 261–275.
Long, A., 2001. Mid-Holocene sea-level change and coastal evolution. Prog. Phys. Geogr. 25 (3), 399–408.
Martins, V., Dubert, J., Jouanneau, J.-M., Weber, O., da Silva, E.F., Patinha, C., Alveirinho Dias, J.M., Rocha, F., 2007. A multiproxy approach of the Holocene evolution of shelf-slope circulation on the NW Iberian Continental Shelf. Mar. Geol. 239 (1–2), 1–18.
Muñoz, A., Acosta, J., Uchupi, E., 2003. Cenozoic tectonics on the Galicia margin, northwest Spain. Geo Mar. Lett. 23 (1), 72–80.
Naughton, F., Goñi, M.F.S., Drago, T., Freitas, M.C., Oliveira, A., 2007. Holocene changes in the Douro estuary (Northwestern Iberia). J. Coast. Res. 23 (3), 711–720.
Okyar, M., Ergin, M., Evans, G., 2005. Seismic stratigraphy of Late Quaternary sediments of western Mersin Bay shelf, (NE Mediterranean Sea). Mar. Geol. 220 (1–4), 113–130.
Oliveira, I., Valle, A., Miranda, F., 1982. Litoral problems in the portuguese west coast. Proc. 18th Coastal Eng. Conf. 3, 1951–1969.
Oliveira, A., Rocha, F., Rodrigues, A., Jouanneau, J., Dias, A., Weber, O., Gomes, C., 2002. Clay minerals from the sedimentary cover from the Northwest Iberian shelf. Prog. Oceanogr. 52 (2–4), 233–247.
Peltier, W.R., Fairbanks, R.G., 2006. Global glacial ice volume and Last Glacial Maximum duration from an extended Barbados sea level record. Quat. Sci. Rev. 25 (23–24), 3322–3337.
Rey Salgado, J., 1993. Relacion morphose dimentaria entre la platforma continental de Galicia y las Rias bajas y su evolucion durante el Cuaternario. Publ. Espec.-Inst. Oceanogr. 17, 1–233.
Rodrigues, A., Magalhães, F., Dias, J.A., 1991. Evolution of the North Portuguese coast in the last 18,000 years. Quat. Int. 9, 67–74.
Rohrlich, V., Wiseman, G., Komornik, A., 1995. Overconsolidated clays from the Israeli Mediterranean coast and inner shore. Eng. Geol. 39 (1–2), 87–94.
Slater, R.A., Gorsline, D.S., Kolpack, R.L., Shiller, G.I., 2002. Post-glacial sediments of the Californian shelf from Cape San Martin to the US–Mexico border. Quat. Int. 92 (1), 45–61.
Sommerfield, C.K., Wheatcroft, R.A., 2007. Late Holocene sediment accumulation on the northern California shelf: oceanic, fluvial, and anthropogenic influences. Geol. Soc. Amer. Bull. 119 (9–10), 1120–1134.
Stuiver, M., Reimer, P.J., Bard, E., Beck, J.W., Burr, G.S., Hughen, K.A., Kromer, B., McCormac, G., Van der Plicht, J., Spurk, M., 1998. INTCAL98 radiocarbon age calibration, 24,000-0 cal BP. Radiocarbon 40 (3), 1041–1083.
van Weering, T.C.E., McCave, I.N., 2002. Benthic processes and dynamics at the NW Iberian margin: an introduction. Prog. Oceanogr. 52 (2–4), 123–128.
Vis, G.-J., Kasse, C., Vandenberghe, J., 2008. Late Pleistocene and Holocene palaeogeography of the Lower Tagus Valley (Portugal): effects of relative sea level, valley morphology and sediment supply. Quat. Sci. Rev. 27 (17–18), 1682–1709.
Vitorino, J., Oliveira, A., Jouanneau, J.M., Drago, T., 2002. Winter dynamics on the northern Portuguese shelf. Part 1: physical processes. Prog. Oceanogr. 52 (2–4), 129–153.

5. Holocene evolution of mud depocentres on a high-energy, low-accumulation shelf (NW Iberia)

Hendrik Lantzsch, Till J. J. Hanebuth, **Vera B. Bender**

MARUM – Center for Marine Environmental Sciences and Faculty of Geosciences, University of Bremen, P.O. Box 330440, 28334 Bremen, Germany.

Quaternary Research **72**, 325–336, doi:10.1016/j.yqres.2009.07.009

Quaternary Research 72 (2009) 325–336

Contents lists available at ScienceDirect

Quaternary Research

journal homepage: www.elsevier.com/locate/yqres

Holocene evolution of mud depocentres on a high-energy, low-accumulation shelf (NW Iberia)

Hendrik Lantzsch *, Till J.J. Hanebuth, Vera B. Bender

MARUM — Center for Marine Environmental Sciences, and Faculty of Geosciences, University of Bremen, P.O. Box 330440, 28334 Bremen, Germany

ARTICLE INFO

Article history:
Received 9 April 2009
Available online 15 August 2009

Keywords:
Holocene
Shelf sedimentation
Mud belt
Radiocarbon dating
Sediment dispersal
NW Iberian Peninsula

ABSTRACT

The high-energy, low-accumulation NW Iberian shelf features three confined Holocene mud depocentres. Here, we show that the evolution of such depocentres follows successive steps. The flooding of inner shelf zones and river catchment areas by the late deglacial sea-level rise provided the precondition for shelf mud deposition. Following this, the Holocene deceleration of the sea-level rise caused a rapid refill of the accommodation space within river valleys. Subsequently, the export of major amounts of fines was initiated. The initial onset and loci of shelf mud deposition were related to deposition-favouring conditions in mid-shelf position or to the presence of morphological highs, which act as sediment traps by providing protection against stronger hydrodynamic energy. The detailed reconstruction of the Holocene depocentre evolution shows for the first time that the expansion of such shelf mud deposits cannot only occur by linear growth off the associated sediment source. Rather, they might develop around centres that are fully disconnected from the source of original sediment supply, and expand later into specific directions. Based on these differences and on the connection of the individual mud depocentres to the material source we propose a conceptual subdivision of the group "mid-shelf mud depocentres".

Introduction

Clastic shelf systems represent a major sink for both terrestrial and marine materials on the sediment pathway from the coast to the continental slope. The very dynamic nature of shelves finds its geological expression in a large lateral and stratigraphical variability of the sedimentation patterns that is usually attributed to external forcing by changes in sea level, tectonics, climate, and terrigenous input. However, shelf systems show considerable self-organization by the interaction of bathymetry, wave and current regimes. During the Holocene sea-level highstand, this interplay results particularly in deposition of mud on continental shelves. In recent years, those mud deposits became of major interest due to their role in material budgeting (Durrieu de Madron et al., 2000; Lesueur et al., 2001; Jouanneau et al., 2002; Sommerfield and Wheatcroft, 2007) and as high-resolution climate archives (Martins et al., 2007; Naughton et al., 2007b; Bernárdez et al., 2008; Hanebuth and Lantzsch, 2008; Hanebuth and Henrich, 2009).

The challenge of coring the base of mud belts due to frequently occurring basal sandy lag deposits led to a general lack of knowledge concerning (1) the precise timing of growth initiation, (2) spatial and temporal sedimentary evolution of these highstand depocentres, and (3) role of the forces controlling this development. Closing these gaps should provide a new view on the dominant forces controlling the overall sediment distribution, and on the interpretation of climatic fluctuations within this framework.

We present new data from the NW Iberian shelf including a grid of 1300 km shallow-seismic profiles, 15 sediment cores, and 30 radiocarbon dates. This study (1) analyses the mechanisms for the spatial and temporal Holocene mud deposition, and (2) provides a concept of mid-shelf mud depocentres on high-energy, low-accumulation shelf systems.

Regional settings

Morphology and geology

The NW Iberian shelf is generally narrow with a maximum extension of 50 km in front of the Douro River (Fig. 1). The shelf break occurs in water depths of 160 to 180 m (Dias et al., 2002) and is cut by the Porto submarine canyon at the northern Portuguese continental shelf at 41°20′N. The outer shelf is characterised by basement outcropping south of 42°00′N (Rey Salgado, 1993; Dias et al., 2002; Oliveira et al., 2002; Fig. 1). In contrast, on the inner shelf, plutonic and metamorphic bedrock is present north of 41°30′N (Fig. 1).

Most prominent features of the Spanish coast are the four deep Rías Baixas (Muros, Arosa, Pontevedra, Vigo), which represent Tertiary river valleys, drowned during the last deglacial sea-level rise (Rey Salgado, 1993; Oliveira et al., 2002). In contrast, the Portuguese coastline is smoothened and characterised by the estuaries of the Minho, Lima, Cávado, Ave and Douro Rivers (Fig. 1).

* Corresponding author. Fax: + 49 421 218 65219.
E-mail address: lantzsch@uni-bremen.de (H. Lantzsch).

0033-5894/$ – see front matter © 2009 University of Washington. Published by Elsevier Inc. All rights reserved.
doi:10.1016/j.yqres.2009.07.009

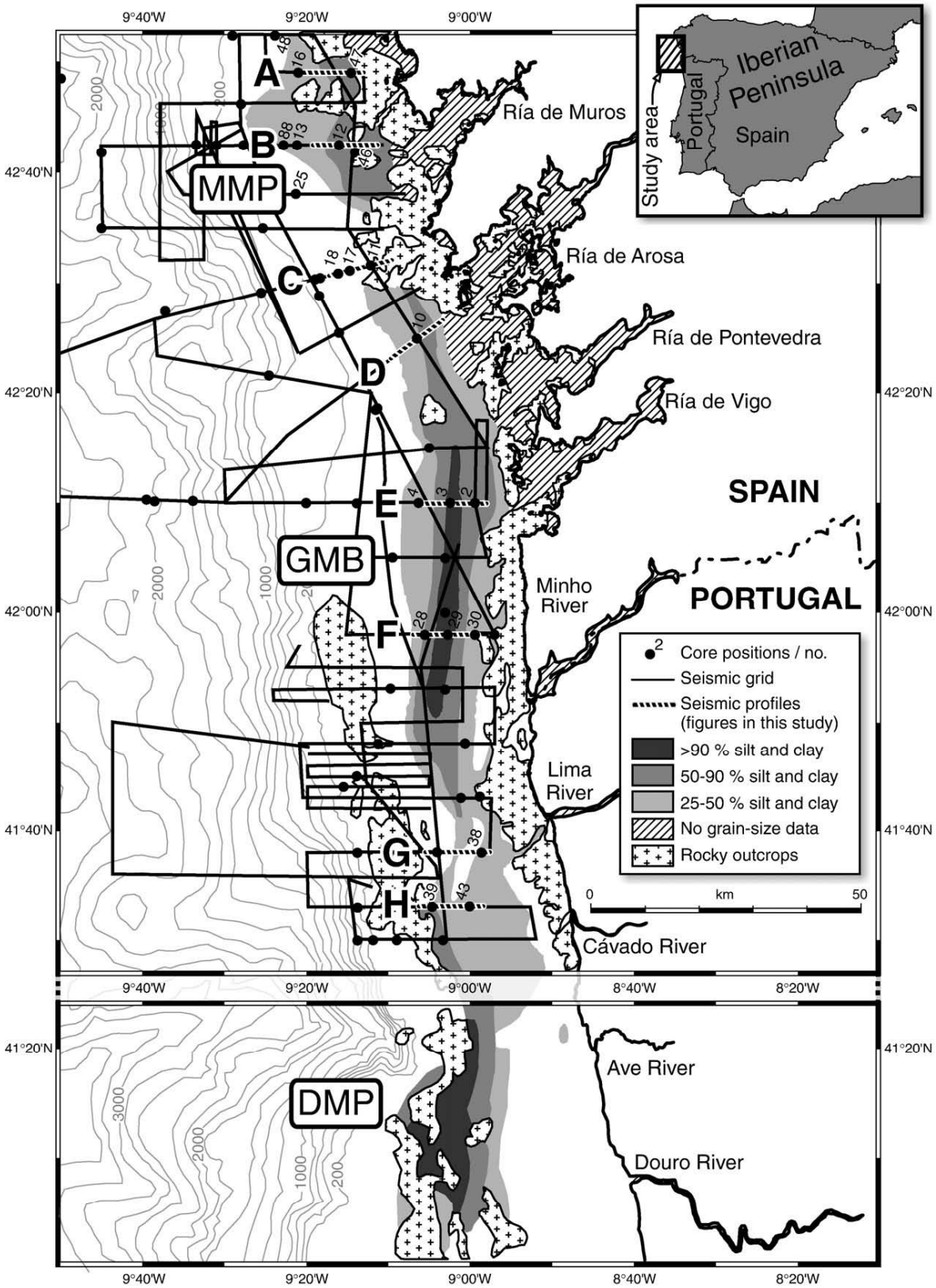

Figure 1. Map of the study area and the adjacent southern part including the position of the Douro River. The shelf surface geology is adopted from Dias et al. (2002). No grain-size measurements are applied to the Rías and river valleys. The Muros Mud Patch (MMP), Galicia Mud Belt (GMB) and Douro Mud Patch (DMP) are displayed in grey. Black lines represent the seismic profiles obtained during Cruise P342. Characters A to H represent seismic profiles shown in Figures 2 and 3. Core positions of Cruises P342 and P366/3 are marked by black dots. Cores used in this study are labelled in short form with 11002-3 being position 2 (P342), for instance and 13046-2 being position 46 (P366/3).

Table 1
List of the GALIOMAR sediment vibrocores of this study.

Core no. (GeoB)	Latitude (N)	Longitude (W)	Water depth [m]	Recovery [m]
11002-3	42°10.00	8°59.24	111	4.34
11003-3	42°10.00	9°02.24	129	4.54
11010-2	42°25.00	9°06.28	119	4.10
11011-2	42°31.38	9°12.07	100	4.85
11012-2	42°42.29	9°16.00	119	4.28
11017-2	42°31.10	9°14.40	120	4.88
11018-2	42°30.54	9°16.04	125	4.00
11028-2	41°57.59	9°05.29	127	4.59
11029-2	41°57.59	9°02.42	114	4.88
11030-2	41°58.00	8°59.24	94	4.60
11038-2	41°38.03	8°58.27	78	4.88
11039-2	41°33.03	9°04.38	99	4.28
11043-2	41°33.05	9°00.03	84	4.51
13046-2	42°41.80	9°14.00	106	2.41
13047-2	42°49.00	9°14.47	94	4.85

Oceanography

The NW Iberian margin is characterised by strong seasonal variations between winter and summer regimes (Dias et al., 2002; Vitorino et al., 2002). The summer situation is dominated by an equatorward directed along-shelf current, low-energy conditions, and occasional wind-driven upwelling. In contrast, highly energetic hydrodynamic conditions during the winter season result in (1) a poleward-directed current on the mid-shelf, (2) intensified river runoff due to both, generally increased precipitation and episodic river floods after storms, and (3) a shelf-wide wind-driven downwelling cell. These winter conditions are proposed to control the modern sediment distribution on the shelf (Dias et al., 2002; Vitorino et al., 2002). Therefore, we consider the NW Iberian shelf as being a high-energy sedimentary shelf system. The described oceanographic pattern is suggested to have been persistent at least over the past 4700 calibrated years before present (cal yr BP in the following; Bernárdez et al., 2008).

The sedimentary system

The Douro River is considered as the main source of fine sediments on the shelf (Araújo et al., 2002; Dias et al., 2002). In contrast, the export from the Rías Baixas is suggested to be negligible (Rey Salgado, 1993). Fine-grained fluviogenic sediments are frequently re-suspended by winter storms and transported to the north by the poleward-flowing bottom current (Dias et al., 2002). This availability of fine sediments leads to the development of well-defined areas of mud deposition in around 100 to 120 m modern water depth (Dias et al., 2002; Oliveira et al., 2002). Here, we use the term "Galicia Mud Belt" (GMB), as introduced by Lantzsch et al. (2009), due to its elongated shape running contour-parallel in mid-shelf position. The Muros and Douro mud depocentres are patch-shaped with minor elongation compared to the GMB and are, therefore, addressed as "Muros Mud Patch" (MMP) and "Douro Mud Patch" (DMP).

Due to relict sands and massive glauconite formation on the outer shelf (Dias and Nittrouer, 1984; Odin and Lamboy, 1988), and relatively low sedimentation rates (Jouanneau et al., 2002), the NW Iberian shelf is considered to represent a low-accumulation sedimentation system (Lantzsch et al., 2009). In contrast to conditions on a fully sediment-starved shelf, which is bare of any remarkable modern sedimentation (e.g. the New Jersey shelf; Goff et al., 2005), such a low-accumulation regime is characterised by the presence of confined sediment bodies as a result of persistent Holocene sedimentation.

Materials and methods

Geophysical profiling

Sediment-acoustic data were collected by means of a Boomer system during the GALIOMAR (Galician Ocean Margin Expedition) cruise in 2006 with the German research vessel POSEIDON (P342; Hanebuth et al., 2007). The frequency band of the Boomer was between 500 Hz and 10 kHz with a main frequency of around 2–3 kHz. The Boomer was shot every second with a two-second break every six shots for firing an airgun. The vertical signal resolution of the Boomer system is about 0.5 m. In total, about 1300 km of shallow-seismic lines were collected (Fig. 1).

Sediment coring

Overall, 66 sediment cores (up to 5 m long) were collected on the NW Iberian shelf and, to a minor extend, at the continental slope during the two GALIOMAR cruises P342 in 2006 and P366/3 in 2008 (Fig. 1; Table 1). A vibrocorer (VKG-6; Thomas Schmidt, Rostock, Germany) was used to recover sandy sediments from up to 230 m water depth. At greater water depths, sediment was retrieved using a gravity corer. The modern sediment surface was sampled by a giant box corer at each core location. In this study, the stratigraphic

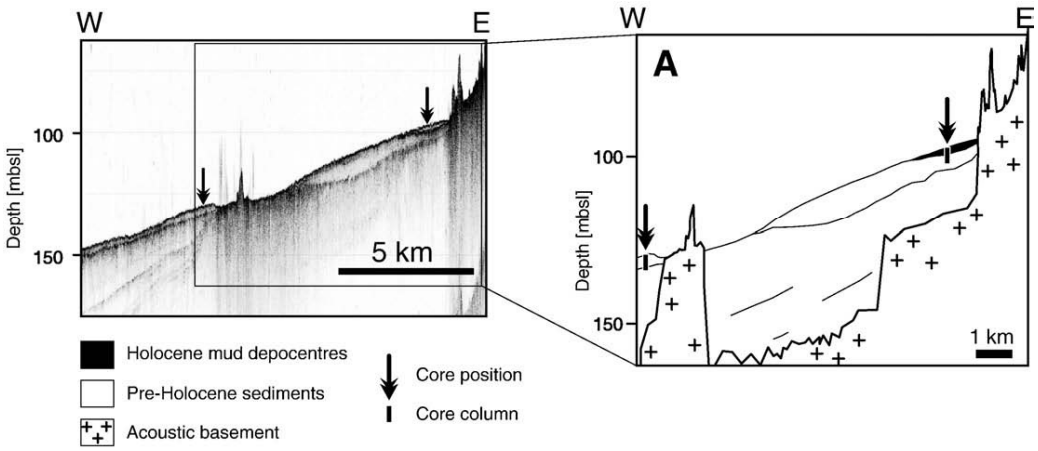

Figure 2. Boomer profile A of the respective seismic profile A shown in Figure 1 and interpretation of the architectural units following the work of Lantzsch et al. (2009). Black arrows indicate sediment-core positions. Depth on *y*-axis is given in metres below modern sea level (mbsl). The uninterpreted Boomer profiles A–H are displayed in the report of Cruise P342 (Hanebuth et al., 2007) and the interpretation of Profiles B and E–G is shown in Lantzsch et al. (2009).

interpretation of the mud deposits is based on Boomer profiles and 15 sediment vibrocores, and follows the late Quaternary subdivision of the NW Iberian stratigraphic shelf architecture as recently established by Lantzsch et al. (2009; Fig. 2).

Analyses in the lab

Core samples from the mud deposits are investigated in 10-cm intervals. The coarse fraction (>63 μm) was separated from the fine fraction (<63 μm) by wet sieving. The coarse fraction was then sonic-sifted into grain-size subfractions. The sediments have been classified according to their grain size using the scheme of Blair and McPherson (1999) and the results were used to corroborate the visual core description.

The selection of material for radiocarbon dating requires special care on continental shelves. Only delicate material of fresh preservation was measured in order to avoid age biasing due to re-deposition of older material. Monospecific samples were preferably selected. However, due to the lack of such a material in some samples, a selection of foraminifers and mollusc shells was necessary. As a result, 30 radiocarbon dates on 13 cores are displayed in this study (Table 2). Radiocarbon measurement was carried out by the Leibniz Laboratory in Kiel (Germany), and the Poznań Radiocarbon Laboratory (Poland). The raw ^{14}C ages were corrected using a standard marine reservoir effect of 400 yr, and converted into 1-sigma calibrated ages with the Calib 5.0.1 software (Stuiver et al., 1998). Dates with a conventional age older than 22 ka were calibrated with the function of Bard et al. (1998).

Results

The NW Iberian shelf mud deposits represent the uppermost acoustic unit in the Boomer profiles and show a sheet-like to wedge-shaped appearance (Figs. 2 and 3). Sediment cores, which were taken on these seismic profiles, show a wide range of sedimentary facies types. The cores are mainly composed of homogenous fine sands, but distinct layers of shell-fragment and siliceous gravels, and mud appear in nearly all cores as well (Fig. 3). The mud deposits are generally characterised by more than 25% fine fraction and overlie homogenous fine sands or gravels with mostly less than 10% mud contents (Fig. 3). Generally, the boundary between mud and underlying coarser sediments is sharp. Only Cores 11003-3 and 13046-2 show a different sedimentation pattern with a gradual fining-upward trend from pure sandy deposits towards mud deposition (Figs. 3B, E).

17 radiocarbon dates were measured on the gravels and fine sands underlying the mud deposits and display ages between 33,860 and 6460 cal yr BP (Table 2; Fig. 3). Two radiocarbon ages are older than 42,000 ^{14}C yr BP, i.e. beyond the limit of the radiocarbon method (Fig. 3C). Eleven radiocarbon measurements on the NW Iberian shelf mud deposits reveal ages between 5388 and 458 cal yr BP (Fig. 3). Most of these samples were taken at the base of the mud depocentres and show a considerable age offset between central and marginal core positions.

Three confined mud depocentres are observed on the NW Iberian shelf — the Muros Mud Patch (MMP), the Galicia Mud Belt (GMB), and the Douro Mud Patch (DMP). The *MMP* represents the northernmost of the mud deposits and occurs down to about 120 m water depth according to the sediment cores and surface samples in our study. The Boomer profiles of the MMP show a transparent acoustic facies, and a slightly decreasing thickness from 1.5 m to about 1 m in seaward direction, which is corroborated by the similarly seaward-thinning trend of the mud deposits in Cores 13047-2, 13046-2, and 11012-2 (Figs. 3A, B). Moreover, a grain-size coarsening is observed in the cores and surface samples in seaward direction (Fig. 3B). As a result, mud contents go generally below 25% towards the outer shelf (Sites 13, 16, 25, 48 and 88 in Fig. 1). Comparably low mud contents are also

Table 2
Radiocarbon dates and age calibration.

Lab no.[a]	Core no. (GeoB)	Depth in core (cm)	Material[b]	Age (^{14}C yr BP)	Age (cal yr BP, 1σ)[c]
KIA 33665	11002-3	250	bF	2715 ± 35	2455–2342
KIA 33664	11002-3	435	bF, bv pieces, gp	4955 ± 45	5388–5249
Poz-24670	11003-3	240	bF	7840 ± 50	8370–8260
Poz-22923	11003-3	360	bF	10,770 ± 50	12,320–12,100
Poz-24771	11003-3	399	bF	13,080 ± 70	14,810–15,110
Poz-22946	11010-2	377	*E. crispum*	15,540 ± 80	18,690–18,220
Poz-22925	11012-2	100	bF	3995 ± 35	4068–3949
Poz-22948	11012-2	320	*E. crispum*	14,820 ± 80	17,550–17,070
KIA 33677	11017-2	130	*E. crispum*	21,390 ± 200	25,540–24,910
KIA 33683	11017-2	247	*E. crispum*	28,520 ± 480	33,860–32,790[d]
KIA 33684	11017-2	417	*E. crispum*	>42,090	Uncalibrated
KIA 33685	11017-2	486	bF	>44,990	Uncalibrated
KIA 33693	11018-2	153	*E. crispum*	20,420 ± 230	24,280–23,690
KIA 33695	11018-2	399	*E. crispum*	22,030 ± 220	26,200–25,690[d]
Poz-21470	11028-2	140	bF	2555 ± 30	2290–2184
Poz-21471	11028-2	416	*E. crispum*	16,780 ± 80	19,760–19,440
Poz-22950	11028-2	429	*E. crispum*	17,310 ± 190	20,240–19,860
KIA 33687	11029-2	103	bF	850 ± 30	503–458
Poz-24772	11029-2	360	bF	2910 ± 35	2737–2669
Poz-27847	11029-2	400	bF	4300 ± 35	4490–4385
KIA 33689	11029-2	488	Echinoderm pieces	12,740 ± 80	14,480–14,080
Poz-21472	11030-2	220	bF	2940 ± 35	2749–2693
Poz-21473	11030-2	460	bF, bv	10,740 ± 50	12,260–12,040
Poz-22951	11038-2	120	bF	3165 ± 35	3013–2888
Poz-22952	11038-2	460	bF, gp	16,880 ± 90	19,800–19,500
KIA 33709	11039-2	178	bF, bv, gp	6110 ± 70	6630–6460
KIA 33714	11039-2	310	bv, gp	18,480 ± 150	21,810–21,180
Poz-26858	13046-2	135	bF	4135 ± 35	4260–4135
Poz-26856	13046-2	210	bF	8750 ± 50	9480–9390
Poz-26859	13047-2	136	bF, pF, gp	4900 ± 40	5297–5135

[a] Radiocarbon laboratory: KIA = Leibniz Laboratory in Kiel (Germany); Poz = Poznań Radiocarbon Laboratory (Poland).
[b] Material: bF = benthic foraminifers; *E. crispum* = *Elphidium crispum* (monospecific sample); bv = bivalve; gp = gastropod.
[c] For reservoir correction, the conventional age of 400 years is applied using CALIB 5.0.1. (Stuiver et al., 1998).
[d] Age calibration is based on the function of Bard et al. (1998).

observed in surface samples and cores of the area between MMP and GMB (Fig. 3C). Radiocarbon samples of the MMP show ages between 5297 and 3949 cal yr BP (Table 2; Figs. 3A, B). In Core 13046-2, mud contents of more than 25%, defining the MMP, are reached between 9480 cal yr BP and 4135 cal yr BP (Fig. 3B). In contrast, mud deposition in Core 11012-2 has started at 4068–3949 cal yr BP (Fig. 3B), which indicates a later onset of mud deposition in seaward parts of the MMP.

The *GMB* shows an elongated shape and stretches parallel to the coast in mid-shelf position between Ría de Arosa and Lima River. The central part of the GMB, characterised by more than 90% fine fraction, is situated in around 120 m water depth between the Ría de Pontevedra and the mouth of the Minho River (Fig. 1). A wedge geometry and distinct internal stratification are observed in the Boomer profiles in areas with a maximum thickness of 4 m (Figs. 3E, F). Marginal parts, i.e. in seaward and landward direction as well as to the north and to the south, show a decreasing thickness (Figs. 3D, G), which is corroborated by a cored mud thickness of down to 1.2 m in marginal positions (Figs. 3D–G). The contact between GMB and DMP is transitional and characterised by a limited thickness and coarser grain size compared to the well-defined centres of GMB and DMP (Figs. 1 and 3G). Radiocarbon ages of the GMB display a range between 5388 and 458 cal yr BP (Table 2; Figs. 3D–F). In the cores of Profile E, mud contents of more than 25% are reached between 8370 and 5249 cal yr BP (Fig. 3E). Similar to the radiocarbon dates from the MMP, the base of the GMB shows younger ages towards the margin of the depocentre. This is most obvious in Profile F (Fig. 3F) where marginal cores show a later onset of mud deposition (2290–2184 cal yr BP in Core 11028-2, 2749–2693 cal yr BP in Core 11030-2) than the central core (4490–4385 cal yr BP in Core 11029-2). In addition, an age range of 3013–2888 cal yr BP indicates a later initial deposition of mud in the marginal southern part (Fig. 3G).

The *DMP* is located in mid-shelf position in front of the Douro River and shows a slightly elongated extension towards the north (Fig. 1). In contrast to the GMB, the DMP is characterised by a transparent acoustic facies, and its distribution is related to the occurrence of rocky outcrops at a water depth of around 100 m (Fig. 1). The modern DMP centre is situated slightly southward of the study area. Although the surface mud contents of the DMP within the study area indicate a relatively homogenous distribution (Fig. 1), Boomer Profile H, and respective sediment cores 11039-2 and 11043-2 show that the thickness of the DMP is not distributed equally (Fig. 3H). Two areas of increased thickness are recognisable which are connected with each other by a thin blanket. The area east of the basement elevations on the outer shelf shows a maximum thickness of about 1.5 m, thinning eastward. Further landward, a maximum thickness of about 3 m is reached, finally gradually thinning towards the inner shelf (not shown).

Mud-depocentre evolution

Initial onset of mud deposition

According to the radiocarbon dating on sediments of the Muros Mud Patch (MMP) and Galicia Mud Belt (GMB), the first onset of major mud deposition is defined by a transition from pure fine sands towards mud contents of more than 25%. This transition marks the initial onset of the MMP between 9480 and 4135 cal yr BP (Figs. 3B and 4A) and of the GMB between 8370 and 5249 cal yr BP (Figs. 3E and 4A). Hence, this gradual pattern can be considered as a general mechanism of mud-belt initiation on the NW Iberian shelf. The initial accumulation of significant amounts of fine sediments, recorded by an increasing mud content in cores of the central MMP and GMB was most probably related to the drowning of the inner shelf zone during the late phase of deglacial sea-level rise and the establishment of the quasi-modern oceanographic conditions. Subsequently, the latest postglacial sea-level rise has resulted in the flooding of river valleys. Since the Douro River is considered as being the main source for the mud deposits on the NW Iberian shelf (Araújo et al., 2002), the initial evolution of these mud depocentres should be closely related to the development of this estuary. Drago et al. (2006) observed a change from a continental sedimentary facies towards marine conditions inside the Douro River valley related to this early Holocene flooding from ~9800 to ~6000 cal yr BP. Afterwards, the deceleration in Holocene sea-level rise has caused a shift in the balance between rate of sea-level rise and sediment supply, which led to a gradual refilling of the Douro estuary as documented by Drago et al. (2006) and Naughton et al. (2007a). Observations by other authors (Dabrio et al., 2000; Boski et al., 2002; Sommerfield and Wheatcroft, 2007; Vis et al., 2008) show a similar mechanism of estuarine infill. According to Long (2001), the available accommodation space within most of the worldwide estuaries was largely filled between ~7800 and ~4400 cal yr BP, which resulted in increased terrigenous export to the shelf. This enhanced export can be considered as one main reason for the initiation and further expansion of shelf mud depocentres.

Expansion of the mud depocentres

The detailed stratigraphic analysis of the NW Iberian shelf mud deposits on the base of Boomer profiles, sediment cores, and radiocarbon dates elucidates here for the first time that the evolution of such mid-shelf fine depocentres on a low-accumulation, high-energy shelf is not uniform but unexpectedly complex. The initial onset of the *MMP* is marked by a measured age of 5297–5135 cal yr BP in the northern part (Fig. 3A), and a gradual transition from pure fine sand to mud between 9480 and 4135 cal yr BP (Site 46 in Fig. 1; Fig. 3B). A basal age of 4068–3949 cal yr BP further seaward (Fig. 3B) indicates a temporal and spatial expansion of the MMP in offshore direction (Figs. 4A, B). This quasi-concentric and continuous broadening hints to the point that, although the Rías Baixas are considered to act mainly as sediment traps (Rey Salgado, 1993), the Ría de Muros is the main source for the muddy sediments of the MMP. An additional contribution of fines from the adjacent northern bay between Ría de Muros and Cape Finisterre is indicated by the northward extension of the MMP (Site 47 in Fig. 1; Fig. 3A). Consequently, the MMP does not represent a northward extension of the GMB as was suggested by previous studies (Dias et al., 2002; Oliveira et al., 2002) but rather represents an individual depocentre. Further indications for this source connection are the decrease in the MMP thickness towards the mid-shelf and the coarser grain size in seaward direction (Figs. 1 and 3A, B). The contribution of mud from the Ría de Muros to the shelf is most probably restricted to the autumn–winter period when (1) the continental runoff is enhanced, and (2) the expansion of river plumes reaches its maximum extension towards the shelf during upwelling conditions (Álvarez-Salgado et al., 2000; Otero et al., 2008).

The location of the MMP is controlled by several factors. According to McCave (1972) and Hill et al. (2007), for instance, the dominant forces influencing the distribution of mid-shelf mud belts are sediment input and the hydrodynamic conditions on the shelf (i.e. the effect of waves and shelf currents). Other authors (Edwards, 2002; Hanebuth and Lantzsch, 2008) additionally emphasised the influence of morphological features, such as structural highs and morphological steps, on the formation of mud deposits. Considering the low sediment export from the Rías Baixas, the interplay of morphological features and hydrodynamic conditions should be the key factor for the MMP formation. Hence, rocky outcrops in the inner to mid-shelf region have most probably strong influence on the shape of the MMP by trapping material due to a sheltering of sediments against stronger hydrodynamic energy. Therefore, those morphological features are considered as being the dominant parameter enabling MMP deposition. Otherwise, a sandy inner shelf would be expected in such a high-energy environment, as it is the case for the area in front of the Douro River mouth, for instance (Fig. 1).

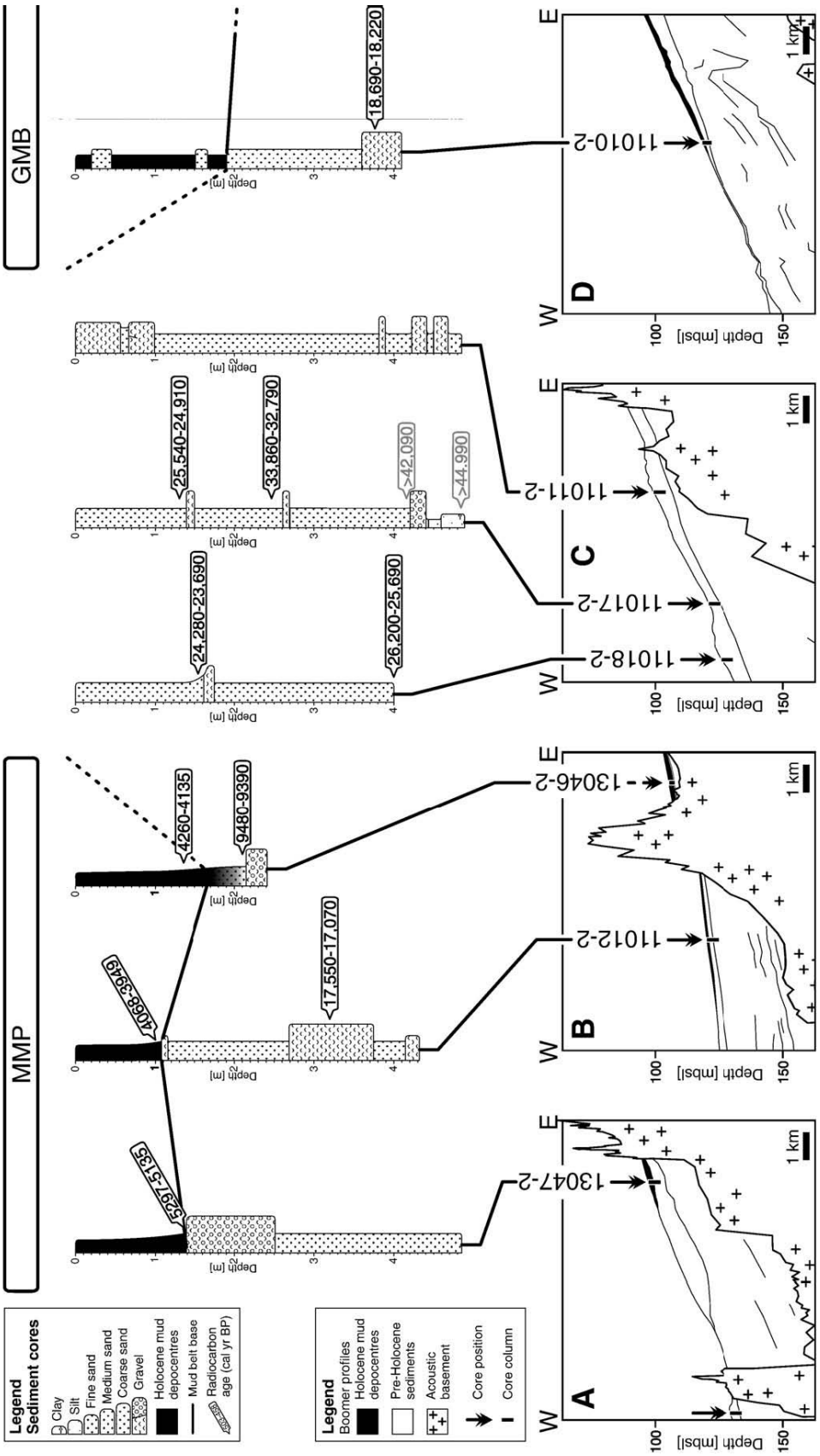

Figure 3. Interpretation of the Boomer profiles A to H and respective sediment-core records taken on these profiles. Lithology, grain size and radiocarbon ages are shown in the sediment-core columns. The locations of Profiles A–H are shown in Figure 1. Black arrows in the Boomer profiles indicate sediment-core positions. Unlabelled arrows indicate sediment cores not displayed in this study. MMP: Muros Mud Patch, GMB: Galicia Mud Belt, DMP: Douro Mud Patch. See Figure 1 for the exact position of Core 13046-2 (placed slightly southward of Profile B).

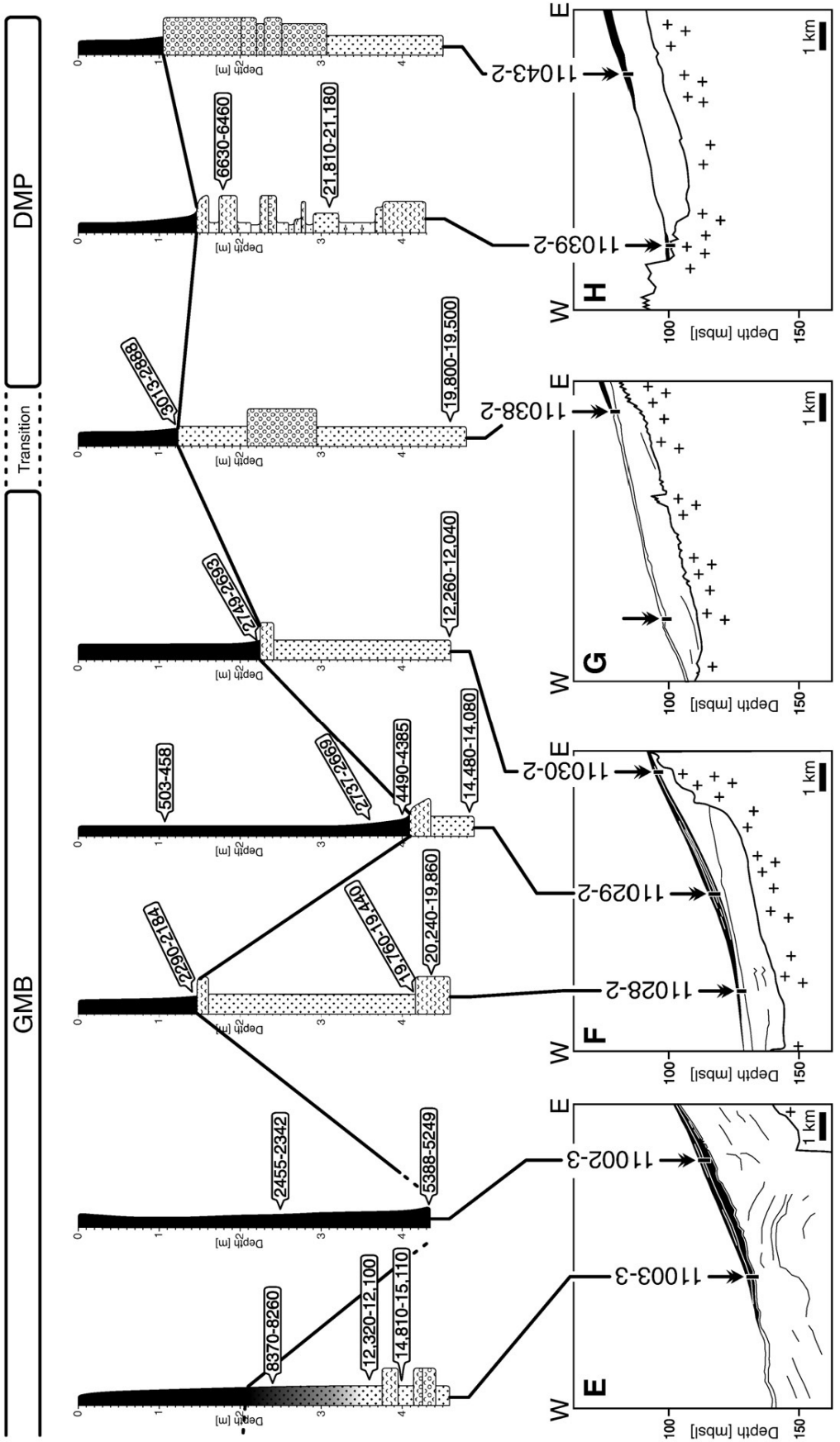

Figure 3 (*continued*).

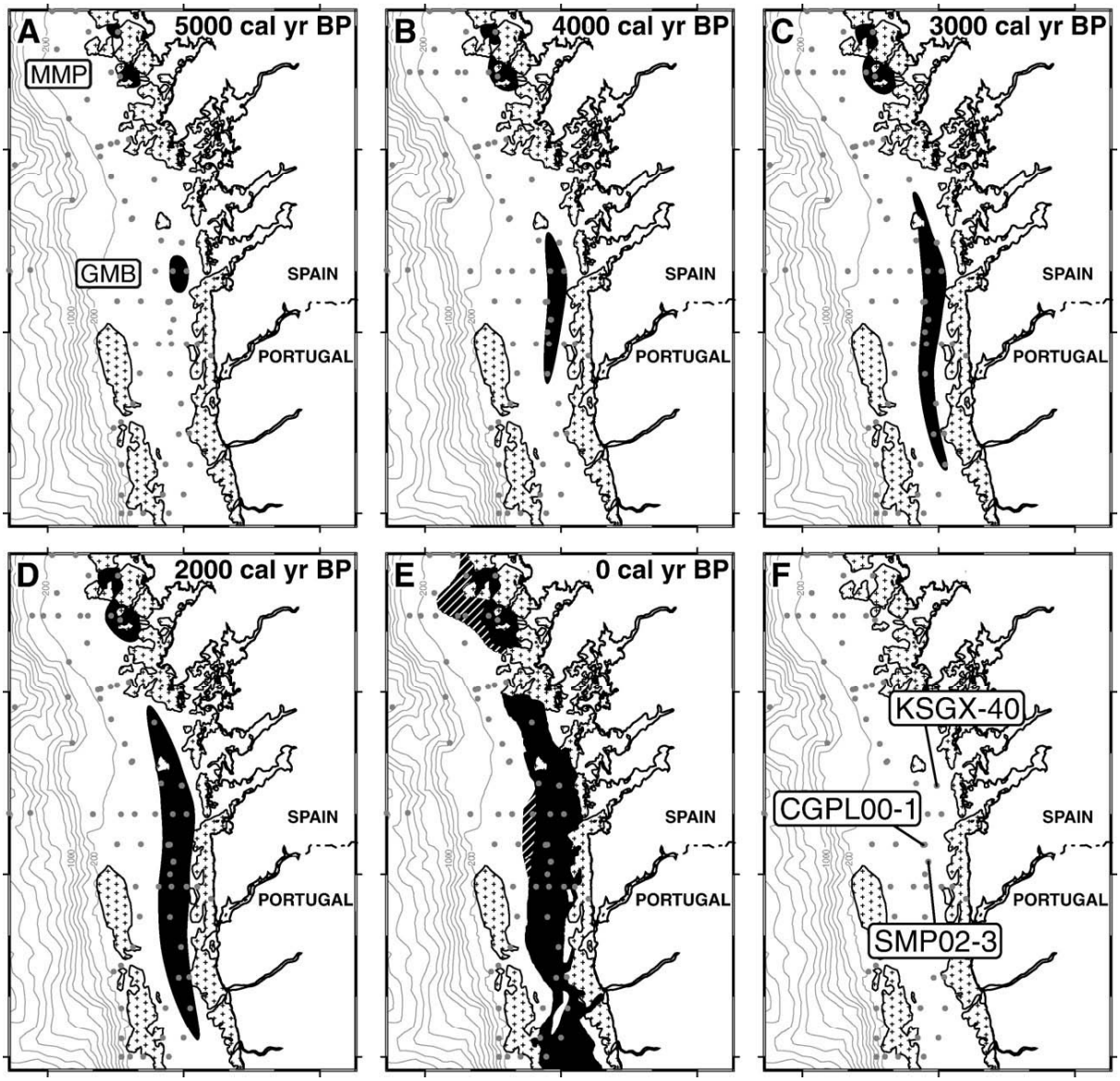

Figure 4. Initial onset and further expansion of the Muros Mud Patch (MMP) and the Galicia Mud Belt (GMB). Black areas indicate mud contents >25%. Core positions of this study are indicated by grey dots and core locations of other studies are displayed in box F (CGPL00-1: González-Álvarez et al., 2005; KSGX-40: Martins et al., 2007; SMP02-3: Bernárdez et al., 2008). The present-day mud-belt distribution in box E is adopted from Dias et al. (2002). Streaked areas indicate discrepancies between the study of Dias et al. (2002) and the own grain-size measurement on surface samples.

Mud-belt sediments in the area between MMP and GMB are neither detected in the cores and surface samples of our study (Figs. 3C and 4E), nor mapped by Dias et al. (2002; Fig. 1). Although we cannot exclude some trapping of fine sediments in shallower water depths, the reason for this particular non-deposition should be found in the pronounced northern rim of the Ría de Arosa, which is characterised by rocky outcrops extending far across the mid-shelf (Dias et al., 2002; Fig. 1). These outcrops seem to act as a sediment barrier due to either (1) their high elevation preventing sediment transit, or (2) enhanced hydrological energy in this area caused by reflection of incoming waves and/or (3) deflection of the poleward shelf current, which might result in an off-shelf export of fine sediments at the southern rim of this barrier. However, mud contents below 25% are also found in our study at Sites 13, 16 and 88 in the MMP (and Site 4 in the GMB; Fig. 1). This pattern is contrasting the mud distribution mapped by Dias et al. (2002; Fig. 4E), which might point to a strong influence of either seasonal or annual variations in the extent of the modern margins of the main mud depocentres. Above all, frequently appearing storm events might lead to intensive re-mobilisation (Vitorino et al., 2002) and, thus, margin re-shaping in these areas.

The formation of the *GMB* did not take place continuously over the whole area but in successive steps. The initial onset of the GMB is displayed by a gradual development from fine sands towards mud deposition between 8370 and 5249 cal yr BP in the region of Profile E (Figs. 3E and 4A). However, the onset of the GMB varies largely across the shelf. Martins et al. (2007) reported deposition of >25% mud in front of the Ría de Vigo (KSGX-40; Fig. 4F) from ~2500 cal yr BP. This age indicates a northward contour-parallel expansion of the mud belt (Figs. 4A, B). The extension of the Galicia Mud Belt, however, did not only appear into northward direction alone. Profile F further south displays mud deposition starting at 4490–4385 cal yr BP and deposition of fines in Profile G is recorded not earlier than 3013 cal yr BP (Figs. 3G, F and 4A, B). In addition, Bernárdez et al. (2008)

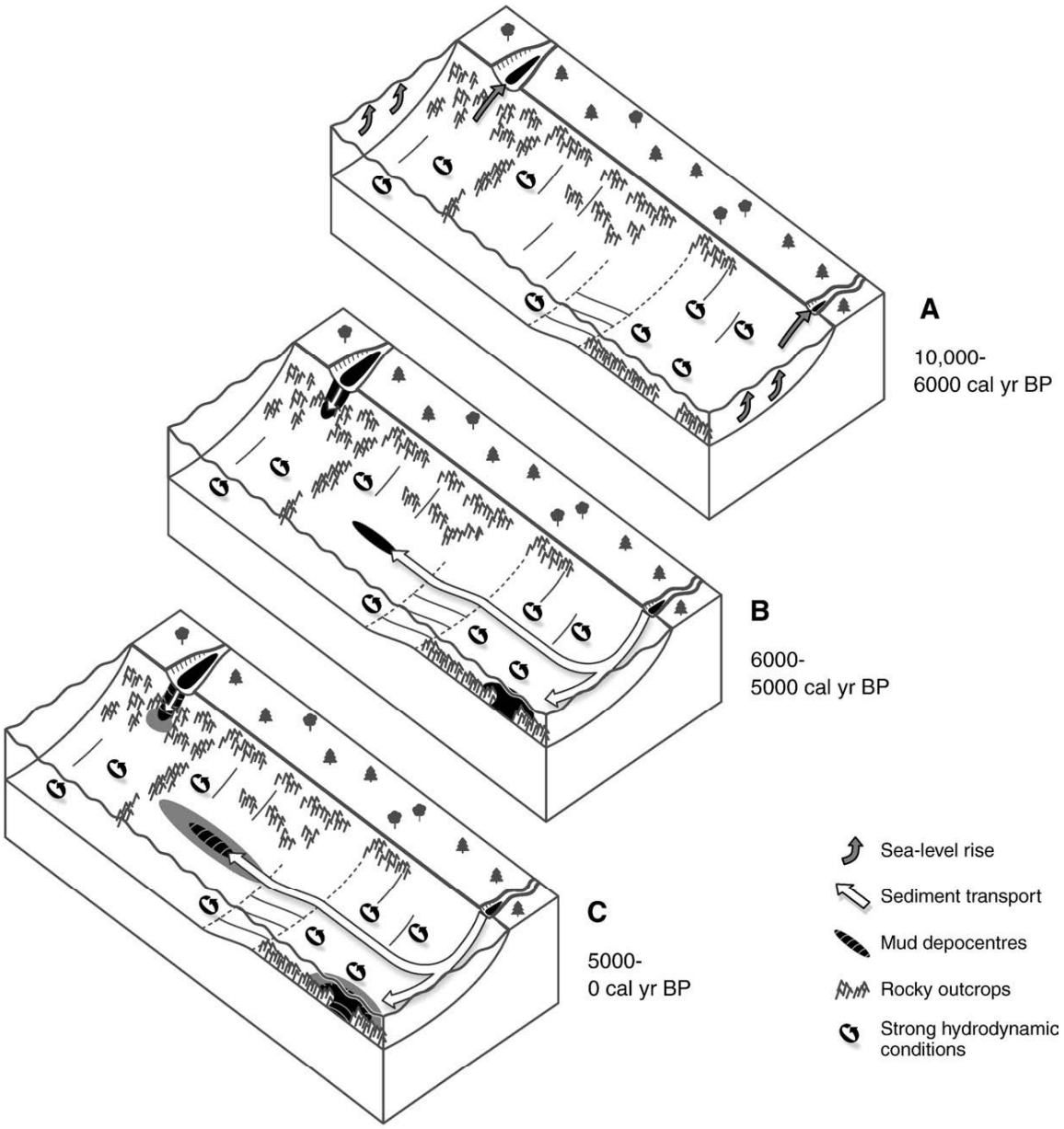

Figure 5. Schematic block diagram showing (A) the flooding of the Rías and estuaries due to the deglacial/early Holocene sea-level rise, (B) the onset of major mud deposition on the NW Iberian shelf, and (C) the further expansion of these fine-grained depocentres.

recently published an increasing mud content in fine sands between ~4700 and ~3300 cal yr BP (SMP02-3; Fig. 4F). The lateral expansion of the GMB was not only restricted to N–S direction paralleling the bathymetry. For instance, cores in Profile F directly display the extension history in W–E direction (Fig. 3F). Mud deposition started at 4490–4385 cal yr BP in Core 11029-2, which is located in the central part of the modern mud belt. In contrast, Cores 11028-2 and 11030-2 from marginal positions show an onset of the mud belt after 2290 and 2749 cal yr BP, respectively (Figs. 4D, E). In addition, González-Álvarez et al. (2005) reported the initiation of mud at ~2800 cal yr BP in the marginal part of the GMB (CGPL00-1; Fig. 4F). Hence, the detailed reconstruction of the GMB evolution shows that this mud belt started to develop in the area of Profile E, and all marginal parts around the GMB main centre, parallel to the bathymetry as well as in seaward and landward directions, show a successively later time of initiation (Fig. 4). This non-linear extension from a centre points to a development of the GMB detached from the sediment source in the south.

The location of the GMB is related to the deposition-favouring environment in mid-shelf position in contrast to stronger hydrodynamic conditions on inner and outer shelf as previously stated by McCave (1972) and Hill et al. (2007). Hence, the shelf bathymetry and water depth, respectively, determine the position of mid-shelf mud deposition, and the coarsening of GMB sediments towards marginal parts is related to a stronger wave impact towards the inner shelf and intense currents on the outer shelf. The delayed onset of mud sedimentation in the south and generally coarser deposits (muddy fine sands) in the transitional area between GMB and Douro Mud Patch (DMP) should then be related to the elevated bathymetry of this area relative to the centre of the GMB leading to stronger hydrodynamic conditions. In contrast to the MMP, pronounced basement elevations are of minor influence on the GMB distribution.

The modern DMP centre is located slightly south of the study area. Sediment cores have been retrieved from the northern branch of the DMP and a radiocarbon date of 6500 cal yr BP was measured beneath

the DMP deposits in Profile H (Fig. 3H). Consequently, the extension of the DMP towards the north took place later than 6630–6460 cal yr BP. In addition, one single age of 495–677 cal yr BP was recently published by Burdloff et al. (2008) from the central part of the DMP. However, the age of the mud base is not known. Therefore, the spatial and temporal development of this depocentre remains speculative. Nevertheless, the detailed reconstruction of the MMP and the GMB evolution, as examined in this study, illustrates that the modern centres of fine deposition correspond well with the location of the initial onset of mud deposition. In analogy, the initiation of the DMP is suggested to have also started at the position of the modern fine centre and, therefore, clearly detached from the sediment source. This detached development is supported by the mechanism, which controls the DMP formation. The highest sedimentation rates of the DMP are found immediately east of rocky outcrops in about 100 m water depth. Hence, Drago et al. (1999) have suggested a relation of the DMP origin to the topographic relief which might provide a weak hydrodynamic environment on the one hand. On the other hand, these rocks lead to sediment trapping by acting as a barrier within the flow direction of the bottom nepheloid layer. Consequently, the sediments are hindered to move further offshore. Hence, these sediment-protecting and -catching morphological features represent the dominant parameter responsible for DMP deposition. Non-deposition of mud in front of the Douro River might be related to the absence of such pronounced morphological features favouring sediment bypassing and winnowing of fines by winter storms.

As a summary, the evolution of the NW Iberian shelf mud deposits has taken place in succeeding steps. This development is schematically reconstructed in Figure 5. First, the flooding of major estuaries during the late Pleistocene to early Holocene sea-level rise led to accumulation of fine sediments inside the river valleys (Fig. 5A). The export of terrigenous material to the shelf was then initiated by a shift in the balance between rate of sea-level rise and amount of terrigenous sediment supply. Hence, Holocene sea-level stabilisation and decreasing accommodation space within the Douro estuary gave rise to the deposition of larger amounts of fine sediments on the NW Iberian shelf at around 6000–5000 cal yr BP (Drago et al., 1999; Lantzsch et al., 2009; Fig. 5B). This initiated export of sediments provided the prerequisite for the sedimentation of mud on the shelf. Mid-shelf zones are characterised by deposition-favouring hydrodynamic conditions, and the occurrence of morphological features has additionally strongly controlled the location of the initial onset (Fig. 5B) and further extension of the mud depocentres (Fig. 5C). The relatively steady position of the mud deposits on the NW Iberian shelf suggests that no major changes of the general oceanographic setting took place during the Holocene. Consequently, the effect of the hydrodynamic regime and the influence of morphological features essentially control the general mud distribution. Within this framework, Holocene climatic changes cause internal grain-size fluctuations in the sediment cores (González-Álvarez et al., 2005; Martins et al., 2007; Bernárdez et al., 2008).

Conceptual subdivision of mid-shelf mud depocentres

The NW Iberian mud deposits represent mid-shelf mud belts according to the classification of McCave (1972). Nevertheless, these depocentres show considerable differences regarding their overall shaping and loci of formation. Those differences reveal the dominant forces controlling the mud-belt distribution. This study shows that reduced hydrodynamic conditions in mid-shelf environments are not the exclusive mechanism for the formation of mud belts, but that the role of morphological features might be of similar importance. Therefore, we propose a conceptual subdivision here concerning the characteristic distribution of mud deposition. Two main types are observed.

Type 1 mud deposits are attached to the associated sediment source and show an expansion from this sediment source towards the mid-shelf (Fig. 6). Additionally, sediment coarsens and thickness decreases with distance to the source. Type 1 can be further subdivided concerning the dominant forces, which control the distribution of fines. The common *Type 1a*, though not developed on the NW Iberian shelf, is closely related to the deposition-favouring hydrodynamic conditions in mid-shelf position (Fig. 6). In contrast to this mid-shelf mud, large areas of inner and outer shelf are typically characterised by sand draping due to the impact of storm wave activity and strong shelf currents (McCave, 1972). Nevertheless, the

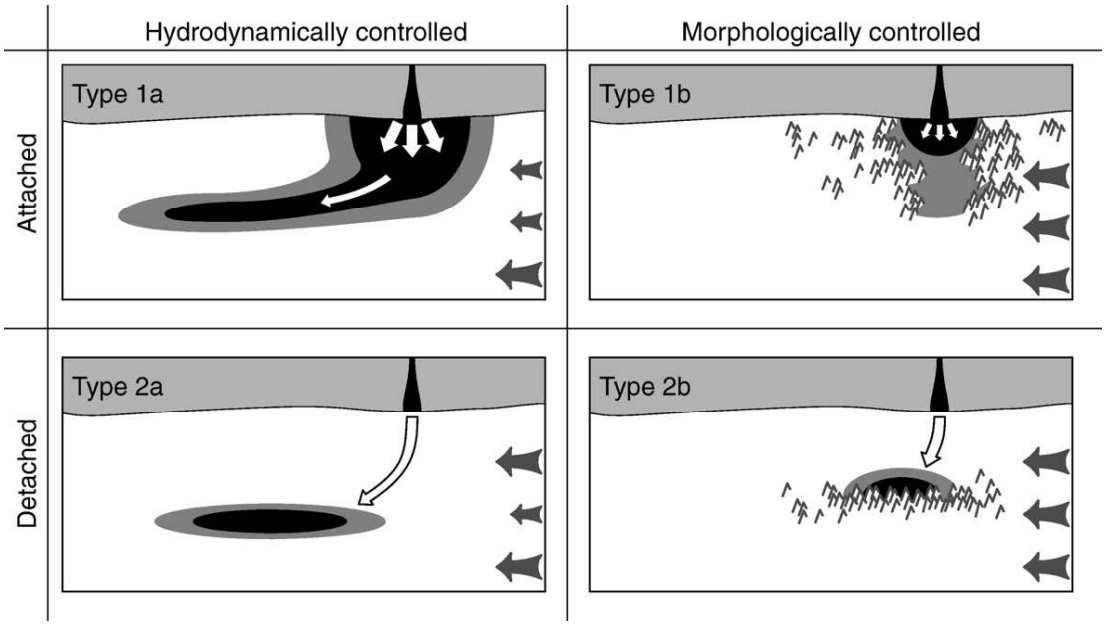

Figure 6. Types of Holocene mud depocentres. Type 1 is attached to the sediment source, Type 2 is detached. The sediment distribution of Types 1a and 2a is related to the deposition-favouring hydrodynamic conditions in mid-shelf position, whereas Types 1b and 2b are strongly controlled by the occurrence of morphological features. White arrows indicate sediment input and transport, grey arrows the strength of the hydrodynamic regime on inner, mid-, and outer shelf.

Type 1a depocentre is attached to the sediment source. Hence, either higher sediment input or a weak hydrodynamic regime close to the source favour mud deposition on the inner shelf. Therefore, this type does not occur under the low-accumulation, high-energy setting of the NW Iberian shelf. Examples for Type 1a are the mud belt off SW Africa (Meadows et al., 2002), the Gulf of Lions mud belt (Durrieu de Madron et al., 2000), and the Ebro mud belt (Díaz et al., 1996). In these cases, the sediment input by a major river leads to the development of a prodelta and of a connected adjacent, elongated mid-shelf mud belt. Hence, mud belts, which are in contact with a prodelta, are typical representatives of Type 1a. *Type 1b*, in contrast, shows an influence of morphological features (Fig. 6), as it is the case for the MMP. There, deposition is related to rocky outcrops on the inner and mid-shelf. Those elevations act as sediment traps and shelter the sediments against strong hydrodynamic conditions which prevent as well an extended deposition of mud on the shelf, as it is the case for Type 1a. By now, other examples for Type 1b from literature are, to our knowledge, not known, what might be due to generally few publications dealing with such small-scale mud entrapments. In addition, Type 1b represents a special morphological setting, which should be restricted to high-energy, low-accumulation shelves. An absence of such morphological barriers would cause non-deposition and erosion of fines.

The most characteristic feature of *Type 2* mud deposits is their development detached from the sediment source (Fig. 6). Those areas are characterised by extensive sand draping on inner and outer shelf due to strong hydrodynamic conditions. Therefore, this type should be typical for low-accumulation and high-energy shelf regimes. As for Type 1, a further subdivision can be applied. The distribution of *Type 2a* mud belts is strongly dependent on weak hydrodynamic conditions, which are usually located in mid-shelf position (Fig. 6). On inner and outer shelf, the impact of the wave base and strong currents, respectively, prevents a deposition of fines. Therefore, Type 2a represents the textbook-style example of a mid-shelf mud belt as defined by McCave (1972). The GMB shows all of these characteristics and various other examples fulfilling these criteria have been reported in literature such as the mud belt off the Russian River in northern California (Demirpolat, 1991), the Grande Vasiere Mud Belt in the Bay of Biscay (Lesueur et al., 2001), and the Huksan Mud Belt in the southeastern Yellow Sea (Lee and Chu, 2001). In all these cases, pronounced morphological features are either absent or of minor importance for the distribution of these mud deposits. This morphological influence becomes the dominant control in *Type 2b* mud belts, which represents, again, a special depositional setting on a high-energy, low-accumulation shelf system. Those mud deposits are formed due to the occurrence of morphological features (Fig. 6). The water depth is of subordinate importance and Type 2b mud belts might occur divergently from the optimal water depth that would be characterised by the weakest hydrodynamic conditions in case of an absence of morphological elevations. The DMP represents a well-suited example for Type 2b. However, examples from literature for the influence of morphological features on the mud depocentre distribution are scarce. Edwards (2002) reported north of Monterey Bay (California) topographic highs on the mid-shelf to act as barriers for fine sediments and to lead to sediment ponding. Jouanneau et al. (2008) observed sediment trapping related to rocky outcrops on the Basque shelf (Bay of Biscay). Nevertheless, the influence of these morphological features is of minor importance for the general sediment distribution, and a dominant influence such as reported by Drago et al. (1999) for the NW Iberian shelf system is not present in those shelf settings.

Conclusions

The Holocene mud deposits on the NW Iberian shelf provide a new view on the evolution of mid-shelf mud depocentres in high-energy, low-accumulation sedimentary shelf regimes. The observed differential lateral onset and dynamic of expansion reveal exemplarily the major controls on the development of such mud depocentres.

The deceleration in early Holocene sea-level rise was conducive to the deposition of fines on the shelf. This initial mud deposition is marked by a transition of fine sands towards mud in sediment cores from the central Muros Mud Patch between 9480 and 4135 cal yr BP and from the Galicia Mud Belt between 8370 and 5249 cal yr BP. The detailed analysis of the mud-depocentre evolution reveals that the Galicia Mud Belt started to develop in a main centre detached from the coastal source of original sediment supply. The succeeding development of this mud belt was surprisingly non-linear. The expansion towards the sediment source as well as towards the north following the current direction is contrasting the linear development of the Muros Mud Patch which took indeed place from the sediment source towards the mid-shelf as generally expected for shelf mud deposits.

The location of the initial onset of these depocentres and their further expansion was most probably determined by the deposition-favouring hydrodynamic conditions in mid-shelf position, and the occurrence of morphological features, which act as sediment traps.

Following these characteristics, two main types of fine depocentres can be defined. Type 1 is attached to the associated sediment source and shows an expansion from this source towards the mid-shelf. The distribution of Type 1a is dominantly controlled by the deposition-favouring hydrodynamic conditions in mid-shelf position. In contrast, the position of Type 1b deposits is strongly influenced by the occurrence of morphological features such as local elevations in basement, which trap sediments by sheltering the deposits against stronger hydrodynamic conditions.

Type 2 mud deposits emplace in detachment from the sediment source. Reason is either low sediment input or strong hydrodynamic conditions along inner shelf and shore zone. This detached evolution is proposed to be a characteristic feature of low-accumulation sedimentary shelf systems in contrast to input-dominated shelves where excessive supply overshadows the effect of other forces. Similar to Type 1, Type 2 can be further subdivided. Whereas the distribution of Type 2a is dominantly controlled by the hydrodynamic conditions related to water depth, Type 2b is largely influenced by defined morphological features.

Further studies should focus on the initial onset and development of other mud belts to get a deeper insight into the evolution of such depocentres and further support the proposed conceptual subdivision by a well-dated stratigraphy.

Acknowledgments

Special thanks go to Sebastian Krastel and Hannes Riepshoff for their contribution to this project. We also wish to thank Captain Michael Schneider and his complete crew on RV POSEIDON for their outstanding support. We are thankful to Rüdiger Henrich for providing the opportunity to conduct this study. This work was funded through DFG-Research Center/Excellence Cluster “The Ocean in the Earth System“.

References

Álvarez-Salgado, X.A., Gago, J., Míguez, B.M., Gilcoto, M., Pérez, F.F., 2000. Surface waters of the NW Iberian margin: upwelling on the shelf versus outwelling of upwelled waters from the Rías Baixas. Estuarine, Coastal and Shelf Science 51 (6), 821–837.

Araújo, M.F., Jouanneau, J.M., Valério, P., Barbosa, T., Gouveia, A., Weber, O., Oliveira, A., Rodrigues, A., Dias, J.M.A., 2002. Geochemical tracers of northern Portuguese estuarine sediments on the shelf. Progress in Oceanography 52 (2–4), 277–297.

Bard, E., Arnold, M., Hamelin, B., Tisnerat-Laborde, N., Cabioch, G., 1998. Radiocarbon calibration by means of mass spectrometric Th-230/U-234 and C-14 ages of corals: an updated database including samples from Barbados, Mururoa and Tahiti. Radiocarbon 40 (3), 1085–1092.

Bernárdez, P., González-Álvarez, R., Francés, G., Prego, R., Bárcena, M.A., Romero, O.E., 2008. Late Holocene history of the rainfall in the NW Iberian peninsula — evidence from a marine record. Journal of Marine Systems 72 (1–4), 366–382.
Blair, T.C., McPherson, J.G., 1999. Grain-size and textural classification of coarse sedimentary particles. Journal of Sedimentary Research 69 (1), 6–19.
Boski, T., Moura, D., Veiga-Pires, C., Camacho, S., Duarte, D., Scott, D.B., Fernandes, S.G., 2002. Postglacial sea-level rise and sedimentary response in the Guadiana Estuary, Portugal/Spain border. Sedimentary Geology 150 (1–2), 103–122.
Burdloff, D., Araújo, M.F., Jouanneau, J.M., Mendes, I., Monge Soares, A.M., Dias, J.M.A., 2008. Sources of organic carbon in the Portuguese continental shelf sediments during the Holocene period. Applied Geochemistry 23 (10), 2857–2870.
Dabrio, C.J., Zazo, C., Goy, J.L., Sierro, F.J., Borja, F., Lario, J., González, J.A., Flores, J.A., 2000. Depositional history of estuarine infill during the last postglacial transgression (Gulf of Cadiz, Southern Spain). Marine Geology 162 (2–4), 381–404.
Demirpolat, S., 1991. Surface and near-surface sediments from the continental shelf off the Russian River, Northern California. Marine Geology 99 (1–2), 163–173.
Dias, J.M.A., Nittrouer, C.A., 1984. Continental shelf sediments of northern Portugal. Continental Shelf Research 3 (2), 147–165.
Dias, J.M.A., Gonzalez, R., Garcia, C., Diaz-del-Rio, V., 2002. Sediment distribution patterns on the Galicia-Minho continental shelf. Progress in Oceanography 52 (2–4), 215–231.
Díaz, J., Palanques, A., Nelson, C.H., Guillén, J., 1996. Morpho-structure and sedimentology of the Holocene Ebro prodelta mud belt (northwestern Mediterranean Sea). Continental Shelf Research 16 (4), 435–456.
Drago, T., Araújo, F., Valério, P., Weber, O., Jouanneau, J.M., 1999. Geomorphological control of fine sedimentation on the northern Portuguese shelf. Boletín Instituto Español de Oceanografía 15 (1–4), 111–122.
Drago, T., Freitas, C., Rocha, F., Moreno, J., Cachao, M., Naughton, F., Fradique, C., Araujo, F., Silveira, T., Oliveira, A., Cascalho, J., Fatela, F., 2006. Paleoenvironmental evolution of estuarine systems during the last 14,000 years — the case of Douro estuary (NW Portugal). Journal of Coastal Research 1, 186–192.
Durrieu de Madron, X., Abassi, A., Heussner, S., Monaco, A., Aloisi, J.C., Radakovitch, O., Giresse, P., Buscail, R., Kerherve, P., 2000. Particulate matter and organic carbon budgets for the Gulf of Lions (NW Mediterranean). Oceanologica Acta 23 (6), 717–730.
Edwards, B.D., 2002. Variations in sediment texture on the northern Monterey Bay National Marine Sanctuary continental shelf. Marine Geology 181 (1–3), 83–100.
Goff, J.A., Austin, J.J.A., Gulick, S., Nordfjord, S., Christensen, B., Sommerfield, C., Olson, H., Alexander, C., 2005. Recent and modern marine erosion on the New Jersey outer shelf. Marine Geology 216 (4), 275–296.
González-Álvarez, R., Bernárdez, P., Pena, L.D., Francés, G., Prego, R., Diz, P., Vilas, F., 2005. Paleoclimatic evolution of the Galician continental shelf (NW of Spain) during the last 3000 years: from a storm regime to present conditions. Journal of Marine Systems 54 (1–4), 245–260.
Hanebuth, T., Bender, V., Bujan, S., Elvert, M., Frederichs, T., Kockisch, B., Krastel-Gudegast, S., Lantzsch, H., Mena Rodríguez, Á., Schmidt, F., Strozyk, F., Wagner Friedrichs, M., 2007. Report and first results of the Poseidon cruise P342 GALIOMAR, Vigo — Lisboa (Portugal), August 19th–September 06th, 2006. Distribution pattern, residence times and export of sediments on the Pleistocene/Holocene Galician Shelf (NW Iberian Peninsula). Berichte, Fachbereich Geowissenschaften, University of Bremen 255, 203 pp.
Hanebuth, T.J.J., Henrich, R., 2009. Recurrent decadal-scale dust events over Holocene western Africa and their control on canyon turbidite activity (Mauritania). Quaternary Science Reviews 28 (3–4), 261–270.
Hanebuth, T.J.J., Lantzsch, H., 2008. A Late Quaternary sedimentary shelf system under hyperarid conditions: unravelling climatic, oceanographic and sea-level controls (Golfe d'Arguin, Mauritania, NW Africa). Marine Geology 256 (1–4), 77–89.
Hill, P.S., Fox, J.M., Crockett, J.S., Curran, K.J., Friedrichs, C.T., Rockwell Geyer, W., Milligan, T.G., Ogston, A.S., Puig, P., Scully, M.E., Traykovski, P.A., Wheatcroft, R.A., 2007. Sediment delivery to the seabed on continental margins. In: Nittrouer, C.A., Austin, J.A., Field, M.E., Kravitz, J.H., Syvitski, J.P.M., Wiberg, P.L. (Eds.), Continental Margin Sedimentation — From Sediment Transport to Sequence Stratigraphy. Blackwell Publishing, International Association of Sedimentologists Special Publication 37, Malden, Oxford, Carlton, pp. 49–98.
Jouanneau, J.M., Weber, O., Drago, T., Rodrigues, A., Oliveira, A., Dias, J.M.A., Garcia, C., Schmidt, S., Reyss, J.L., 2002. Recent sedimentation and sedimentary budgets on the western Iberian shelf. Progress in Oceanography 52 (2–4), 261–275.
Jouanneau, J.M., Weber, O., Champilou, N., Cirac, P., Muxika, I., Borja, A., Pascual, A., Rodríguez-Lázaro, J., Donard, O., 2008. Recent sedimentary study of the shelf of the Basque country. Journal of Marine Systems 72 (1–4), 397–406.
Lantzsch, H., Hanebuth, T.J.J., Bender, V.B., Krastel, S., 2009. Sedimentary architecture of a low-accumulation shelf since the Late Pleistocene (NW Iberia). Marine Geology 259 (1–4), 47–58.
Lee, H.J., Chu, Y.S., 2001. Origin of inner-shelf mud deposit in the southeastern Yellow Sea: Huksan Mud Belt. Journal of Sedimentary Research 71 (1), 144–154.
Lesueur, P., Jouanneau, J.M., Boust, D., Tastet, J.P., Weber, O., 2001. Sedimentation rates and fluxes in the continental shelf mud fields in the Bay of Biscay (France). Continental Shelf Research 21 (13–14), 1383–1401.
Long, A., 2001. Mid-Holocene sea-level change and coastal evolution. Progress in Physical Geography 25 (3), 399–408.
Martins, V., Dubert, J., Jouanneau, J.-M., Weber, O., da Silva, E.F., Patinha, C., Alveirinho Dias, J.M., Rocha, F., 2007. A multiproxy approach of the Holocene evolution of shelf-slope circulation on the NW Iberian Continental Shelf. Marine Geology 239 (1–2), 1–18.
McCave, I.N., 1972. Transport and escape of fine-grained sediment from shelf areas. In: Swift, D.J.P., Duane, D.B., Pilkey, O.H. (Eds.), Shelf Sediment Transport: Process and Pattern. Dowden, Hutchinson and Ross, Inc., Stroudsburg, pp. 225–244.
Meadows, M.E., Rogers, J., Lee-Thorp, J.A., Bateman, M.D., Dingle, R.V., 2002. Holocene geochronology of a continental-shelf mudbelt off southwestern Africa. Holocene 12 (1), 59–67.
Naughton, F., Goñi, M.F.S., Drago, T., Freitas, M.C., Oliveira, A., 2007a. Holocene changes in the Douro estuary (Northwestern Iberia). Journal of Coastal Research 23 (3), 711–720.
Naughton, F., Bourillet, J.F., Fernanda, M., Goñi, S., Turon, J.L., Jouanneau, J.M., 2007b. Long-term and millennial-scale climate variability in northwestern France during the last 8850 years. Holocene 17 (7), 939–953.
Odin, G.S., Lamboy, M., 1988. Glaucony from the Margin off Northwestern Spain. In: Odin, G.S. (Ed.), Green Marine Clays. Developments in Sedimentology, 45. Elsevier, Amsterdam, Oxford, New York, pp. 249–275.
Oliveira, A., Rocha, F., Rodrigues, A., Jouanneau, J., Dias, A., Weber, O., Gomes, C., 2002. Clay minerals from the sedimentary cover from the Northwest Iberian shelf. Progress in Oceanography 52 (2–4), 233–247.
Otero, P., Ruiz-Villarreal, M., Peliz, A., 2008. Variability of river plumes off Northwest Iberia in response to wind events. Journal of Marine Systems 72 (1–4), 238–255.
Rey Salgado, J., 1993. Relación morfosedimentaria entre la plataforma continental de Galicia y las Rías Bajas y su evolución durante el Cuaternario. Publicaciones Especiales, Instituto Español de Oceanografía 17, 1–233.
Sommerfield, C.K., Wheatcroft, R.A., 2007. Late Holocene sediment accumulation on the northern California shelf: oceanic, fluvial, and anthropogenic influences. Geological Society of America Bulletin 119 (9–10), 1120–1134.
Stuiver, M., Reimer, P.J., Bard, E., Beck, J.W., Burr, G.S., Hughen, K.A., Kromer, B., McCormac, G., Van der Plicht, J., Spurk, M., 1998. INTCAL98 radiocarbon age calibration, 24,000–0 cal BP. Radiocarbon 40 (3), 1041–1083.
Vis, G.-J., Kasse, C., Vandenberghe, J., 2008. Late Pleistocene and Holocene palaeogeography of the Lower Tagus Valley (Portugal): effects of relative sea level, valley morphology and sediment supply. Quaternary Science Reviews 27 (17–18), 1682–1709.
Vitorino, J., Oliveira, A., Jouanneau, J.M., Drago, T., 2002. Winter dynamics on the northern Portuguese shelf. Part 2: bottom boundary layers and sediment dispersal. Progress in Oceanography 52 (2–4), 155–170.

6. Control of sediment supply, palaeoceanography and morphology on late Quaternary sediment dynamics at the Galician continental slope

Vera B. Bender [a, b], Till J. J. Hanebuth [b], Anxo Mena [c], Karl-Heinz Baumann [a], Guillermo Francés [c], Tilo von Dobeneck [a]

[a] *MARUM – Center for Marine Environmental Sciences, University of Bremen, P.O. Box 330 440, 28334 Bremen, Germany.*

[b] *Faculty of Geosciences, University of Bremen, Klagenfurter Strasse, 28359 Bremen, Germany.*

[c] *Dpt. Xeociencias Mariñas e. O. T., Fac. Ciencias do Mar, Universidade de Vigo, CUVI, 36310 Vigo, España.*

Geo-Marine Letters **32**, 313–335, doi: 10.1007/s00367-012-0282-2

Geo-Mar Lett (2012) 32:313–335
DOI 10.1007/s00367-012-0282-2

ORIGINAL

Control of sediment supply, palaeoceanography and morphology on late Quaternary sediment dynamics at the Galician continental slope

Vera B. Bender · Till J. J. Hanebuth · Anxo Mena · Karl-Heinz Baumann · Guillermo Francés · Tilo von Dobeneck

Received: 18 January 2012 / Accepted: 15 February 2012 / Published online: 11 March 2012

Abstract Controls of sediment dynamics at the Galician continental slope (NW Iberia) during the past 30 ka were reconstructed from three new gravity cores (GeoB11035-1, 130206–1, 13071–1) based on sedimentological (e.g. sortable silt, IRD), micropalaeontological (e.g. coccoliths), geochemical (AMS ^{14}C, XRF) and geophysical (e.g. magnetic susceptibility) diagnostics. The data are consistent with existing regional knowledge that, during marine isotope stages 3–1, variations in detrital input, marine productivity and sea level were the essential drivers of sediment availability on the slope, whereas deep-water current velocities controlled sediment deposition: (1) the period prior to 30 cal ka BP is characterized by minor but systematic variations in various proxies which can be associated with D-O cycles; (2) between 30 and 18 cal ka BP, high detrital input and steady slope-parallel currents led to constant sedimentation; (3) from the LGM until 10 cal ka BP, the shelf-transgressive sea-level rise increased the detrital particle flux; sedimentation was influenced by significantly enhanced deep-water circulation during the Bølling/Allerød, and subsequent slowing during the Younger Dryas; (4) an abrupt and lasting change to hemipelagic sedimentation at ca. 10 cal ka BP was probably due to Holocene warming and decelerated transgression; (5) after 5 cal ka BP, additional input of detrital material to the slope is plausibly linked to the evolution of fine-grained depocentres on the Galician shelf, this being the first report of this close shelf–slope sedimentary linkage off NW Iberia. Furthermore, there is novel evidence of the nowadays strong outer shelf Iberian Poleward Current becoming established at about 15.5 cal ka BP. The data also demonstrate that small-scale morphologic features and local pathways of sediment export from the neighbouring shelf play an important role for sediment distribution on the NW Iberian slope, including a hitherto unknown sediment conduit off the Ría de Arousa. By implication, the impact of local morphology on along- and down-slope sediment dynamics is more complex than commonly considered, and deserves future attention.

Electronic supplementary material The online version of this article (doi:10.1007/s00367-012-0282-2) contains supplementary material, which is available to authorized users.

V. B. Bender (✉) · T. J. J. Hanebuth
MARUM – Center for Marine Environmental Sciences,
University of Bremen,
P.O. Box 330 440, 28334 Bremen, Germany
e-mail: vbender@uni-bremen.de

A. Mena · G. Francés
Departamento de Xeociencias Mariñas e O.T.,
Facultad de Ciencias do Mar, Universidade de Vigo,
36310 CUVI, Vigo, Spain

K.-H. Baumann · T. von Dobeneck
Faculty of Geosciences, University of Bremen,
P.O. Box 330 440, 28334 Bremen, Germany

Introduction

At centennial to millennial timescales, the essential drivers of sedimentation along passive continental margins are (1) the sources and magnitude of detrital input with (2) primary production providing the basic 'ingredients', whereas (3) oceanographic (especially intermediate- and deep-water currents) and (4) sea-level conditions regulate transport and depositional processes. These four elements are ultimately controlled by climate at various spatiotemporal scales.

Within the framework of the European OMEX (Ocean Margin EXchange) projects, the NW Iberian margin has

been well studied in terms of modern oceanography and sedimentation (see introductory overviews in van Weering et al. 1998, and van Weering and McCave 2002). Indeed, the last decade has seen a considerable advance in knowledge on the late Pleistocene palaeoceanographic history of the western Iberian margin as a whole (e.g. Schönfeld and Zahn 2000; Thomson et al. 2000; Eynaud et al. 2009; Salgueiro et al. 2010). This includes a series of abrupt climate shifts during marine isotope stage (MIS) 3 (e.g. Shackleton et al. 2000; de Abreu et al. 2003; Schönfeld et al. 2003), known from Greenland ice cores as Dansgaard-Oeschger (D-O) cycles (e.g. Dansgaard et al. 1993; Grootes et al. 1993). Moreover, phases of extensive iceberg discharge into the North Atlantic known as Heinrich (H) events (Heinrich 1988) have been tracked by their ice-rafted debris (IRD) as far as the southern Portuguese margin (Lebreiro et al. 1996). On the other hand, comparatively few studies have focused on late Pleistocene sedimentary processes and products on the western slope of the Iberian margin (e.g. Baas et al. 1997; Hall and McCave 2000; Lebreiro et al. 2009), and even fewer on the morphologically complex Galician continental slope sector (e.g. Hall and McCave 2000).

It appears natural to regard the continental slope as an open system, strongly affected by the evolution of the adjacent shelf. Surprisingly, these two adjoining sedimentary environments are commonly studied separately. The late Quaternary deglacial sedimentary evolution of the NW Iberian continental shelf, including its late Holocene muddy depocentre, is very well documented (e.g. González-Álvarez et al. 2005; Martins et al. 2007; Lantzsch et al. 2009a, b, 2010). Within this context, the present study explores the linkage of sediment dynamics on the Galician slope with the last deglacial shelf evolution in this key eastern Atlantic boundary region.

The aim is to unravel the late Quaternary interplay of local slope morphology as well as regional oceanography and sea-level variations as drivers of sediment dynamics on the NW Iberian slope. For this purpose, sedimentological (grain-size distribution, carbonate content, X-radiographies and IRD counts), micropalaeontological (coccolith assemblages, *Neogloboquadrina pachyderma* (sin) counts), geochemical (AMS ^{14}C dating, XRF elemental scans) and geophysical (magnetic susceptibility, seismic reflection profiles) diagnostics were investigated in three new gravity cores from the Galician slope.

Physical setting

The NW Iberian continental margin off Galicia presents a diverse and complex morphology (see Fig. 1a). Compared to the Portuguese sector, the coast is rougher and rockier. The mostly crystalline Palaeozoic and Precambrian littoral is cut by the deep 'Rías Baixas', old Tertiary river valleys drowned during the last sea-level rise (Rey Salgado 1993; Oliveira et al. 2002a). The adjoining narrow shelf (maximum width of 40 km off the Miño River) has a series of rocky outcrops in its inner and outer sectors (Dias et al. 2002). Another prominent feature is the Galician mud belt (GMB), a fine-grained mid-shelf depocentre of fluvially derived muds (e.g. Lantzsch et al. 2009a). The inner and outer shelf as well as the shelf break are covered with sandy, partly glauconitic sediments (Dias et al. 2002; Lantzsch et al. 2009b). The shelf break is generally reached at 160–180 m water depth.

A very steep and irregular slope extends to about 2,000 m water depth (Lallemand et al. 1985), its lower sector interrupted by several structural highs. Further west there is the Galicia Bank, a flat-topped submarine plateau at <700 m water depth. The Galician shelf and Galicia Bank enclose a <3,000 m deep and ±50 km wide trough, the Galician interior basin (Fig. 1a). Abyssal depths are reached only north, west and south of the Galicia Bank (Biscay abyssal plain to the N, Iberian abyssal plain to the W and S).

Intermediate- and deep-water circulation is constrained by the complex bathymetry. This includes the Eastern North Atlantic Central Water of subtropical ($ENACW_{ST}$; <300 m water depth) as well as of subpolar ($ENACW_{SP}$; >450 m water depth) origin, the Mediterranean Water (MW; ~800–1,100 m), the Deep Intermediate Water (DIW; ~1,490–2,150 m water depth, mixed with Labrador Sea Water), the Lower North Atlantic Deep Water (LNADW; ~2,150–3,450 m water depth), and the Lower Deep Water (LDW; >3,450 m water depth) containing some fraction of Antarctic Bottom Water (Mazé et al. 1997; Varela et al. 2005). Warm, saline $ENACW_{ST}$ and cooler, less dense $ENACW_{SP}$ coalesce off Cape Finisterre, forming the Finisterre Front (Fig. 1b).

Surface water circulation is controlled mainly by the North Atlantic subtropical gyre in combination with the seasonally reversing wind regimes. As the easternmost branch of the subtropical gyre, the Portugal Current flows equatorwards (Varela et al. 2005; Fig. 1b). The emergence of an associated coastal current, the Portugal Coastal Current (PCC) flowing southwards at about 10°W, appears to be linked to upwelling caused by the N–NW summer wind regime (April–August). The PCC carries cold and nutrient-rich $ENACW_{SP}$ to offshore Galicia. During the winter season (September–March), SW winds prevail and PCC flow is negligible (Álvarez-Salgado et al. 2003). Over the shelf and upper slope, a countercurrent called the Iberian Poleward Current (IPC) flows northwards, transporting mainly $ENACW_{ST}$. IPC appearance has formerly been linked to winter conditions (Haynes and Barton 1990) but newer observations by Fiúza et al. (1998) and modelling results of Peliz et al. (2003a, b) suggest that wind stress has a relatively low influence of only 20% compared to that of

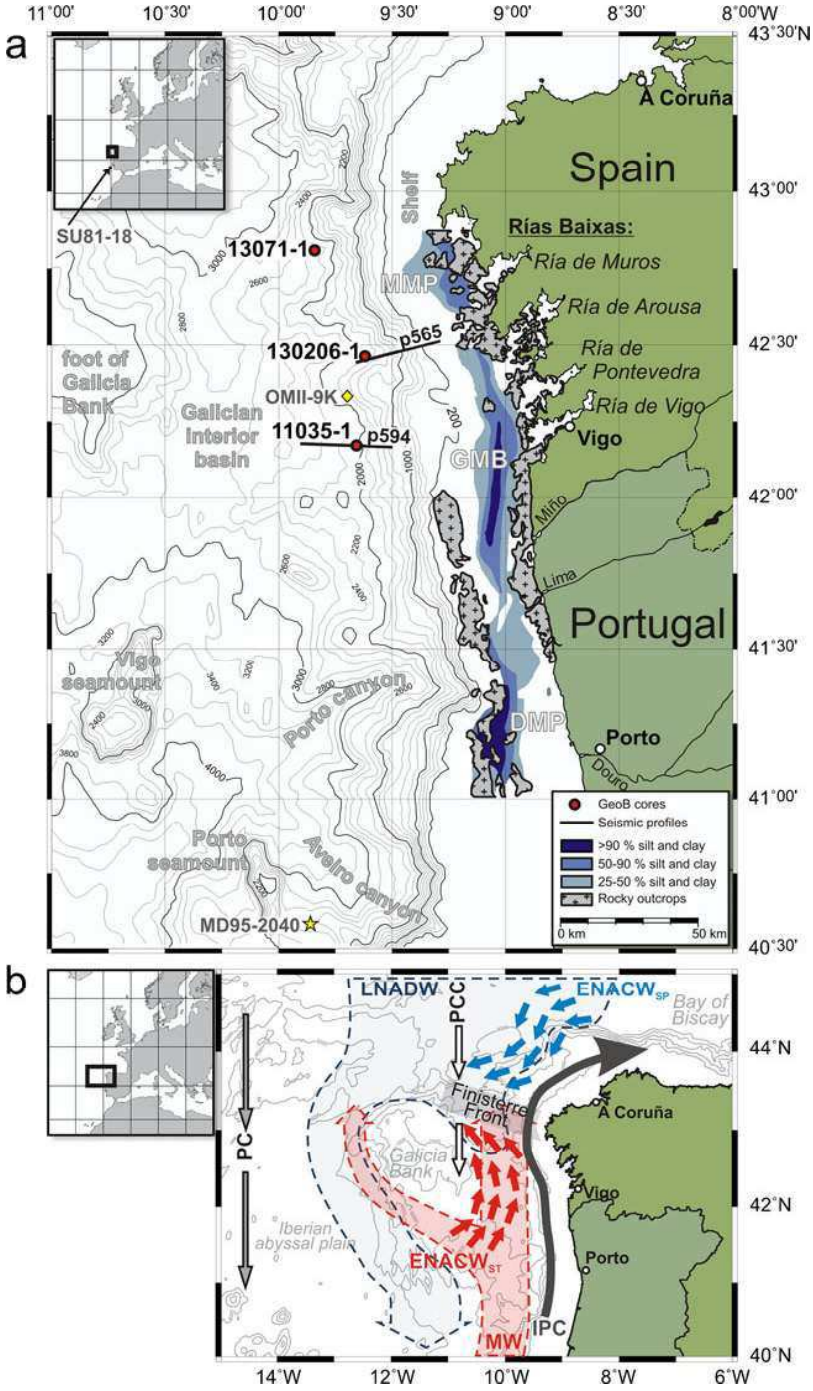

Fig. 1 The NW Iberian continental margin. **a** Map of bathymetric and lithologic features, as well as locations of the three GeoB cores (present study), cores MD95-2040 (e.g. de Abreu et al. 2003) and OMII-9K (Hall and McCave 2000), and SU81-18 (Bard et al. 2000) south of the study area (*inset*). Shelf geology modified from Dias et al. (2002) and Lantzsch et al. (2009a). *MMP* Muros mud patch, *GMB* Galician mud belt, *DMP* Douro mud patch. **b** Main circulation patterns (for data sources, see main text; isobath interval 1,000 m; 200 m indicated in **a**), showing surface circulation (*solid arrows*) and deep-water masses. Note that the latter are not able to pass over the Galician interior basin. *PC* Portugal Current, *PCC* Portugal Coastal Current, *IPC* Iberian Poleward Current, *MW* Mediterranean Water, *LNADW* Lower North Atlantic Deep Water

interactions between meridional density gradients and topography. Below the two species of ENACW, the MW (also known as Mediterranean Outflow Water) flows northwards with two distinct cores at ~800 and ~1,100 m water depth (Iorga and Lozier 1999; Varela et al. 2005). In CTD data, the lower boundary of the MW with the underlying DIW is very gradual and difficult to constrain. CTD data from the world ocean circulation experiment (eWOCE, www.ewoce.org) indicate that the Galician interior basin, with its <3,000 m water depth, acts as a structural barrier for deeper northern and southern water masses like the LNADW and LDW respectively (Fig. 1b).

Not much is known regarding past surface and subsurface circulation patterns off Galicia. Since the modern circulation is driven mainly by the North Atlantic subtropical gyre, glacial surface circulation should have been somewhat

different, with the polar front reaching as far south as Portugal during extreme cold events (e.g. Younger Dryas, Heinrich events; Eynaud et al. 2009). Indeed, some information exists on MW variability since the last glacial maximum (LGM) on the western and southern Portuguese margin and in the Gulf of Cadiz (Schönfeld and Zahn 2000; Rogerson et al. 2005; Voelker et al. 2006). Palaeoceanographic reconstructions based on, for example, benthic foraminifer and grain-size proxies revealed that the MW was denser and flowing at greater depths (~2,000 m) during the last glacial (Schönfeld and Zahn 2000; Rogerson et al. 2005), and also during cold periods like Heinrich events and D-O stadials (Llave et al. 2006; Voelker et al. 2006). However, it appears not to have reached further north than 39°N in its glacial mode (Schönfeld and Zahn 2000). The modern, twin-core MW flow pattern over the Galician interior basin was established at ca. 7,500 uncalibrated ^{14}C years BP (~8.3 cal ka BP; Schönfeld and Zahn 2000).

Modern Galician slope sedimentation is dominated by biogenic production in surface nepheloid layers and settling from intermediate nepheloid layers at the ENACW level (~450 m, Varela et al. 2005; Hall et al. 2000; McCave and Hall 2002). The existence of intermediate nepheloid layers is strongly linked to bottom nepheloid layer formation on the Galician shelf and upper slope, in turn coupled to downwelling conditions typically occurring in winter (Dias et al. 2002; Oliveira et al. 2002b; Vitorino et al. 2002). As a consequence, the uppermost slope and shelf break are today regions of resuspension and winnowing—thus, non-deposition (Hall et al. 2000; McCave and Hall 2002)—contrasting with hemipelagic sedimentation on the lower slope. Further south along the Portuguese margin, sediment supply by turbidity currents through major canyons (e.g. Nazaré Canyon; Milkert et al. 1996) played an additional and significant role during the late Pleistocene (Baas et al. 1997). Similar sediment conduits may exist on the Galician continental slope but to date these have not been reported in the literature. Most recently, Hernández-Molina et al. (2011) pointed out that water-mass flow patterns around Iberia have high potential for contouritic sediment transport and deposition, and that the role of such has been significantly underestimated in the past.

The late Pleistocene sedimentary history of the Galician continental slope is only sparsely known. In general during glacial times and associated sea-level lowstands, fluvial sediment supply to the shelf break and slope was probably more direct and therefore enhanced (Weaver et al. 2000; Nittrouer et al. 2007). Higher mass accumulation rates found in OMEX core OMII-9K off the Ría de Pontevedra (see Fig. 1a) during MIS 2 support this notion (Hall and McCave 2000). Palaeocurrent reconstructions from the same core showed that slow bottom flow, driven by weaker thermohaline circulation, and subsequent deposition of finer material apparently were persistent features during colder periods (e.g. Younger Dryas, YD) and, vice versa, faster flow a characteristic of warmer periods (e.g. Bølling/Allerød, B/A; Hall and McCave 2000). For the Portuguese slope, Baas et al. (1997) report that hemipelagic sedimentation prevailed during the Holocene, whereas in earlier times there was an additional input of terrigenous material from local and distant sources by low-concentration turbidity currents, contour currents and icebergs (Heinrich layers) under the control of sea level and climate. Such processes are far from being understood in equivalent detail for the Galician slope. In fact, core OMII-9K is to date the only sedimentological record from this highly complex margin sector, where sedimentary patterns are very likely to be strongly influenced by the regional and local morphology.

Materials and methods

Sediment core GeoB11035-1 (42°10.3′N, 09°39.47′W, 2,045 m water depth) was recovered during the German R/V *Poseidon* expedition 342 in 2006 from about 60 km off the Ría de Vigo. Sediment cores GeoB130206-1 (42°27.51′N, 09°37.19′W) and GeoB13071-1 (42°48.49′N, 09°50.55′W) were recovered during R/V *Poseidon* expedition 366/3 in 2008. Site 130206 is at 1,704 m water depth about 50 km off the Ría de Arousa, and site 13071 at 2,274 m water depth about 50 km off Cape Finisterre. Sites 11035 and 130206 are today under DIW influence, whereas site 13071 is some 100 m deeper and today situated at the DIW–LNADW boundary. As all sites lie well above the modern (4,500 m) and glacial (4,200 m) lysoclines (Crowley 1983), any effects of carbonate dissolution are negligible.

Seismic reflection lines across sites 11035 and 130206 were shot during R/V *Poseidon* expedition 342. This was by means of a Mini-GI-Gun (2×0.25 l, 50–500 Hz, ~140–150 bar) and a 100-m-long 16-channel streamer (eight hydrophones per group, 6.25 m channel distance).

All cores were investigated by non-destructive logging methods before sub-sampling. Magnetic susceptibility and X-ray fluorescence (XRF) were measured on the undisturbed archive halves of all three cores. Magnetic susceptibility was logged using an automated Bartington® MS2F sensor at 1 cm spacing. XRF scans were performed with an AVAATECH XRF core scanner at 10 kV for the light elements Al to Fe (all three cores) and, additionally, at 30 kV for the heavy elements Rb to Ba (GeoB11035-1 only) at intervals of 2 cm (GeoB11035-1) and 1 cm (GeoB130206-1 and GeoB13071-1).

For radiographic assessments, sediment slabs of 25×10×1 cm were cut from the entire lengths of all cores. The slab samples were exposed for 210 s at 48 kV in a Faxitron 43855A X-ray cabinet, and developed negatives were digitized at 600 dpi.

Total organic carbon (TOC) was quantified on 10 mg of pulverized bulk sub-samples with a LECO CS-200 system. Total carbon (TC) was analyzed in a separate measurement on 25 mg of the pulverized bulk sub-samples with a VarioELIII elemental analyzer in CHN mode. Carbonate contents were calculated from the difference of TC and TOC.

Sub-samples for grain-size analyses were collected every 10 cm and washed through a 63 μm mesh sieve to separate the sand from the mud fractions. Each sand fraction was subsequently sub-fractionated into very fine (63–125 μm), fine (125–250 μm), medium (250–500 μm), coarse (500–1,000 μm) and very coarse sand (>1,000 μm; Blair and McPherson 1999) by means of a Fritsch Analysette Sonic Sifter. Particles larger than 2 mm (gravel) were never present.

Grain-size distributions of the mud fractions (<63 μm) were analyzed by means of a Micromeritics SediGraph 5100, using one series of non-treated aliquots and another series of decarbonated aliquots (acid leaching of $CaCO_3$ with 12.5% HCl) to obtain bulk and terrigenous mud grain-size distributions respectively. Based on McCave and Hall (2006), sortable silt (terrigenous 10–63 μm fraction) mean grain size ($\overline{SS}$) and content (dry wt%, SS%) were calculated as proxies for bottom current flow speed. More recently, Law et al. (2008) suggested to shift the lower cut-off diameter for sortable silt in cohesive sediments (>7.5% clay, <4 μm) from 10 μm up to 16 μm, whereby the 10–16 μm fraction may be less affected by current sorting than previously thought. However, more studies would be needed to confirm these results and, therefore, the established 10 μm lower boundary for sortable silt in deep-sea settings originally proposed by McCave et al. (1995) was retained in the present study.

Coccolith abundance and species diversity of core GeoB11035-1 were analyzed at 5–10 cm intervals, sample preparation being according to the combined dilution/filtering technique described by Andruleit (1996). Between 50 and 100 mg dry bulk sediment was brought into suspension using tap water, and insonified for less than 30 s. After dilution with a rotary splitter, each suspension was filtered onto polycarbonate membrane filters (0.4 μm pore size), and then dried at 40°C for 24 h before <1×1 cm filter aliquots were mounted on an aluminium stub. In each case, at least 300 coccoliths were counted under a Zeiss DSM 940A scanning electron microscope at 3,000× magnification. Coccolith counts were converted into numbers per gram dry bulk sediment.

In core GeoB11035-1, *N. pachyderma* (sin) and IRD counts were done at varying sample resolution (1–9 cm) using aliquots wet sieved through 63 and 150 μm mesh sieves. The >150 μm fractions were split to obtain a minimum number of 300 particles per count. Counts are reported as number/gram bulk sediment.

AMS ^{14}C measurements were performed at the Leibniz Laboratory in Kiel (Germany) and the Poznan Radiocarbon Laboratory (Poland), on specimens of *Globigerina bulloides* hand-picked from the >250 μm fractions of nine selected samples. All dates are reported in calibrated kilo annum before present (cal ka BP), corrected for a conservative marine reservoir effect of 400 years and converted into 1-sigma calibrated ages using Calib 5.0.1 (Stuiver et al. 1998). Dates with a conventional age older than 22 ka were calibrated based on Bard et al. (1998).

An age model for core GeoB11035-1 served for stratigraphic correlation with cores GeoB130206-1 and GeoB13071-1 via Ca/Fe and magnetic susceptibility records. The age model of GeoB11035-1 is based primarily on five radiocarbon dates refined by correlation (AnalySeries 2.0; Paillard et al. 1996) of the high-resolution XRF Ca/Ti record with the well-dated GISP II $\delta^{18}O$ record (Stuiver and Grootes 2000), assuming that all Ca is of biogenic origin (correlation coefficient of XRF Ca (cps) versus carbonate (wt%) is 0.92), and that marine carbonate productivity increased during warmer periods with zero lag. In the lower part of core GeoB11035-1, Heinrich layers 4, 5 and 6 were used as additional tie points, identified by X-radiographies, higher magnetic susceptibility values, and greater abundances of *N. pachyderma* (sin) and IRD (see below, and Fig. 1a–c in the online electronic supplementary material for this article). Age assignments of these layers are based on de Abreu et al. (2003) for the well-studied core MD95-2040 (see Fig. 1a). This amounted to a total of 17 age tie points for core GeoB11035-1 (cf. Table 1).

Results

Seismic data

Crossing core site GeoB11035 (Fig. 1a), the eastern part of reflection seismic profile p594 (Fig. 2a) encompasses the steep (~9°) continental slope at about 1,300 m water depth (1,750 ms TWT, two-way travel time; time-to-depth conversion is based on 1,500 m/s sound velocity in the water column and uppermost water-saturated sediments). Below ~1,700 m water depth (2,275 ms TWT), the slope angle decreases to ~2.3°. Outcropping basement, approx. 120 m high, interrupts the slope ca. at shot point (SP) 5,150. Sediments filling the trough between the steep slope and the basement outcrop show an upper stratified seismic facies and a lower chaotic seismic facies. Such chaotic facies are indicative of mass-wasting deposits (e.g. Brown and Fisher 1977), suggesting initial gravity-driven sediment transport filling this trough. On both sides of the basement outcrop, focusing of slope-parallel currents has resulted in the formation of moats. Overspills from suspended sediments transported contour-parallel through these moats built up

Table 1 Age model tie points (^{14}C age at base of GeoB11035-1 (*asterisk*) is not considered because beyond radiocarbon limits)

Depth in core (cm)	Tie point type/lab. code	Conventional AMS ^{14}C age (years)	1σ calibrated (cal years BP)	Intercept (cal ka BP)	Assigned age (cal ka BP)	Reference
Core GeoB11035-1						
0.00	Core top	–	–	–	0.00	
37.56	Correlation[a]	–	–	–	9.71	Stuiver and Grootes (2000)
58.00	KIA 33701[b]	11,110±70	12,710–12,825	12.77±0.06	12.77	Stuiver et al. (1998)
79.97	Correlation[a]	–	–	–	14.46	de Abreu et al. (2003)
135.00	KIA 33708[b]	14,940±100	17,280–17,805	17.54±0.26	17.54	Stuiver et al. (1998)
250.00	Poz-23451[c]	18,250±100	20,870–21,290	21.08±0.21	21.08	
264.35	Correlation[a]	–	–	–	23.99	Stuiver and Grootes (2000)
286.01	Correlation[a]	–	–	–	30.10	
300.00	Poz-31023[c]	27,700±270	31,650–32,260	31.96±0.30	31.96	Bard et al. (1998)
320.02	Correlation[a]	–	–	–	32.91	Stuiver and Grootes (2000)
339.99	Correlation[a]	–	–	–	35.71	
346.50	Top of H4	–	–	–	38.36	de Abreu et al. (2003)
351.00	Base of H4	–	–	–	40.16	
390.00	Poz-23452[c]	38,200±1,400	41,945–44,920	43.43±1.49	43.43	Bard et al. (1998)
420.00	Base of H5	–	–	–	46.92	de Abreu et al. (2003)
486.50	Top of H6	–	–	–	58.30	
492.50	Base of H6	–	–	–	61.90	
494.00	KIA 33718[b]	46,620±5,250	46,775–57,390*	52.08±5.31*	–	Bard et al. (1998)
Core GeoB13071-1						
0.00	Core top	–	–	–	0.00	
33.00	Correlation[d]	–	–	–	9.78	
82.00	Poz-27844[c]	12,670±60	14,030–14,210	14.12±0.09	14.12	Stuiver et al. (1998)
227.79	Correlation[d]	–	–	–	17.82	
276.00	Poz-27927[c]	24,840±520	28,120–29,310	28.71±0.59	28.71	Bard et al. (1998)
Core GeoB130206-1						
0.00	Core top	–	–	–	0.00	
10.00	Correlation[d]	–	–	–	3.09	
30.00	Correlation[d]	–	–	–	9.79	
121.00	Correlation[d]	–	–	–	14.46	
189.01	Correlation[d]	–	–	–	17.76	
469.00	Poz-27845[c]	25,140±150	28,885–29,230	29.06±0.17	29.06	Bard et al. (1998)

[a] Correlation with δ^{18}O record of GISPII. [b] Leibniz Laboratory, Kiel, Germany. [c] Poznan Radiocarbon Laboratory, Poland. [d] Correlation with GeoB11035-1 according to Fig. 3

~20 m high stratified levees. Lateral extensions of these deposits show continuous stratified reflectors with strata thickness decreasing basinwards. This geometry suggests sustained current-related slope-parallel sediment transport and draped deposition for the younger past. Between SPs 4,250 and 3,700 is a lens of chaotic seismic facies about 100 m below seafloor (~3,300 ms TWT). Such intercalated chaotic seismic facies occur frequently below 200 m sediment depth and are plausibly explained by relatively active mass movement in earlier times.

Seismic profile p565 reported in Fig. 2b runs slightly south of site GeoB130206 (cf. Fig. 1a). In the ENE part of the profile, the outer shelf is covered by a stratified sediment wedge up to 90 m thick and thinning to only 5 m in front of a shelf-edge basement outcrop at ~350 m water depth (~470 ms TWT). WSW of this outcrop, a sediment wedge several metres thick can be recognized. The adjacent upper slope is very steep, reaching 33° between 600 and 1,000 m water depth (~800–1,330 ms TWT). Attempts at seafloor sampling with a giant box corer in this area during R/V *Poseidon* expeditions 342 and 366 failed; it is assumed that this section of the upper slope is currently sediment starved. Below 1,350 m water depth (~1,775 ms TWT), the slope gradient abruptly decreases to ~2°. Further west, several terraces of well-stratified deposits overlie the stratified filling of a U-shaped basement depression. These are incised by an 80-m-deep and 1-km-wide channel (ca. SP

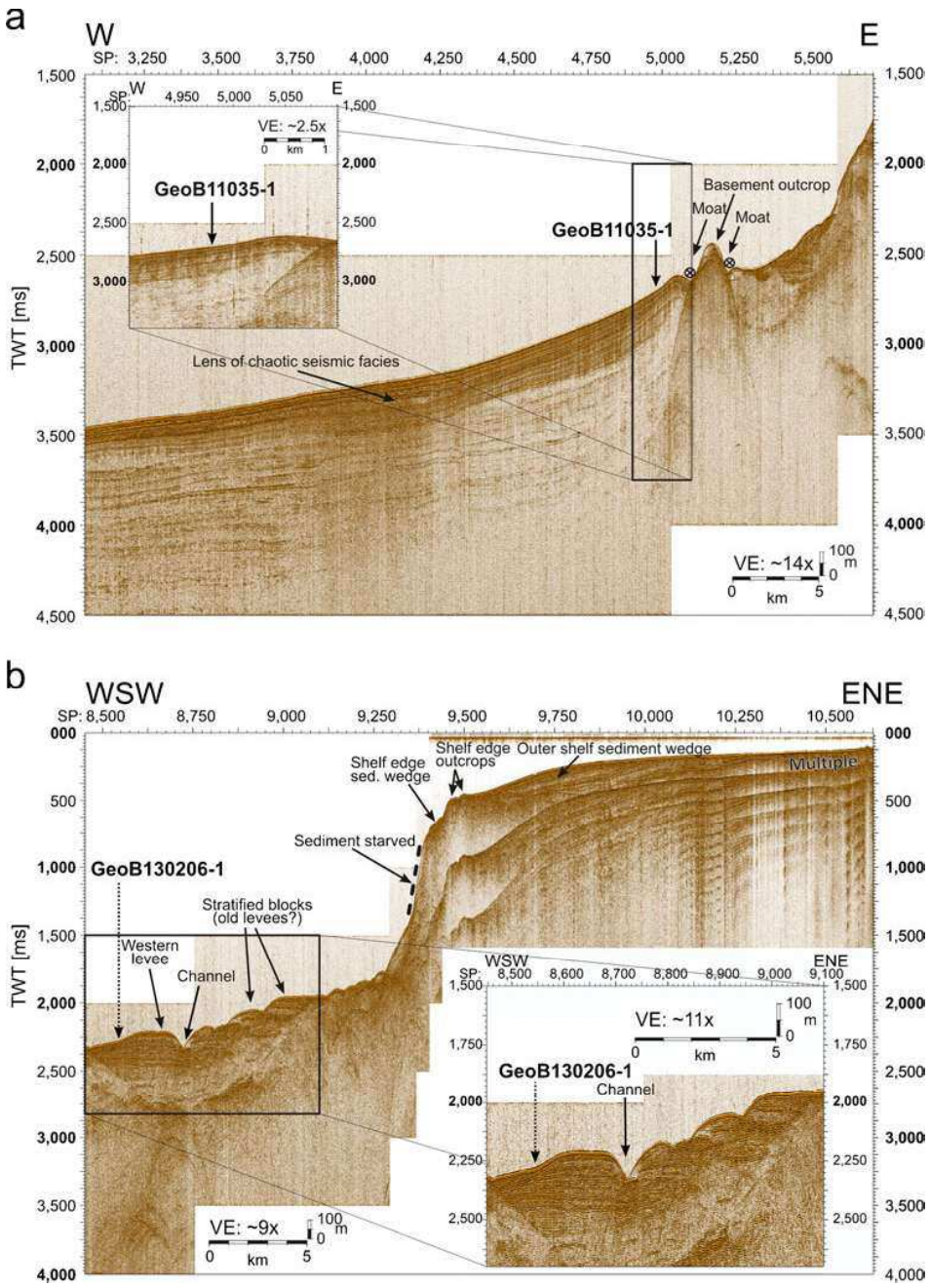

Fig. 2 **a** Seismic profile p594 off the Ría de Vigo, incorporating coring site GeoB11035. The very regularly stratified seismic facies suggests rather constant current-dominated sediment transport and depositional processes west of the basement outcrop. **b** Seismic profile p565, showing an approx. 80-m-deep channel in the western part (cf. enlargement). Note that coring site GeoB130206 is approx. 1 km north of this profile and has been projected onto it by shortest distance. It is thus likely that core GeoB130206-1 was recovered from inside the channel or its western levee. *TWT* Two-way travel time, *SP* shot point

8,725). The precise orientation of the channel is uncertain but a SE–NW direction and slightly meandering pattern are likely. The sediment bodies to the WSW and ENE of the channel are well stratified down to about 200 m sediment thickness (ca. 2,500 ms TWT at SP 8,725), representing the channel's levees. The sediments beneath the levees and channel show a chaotic and transparent seismic facies, pointing to mass-wasting processes initially filling the U-shaped basement valley.

Core GeoB13071-1 was recovered north of the other two cores in a zone of acoustically stratified sediments at the foot of the continental slope (unpublished onboard cruise data). The slope morphology suggests a close-by canyon

structure. These stratified deposits represent the first modern sediment depocentre below the shelf break, as is the case for the two other core localities.

Chronostratigraphy

Of the six radiocarbon-dated levels in core GeoB11035-1, five gave reliable ages and were used for the age model (Table 1, Fig. 3; cf. the core base sample dated beyond radiocarbon limits). Two radiocarbon-dated levels in core GeoB13071-1 gave results consistent with the preliminary stratigraphy, and these were incorporated into the age model of this core. For GeoB130206-1, only the core base was AMS ^{14}C dated. This core is only half the age of GeoB11035-1 at a similar core depth (i.e. double the sedimentation rate; cf. below) but is situated close to a sediment conduit (cf. above); therefore, this core base age has been retained.

Linear sedimentation rates (LSRs; Figs. 4a, 5a and 6a) were calculated on the basis of the age tie points described above. It should be noted that GeoB130206-1 exhibits a series of fine sandy proximal turbidites (see Fig. 1d in the electronic supplementary material). Assuming instantaneous deposition of these layers, the age model of GeoB130206-1 was corrected by assigning zero time progression for the respective depth intervals. Seeing that turbidity currents can enforce significant erosion, this adds an undefined degree of uncertainty to the age model of GeoB130206-1.

Of the three cores, only GeoB11035-1 reaches back to MIS 4 (Fig. 3). Heinrich layers 6 (H6), 5 (H5) and 4 (H4) can be clearly identified in the lowest 2 m section of this core. H4 is the most striking feature not only in the X-ray image but also in all other records for GeoB11035-1 (cf. Fig. 1 in the electronic supplementary material). The H4 event layer is characterized by an extremely high magnetic susceptibility (up to 1,600 × 10^{-6} SI) together with a

Fig. 4 Lithology of GeoB11035-1: **a** linear sedimentation rate (*LSR*), **b** Ti/K, **c** Si/Ti and **d** Ca/Fe ratios, **e** bulk $CaCO_3$ content, **f** sortable silt (10–63 μm) content (SS%) and **g** mean grain size ($\overline{SS}$), **h** bulk sediment grain-size composition differentiated into contents of clay, silt, sand <150 μm ("very fine"), and sand >150 μm, **i** grain-size composition of bulk and decarbonated (terrigenous) mud, as well as corresponding sand content of bulk sediments (*white circles in upper panel*). *Vertical grey bars* indicate the Younger Dryas (YD), the last glacial maximum (LGM, following the EPILOG definition of Mix et al. 2001), and H layer 4 (H4)

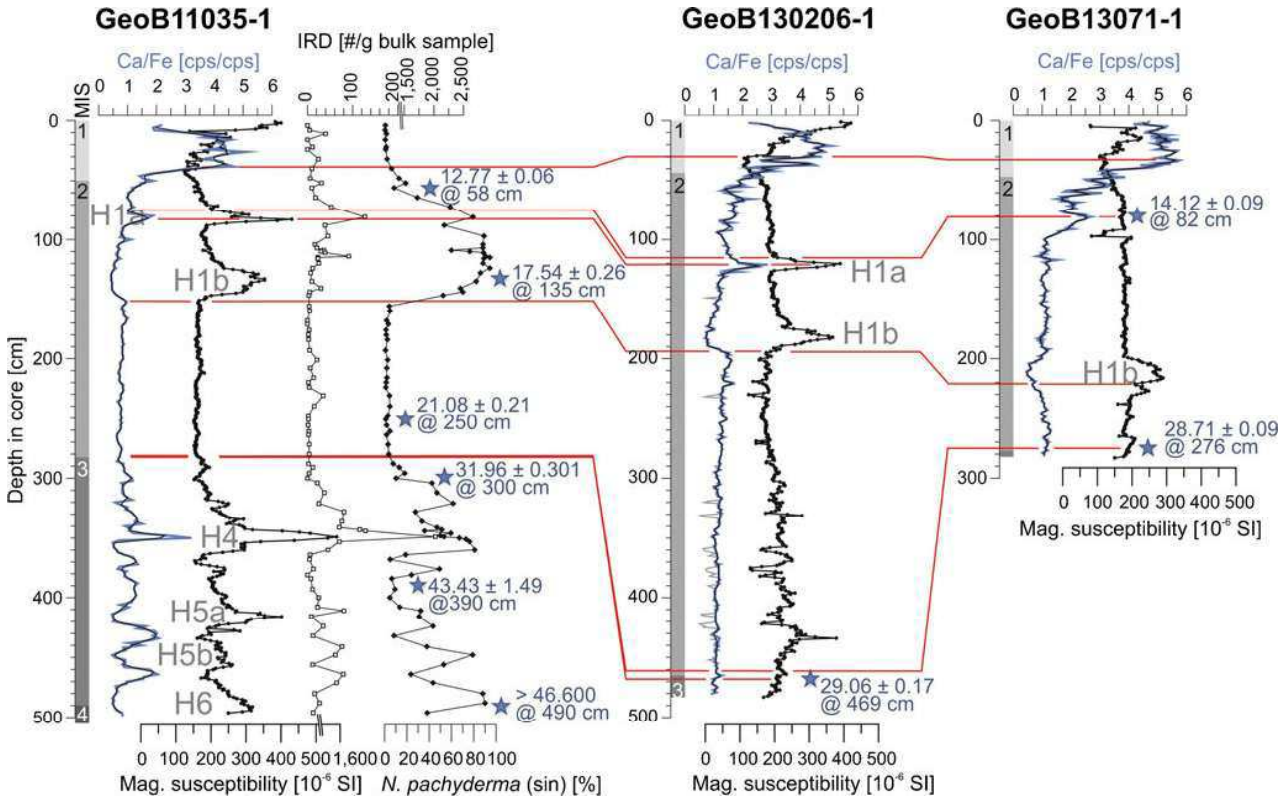

Fig. 3 Inter-core correlation of Ca/Fe ratios (*black line* 3-step running average) and magnetic susceptibility (*circles*) supported by radiocarbon dates (*stars*) as basis for the chronostratigraphy of the three study cores. Heinrich layers (*H*) are labelled if recognizable in Ca/Fe ratios and/or magnetic susceptibility (note extremely high SI values for H4 in GeoB11035-1). For GeoB11035-1, H layer identification was additionally supported by IRD (*squares*) and *N. pachyderma* (sin) (*diamonds*) counts. Underlain (*grey*) negative peaks in the Ca/Fe record of GeoB130206-1 are associated with fine sandy turbidites

Geo-Mar Lett (2012) 32:313–335

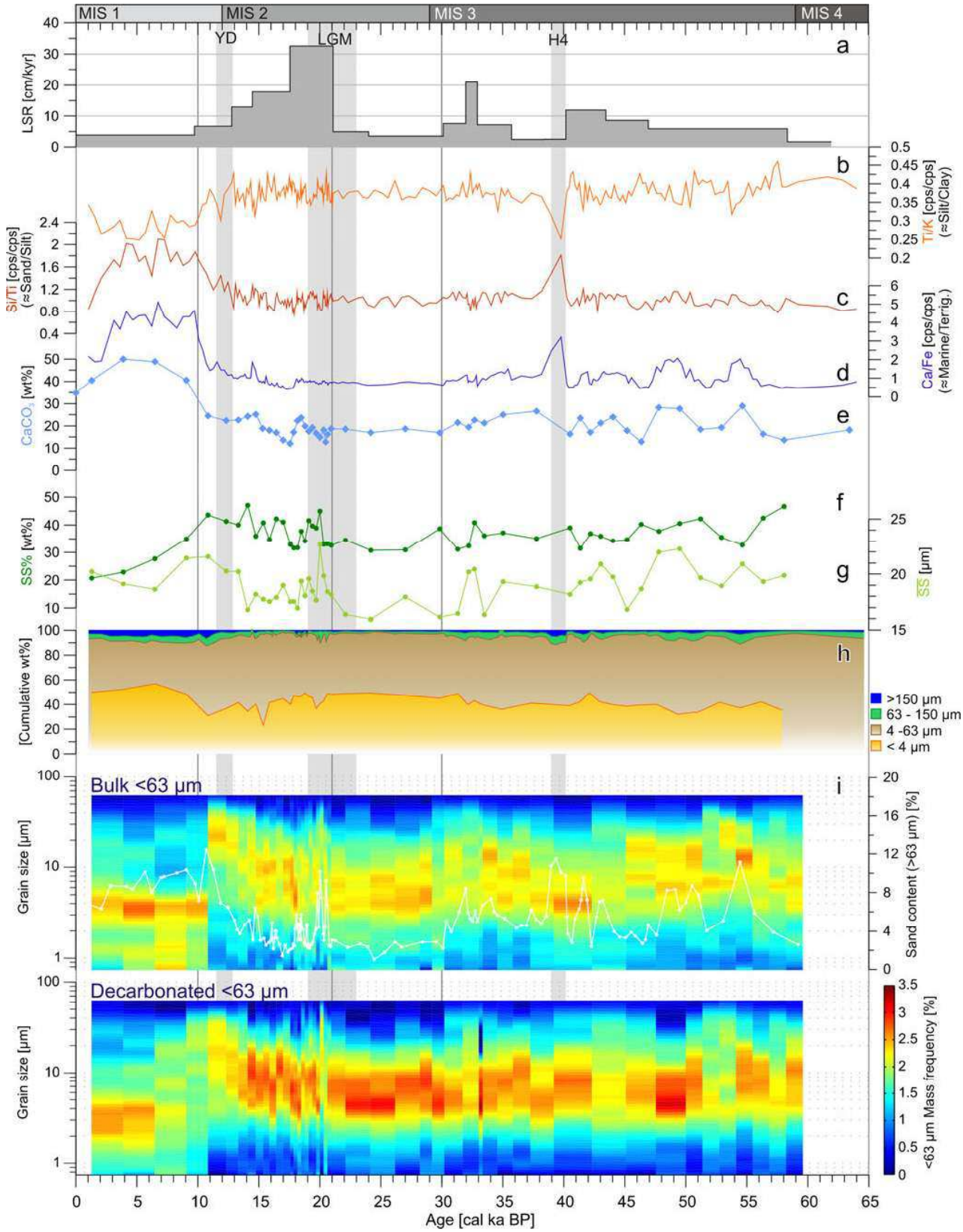

significantly increased Ca/Fe ratio, pointing to a considerable contribution of detrital carbonate (Figs. 3 and 4). This prominent imprint of H4 is consistent with the findings of Moreno et al. (2002) and de Abreu et al. (2003).

In contrast to core GeoB11035-1, cores GeoB13071-1 and GeoB130206-1 both end at ca. 30 cal ka BP. This can possibly be explained by the occurrence of relatively coarse (therefore, difficult to penetrate) Heinrich layer 3 (H3) sediments, dated at 30.2–29.0 cal ka BP on the western Iberian margin (de Abreu et al. 2003). Radiographs of GeoB11035-1 show an irregular and slightly bioturbated layer of fine sand at 285–286 cm core depth (corresponding to 30.1–29.8 cal ka BP). However, this layer has not been detected by other methods and it remains speculative if it is genetically associated with H3.

H1 is marked by two discrete peaks in GeoB11035-1 and GeoB130206-1 (Fig. 3). In GeoB13071-1, only the older peak is clearly recognizable. This two-phase deposition of H1 appears to be a broad feature in the eastern subtropical North Atlantic (Lebreiro et al. 1996; Naughton et al. 2007a, 2009). Bard et al. (2000) also identified two distinct depositional phases for H1 centred at 17.5 (H1b) and 16 cal ka BP (H1a). In core GeoB11035-1, the corresponding values are 17.54±0.26 and ca. 14.5 cal ka BP. de Abreu et al. (2003) observed only a single depositional phase for H1 between 17.6 and 14.9 cal ka BP off Portugal.

MIS 1 (Holocene) is represented in all three cores within the top ~50 cm. It is easily identifiable by lighter colours and a rather sharp increase in the topmost Ca/Fe ratios (Fig. 3). The Ca/Fe ratios of all three cores decrease again towards the modern sediment surface, but do not reach pre-Holocene values. Noteworthy is that the Holocene parts of all Ca/Fe ratios and susceptibility records are not as easy to correlate as the pre-Holocene parts.

Lithostratigraphy of GeoB11035-1

For all three cores combined, the data reveal that Si is bound to the very fine to fine sand fraction, presumably as quartz. Ti is associated with a medium silt grain-size spectrum of ca. 10~30 μm, and K appears to be bound to terrigenous clay minerals (ca. 2 μm). Consequently, the Ti/K (Figs. 4b, 5b and 6b) and Si/Ti (Figs. 4c, 5c and 6c) ratios approximate terrigenous silt/clay and sand/silt ratios respectively (cf. grain-size distributions in parts f–i of these three figures). The Ca/Fe ratio (Figs. 4d, 5d and 6d), a widely used marine/terrigenous proxy, closely mirrors variations in total $CaCO_3$ in all three cores (Figs. 4e, 5e and 6e), with the exception of H4. Here, an increase in Ca/Fe and decrease in $CaCO_3$ suggest the presence of other Ca-bearing minerals (e.g. anorthite, dolomite). In terms of core-specific trends, the stratigraphic sequence of GeoB11035-1 can be subdivided into the four intervals described below.

Fig. 5 Lithology of GeoB13071-1: **a** linear sedimentation rate (*LSR*), **b** Ti/K, **c** Si/Ti and **d** Ca/Fe ratios, **e** bulk $CaCO_3$ content, **f** sortable silt (10–63 μm) content (SS%) and **g** mean grain size ($\overline{SS}$), **h** bulk sediment grain-size composition differentiated into contents of clay, silt, and very fine, fine, medium, coarse, and very coarse sand, **i** grain-size composition of bulk and decarbonated (terrigenous) mud, as well as corresponding sand content of bulk sediments (*white circles in upper panel*). *Vertical grey bars* indicate the Younger Dryas (YD) and the last glacial maximum (LGM)

From the core base at *~65 cal ka BP until 30 cal ka BP*, all records show minor variations at about constant levels, with the exception of H4 noted above. LSRs vary between 5 and 12 cm/1,000 years, apart from a short phase of enhanced sedimentation reaching 20.9 cm/1,000 years from 33 to 32 cal ka BP. Silt (63–4 μm) and clay (<4 μm) dominate (Fig. 4h), sand contents (>63 μm) contributing only 2–12% (Fig. 4h, i). $CaCO_3$ contents vary at about 20% and reflect the Ca/Fe trend (Fig. 4e, d). Sortable silt mean grain size ($\overline{SS}$) and content (SS%) fluctuate in the range 16–22 μm and 30–43% respectively (Fig. 4f, g). General variations in grain-size distribution are similar for the bulk and decarbonated mud fractions (upper and lower panels in Fig. 4i), implying that potentially present carbonaceous mud would have a grain size similar to that of terrigenous mud.

Between *30 and 21 cal ka BP*, all records remain very constant and LSR is ~3.5 cm/1,000 years. The sediments are composed of ~98% silt and clay in equal proportions. $\overline{SS}$ is slightly finer with less data scatter (16–20 μm) than for the preceding time interval; accordingly, SS% varies between 30–40% (Fig. 4f, g). Carbonate content decreases slightly to ~18% (Fig. 4e) and total coccolith numbers are relatively low at ~$1{,}000 \times 10^6$ coccoliths/g sediment (Fig. 7c), suggesting reduced biogenic sedimentation. Coccolith diversity is also very low and dominated by *Gephyrocapsa muellerae* and, to a minor degree, *Emiliania huxleyi* (Fig. 7e). At 21 cal ka BP, i.e. at the height of the LGM, LSR reaches a maximum of 32.5 cm/1,000 years and then gradually decreases to 3.8 cm/1,000 years in the Holocene.

The deglaciation period from *21–10 cal ka BP* is characterized by the strongest overall dynamics. At ~20 cal ka BP, there is a very short interval of reduced carbonate content (12%) and highest $\overline{SS}$ (22.6 μm). At 18 cal ka BP, there is a synchronous decrease in the Ca/Fe ratio, $CaCO_3$ and sand contents, and $\overline{SS}$. Whereas the Ca/Fe, $CaCO_3$ and sand values increase only gradually again from 17.5 to 10 cal ka BP, SS% values plateau rapidly at ca. 40% from 17 to ~10 cal ka BP (Fig. 4d–f, i). Likewise, $\overline{SS}$ initially decreases to 17 μm, then increases to 19 μm and varies at about 18 μm until ~14 cal ka BP, when it decreases again to 17 μm. After ~14 cal ka BP, $\overline{SS}$ abruptly increases to vary at about 21 μm until ~10 cal ka BP (Fig. 4g). Similar to the trends for $CaCO_3$, Ca/Fe and sand content, total coccolith abundance and species diversity

Geo-Mar Lett (2012) 32:313–335

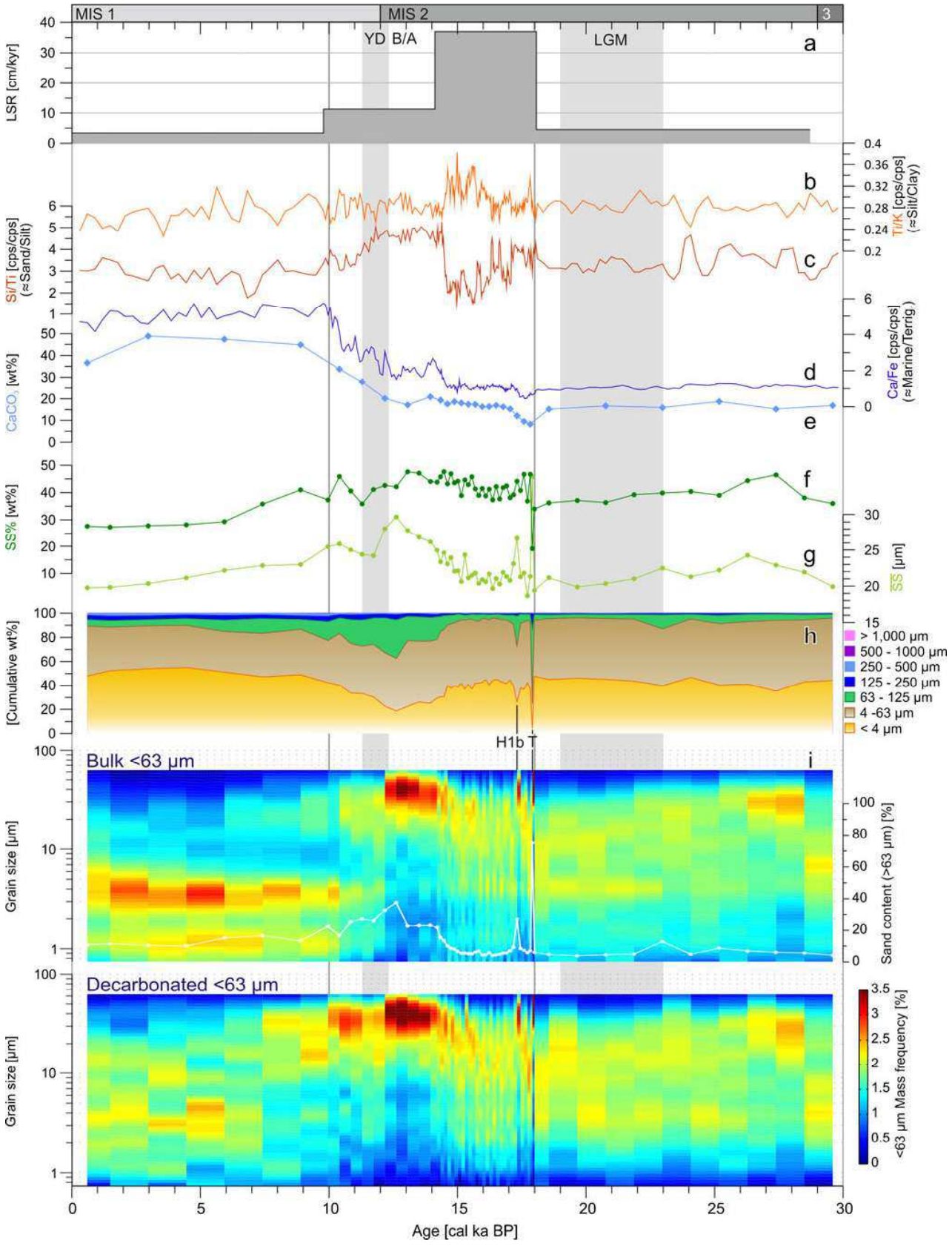

gradually increase from 18–10 cal ka BP (Fig. 7c, e). *N. pachyderma* (sin) relative abundance increases abruptly from 4% at 18.2 cal ka BP to reach a maximum of ca. 95% during H1 (Fig. 7d). Its abundance then gradually decreases during the B/A, with a minor recurrence during the YD. After ~13.5 cal ka BP until the end of this time interval, the coarsening trend of terrigenous mud is maintained but accompanied by poorer sorting, as indicated by the broader grain-size spectra (Figs. 4i and 8b).

The most significant shifts in all records of GeoB11035-1 occur sharply at *10 cal ka BP*. Ca/Fe and $CaCO_3$ values increase to a maximum ($CaCO_3$ reaches 50% in the mid-Holocene); sand content is ~10%. Total coccolith numbers increase to a maximum of about $18{,}000 \times 10^6$ coccoliths/g sediment in the early Holocene, synchronous with maximum species diversity. For the remainder of the Holocene, numbers vary between $4{,}000 \times 10^6$ and $12{,}000 \times 10^6$ coccoliths/g, with a slightly reduced species diversity dominated by *E. huxleyi* (Fig. 7c, e). The mud fractions are rather poorly sorted, with an increased clay component (Fig. 4i). SS% decreases from 34% at ~10 cal ka BP, to 20% in the late Holocene. During the early Holocene (until ~5 cal ka BP), terrigenous silt is significantly reduced, and increased proportions of carbonaceous clay characterize the mud (Figs. 4i and 8a). After *~5 cal ka BP*, there is an input of terrigenous material with a mean grain size of 3 μm, accompanied by a 15% decrease in carbonate content (Figs. 4e and 8a).

Lithostratigraphy of GeoB13071-1

The records of core GeoB13071-1 can be subdivided into stratigraphic intervals with time boundaries similar to those of core GeoB11035-1, except that the oldest interval of the latter core is not reached. A rather stable time interval from *30 to 18 cal ka BP* is characterized by a low LSR of 4.5 cm/1,000 years, and very low carbonate (~15%) and sand contents (~5%; Fig. 5a, e, i). The sand fraction is dominated by very fine sand (Fig. 5h). Compared to GeoB11035-1, much broader mud grain-size spectra indicate poorer sorting associated with a rather bimodal distribution comprising a 3 μm and a ~15 μm component (Figs. 5i and 8k). Between 30–18 cal ka BP, the mud fraction is composed of silt and clay in equal proportions and is mainly of terrigenous origin (Fig. 5h, i). SS% and $\overline{SS}$ vary moderately in the range 30–40% and 20–25 μm respectively (Fig. 5g). An additional 3 μm fraction persists up to and throughout the LGM (Fig. 5i and 8j, k).

Similar to GeoB11035-1, the period *18 to 10 cal ka BP* has the strongest dynamics, including short-duration excursions. An initial maximum LSR of 36.9 cm/1,000 years and subsequent gradual decrease to a Holocene LSR of 3.4 cm/1,000 years are in remarkably good agreement with the corresponding values for core 11035–1. The time interval begins with a fine, distinctive sandy turbidite (Fig. 8l), followed shortly thereafter at ~17.5 cal ka BP by H1b, identified by elevated magnetic susceptibility but slightly finer grain size (very fine sandy silt with ~23% clay) and poorer sorting (Figs. 3, 5i and 8l). With time, the ~15 μm component coarsens whereas the 3 μm component declines (Figs. 5i and 8i, j). This is reflected in the negative correlation between Si/Ti and Ti/K, wherein the increase in Ti mirrors the coarse silt component (Fig. 5c). At about 15.5 cal ka BP, $\overline{SS}$ starts to increase from ~21 μm to reach a maximum of 29.6 μm at the end of the B/A (Fig. 5g). Synchronously, SS% varies between 35–48% with a generally increasing trend (Fig. 5f). By about 14.3 cal ka BP, the onset of the B/A, the 3 μm component is negligible and the grain-size spectrum expands further towards the very fine sand fraction (Figs. 5c, h, i and 8h). This phase of well-sorted coarse silt–very fine sand deposition reaches its maximum by the end of the B/A warm period. At about 12 cal ka BP, sorting diminishes and the 3 μm component emerges again (Fig. 8g). Notably, this clayey component is constituted mainly of carbonate, as shown by its absence in the decarbonated (~terrigenous) grain-size spectrum and by the corresponding Ca/Fe and $CaCO_3$ values (Fig. 8e–g).

As in core GeoB11035-1, a major compositional change occurs at ca. *10 cal ka BP*. From then to the present day, Ca/Fe and $CaCO_3$ are at a maximum (close to 50%). There is an additional medium sand component composed mainly of planktic and benthic foraminifers; the 3 μm carbonate component is clearly present in the fine fraction, and an ~1 μm carbonate component is newly added (Fig. 8e, f). SS% and $\overline{SS}$ decrease markedly from 41.5% and 25.5 μm at the beginning of this interval, to ~28% and ~21 μm respectively at about *5 cal ka BP*, and stabilize around these values for the remainder of the interval (Fig. 5f, g). As in core GeoB11035-1, a distinct terrigenous fine silt/clay component with a mean of ~3 μm is reintroduced at about 5 cal ka BP (Fig. 8e).

Lithostratigraphy of GeoB130206-1

The records of GeoB130206-1 are overall similar to those of GeoB11035-1 and GeoB13071-1 but show some interesting differences. The period *30~20 cal ka BP* is characterized by a background sedimentation of ~15% carbonate content. The

Fig. 6 Lithology of GeoB130206-1: **a** turbidite-corrected linear sedimentation rate (*LSR*), **b** Ti/K, **c** Si/Ti and **d** Ca/Fe ratios (underlain *green peaks* are extreme values associated with fine sandy turbidites), **e** bulk $CaCO_3$ content, **f** sortable silt (10–63 μm) content (SS%) and **g** mean grain size ($\overline{SS}$), **h** bulk sediment grain-size composition differentiated into contents of clay, silt, and very fine, fine, medium, coarse, and very coarse sand, **i** grain-size composition of bulk and decarbonated (terrigenous) mud, as well as corresponding sand content of bulk sediments (*white circles in upper panel*). *Vertical grey bars* indicate the Younger Dryas (YD) and the last glacial maximum (LGM)

Geo-Mar Lett (2012) 32:313–335

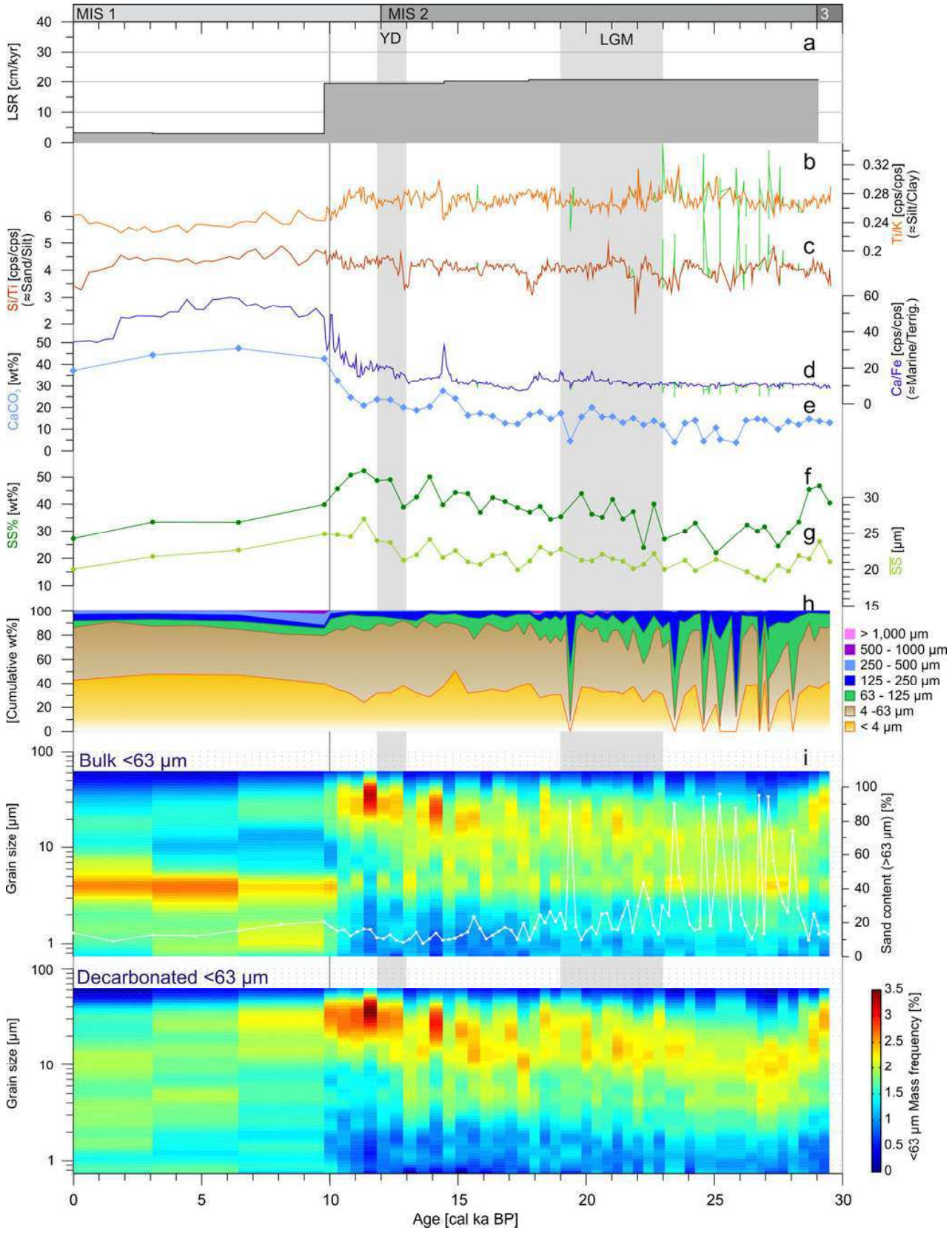

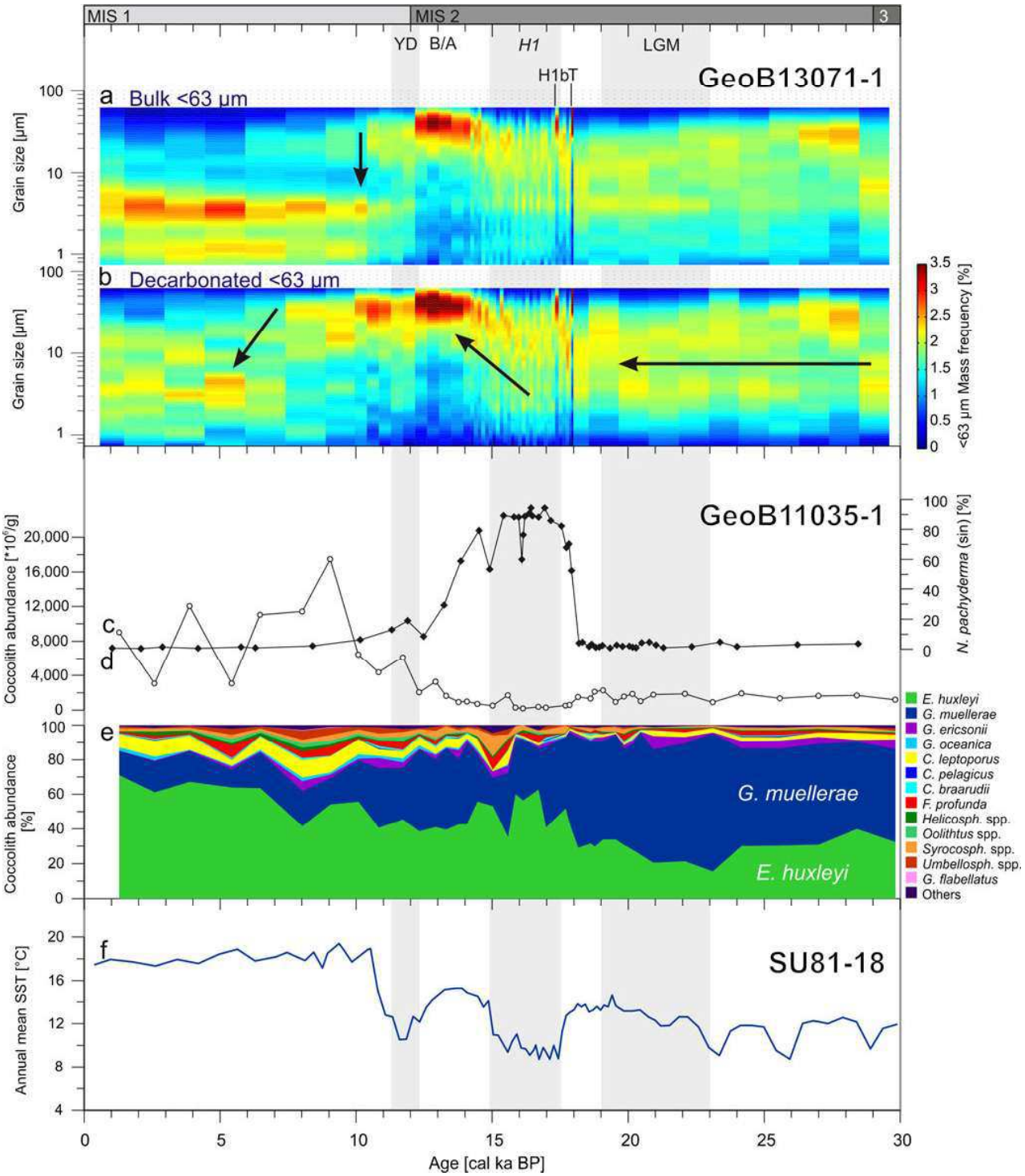

Fig. 7 GeoB13071-1: grain-size composition of bulk (**a**) and decarbonated (terrigenous, **b**) mud, with identification of H1b sediments as well as the turbidite (*T*; cf. Fig. 81). The *arrows* denote the relatively constant pre-LGM conditions, gradual sorting and grain-size increase towards the B/A, abrupt and strong biogenic influence at 10 cal ka BP, and the Holocene terrigenous grain-size shift linked to sea level-induced sediment dynamics on the shelf. **c**–**e** GeoB11035-1: total coccolith abundance (**c**), relative coccolith species abundance (**e**), *N. pachyderma* (sin) counts (**d**). **f** Core SU81-18 (Bard et al. 2000): alkenone-based sea-surface temperature (*SST*) reconstructions. *Vertical grey bars* indicate the Younger Dryas (YD), Bølling/Allerød (B/A), Heinrich event 1 (H1) and the last glacial maximum (LGM)

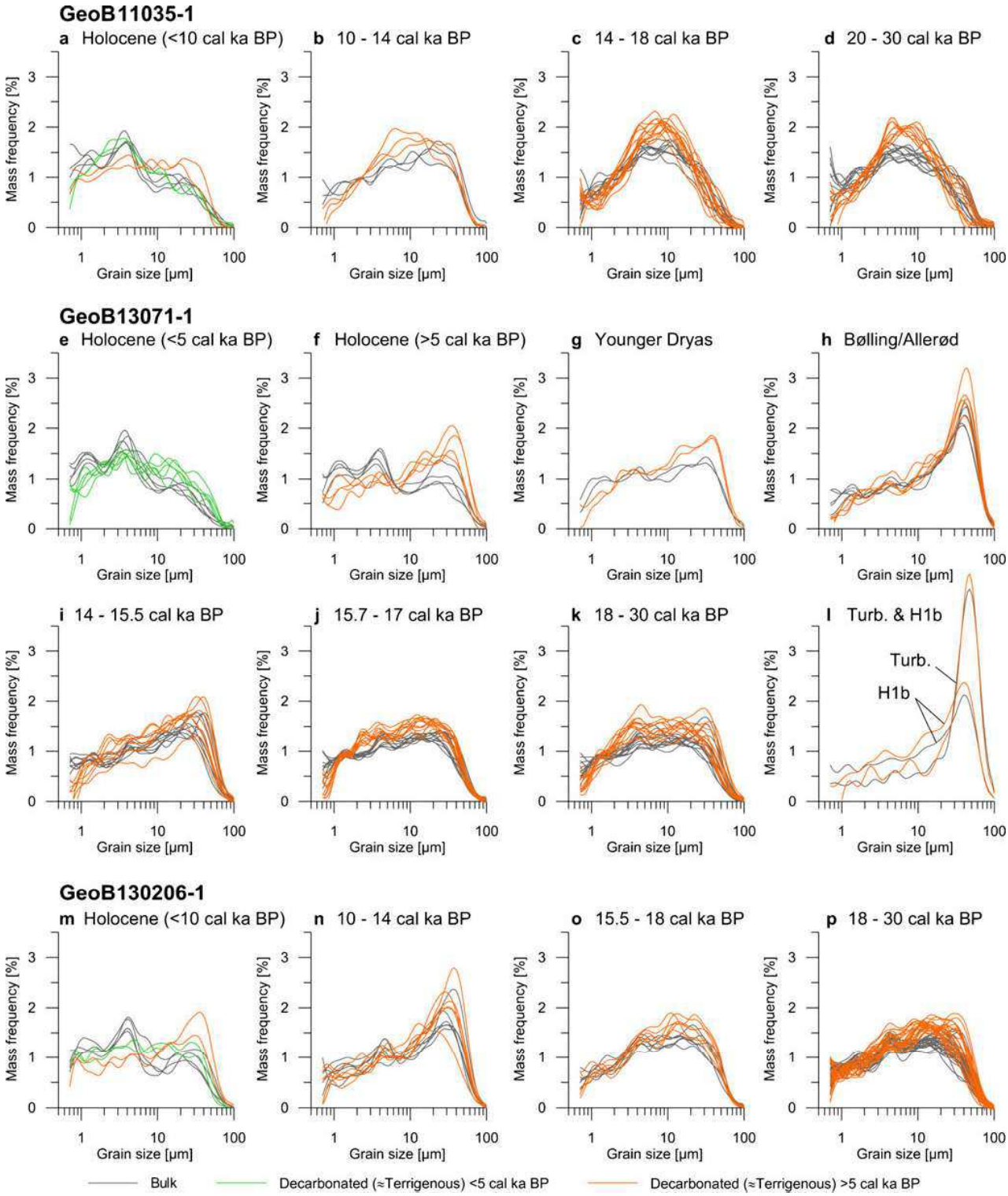

Fig. 8 Bulk (*grey*) and decarbonated (*orange*, *green*) mud grain-size spectra for different time intervals identified in **a**–**d** GeoB11035-1, **e**–**l** GeoB13071-1 and **m**–**p** GeoB130206-1

mud comprises a terrigenous silt component between 30~10 μm (medium–fine silt) and an additional subordinate carbonate component at 4 μm (Figs. 6e, i and 8p). The sortable silt fraction shows strong variations in $\overline{SS}$ and SS% in the range 18–24 μm and 30–50% respectively (Fig. 6f, g). In contrast to cores GeoB11035-1 and 13071–1, a series of fine sandy

turbidite beds can be recognized in this time interval (Figs. 6h, and Fig. 1d in the electronic supplementary material). The LSR (20.6 cm/1,000 years, excluding the turbidite layers) is much higher than at the other two sites and remains at a constantly high level throughout the period *20~10 cal ka BP*, whereas it peaks at the other two sites (Figs. 4a, 5a and 6a). This time interval is also characterized by a slight increase in Ca/Fe and $CaCO_3$ (the latter from 15 to 20%); sand content varies between 15 and 20%, with mainly terrigenous very fine to fine sands (Fig. 6h). SS% gradually increases from 35 to 50%, together with an increase in $\overline{SS}$ from 21 to 23 μm until ~14 cal ka BP. During a short interval at ~14 cal ka BP, represented by only one well-sorted sample, $\overline{SS}$ increases to 24 μm and SS% reaches 50%, probably corresponding to the B/A. During the subsequent YD, $\overline{SS}$ and SS% decrease before increasing again up to their highest values of 27 μm and 52% respectively (Fig. 6f, g). Noteworthy is that, until 13 cal ka BP, a terrigenous very fine silt component at ~4 μm is present which is then completely absent between 13~10 cal ka BP (Figs. 6i and 8n).

As in the case of the other two cores, the strongest change in composition occurs at *10 cal ka BP*. Carbonate content reaches 45% and the sand fraction (up to 20%) consists mainly of planktic and benthic foraminifers. An LSR of 3.2 cm/1,000 years compares well with the findings for the other sites (Fig. 6a). The mud is abruptly dominated by a 4 μm carbonate component; the remaining terrigenous mud fraction is poorly sorted (Fig. 8m). This is reflected by $\overline{SS}$ and SS% decreasing from 25 μm and 40% at ~10 cal ka BP, to 20 μm and 27% respectively in recent times (Fig. 6f, g). The return of a terrigenous clay component (3~4 μm) at *~5 cal ka BP* recognized in cores GeoB11035-1 and 13071–1 is not clearly seen in core GeoB130206-1; nevertheless, a slight decrease in Ca/Fe, $CaCO_3$ and Si/Ti hints at a growing influence of terrigenous silt after 5 cal ka BP (Figs. 6c–e, h and 8m).

Discussion

Transport modes: hemipelagic, contouritic and down-slope sedimentation

To distinguish current-induced deposition from down-slope or hemipelagic sediment input, McCave and Hall (2006) proposed that increased sorting during current transport should be reflected in concurrent increases in sortable silt mean grain size ($\overline{SS}$) and content (SS%). Indeed, $\overline{SS}$ vs. SS% relationships reveal distinct differences between (late) Holocene and deglacial datasets for all three GeoB cores (Fig. 9a–c). Holocene sedimentation off Galicia is clearly rooted in hemipelagic settling (as discussed further below). By contrast, the higher $\overline{SS}$ and SS% values of deglacial sediments are interpreted to reflect contouritic sediment transport. For cores GeoB11035-1 and GeoB13071-1, increased sediment supply during the deglacial period (LSRs reaching 37 cm/1,000 years in core 13071–1) is not associated with a recognizable change in transport mode compared to the period prior to ~18 cal ka BP (Fig. 9a, b). This is not the case for core 130206–1, where the signatures for the latter time period suggest decreased current-induced sorting associated with much broader data scatter overlapping even with the Holocene dataset (Fig. 9c). In core 130206–1, the period prior to ~18 cal ka BP is characterized by frequently occurring clean fine sandy turbidites, whereas the reduced sorting of the muddy background suggests simple hemipelagic settling from the water column (rather than contouritic sedimentation; Fig. 9c). Thus, massive reworking on the Galician shelf during the pre-LGM sea-level regression (see discussion below) led to off-shelf transport of the fine fraction in the form of nepheloid layers, whereas sand transport was event-like via turbidity currents in the area of site GeoB130206. Contouritic transport at site

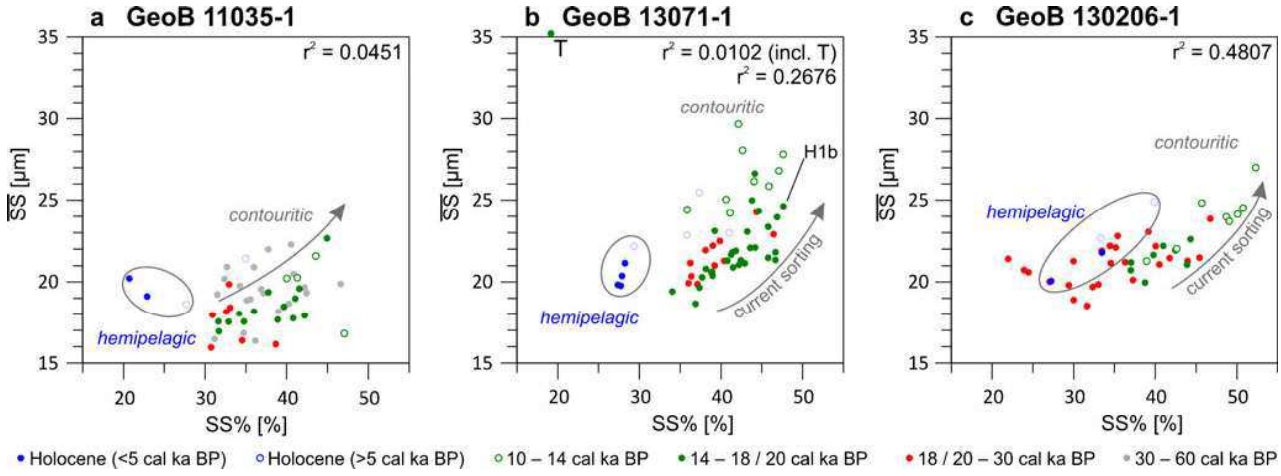

Fig. 9 Sortable silt mean grain size ($\overline{SS}$) vs. content (SS%) plots for the three study cores; in combination with other proxy data, these served to deduce three general sediment supply processes: hemipelagic settling, as well as contouritic and turbiditic (*T*) transport

GeoB130206 is more important after 18 cal ka BP at the time when turbidity current activity declined, adding evidence to the contour current–turbidity current interaction concept proposed by Mulder et al. (2006).

Influence of local morphology on sedimentation patterns

In addition to the frequent occurrence of fine sandy turbidites characterizing site GeoB130206 prior to 18 cal ka BP (cf. above), a constantly high LSR of ~20 cm/1,000 years until 10 cal ka BP, i.e. throughout the post-glacial sea-level rise (Fig. 6), contrasts with sites GeoB11035 and GeoB13071 then experiencing their highest LSRs. At ~10 cal ka BP, however, the LSRs decrease to similarly low levels at all three sites. This "permanently" high pre-Holocene LSR, as well as the greater occurrence of turbidite beds in GeoB130206-1 are interpreted as resulting from the site's proximity to the channel identified on seismic profile p565 (Fig. 2b). This channel would have acted as an efficient *sediment conduit* not only for the turbidity current succession associated with the early sea-level fall but also for the focused off-shelf transport of terrigenous mud (cf. discussion above). This direct terrigenous feeding of the conduit would have been cut off by rising sea level at ca. 10 cal ka BP, causing the observed overall decrease in siliciclastic supply to the Galician slope. These findings convincingly demonstrate how the general sedimentation patterns spanning the past 30 cal ka BP at site 130206 can be teased apart from site-specific overprinting rooted in the local morphology.

The combined findings of well-stratified sediments in the vicinity of site GeoB11035, moats on both sides of the outcrop (cf. seismic profile p594, Fig. 2a), and sortable silt evidence from core GeoB11035-1 point to sustained pre-Holocene *contouritic sediment transport* in this area. LSRs from core GeoB11035-1 indicate main deposition during cold (glacial periods) and deglacial periods, when detrital material was abundantly available. Using long-range side scan sonar and drilling data, Gardner and Kidd (1987) suggested that the most important sediment transport off NW Iberia was generally slope-parallel and directed northwards since the latest Miocene. Similar to site GeoB1135, therefore, contouritic sediment transport and depositional conditions can be expected for site GeoB13071, and series of such contourites presumably exist at the Galician continental margin. Nevertheless, terrigenous mud grain-size spectra differ significantly between these two cores. The mud fraction is moderately well sorted at ca. ~8 μm for GeoB11035-1, and less well sorted with a bimodal distribution comprising coarser silt (10~30 μm) and clayey (3 μm) components for GeoB13071-1. Furthermore, the GeoB11035-1 $\overline{SS}$ versus SS% relationship shows a finer $\overline{SS}$ spectrum but with a similarly focused data distribution (Fig. 9). Assuming contouritic transport for both deposits, overall better sorted terrigenous mud grain-size spectra at a finer mean grain size for GeoB11035-1 suggest a longer slope-parallel transport pathway, depositing the coarser grain-size components before reaching the site of this core. Generally finer $\overline{SS}$ values alternatively point to site GeoB11035 being less exposed to the bottom current regime, maybe due to a local morphologic position outside the main current core. By contrast, site GeoB13071 appears to receive additional, less well-sorted mud (cf. Fig. 8c, d, j, k). An extensive high-turbidity plume close to the shelf break at 42°30′N (ca. 35 km south of site GeoB13071 and north of site GeoB11035; Fig. 1a) has been observed under modern conditions (Hall et al. 2000). On the shelf, glauconite-rich fine sands in the same area have been interpreted as an outer shelf palimpsest facies (Lantzsch et al. 2009b). Both findings indicate active winnowing and resuspension processes—thus, an active shelf mud export in the area around 42°30′N.

Under northward-flowing intermediate- and deep-water currents, the newly exported mud would experience little sorting before reaching site GeoB13071. The data for core GeoB13071-1 therefore add evidence that this major *shelf export pathway*, delivering additional coarser mud fractions to the slope-parallel transport system, is not just a modern feature (Dias et al. 2002) but has been active over the past 30 cal ka BP.

External control on sedimentation patterns: sediment availability, sea level and palaeoceanography

Galician continental margin sedimentation since 65 cal ka BP can be described by four successive time intervals. From *65 to 30 cal ka BP*, sedimentation was dominated by siliciclastic terrigenous mud, low pelagic carbonate input and minor lithologic variability. Roucoux et al. (2005) identify similar minor variability in Iberian hinterland vegetation from 65 to 31 cal ka BP, with slightly wetter interstadials and cooler and drier stadials which may have modified river runoff and the flux of fine detritus. The resolutions of GeoB11035-1 proxy records are too low to directly link grain-size and sorting variations with specific stadial/interstadial cycles; however, such cycles can most likely explain the observed variability. The ~1,500-year D-O cycles (Dansgaard et al. 1993) largely characterize North Atlantic climate during this time interval. Reduced formation of North Atlantic deep water during stadials decelerates the Atlantic meridional overturning circulation (AMOC), reducing deep-water current velocities (Broecker et al. 1985; Ganopolski and Rahmstorf 2001) and consequently enabling deposition of finer-grained material marked by reduced sorting. Vice versa, during interstadials enhanced AMOC hampers deposition of finer particles, leading to grain-size spectra coarsening. Hypothetically, D-O-related short-lasting changes in terrigenous fluvial input and deep-water current velocity might thus explain the observed

sedimentary fluctuations between 65–30 cal ka BP. A water-mass candidate carrying these sediments is MW, which flowed more vigorously and 500–800 m deeper (near the 2,000 m isobath) during cold periods (e.g. Schönfeld and Zahn 2000; Rogerson et al. 2005; Voelker et al. 2006). Nevertheless, MW in its glacial mode does not seem to extend farther north than 39°N (Schönfeld and Zahn 2000). Instead, at the Tore seamount (39°N) northward-flowing Southern Ocean Water replaced southward-flowing NADW below 2,000 m water depth during MIS 2 (Lebreiro et al. 1997). Glacial intermediate- and deep-water current velocity off Galicia is thus coupled to AMOC variations (reduced during stadials and enhanced during warming episodes) rather than to changes in MW flow, which appears to be more significant in the Gulf of Cadiz and off SW Portugal. This concept of palaeocurrent variability off Galicia is supported by reduced palaeocurrent speeds during colder periods documented in core OMII-9K (Fig. 1a; Hall and McCave 2000).

The time interval between *30 and 18 cal ka BP* is more stable; the lithological dominance of terrigenous mud from the previous interval is perpetuated and even slightly increased. At 30 cal ka BP, northern hemisphere ice caps approached their maximum volume and remained constant for the following 11 ka, this being a time of global sea-level fall and lowstand (Lambeck et al. 2002; Peltier and Fairbanks 2006; Hanebuth et al. 2009). Turbidite deposition at site GeoB130206 would have been most active during early rapid sea-level fall (30~23 cal ka BP) and fine sand input significantly reduced from 23 to 19.5 cal ka BP when sea level stabilized at its lowstand position of ~130 m below the modern sea level (Peltier and Fairbanks 2006; Hanebuth et al. 2009; Fig. 6). The coastline off Galicia was located at today's mid-shelf position at that time. Consequently, the flux of fluvially derived terrigenous material, as the dominating sediment sources off Galicia, would have been much more direct to the slope during high-glacial times, explaining the observed dominance of terrigenous mud (Fig. 10a). The Iberian continental palaeoclimate is characterized by remarkably constant cold and arid conditions between 31 and 23 cal ka BP (Roucoux et al. 2005). Alkenone-based sea-surface temperature reconstructions from the SW Iberian margin also indicate relatively cool temperatures of ~12°C for this pre-LGM interval (Bard et al. 2000), keeping pelagic carbonate production low and thus explaining the low coccolith abundance in GeoB11035-1 (Fig. 7d). At 23 cal ka BP these cold and arid climatic conditions became less severe and humidity actually increased over Iberia during the LGM (Roucoux et al. 2005; Naughton et al. 2007a; Voelker et al. 2009), agreeing with the statement of Mix et al. (2001) that the LGM does not always correspond to the coldest glacial period. The general sediment composition off Galicia appears to be strongly controlled by sea level, whereas the shift to cold and more humid conditions did not have a significant influence. The last turbidite in GeoB130206-1 at 19.4 cal ka BP may be associated with an abrupt and pulse-like first rise in sea level exactly at this time (Clark et al. 2004; Hanebuth et al. 2009); the turbidite bed of GeoB13071-1 at 17.9 cal ka BP could reflect the initiation of large-scale shelf sand reworking when sea level rose over the northern Galician shelf.

Post-LGM sedimentation off Galicia from *18 to 10 cal ka BP* was still mainly siliciclastic. The ongoing sea-level rise (Peltier and Fairbanks 2006) would have caused strong reworking of the outer to mid-shelf sediments. During early deglacial sea-level rise (18–15 cal ka BP), immense reworking has been documented on the mid-shelf (Lantzsch et al. 2009b, 2010). The sand fraction would have been directly re-deposited on the outer shelf, whereas silt and clay would have been exported by winnowing (Lantzsch et al. 2010), producing LSRs of up to 37 cm/1,000 years (GeoB13071-1) on the slope. This concept is supported by highest mass accumulation rates during MIS 2 in core OMII-9K (Hall and McCave 2000), and other reconstructions from the western Portuguese margin reporting enhanced input of fine terrigenous sediments during glacials, especially during H1 from 18 to 15 cal ka BP (de Abreu et al. 2003; Lebreiro et al. 2009; Sierro et al. 2009).

From *15.5 cal ka BP* onwards, the grain-size data show significant coarsening from medium silt to coarse silt and very fine sand (GeoB13071-1). To transport and export this coarse material in the course of persisting transgressive reworking—material which was previously directly re-deposited on the outer shelf—the hydrodynamic energy would need to have intensified significantly by ~15.5 cal ka BP over the Galician outer shelf. A hypothetical mechanism leading to the observed time lag between sea level-induced reworking on the outer shelf and export to the slope starting at 15.5 cal ka BP could be the time-lagged onset of a strong outer shelf current. Under modern oceanographic conditions, the Iberian Poleward Current plays a significant role in sediment transport over the Galician shelf (Dias et al. 2002). Origin, occurrence and seasonality of the IPC remain controversial. Latest studies suggest an origin largely from NE Atlantic meridional density gradients and topographic interactions (Peliz et al. 2003a, b), meaning that the IPC is linked to NE Atlantic oceanographic patterns. Moreover, it appears that the existence of the IPC is linked to the Portugal Current, in turn being the easternmost branch of the North Atlantic subtropical gyre. Palaeoceanographic studies from the western Iberian margin indicate that the polar front receded at the end of H1 at ~15.5 cal ka BP (Eynaud et al. 2009; Voelker et al. 2009; see also Figs. 2 and 3 in the electronic supplementary material), enabling the subtropical gyre to extend further north. Due to this shift, a powerful poleward outer shelf current, analogous to the modern IPC, might have started to evolve at ca. 15.5 cal ka BP. Consequently, the Galician upper slope and outer shelf

circulation would have experienced a remarkable directional change from southerly flowing water masses (e.g. $ENACW_{SP}$) prior to 15.5 cal ka BP, to the northerly flowing IPC transporting $ENACW_{ST}$ nowadays (Varela et al. 2005; Fig. 10a, b).

Deep-water currents controlling deposition on the slope experience significant modifications by climatic changes. The grain-size data show reduced current sorting of terrigenous mud during the period ~18 to ~15 cal ka BP (Fig. 9). Sea-surface temperatures off SW Portugal (core SU81-18; Fig. 7f; Bard et al. 2000) and onshore pollen records (Roucoux et al. 2005) show a significant relative cooling during H1 (17.5 to 14.9 cal ka BP; de Abreu et al. 2003). Furthermore, a northern Galician speleothem record indicates that the time interval 18.2–15.4 cal ka BP was NW Iberia's driest and coldest phase of the past 25 cal ka BP (Moreno et al. 2010). Numerical modelling indicates that Heinrich events can cause a collapse or at least a slowdown of deep-water thermohaline circulation (Seidov and Maslin 1999), and geochemical data from the subtropical Atlantic show a nearly total shutdown of AMOC between 17.5~15 cal ka BP (McManus et al. 2004). The present grain-size data thus support the earlier interpretation of reduced current speeds during cold periods (Hall and McCave 2000); furthermore, they show less effective current-induced sorting during such cold periods.

Between 14 and 12.5 cal ka BP, the grain-size data reveal a decrease of the 3~4 μm component and a shift towards coarse silt (~30 μm; bulk and terrigenous mud; Fig. 7a, b); $\overline{SS}$ values indicate increasing near-bottom flow speed. Maximum near-bottom flow speeds are reached at the end of the B/A warm phase. Following the above conceptual model, this development is in remarkable accordance with an abruptly resuming AMOC at ~14.7 cal ka BP (onset of the B/A warm phase), reaching maximum flow speed intensity at 14.2 cal ka BP and remaining constant until 12.5 cal ka BP (McManus et al. 2004). This strengthening of deep-water currents associated with B/A warming would condition the abrupt shift towards the observed better sorted mud fraction, again supporting the interpretation of core OMII-9K which shows a similar sedimentary pattern, indicative of faster bottom current flow during the B/A warming (Hall and McCave 2000; see also Fig. 4 in the electronic supplementary material).

The well-sorted very coarse silt and very fine sand sedimentation is interrupted by a ~1,000 year period marked by poorer sorted terrigenous mud grain-size distributions (Fig. 7b), and decreased $\overline{SS}$ and SS% (Fig. 8f, g), suggesting reduced current strength. This current strength reduction coincides with YD cooling (Fig. 7d, f) when, as in the H1 interval, AMOC was significantly reduced (McManus et al. 2004). Contrasting with the preceding 18–15 cal ka BP initial deglacial sea-level rise interval, the sedimentary expression of weakened deep-water circulation is this time not overprinted by enhanced detrital input. Instead, LSRs decrease gradually together with decreasing $\overline{SS}$ and SS% from the B/A until 10–8 cal ka BP (Figs. 4, 5 and 7).

Although small amounts of terrigenous coarse silt (~30 μm) still arrive at the slope up to ~8 cal ka BP (e.g. Fig. 7a, b), the most dramatic shift in the sedimentary pattern occurs at *~10 cal ka BP* synchronously at all three sites, marking the onset of the Holocene regime (e.g. Fig. 7). At 10 cal ka BP the eustatic sea-level rise decelerated significantly and sea level was already close to the modern coasts (ca. –30 m; Peltier and Fairbanks 2006), creating wide accommodation space on the inner shelf and within the Galician Rías Baixas (40–45 m deep), where storage of detrital material is promoted today (Drago et al. 2006; Naughton et al. 2007b). Reflecting the end of transgressive reworking on the shelf, the top of the sandy transgressive unit (U2) on the shelf dates to ca. 10 cal ka BP (Lantzsch et al. 2009b, 2010). Besides the subsequently decreased supply, the sortable silt data indicate decelerated slope currents from the early Holocene onwards, additionally leading to the disappearance of the ~30 μm silt fraction. Noteworthy is that the modern flow pattern of MW along the western Iberian margin was established at this time (ca. 8 cal ka BP at the northern Portuguese margin; Schönfeld and Zahn 2000). The fading out of coarse silt on the slope during the early Holocene would thus be a combined result of (1) decreasing supply due to the termination of mid-shelf sediment reworking and gradual refill of NW Iberian estuaries, both being associated with the decelerating sea-level rise, and (2) decelerated slope currents related to the establishment of the modern intermediate-water flow patterns along western Iberia. Furthermore, from 10 cal ka BP onwards, the abundant appearance of planktonic and benthic foraminifers, more than fivefold increases in coccolith numbers, higher coccolith species diversity, and the mud fraction dominated by ~4 μm carbonate suggest significantly increased Holocene primary production (Fig. 7c, e). Sequential with this increase in marine productivity, a decrease in the relative abundance of *N. pachyderma* (sin) of GeoB11035-1 (Fig. 7d) is consistent with a retreat of polar waters off NW Iberia (cf. Fig. 3 in the online electronic supplementary material; Eynaud et al. 2009). Although a certain effect of reduced carbonate dilution by lower detrital supply cannot be excluded, these combined evidences plausibly indicate that marine productivity was greatly enhanced along the Galician continental margin from ~10 cal ka BP onwards by the Holocene warming (documented off western Iberia by, for example, Bard et al. 2000, de Abreu et al. 2003, and Schönfeld et al. 2003). Similar observations have been documented for the Gulf of Cadiz and the Alboran Sea (Colmenero-Hidalgo et al. 2004), suggesting a general pattern of increased productivity around Iberia during the Holocene.

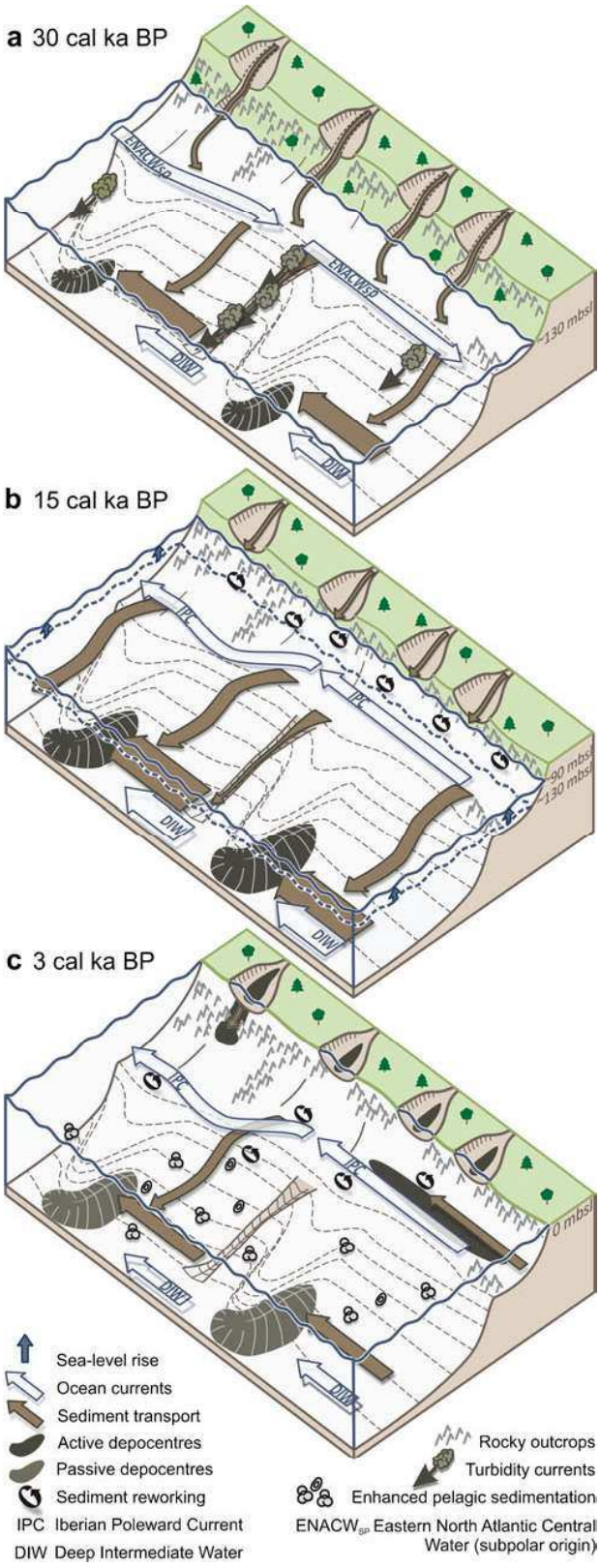

Fig. 10 Schematic illustration of late Quaternary sediment dynamics on the Galician continental slope to about 3,000 m water depth in the Galician interior basin: **a** direct and continuous detrital input, as well as turbidity currents channelized by sediment conduits dominate during the maximum regression at ca. 23 ka; **b** onset of IPC circulation along the outer shelf marks the deglacial transgression, resulting in a main outer shelf current reversal and strong reworking on the middle to inner shelf; **c** after the flooding and refilling of the Galician rías, present-day dynamics are driven by seasonal resuspension from the mid-shelf mud depocentres and small-scale shelf export, whereas pelagic sedimentation is greatly enhanced

Furthermore, this Holocene hemipelagic sedimentary pattern off Galicia is regionally consistent with the findings of, for example, Baas et al. (1997) and Lebreiro et al. (2009) for the Portuguese margin.

Besides the clear dominance of biogenic carbonate, minor variations in detrital input are recognizable in the Holocene mud grain-size spectra. After *~5 cal ka BP*, all $CaCO_3$ and Ca/Fe records experience a slight decrease, whereas a terrigenous ~3 μm component appears in the grain-size spectra (e.g. Fig. 7b). Since sea-surface temperatures and coccolith diversity do not change significantly, this relative increase in terrigenous mud evidently is an unaltered input signal. Under modern conditions, fine sediments are frequently resuspended from the Galician mid-shelf mud belt by deep storm-related turbulence (Dias et al. 2002; Vitorino et al. 2002), and transported off-shelf in the form of intermediate nepheloid layers (Hall et al. 2000; Fig. 10c). The concurrent reappearance of terrigenous mud on the slope and initial formation of the Galician mid-shelf mud belt as early as 5.3 cal ka BP (Lantzsch et al. 2009a) point towards the onset of this resuspension–export process at ca. 5 cal ka BP. The higher frequency of storm tracks over NW Iberia after 4.5 cal ka BP have been interpreted from Ría de Muros sediments by Pena et al. (2010), whereas a shift to less stormy conditions at 2.8 cal ka BP has been reported for a Galician outer shelf sediment record (González-Álvarez et al. 2005). However, the latter is drawn from a sandy-to-muddy lithofacies change at 2.8 cal ka BP, which could also be interpreted in terms of a time-transgressive lateral expansion of the Galician mud belt (Lantzsch et al. 2009b). Holocene sample and age tie point resolution of the present study is too low to clearly differentiate whether the additional terrigenous mud on the slope after ca. 5 cal ka BP is directly due to Galician mud belt initiation, or whether a climatic shift to stormier conditions at 4.5 cal ka BP was necessary to foster the export. Nevertheless, a sedimentary shelf–slope linkage is clearly evident, and the establishment of a modern large-scale storm-driven mud resuspension–export pattern between 4–5 cal ka BP along the Galician ocean margin is plausible (Fig. 10c). A similar mid-Holocene sea level-induced initiation of a fine-grained depocentre has been documented also for the southern Iberian mid-shelf (Rosa et al. 2011)—

evidently, the impact of shelf depocentre evolution on slope sedimentary patterns cannot be disregarded.

Conclusions

Multiproxy investigation of three new cores from the Galician continental slope revealed four periods with distinct sedimentary signatures over the past 65 ka. Spanning the marine isotope stages 3 to 1, variations in detrital input, marine productivity and sea level were the essential drivers of sediment availability on the slope, whereas deep-water current velocities and local morphology controlled sediment deposition:

1. the period prior to 30 cal ka BP is characterized by minor but systematic variations in various proxies which can be attributed to D-O cycles;
2. between 30 and 18 cal ka BP, high detrital input and steady slope-parallel currents led to a constant sedimentation regime;
3. from the LGM until 10 cal ka BP, the shelf-transgressive sea-level rise caused an increased detrital particle supply resulting in highly terrigenous deposits; in particular, the strong outer shelf Iberian Poleward Current was established at about 15.5 cal ka BP; sedimentation on the slope was significantly influenced by enhanced AMOC strength during the Bølling/Allerød, and subsequent slowing during the Younger Dryas;
4. an abrupt and lasting change to highly biogenic sedimentation at ca. 10 cal ka BP is probably due to the Holocene warming as well as to decelerated transgression on the inner shelf resulting in strongly reduced terrigenous supply; however, additional input of fine-grained detrital material after 5 cal ka BP was contemporaneous with the initiation of fine-grained depocentres on the middle Galician shelf, both plausibly linked to the readjusting sediment export from the major drowned river mouth estuaries;
5. the area off the Ría de Vigo is fed by mature sediments from slope-parallel deep-ocean currents building a significant contourite body, whereas the data suggest the strong influence of a nearby active sediment export pathway on the shelf off the Ría de Arousa/Ría de Muros (north of 42°30′N);
6. the newly discovered channel off the Ría de Arousa was active only in pre-Holocene times.

The combined findings of this study underline that only precise knowledge of sediment architecture and composition enables differentiating between independent but interacting contributions of local slope and shelf morphology, regional sedimentation patterns, and their palaeoclimatic and palaeoceanographic variations as drivers of sediment dynamics. By implication, sediment dynamics particularly in morphologically complex settings are less straightforward than commonly considered and thus deserve further attention in future.

Acknowledgements This study was funded through the DFG Graduate College "Proxies in Earth History (EUROPROX)" and DFG-Research 642 Center/Cluster of Excellence "The Ocean in the Earth System", as well as the GRACCIE (Consolider-Ingenio, CDS 2007–00067) and CONTOUR-IBER (CTM2008-06399-C04-01/MAR) projects. We wish to thank Captain M. Schneider and his crew of R/V *Poseidon* for the professional but cordial atmosphere during cruises Pos-342 and Pos-366/3. Sebastian Krastel-Gudegast and Marion Castex are thanked for their supporting work. Furthermore, we are grateful to Susana Lebreiro, Calvin Campbell and two anonymous reviewers for their very constructive comments on earlier versions of this manuscript, as well as to the journal editors for helpful feedback.

References

Álvarez-Salgado XA, Figueiras FG, Pérez FF, Groom S, Nogueira E, Borges A, Chou L, Castro CG, Moncoiffé G, Ríos AF, Miller AEJ, Frankignoulle M, Savidge G, Wollast R (2003) The Portugal coastal counter current off NW Spain: new insights on its biogeochemical variability. Prog Oceanogr 56:281–321. doi:10.1016/S0079-6611(03)00007-7

Andruleit H (1996) A filtration technique for quantitative studies of coccoliths. Micropaleontology 42:403–406

Baas JH, Mienert J, Abrantes F, Prins MA (1997) Late quaternary sedimentation on the Portuguese continental margin: climate-related processes and products. Palaeogeogr Palaeoclimatol Palaeoecol 130:1–23. doi:10.1016/S0031-0182(96)00135-6

Bard E, Arnold M, Hamelin B, Tisnerat-Laborde N, Cabioch G (1998) Radiocarbon calibration by means of mass spectrometric $^{230}Th/^{234}U$ and ^{14}C ages of corals: an updated database including samples from Barbados, Mururoa and Tahiti. Radiocarbon 40:1085–1092

Bard E, Rostek F, Turon JL, Gendreau S (2000) Hydrological impact of Heinrich events in the subtropical northeast Atlantic. Science 289:1321–1324. doi:10.1126/science.289.5483.1321

Blair TC, McPherson JG (1999) Grain-size and textural classification of coarse sedimentary particles. J Sediment Res 69:6–19

Broecker WS, Peteet DM, Rind D (1985) Does the ocean–atmosphere system have more than one stable mode of operation? Nature 315:21–26. doi:10.1038/315021a0

Brown LF, Fisher WL (1977) Seismic-stratigraphic interpretation of depositional systems: examples from Brazilian rift and pull-apart basins. In: Payton CE (ed) Seismic stratigraphy - applications to hydrocarbon exploration. AAPG Memoir, pp 213–248

Clark PU, McCabe AM, Mix AC, Weaver AJ (2004) Rapid rise of sea level 19,000 years ago and its global implications. Science 304:1141–1144. doi:10.1126/science.1094449

Colmenero-Hidalgo E, Flores JA, Sierro FJ, Bárcena MA, Löwemark L, Schönfeld J, Grimalt JO (2004) Ocean surface water response to short-term climate changes revealed by coccolithophores from the Gulf of Cadiz (NE Atlantic) and Alboran Sea (W Mediterranean). Palaeogeogr Palaeoclimatol Palaeoecol 205:317–336. doi:10.1016/j.palaeo.2003.12.014

Crowley TJ (1983) Calcium carbonate preservation patterns in the Central North Atlantic during the last 150,000 years. Mar Geol 51:1–14. doi:10.1016/0025-3227(83)90085-3

Dansgaard W, Johnsen SJ, Clausen HB, Dahljensen D, Gundestrup NS, Hammer CU, Hvidberg CS, Steffensen JP, Sveinbjornsdottir

AE, Jouzel J, Bond G (1993) Evidence for general instability of past climate from a 250-kyr ice-core record. Nature 364:218–220. doi:10.1038/364218a0

de Abreu L, Shackleton NJ, Schönfeld J, Hall M, Chapman M (2003) Millennial-scale oceanic climate variability off the Western Iberian margin during the last two glacial periods. Mar Geol 196:1–20. doi:10.1016/S0025-3227(03)00046-X

Dias JMA, Gonzalez R, Garcia C, Diaz-del-Rio V (2002) Sediment distribution patterns on the Galicia-Minho continental shelf. Prog Oceanogr 52:215–231. doi:10.1016/S0079-6611(02)00007-1

Drago T, Freitas C, Rocha F, Moreno J, Cachao M, Naughton F, Fradique C, Araújo F, Silveira T, Oliveira A, Cascalho J, Fatela F (2006) Paleoenvironmental evolution of estuarine systems during the last 14000 years - the case of Douro estuary (NW Portugal). J Coast Res 1:186–192

Eynaud F, de Abreu L, Voelker A, Schönfeld J, Salgueiro E, Turon JL, Penaud A, Toucanne S, Naughton F, Goñi MFS, Malaizé B, Cacho I (2009) Position of the Polar Front along the western Iberian margin during key cold episodes of the last 45 ka. Geochem Geophys Geosyst 10:1–21. doi:10.1029/2009GC002398

Fiúza AFG, Hamann M, Ambar I, Díaz del Río G, González N, Cabanas JM (1998) Water masses and their circulation off western Iberia during May 1993. Deep-Sea Res I 45:1127–1160. doi:10.1016/S0967-0637(98)00008-9

Ganopolski A, Rahmstorf S (2001) Rapid changes of glacial climate simulated in a coupled climate model. Nature 409:153–158. doi:10.1038/35051500

Gardner JV, Kidd RB (1987) Sedimentary processes on the northwestern Iberian continental margin viewed by long-range side-scan sonar and seismic data. J Sediment Petrol 57:397–407

González-Álvarez R, Bernárdez P, Pena LD, Francés G, Prego R, Diz P, Vilas F (2005) Paleoclimatic evolution of the Galician continental shelf (NW of Spain) during the last 3000 years: from a storm regime to present conditions. J Mar Syst 54:245–260. doi:10.1016/j.jmarsys.2004.07.015

Grootes PM, Stuiver M, White JWC, Johnsen S, Jouzel J (1993) Comparison of oxygen-isotope records from the GISP2 and GRIP Greenland ice cores. Nature 366:552–554. doi:10.1038/366552a0

Hall IR, McCave IN (2000) Palaeocurrent reconstruction, sediment and thorium focussing on the Iberian margin over the last 140 ka. Earth Planet Sci Lett 178:151–164. doi:10.1016/S0012-821X(00)00068-6

Hall IR, Schmidt S, McCave IN, Reyss JL (2000) Particulate matter distribution and $^{234}Th/^{238}U$ disequilibrium along the Northern Iberian Margin: implications for particulate organic carbon export. Deep-Sea Res I 47:557–582. doi:10.1016/S0967-0637(99)00065-5

Hanebuth TJJ, Stattegger K, Bojanowski A (2009) Termination of the last glacial maximum sea-level lowstand: the Sunda-Shelf data revisited. Global Planet Change 66:76 84. doi:10.1016/j.gloplacha.2008.03.011

Haynes R, Barton ED (1990) A poleward flow along the Atlantic coast of the Iberian Peninsula. J Geophys Res Oceans 95:11425–11441. doi:10.1029/JC095iC07p11425

Heinrich H (1988) Origin and consequences of cyclic ice rafting in the northeast Atlantic Ocean during the past 130,000 years. Quat Res 29:142–152. doi:10.1016/0033-5894(88)90057-9

Hernández-Molina FJ, Serra N, Stow DAV, Llave E, Ercilla G, Van Rooij D (2011) Along-slope oceanographic processes and sedimentary products around the Iberian margin. Geo-Mar Lett 31:315–341. doi:10.1007/s00367-011-0242-2

Iorga MC, Lozier MS (1999) Signatures of the Mediterranean outflow from a North Atlantic climatology: 1. Salinity and density fields. J Geophys Res 104:25985–26009. doi:10.1029/1999JC900115

Lallemand S, Mazé JP, Monti S, Sibuet JC (1985) New bathymetric map of the northeast Atlantic Ocean. C R Acad Sci Série II 300:145–149

Lambeck K, Yokoyama Y, Purcell T (2002) Into and out of the last glacial maximum: sea-level change during oxygen isotope stages 3 and 2. Quat Sci Rev 21:343–360. doi:10.1016/S0277-3791(01)00071-3

Lantzsch H, Hanebuth TJJ, Bender VB (2009a) Holocene evolution of mud depocentres on a high-energy, low-accumulation shelf (NW Iberia). Quat Res 72:325–336. doi:10.1016/j.yqres.2009.07.009

Lantzsch H, Hanebuth TJJ, Bender VB, Krastel-Gudegast S (2009b) Sedimentary architecture of a low accumulation shelf since the Late Pleistocene (NW Iberia). Mar Geol 259:47–58. doi:10.1016/j.margeo.2008.12.008

Lantzsch H, Hanebuth TJJ, Henrich R (2010) Sediment recycling and adjustment of deposition during deglacial drowning of a low-accumulation shelf (NW Iberia). Cont Shelf Res 30:1665–1679. doi:10.1016/j.csr.2010.06.013

Law BA, Hill PS, Milligan TG, Curran KJ, Wiberg PL, Wheatcroft RA (2008) Size sorting of fine-grained sediments during erosion: results from the western Gulf of Lions. Cont Shelf Res 28:1935–1946. doi:10.1016/j.csr.2007.11.006

Lebreiro SM, Moreno JC, McCave IN, Weaver PPE (1996) Evidence for Heinrich layers off Portugal (Tore seamount: 39° N, 12° W). Mar Geol 131:47–56. doi:10.1016/0025-3227(95)00142-5

Lebreiro SM, Moreno JC, Abrantes FF, Pflaumann U (1997) Productivity and paleoceanographic implications on the Tore seamount (Iberian margin) during the last 225 kyr: foraminiferal evidence. Paleoceanography 12:718–727. doi:10.1029/97PA01748

Lebreiro SM, Voelker AHL, Vizcaino A, Abrantes FG, Alt-Epping U, Jung S, Thouveny N, Gràcia E (2009) Sediment instability on the Portuguese continental margin under abrupt glacial climate changes (last 60 kyr). Quat Sci Rev 28:3211–3223. doi:10.1016/j.quascirev.2009.08.007

Llave E, Schönfeld J, Hernández-Molina FJ, Mulder T, Somoza L, Díaz del Río V, Sánchez-Almazo I (2006) High-resolution stratigraphy of the Mediterranean outflow contourite system in the Gulf of Cadiz during the late Pleistocene: the impact of Heinrich events. Mar Geol 227:241–262. doi:10.1016/j.margeo.2005.11.015

Martins V, Dubert J, Jouanneau JM, Weber O, da Silva EF, Patinha C, Dias JMA, Rocha F (2007) A multiproxy approach of the Holocene evolution of shelf-slope circulation on the NW Iberian continental shelf. Mar Geol 239:1–18. doi:10.1016/j.margeo.2006.11.001

Mazé JP, Arhan M, Mercier H (1997) Volume budget of the eastern boundary layer off the Iberian Peninsula. Deep-Sea Res I 44:1543–1574. doi:10.1016/S0967-0637(97)00038-1

McCave IN, Hall IR (2002) Turbidity of waters over the northwest Iberian continental margin. Prog Oceanogr 52:299–313. doi:10.1016/S0079-6611(02)00012-5

McCave IN, Hall IR (2006) Size sorting in marine muds: processes, pitfalls, and prospects for paleoflow-speed proxies. Geochem Geophys Geosyst 7:1–37. doi:10.1029/2006GC001284

McCave IN, Manighetti B, Robinson SG (1995) Sortable silt and fine sediment size composition slicing: parameters for paleocurrent speed and paleoceanography. Paleoceanography 10:593–610. doi:10.1029/94PA03039

McManus JF, Francois R, Gherardi JM, Keigwin LD, Brown-Leger S (2004) Collapse and rapid resumption of Atlantic meridional circulation linked to deglacial climate changes. Nature 428:834–837. doi:10.1038/nature02494

Milkert D, Weaver PPE, Liu L (1996) Pleistocene and Pliocene turbidites from the Iberia abyssal plain. In: Whitmarsh RB, Sawyer DS, Klaus A, Masson DG (eds) ODP proceedings, scientific results. Ocean Drilling Program, College Station, pp 281–294

Mix AC, Bard E, Schneider R (2001) Environmental processes of the ice age: land, oceans, glaciers (EPILOG). Quat Sci Rev 20:627–657. doi:10.1016/S0277-3791(00)00145-1

Moreno E, Thouveny N, Delanghe D, McCave IN, Shackleton NJ (2002) Climatic and oceanographic changes in the northeast

Atlantic reflected by magnetic properties of sediments deposited on the Portuguese margin during the last 340 ka. Earth Planet Sci Lett 202:465–480. doi:10.1016/S0012-821X(02)00787-2

Moreno A, Stoll H, Jiménez-Sánchez M, Cacho I, Valero-Garcés B, Ito E, Edwards RL (2010) A speleothem record of glacial (25–11.6 kyr BP) rapid climatic changes from northern Iberian peninsula. Global Planet Change 71:218 231. doi:10.1016/j.gloplacha.2009.10.002

Mulder T, Lecroart P, Hanquiez V, Marches E, Gonthier E, Guedes JC, Thiébot E, Jaaidi B, Kenyon N, Voisset M, Perez C, Sayago M, Fuchey Y, Bujan S (2006) The western part of the Gulf of Cadiz: contour currents and turbidity currents interactions. Geo-Mar Lett 26:31–41. doi:10.1007/s00367-005-0013-z

Naughton F, Sánchez Goñi MF, Desprat S, Turon JL, Duprat J, Malaizé B, Joli C, Cortijo E, Drago T, Freitas MC (2007a) Present-day and past (last 25 000 years) marine pollen signal off western Iberia. Mar Micropaleontol 62:91–114. doi:10.1016/j.marmicro.2006.07.006

Naughton F, Sánchez Goñi MF, Drago T, Freitas MC, Oliveira A (2007b) Holocene changes in the Douro estuary (northwestern Iberia). J Coast Res 23:711–720. doi:10.2112/05-0462.1

Naughton F, Sánchez Goñi MF, Kageyama M, Bard E, Duprat J, Cortijo E, Desprat S, Malaizé B, Joly C, Rostek F, Turon JL (2009) Wet to dry climatic trend in north-western Iberia within Heinrich events. Earth Planet Sci Lett 284:329–342. doi:10.1016/j.epsl.2009.05.001

Nittrouer CA, Austin JA, Field ME, Kravitz JH, Syvitski JPM, Wiberg PL (2007) Writing a rosetta stone: insights into continental-margin sedimentary processes and strata. In: Nittrouer CA, Austin JA, Field ME, Kravitz JH, Syvitski JPM, Wiberg PL (eds) Continental margin sedimentation: from sediment transport to sequence stratigraphy. Blackwell, Oxford, pp 1–48

Oliveira A, Rocha F, Rodrigues A, Jouanneau J, Dias A, Weber O, Gomes C (2002a) Clay minerals from the sedimentary cover from the Northwest Iberian shelf. Prog Oceanogr 52:233–247. doi:10.1016/S0079-6611(02)00008-3

Oliveira A, Vitorino J, Rodrigues A, Jouanneau JM, Dias JA, Weber O (2002b) Nepheloid layer dynamics in the northern Portuguese shelf. Prog Oceanogr 52:195–213. doi:10.1016/S0079-6611(02)00006-X

Paillard D, Labeyrie L, Yiou P (1996) Macintosh program performs time-series analysis. Eos 77:379

Peliz A, Dubert J, Haidvogel DB, Le Cann B (2003a) Generation and unstable evolution of a density-driven eastern Poleward Current: the Iberian poleward current. J Geophys Res Oceans 108:1–24. doi:10.1029/2002JC001443

Peliz A, Dubert JS, Haidvogel DB (2003b) Subinertial response of a density-driven eastern boundary poleward current to wind forcing. J Phys Oceanogr 33:1633–1650

Peltier WR, Fairbanks RG (2006) Global glacial ice volume and last glacial maximum duration from an extended Barbados sea level record. Quat Sci Rev 25:3322–3337. doi:10.1016/j.quascirev.2006.04.010

Pena LD, Francés G, Diz P, Esparza M, Grimalt JO, Nombela MA, Alejo I (2010) Climate fluctuations during the Holocene in NW Iberia: high and low latitude linkages. Cont Shelf Res 30:1487–1496. doi:10.1016/j.csr.2010.05.009

Rey Salgado J (1993) Relacion morphose dimentaria entre la platforma continental de Galicia y las Rias bajas y su evolucion durante el Cuaternario. Publ Espec Inst Español Oceanogr 17:1–233

Rogerson M, Rohling EJ, Weaver PPE, Murray JW (2005) Glacial to interglacial changes in the settling depth of the Mediterranean outflow plume. Paleoceanography 20:1–12. doi:10.1029/2004PA001106

Rosa F, Dias J, Mendes I, Ferreira Ó (2011) Mid to late Holocene constraints for continental shelf mud deposition in association with river input: the Guadiana Mud Patch (SW Iberia). Geo-Mar Lett 31:109–121. doi:10.1007/s00367-010-0219-6

Roucoux KH, de Abreu L, Shackleton NJ, Tzedakis PC (2005) The response of NW Iberian vegetation to North Atlantic climate oscillations during the last 65 kyr. Quat Sci Rev 24:1637–1653. doi:10.1016/j.quascirev.2004.08.022

Salgueiro E, Voelker AHL, de Abreu L, Abrantes F, Meggers H, Wefer G (2010) Temperature and productivity changes off the western Iberian margin during the last 150 ky. Quat Sci Rev 29:680–695. doi:10.1016/j.quascirev.2009.11.013

Schönfeld J, Zahn R (2000) Late Glacial to Holocene history of the Mediterranean outflow. Evidence from benthic foraminiferal assemblages and stable isotopes at the Portuguese margin. Palaeogeogr Palaeoclimatol Palaeoecol 159:85–111. doi:10.1016/S0031-0182(00)00035-3

Schönfeld J, Zahn R, de Abreu L (2003) Surface and deep water response to rapid climate changes at the Western Iberian margin. Global Planet Change 36:237–264. doi:10.1016/s0921-8181(02)00197-2

Seidov D, Maslin M (1999) North Atlantic deep water circulation collapse during Heinrich events. Geology 27:23–26. doi:10.1130/0091-7613(1999) 027<0023:NADWCC>2.3.CO;2

Shackleton NJ, Hall MA, Vincent E (2000) Phase relationships between millennial-scale events 64,000-24,000 years ago. Paleoceanography 15:565–569. doi:10.1029/2000PA000513

Sierro FJ, Andersen N, Bassetti MA, Berné S, Canals M, Curtis JH, Dennielou B, Flores JA, Frigola J, Gonzalez-Mora B, Grimalt JO, Hodell DA, Jouet G, Pérez-Folgado M, Schneider R (2009) Phase relationship between sea level and abrupt climate change. Quat Sci Rev 28:2867–2881. doi:10.1016/j.quascirev.2009.07.019

Stuiver M, Grootes PM (2000) GISP2 oxygen isotope ratios. Quat Res 53:277–283. doi:10.1006/qres.2000.2127

Stuiver M, Reimer PJ, Bard E, Beck JW, Burr GS, Hughen KA, Kromer B, McCormac G, Van der Plicht J, Spurk M (1998) INTCAL98 radiocarbon age calibration, 24,000–0 cal BP. Radiocarbon 40:1041–1083

Thomson J, Nixon S, Summerhayes CP, Rohling EJ, Schönfeld J, Zahn R, Grootes P, Abrantes F, Gaspar L, Vaqueiro S (2000) Enhanced productivity on the Iberian margin during glacial/interglacial transitions revealed by barium and diatoms. J Geol Soc 157:667–677. doi:10.1144/jgs.157.3.667

van Weering TCE, McCave IN (2002) Benthic processes and dynamics at the NW Iberian margin: an introduction. Prog Oceanogr 52:123–128. doi:10.1016/S0079-6611(02)00002-2

van Weering TCE, McCave IN, Hall IR (1998) Ocean Margin Exchange (OMEX I) benthic processes study. Prog Oceanogr 42:1–4. doi:10.1016/S0079-6611(98)00025-1

Varela RA, Rosón G, Herrera JL, Torres-López S, Fernández-Romero A (2005) A general view of the hydrographic and dynamical patterns of the Rías Baixas adjacent sea area. J Mar Syst 54:97–113. doi:10.1016/j.jmarsys.2004.07.006

Vitorino J, Oliveira A, Jouanneau JM, Drago T (2002) Winter dynamics on the northern Portuguese shelf. Part 2: bottom boundary layers and sediment dispersal. Prog Oceanogr 52:155–170. doi:10.1016/S0079-6611(02)00004-6

Voelker AHL, Lebreiro SM, Schönfeld J, Cacho I, Erlenkeuser H, Abrantes F (2006) Mediterranean outflow strengthening during northern hemisphere coolings: a salt source for the glacial Atlantic? Earth Planet Sci Lett 245:39–55. doi:10.1016/j.epsl.2006.03.014

Voelker AHL, de Abreu L, Schönfeld J, Erlenkeuser H, Abrantes F (2009) Hydrographic conditions along the western Iberian margin during marine isotope stage 2. Geochem Geophys Geosyst 10:1–30. doi:10.1029/2009GC002605

Weaver PPE, Wynn RB, Kenyon NH, Evan J (2000) Continental margin sedimentation, with special reference to the north-east Atlantic margin. Sedimentology 47:239–256. doi:10.1046/j.1365-3091.2000.0470s1239.x

Electronic Supplementary Material to Bender et al. (2012)

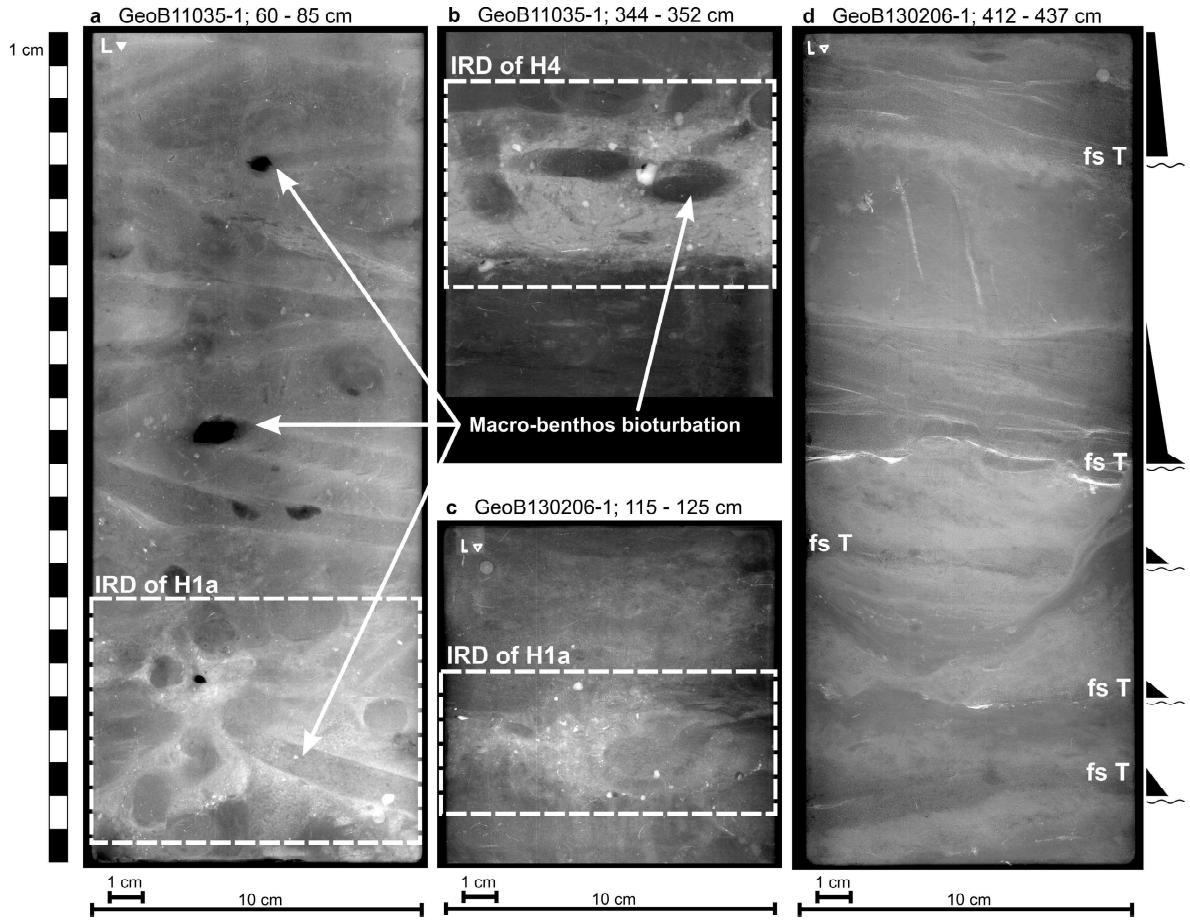

EMS Fig. 1: Radiographic images of **a–c** ice-rafted debris (IRD) layers from cores GeoB11035-1 and GeoB130206-1 associated with Heinrich events H1a and H4. The layers in core GeoB11035-1 are disturbed by macro-benthos bioturbation of *Planolites* and *Zoophycos* type. **d** Successive fine sandy (fs) layers in core GeoB130206-1, interpreted as proximal turbidites (T).

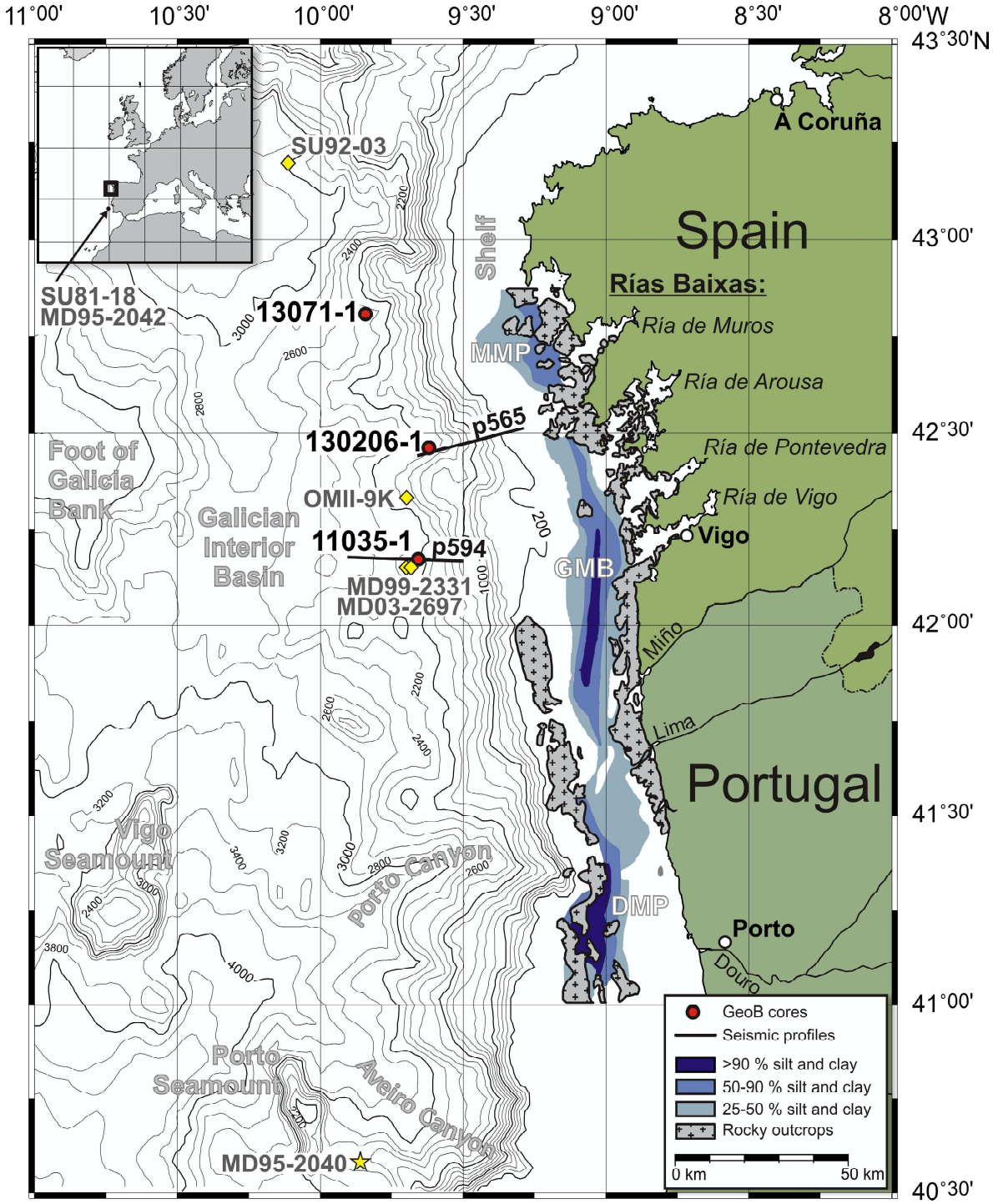

ESM Fig. 2: Site locations of GeoB sediment cores (present study), as well as sediment cores from which data are shown in the following supplementary figures 3 and 4. Cores MD95-2040 (e.g. de Abreu et al. 2003; Salgueiro et al. 2010), MD99-2331 (Eynaud et al. 2009), MD03-2697 (Eynaud et al. 2009), OMII-9K (Hall and McCave 2000), SU92-03 (Salgueiro et al. 2010), as well as south of the study area (inset) core SU81-18 (Bard et al. 2000) and MD95-2042 (e.g. Salgueiro et al. 2010) are indicated. Shelf geology modified from Dias et al. (2002) and Lantzsch et al. (2009). *MMP* Muros mud patch, *GMB* Galician mud belt, *DMP* Douro mud patch.

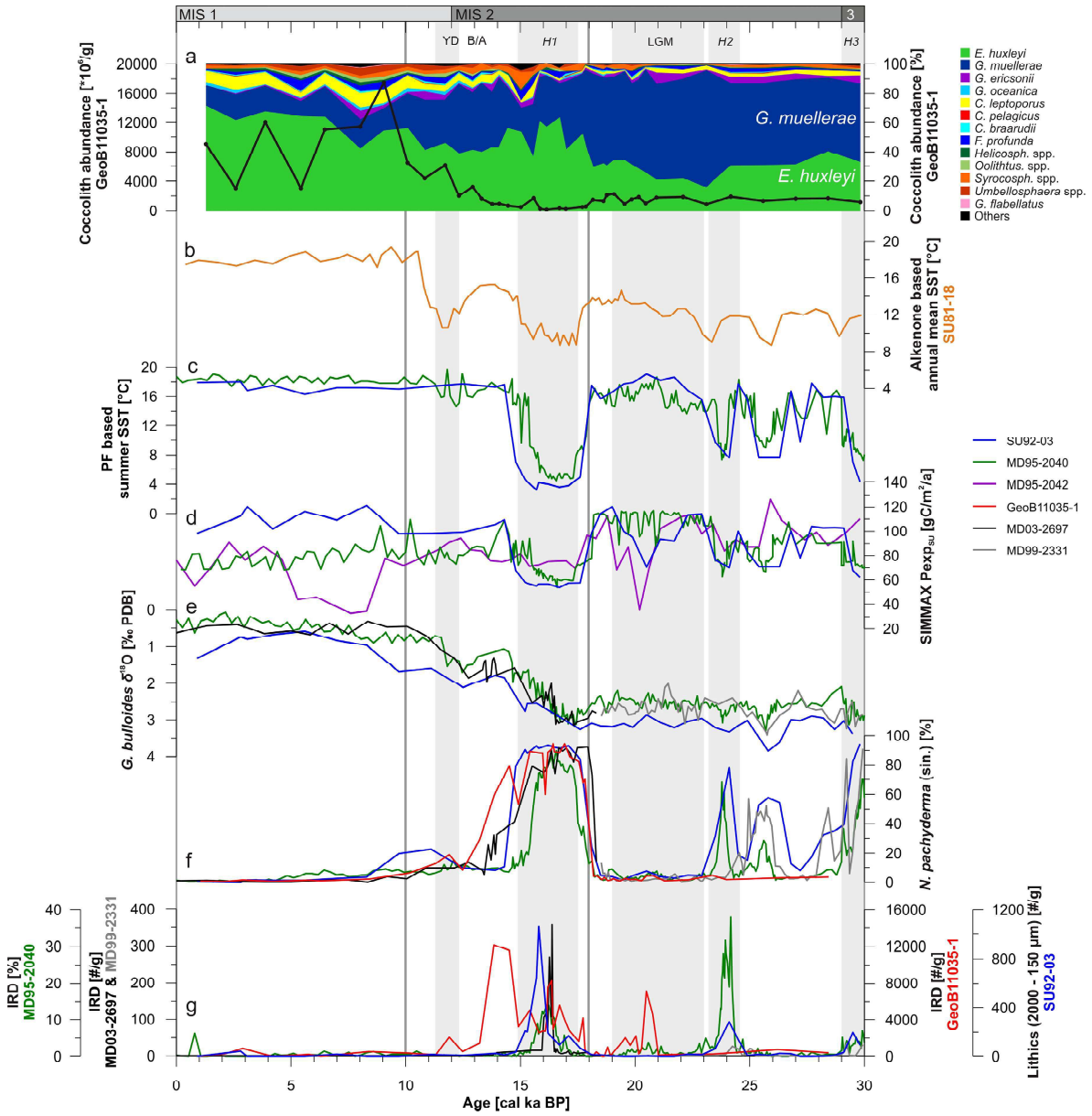

ESM Fig. 3: Comparison of selected paleoceanographic records from the West Iberian margin with paleoceanographic data from core GeoB11035-1. **a** Coccolith total abundance (black line) and cumulative abundance of individual species from GeoB11035-1. **b** Alkenone-based sea-surface temperatures (SST) reconstruction from core SU81-18 (Bard et al. 2000). **c** Planktonic foraminifera based SST reconstructions from cores SU92-03 (*blue*) and MD95-2040 (*green*) (Salgueiro et al. 2010). **d** Summer export productivity reconstructed from SU92-03 (*blue*), MD95-2040 (*green*) and MD95-2042 (*purple*) (Salgueiro et al. 2010). **e** δ^{18}O G. bulloides data from cores SU92-03 (*blue*; Salgueiro et al. 2010), MD95-2040 (*green*; Salgueiro et al. 2010), MD03-2697 (*black*; Eynaud et al. 2009) and MD99-2331 (*gray*; Eynaud et al. 2009). **f** *N. pachyderma* (sin) counts from SU92-03 (*blue*; Salgueiro et al. 2010), MD95-2040 (*green*; Salgueiro et al. 2010), MD03-2697 (*black*; Eynaud et al. 2009) and MD99-2331 (*gray*; Eynaud et al. 2009) and GeoB11035-1 (*red*, this study). **g** IRD counts from SU92-03 (*blue*; Salgueiro et al. 2010), MD95-2040 (*green*; de Abreu et al. 2003), MD03-2697 (*black*; Eynaud et al. 2009) and MD99-2331 (*gray*; Eynaud et al. 2009) and GeoB11035-1 (*red*, this study). For core locations see **ESM Fig. 2.**

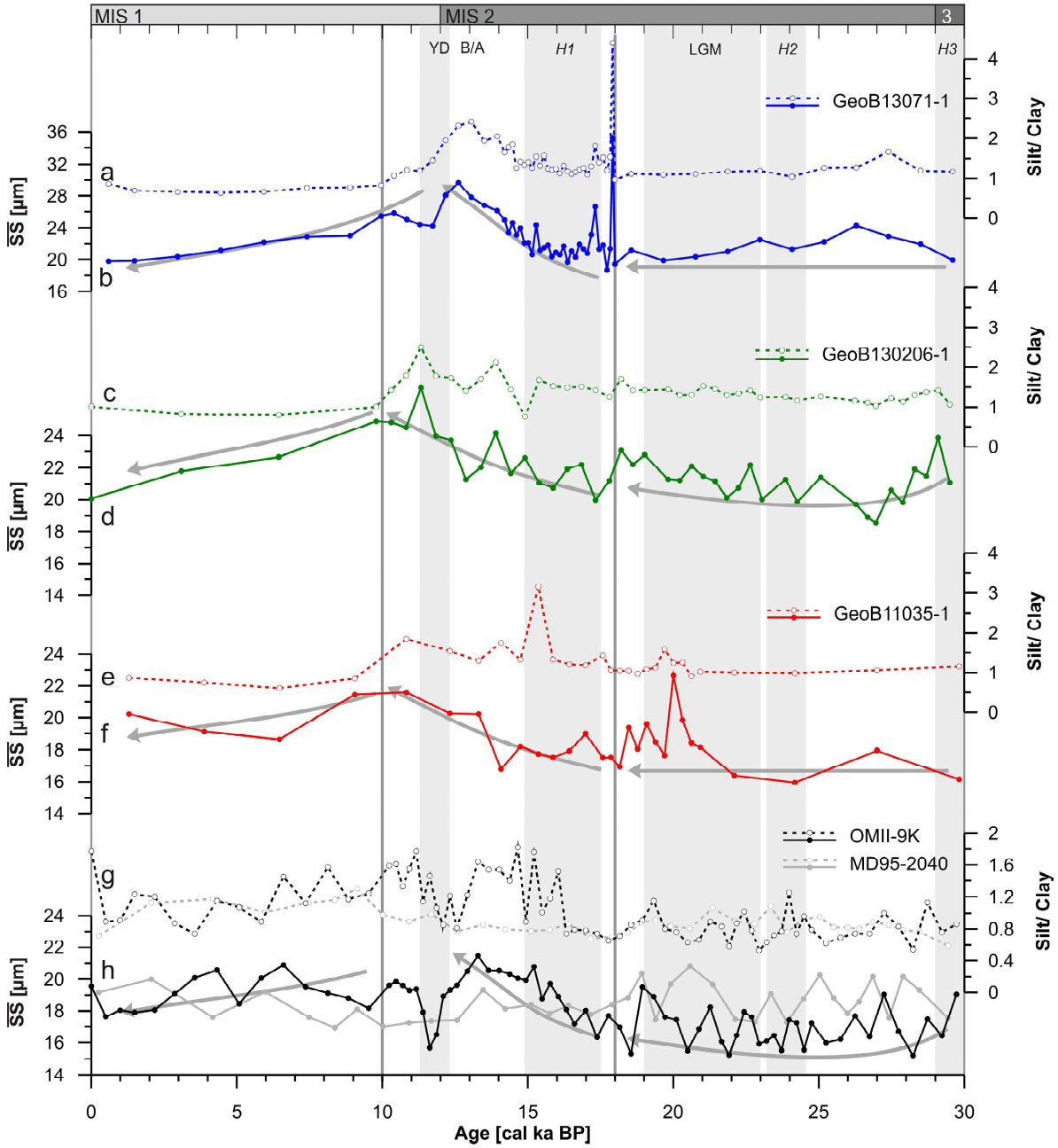

ESM Fig. 4: Comparison of sortable silt mean grain-size ($\overline{SS}$) and silt/ clay ratio from this studies GeoB cores. **a, b** GeoB13071-1 (*blue*), **c, d** GeoB130206-1 (*green*), **e, f** GeoB11035-1 (*red*), with those from **g, h** OMII-9K (*black*) and MD95-2040 (*gray*) (Hall and McCave 2000). For core locations see **ESM Fig. 2.** All records show the same general trends of being rather stable from 30–18 ka BP, increasing current strength (coarsening $\overline{SS}$) towards the end of the deglacial period and a lower rate decreasing trend over the Holocene (*gray* arrows). However, apart from this general trend all cores show clear differences in their details underlining that, though general patterns are consistent over a wider region, local aspects should not be underestimated.

References

Bard E, Rostek F, Turon JL, Gendreau S (2000) Hydrological impact of Heinrich events in the subtropical northeast Atlantic. Science 289:1321-1324. doi:10.1126/science.289.5483.1321

de Abreu L, Shackleton NJ, Schönfeld J, Hall M, Chapman M (2003) Millennial-scale oceanic climate variability off the Western Iberian margin during the last two glacial periods. Mar Geol 196:1-20. doi:10.1016/S0025-3227(03)00046-X

Dias JMA, Gonzalez R, Garcia C, Diaz-del-Rio V (2002) Sediment distribution patterns on the Galicia-Minho continental shelf. Prog Oceanogr 52:215-231.

Eynaud F, de Abreu L, Voelker A, Schönfeld J, Salgueiro E, Turon JL, Penaud A, Toucanne S, Naughton F, Goñi MFS, Malaizé B, Cacho I (2009) Position of the Polar Front along the western Iberian margin during key cold episodes of the last 45 ka. Geochem Geophys Geosyst 10:1-21. doi:10.1029/2009gc002398

Hall IR, McCave IN (2000) Palaeocurrent reconstruction, sediment and thorium focussing on the Iberian margin over the last 140 ka. Earth Planet Sci Lett 178:151-164. doi:10.1016/S0012-821X(00)00068-6

Lantzsch H, Hanebuth TJJ, Bender VB (2009) Holocene evolution of mud depocentres on a high-energy, low-accumulation shelf (NW Iberia). Quat Res 72:325-336. doi:10.1016/j.yqres.2009.07.009

Salgueiro E, Voelker AHL, de Abreu L, Abrantes F, Meggers H, Wefer G (2010) Temperature and productivity changes off the western Iberian margin during the last 150 ky. Quat Sci Rev 29:680-695. doi:10.1016/j.quascirev.2009.11.013

7. Holocene history of shelf sediment export off Southeast South America

Vera B. Bender [a, b], Till J. J. Hanebuth [a]

[a] *MARUM – Center for Marine Environmental Sciences, University of Bremen, Leobener Strasse, 28359 Bremen, Germany.*

[b] *Faculty of Geosciences, University of Bremen, Klagenfurter Strasse, 28359 Bremen, Germany.*

Manuscript in preperation for Continental Shelf Research

Abstract

This study presents evidence for an uppermost slope (220 – 300 m water depth) terrace off Uruguay. From sediment-acoustic data, as well as Neodymium isotopic signatures, grain size analyses, litho- and chronostratigraphic correlation of three gravity cores from the terrace it emerges that contrasting the common morpho-sedimentary contouritic configuration on the Southeast South American continental margin, this uppermost slope terrace is not affected by slope-parallel sediment transport. Rather, the terrace acts as an effective recorder of Holocene shelf sediment export. Siliciclastic fine sands with a grain size of 150 µm draping the outer shelf and originally sourced from the Argentine shelf are identified as the principal sediment source for the terrace. The export of those shelf sediments is primarily controlled by the deglacial sea-level history and sedimentary dynamics on the shelf; rapid early Holocene transgression over the outer shelf led to very high sedimentation rates especially on the outer part of the terrace (>400 cm/kyr); sedimentation rates gradually decrease with decelerating rate of sea-level rise; the deposition of a dominantly sandy unit reflects the flooding of the Rio de la Plata palaeo-channel on the middle shelf, which led to a massively reduced mud dispersal across the shelf; at ca. 7 cal ka BP the approach of modern sea level as well as the onset of modern El Niño Southern Oscillation (strongly influencing fluvial input and shelf circulation) are reflected by a more silty lithology, an additional 20 µm mode in the bulk grain size spectrum, and stabilizing sedimentation rates. Generally high sedimentation rates (min. ca. 50 cm/kyr) enable good temporal resolution and make the terrace sedimentary records prime tools for further paleoceanographic or paleoclimatic studies.

Introduction

The direct study of shelf sediment export through time is often hindered by the lag of suitable records. Outer shelf sedimentary regimes are too dynamic to give the full temporal evolution, and slope records are typically overprinted by sorting processes (e.g., by contour-parallel or downslope transport).

The uppermost slope, directly below the shelf break in many regions is too steep to reliably archive normal sedimentation. Likewise off Southeast South America the upper slope is generally steep (e.g. Urien and Ewing, 1974). Off Argentina the middle slope, below 500 m water depth, is characterized by several morphologic terraces (e.g. Hernández-Molina et al., 2009; Urien and Ewing, 1974). Whereas smaller upper slope terraces characterize the Campos Basin off Southeast Brazil (Viana and Faugères, 1998) no such morphologic steps are as yet known from the Uruguayan ocean margin.

This study presents parametric sediment-acoustic profiles and sediment cores from an exceptional, sediment covered uppermost slope terrace off Uruguay. The general sedimentary process (contouritic versus direct shelf export) building-up the sedimentary strata on the terrace will be discussed based on grain-size data. Moreover, the Holocene history of shelf sediment export will be deciphered via litho- and chronostratigraphic correlation of the terrace sedimentary records.

Regional setting

The western South Atlantic off Southeast South America is dominated by the encounter of the poleward-flowing Brazil current (BC) and the equatorward-flowing Malvinas current (MC), forming the Brazil-Malvinas Confluence (BMC) at intermediate water depths (Peterson and Stramma, 1991; Stramma and England, 1999). On the shelf this pattern is pursued by the coalescence of subantarctic shelf water (SASW) and subtropical shelf water (STSW), forming the subtropical shelf front (STSF) (Piola et al., 2000; Piola et al., 2008) (Fig. 7.1). The density compensated thermohaline structure of the STSF favors the offshore advection of the colliding water masses and makes the STSF a critical component in cross-shelf water transport (Matano et al., 2010; Piola et al., 2008). Circulation on the inner shelf is strongly influenced by the presence of Plata Plume Water (PPW), forming from the huge La Plata river discharge (ca. 23,000 m^3/ s) and minor Patos Lagoon outflow (ca. 1750 m^3/s) (Piola et al., 2000; Piola et al., 2008). As a distinct low-salinity buoyant plume PPW is principally northeast-ward directed and its maximum extension is controlled by the regional along shore wind stress (Möller et al., 2008; Piola et al., 2005).

According to the OCCAM (Ocean Circulation and Climate Advanced Modelling) global ocean model SASW as well as STSW circulate rather fast over the outer shelf, with up to ca. 30 cm/s for the SASW and ca. 20 cm/s for the STSW (Gwilliam, 1996). Thus, both shelf water masses have great sediment transporting potential even up to fine sandy grain sizes (e.g. Miller et al., 1977). Clay-mineralogic analyses between 40° - 27°S suggest that the STSF acts as an effective boundary separating the sandy sediments in the South, from the silty – clayey sediments contributed by La Plata river discharge and Patos lagoon outflow (Campos et al., 2008). Consequently, the Southeast South American shelf is widely covered by siliciclastic sands and bioclastic gravels South of ca. 35°S, whereas North of that latitude a silt to silty clay tongue extends out of the La Plata estuary onto the inner to middle shelf (Martins et al., 2003). Moreover, Neodymium isotopic (εNd) analyses showed that these siliciclastic sands South of ca. 35°S, due to a different

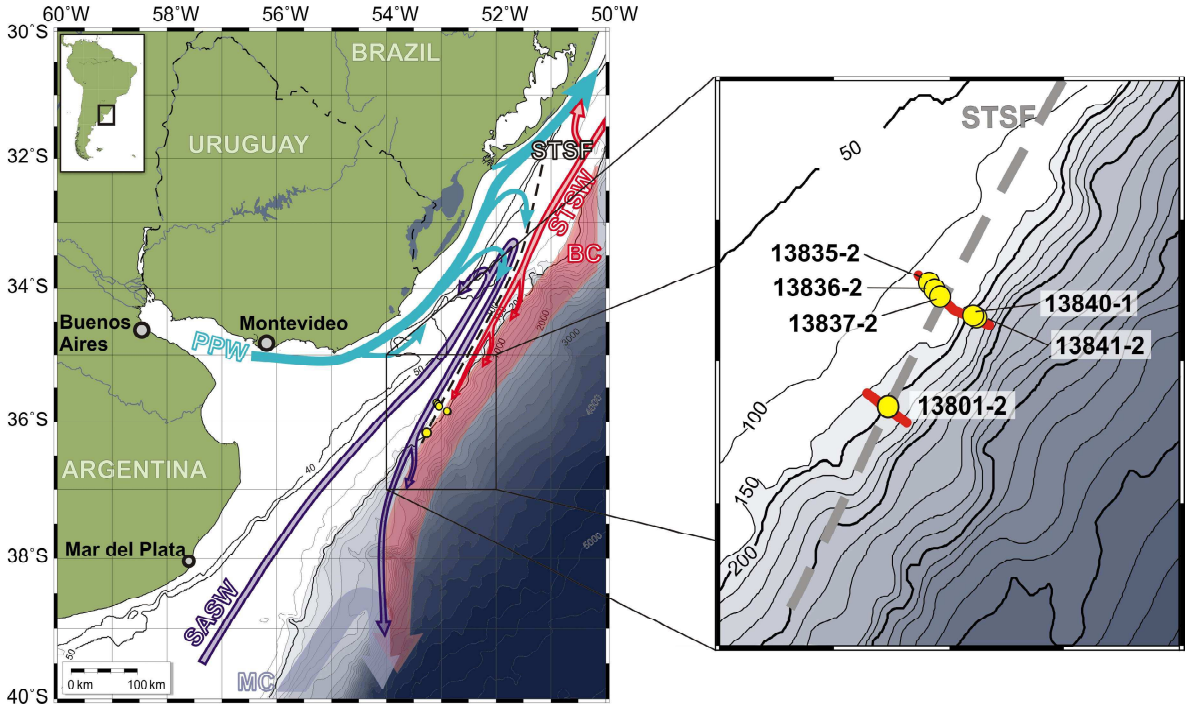

Fig. 7.1: Location of core (*yellow* dots) and parasound profiles (*red* lines) at the Southeast South American continental margin. Oceanographic features representing the mean winter circulation patterns (after Piola et al., 2008); BC: Brazil Current; MC: Malvinas Current; PPW: Plata Plume Water; SASW: Sub-Antarctic Shelf Water; STSF: Sub-Tropical Shelf Front; STSW: Sub-Tropical Shelf Water.

continental source province (younger Andean volcanic rocks – Patagonia; εNd of -4 – 0), inhibit a distinctly heavier εNd signature compared to the terrigenous sediments further North (tholeitic basalts and Paleozoic rocks in the La Plata drainage basin; εNd of -8 – -11; de Mahiques et al., 2008). Between ca. 31° to 34°S the outer shelf is covered by presumably relictic silty clays, assumed to have accumulated there during past sea-level lowstands (Martins et al., 2003).

Material and methods

The studied cores were retrieved from water depths between 130 m to 285 m by vibro- and gravity-coring on the outer shelf and uppermost slope off Uruguay during *R/V METEOR* expedition M78/3a in May/June 2009 (Fig. 7.1 and Table 7.1).

Sub-seafloor imaging was performed with the permanently installed high-frequency sediment echo-sounder ("Parasound" P70, Atlas Elektronik GmbH) system of *R/V METEOR*. The system utilizes the parametric effect to generate three separate signals, of which in this study the secondary low frequency signal with 4 kHz was used for sub-seafloor imaging.

Age determination within the uppermost slope cores is based on nine accelerator mass spectrometer radiocarbon (AMS ^{14}C) dates, performed at the Poznan Radiocarbon Laboratory (Poland). Different types of carbonate were hand-picked from the >250 µm fraction of purposely taken samples for dating (Table 7.2). All dates are converted into 1-sigma calibrated ages using the marine09 calibration data set (Reimer et al., 2009) within the framework of the Calib 6.1.1 software (Stuiver and Reimer, 1993). A correction for a conservative marine reservoir effect of 400 years is included within the calibration data set (Reimer et al., 2009). In the following all ages are given in calibrated thousands of years before present (cal ka BP).

Table 7.1: Meta-data of this study's cores. GC-12: gravity-corer equipped with 12 m core barrel. VC-5: vibro-corer equipped with 5 m core barrel.

GeoB Core	Coring device	Latitude	Longitude	Recovery	Water depth	Location
13801-2	GC-12	36°08.49'S	53°17.96'W	955 cm	241 m	uppermost slope
13840-1	GC-12	35°49.21'S	52°54.56'W	387 cm	232 m	uppermost slope
13841-2	GC-12	35°49.53'S	52°53.87'W	817 cm	285 m	uppermost slope
13835-2	VC-5	35°43.10'S	53°05.13'W	506 cm	131 m	outer shelf
13836-2	VC-5	35°44.72'S	53°03.66'W	507 cm	135 m	outer shelf
13837-2	VC-5	35°46.18'S	53°02.29'W	314 cm	140 m	outer shelf

Samples from the outer shelf cores 13835-2, 13836-2 and 13837-2, used for grain size distribution comparison are dated to be of Holocene age via lithostratigraphic and sediment acoustic profile correlation, supported by two radiocarbon dates.

Lithologs of the uppermost slope cores (13801-2; 13840-1; 13841-2) are primarily based on detailed visual core descriptions. A textural classification after Folk (1968), aided the identification of lithologies and corroborated the visual core description. Moreover, in Cores 13801-2 and 13841-2 identification of internal structures, such as bioturbation, lamination, was supported by continuous 25 x 10 x 1 cm sized down-core X-radiographs.

Table 7.2: Radiocarbon dates and respective calibrated ages.

Lab No.	Core depth [cm]	Material	^{14}C ages [^{14}C yr BP]	1σ calibrated age range [cal yr BP]	Calibrated age (intercept) [cal kyr BP]
GeoB13801-2					
Poz-42421	20	Bulk foraminifera 250 - 1000 µm	800 ± 30	420 - 479	0.45 ± 0.03
Poz-42425	50	Bulk foraminifera 250 - 1000 µm	1155 ± 30	665 - 723	0.69 ± 0.03
Poz-42422	209	*Uvigerina bifurcata*	3730 ± 50	3572 - 3720	3.65 ± 0.07
Poz-42423	375	Bulk biogen. carbonate 250 - 1000 µm	5890 ± 40	6265 - 6353	6.31 ± 0.04
Poz-42424	404	Bulk biogen. carbonate 250 - 1000 µm	6535 ± 35	6998 - 7118	7.06 ± 0.06
Poz-35195	540	*Uvigerina bifurcata*	8180 ± 40	8589 - 8733	8.66 ± 0.07
Poz-42426	686	*Uvigerina bifurcata*	8970 ± 50	9539 - 9688	9.61 ± 0.07
Poz-42427	750	Bulk foraminifera 125 - 1000 µm	9130 ± 60	9771 - 10032	9.90 ± 0.13
Poz-35197	945	Fresh bivalves of *Yoldiella* genus	9560 ± 50	10366 - 10503	10.43 ± 0.07
GeoB13840-1					
Poz-36078	313	*Uvigerina bifurcata*	7880 ± 40	8312 - 8386	8.35 ± 0.04
Poz-36079	384	*Uvigerina bifurcata*	8660 ± 50	9279 - 9406	9.34 ± 0.06
GeoB13841-2					
Poz-42435	34 - 35.5	*Globobulimina* spp.	2170 ± 30	1750 - 1810	1.78 ± 0.03
Poz-36080	183 - 188	Fresh bivalves of *Yoldiella* genus	9190 ± 50	9920 - 10106	10.01 ± 0.09
Poz-36081	400	Fresh bivalves of *Yoldiella* genus	9690 ± 50	10505 - 10588	10.55 ± 0.04
Poz-36082	545 - 547	Fresh bivalves of *Yoldiella* genus	9960 ± 50	10812 - 11065	10.94 ± 0.13
Poz-36084	782	Fresh bivalves of *Yoldiella* genus	10430 ± 50	11361 - 11637	11.50 ± 0.14

Cores 13801-2 and 13841-2 were continuously sampled for grain size analysis every 10 cm and every 20 cm, respectively. Whereas in total a set of 12 samples was taken from selected levels within the outer shelf cores 13835-2, 13836-2 and 13837-2. Core 13840-1 was not sampled for grain size analysis. Grain size distributions from 2000 – 0,4 µm were analyzed with a Coulter Laser Particle Sizer LS200. One series of aliquots was analyzed un-treated ("bulk" in the following) and a second series was digested in successive steps with 35% H_2O_2, 10% HCl and 6% NaOH to remove organic carbon, biogenic carbonate and opal respectively ("terrigenous" in the following).

Selected samples from Core 13801-2 were analyzed for their Neodymium (Nd) isotopic composition at the Geochronological Research Center of the University of São Paulo. For comparability sample preparation and analytical procedure followed the description given by de Mahiques et al. (2008) based on Sato et al. (1995). Analyses were performed with a multicollector Finnigan MAT262 mass spectrometer. Sample Nd ratios were normalized to a $^{146}Nd/^{144}Nd$ ratio of 0,7219, and εNd values were calculated following the equation given by Hamilton et al. (1983).

Results

Parasound profiling revealed the existence of a ca 20 km long and maximum 5.5 km wide morphological terrace at the uppermost slope off Uruguay (ca. 250 m mean water depth of the terrace; Figs. 7.2 and 7.3).

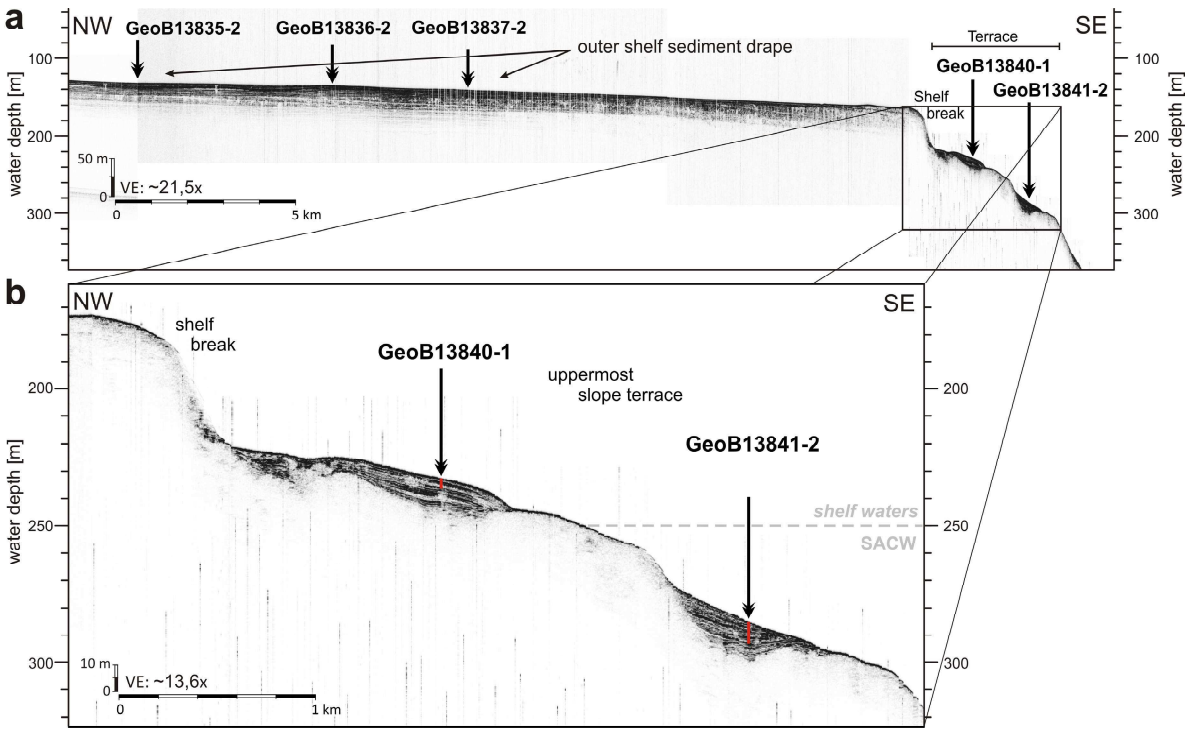

Fig. 7.2: (a) Parasound profile line crossing the sediment core locations GeoB13835-2; GeoB13836-2; GeoB13837-2 (cf. Fig. 7.1) on the outer shelf and GeoB13840-1 and GeoB13841-2 on the uppermost slope terrace. (b) Blow-up of the profile section across the uppermost slope terrace. Note the separation of a shelf proximal and shelf distal depocentre on the uppermost slope terrace by an acoustic basement high. Vertical red bars indicate the approximate core penetration depth. The dashed gray line indicates the modern vertical water mass boundary between shelf water masses and underlying South Atlantic Central Water (SACW) according to Piola and Matano (2001).

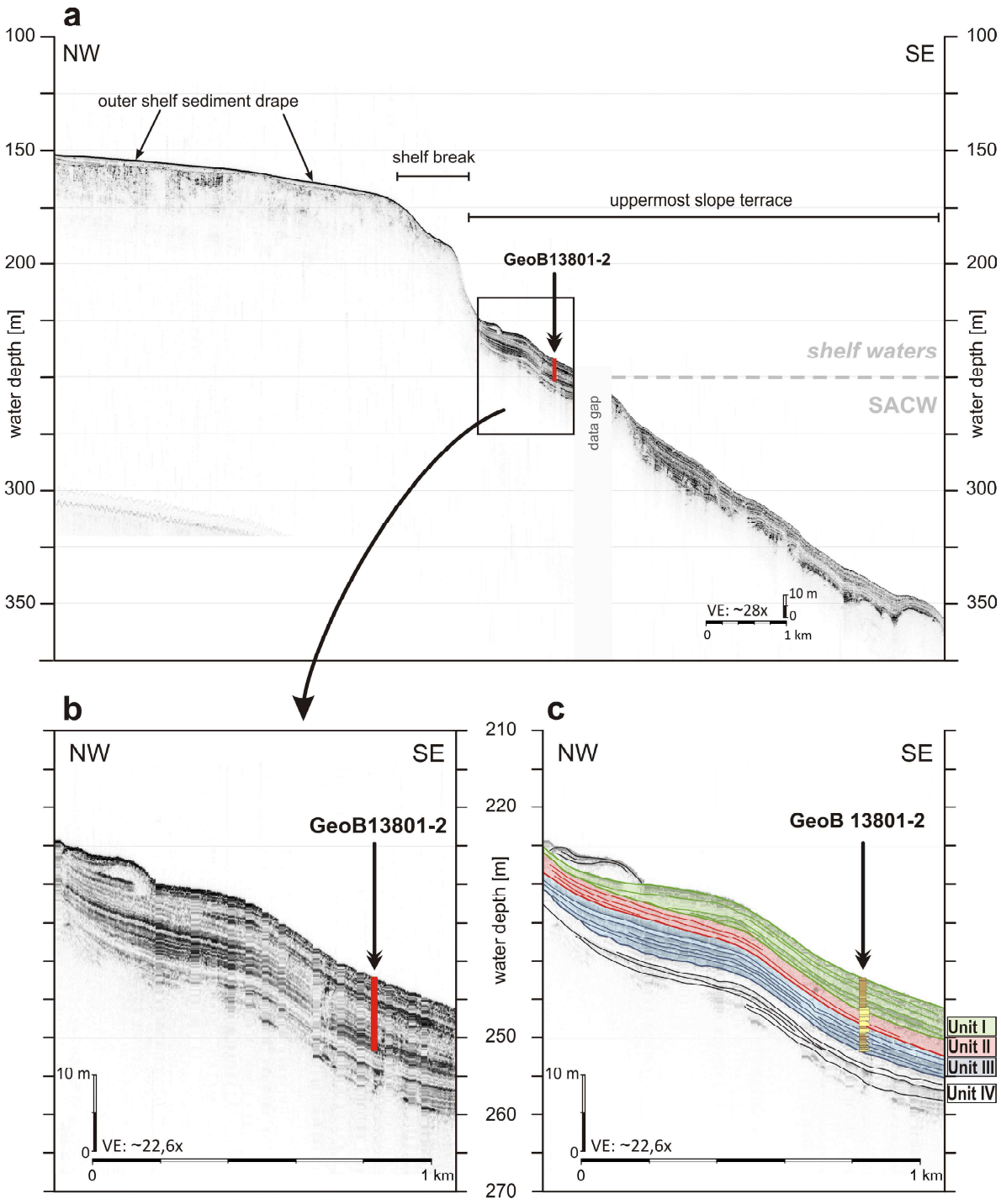

Fig. 7.3: (a) Parasound profile line from the outer shelf down to the uppermost slope terrace outer margin, crossing the sediment core location of GeoB13801-2 (cf. Fig. 7.1). (b and c) original and interpreted blow-up of the profile section across the location of GeoB13801-2. Note the generally undisturbed stratification at the coring location. Vertical red bars indicate approximate core penetration depth. The dashed gray line indicates the present-day vertical water mass boundary between shelf water masses and underlying South Atlantic Central Water (SACW) (Piola and Matano, 2001).

At ca. 35°50'S (Fig. 7.2) the outer shelf is covered by a thin (<5 m) sediment drape of homogenous fine sands partially recovered by vibrocores 13835-2; 13836-2 and 13837-2 (Lantzsch et al. subm.). The shelf break occurs at a water depth of 180 m (Fig. 7.2b). Below a very steep step of ca. 9°, a 3.5-km wide terrace occurs between 220 – 300 m water depth with an average slope angle of 1.5° (Fig. 7.2b and b). The slope significantly steepens again to ca. 6° below 300 m

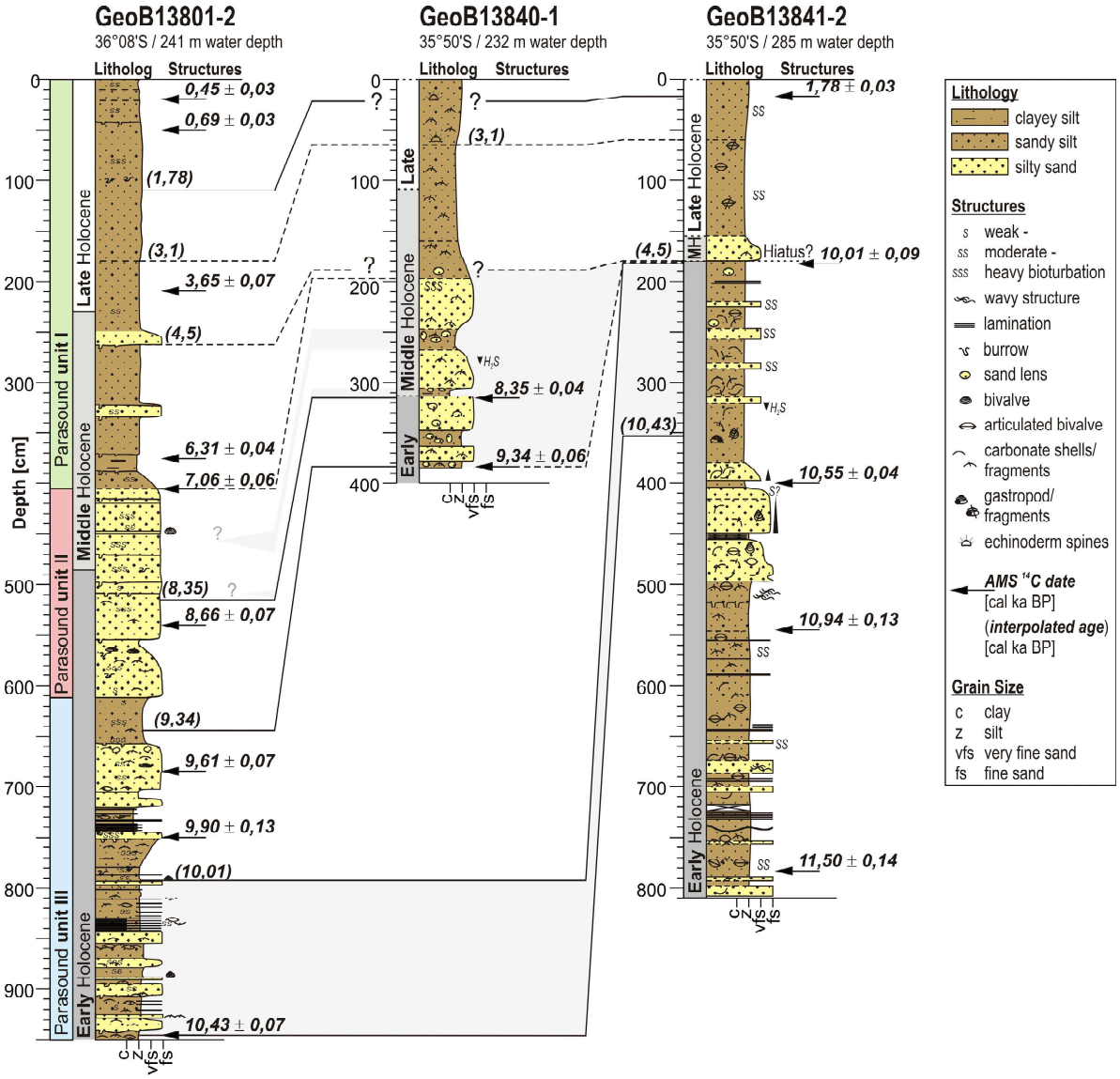

Fig. 7.4: Chronostratigraphic (solid lines) and lithostratigraphic (dashed lines) correlation between the three uppermost slope terrace cores. Radiocarbon dates are given to the right of the core columns at the respective sampling depth, interpolated ages transferred from the age model of GeoB13801-2 (Fig. 7.5) are given in parentheses. All ages are in calibrated ka BP (cal ka BP). To the left of GeoB13801-2 the respective units inferred from Fig. 7.3c are given.

water depth (Fig. 7.2a). Two sedimentary depocentres are developed on the terrace, which at this latitude (35°50'S) are separated by an acoustic basement high (Fig. 7.2b). The upper depocentre between 220 – 245 m water depth is maximum 12 m thick. Towards the Southeast the nicely stratified acoustic facies is punctually blanked out, suggesting normal sedimentation with subordinate secondary internal movement (e.g. creeping) (Fig. 7.2b). Core 13840-1 was taken from this upper depocentre (Fig. 7.2b). The lower depocentre between ca. 270 – 300 m water depth is up to 15 m thick and its surficial morphology is levelling out the underlying acoustic basement depression (Fig. 7.2b). This lower depocentre is internally less well stratified compared to the upper one, and similarly exhibiting small blanking spots. The upper 8 m of this outer depocentre were sampled by gravity core GeoB13841-2 (Fig. 7.2b).

At 36°8'S (Fig. 7.3), in the same way than the northerly profile, the outer shelf is covered with a thin (max. 3 m) sediment drape. The shelf break occurs in two steps at 175 m and 195 m water depth, before the slope angle steepens up to 7° (Fig. 7.3a). Between ca. 225 – 350 m water

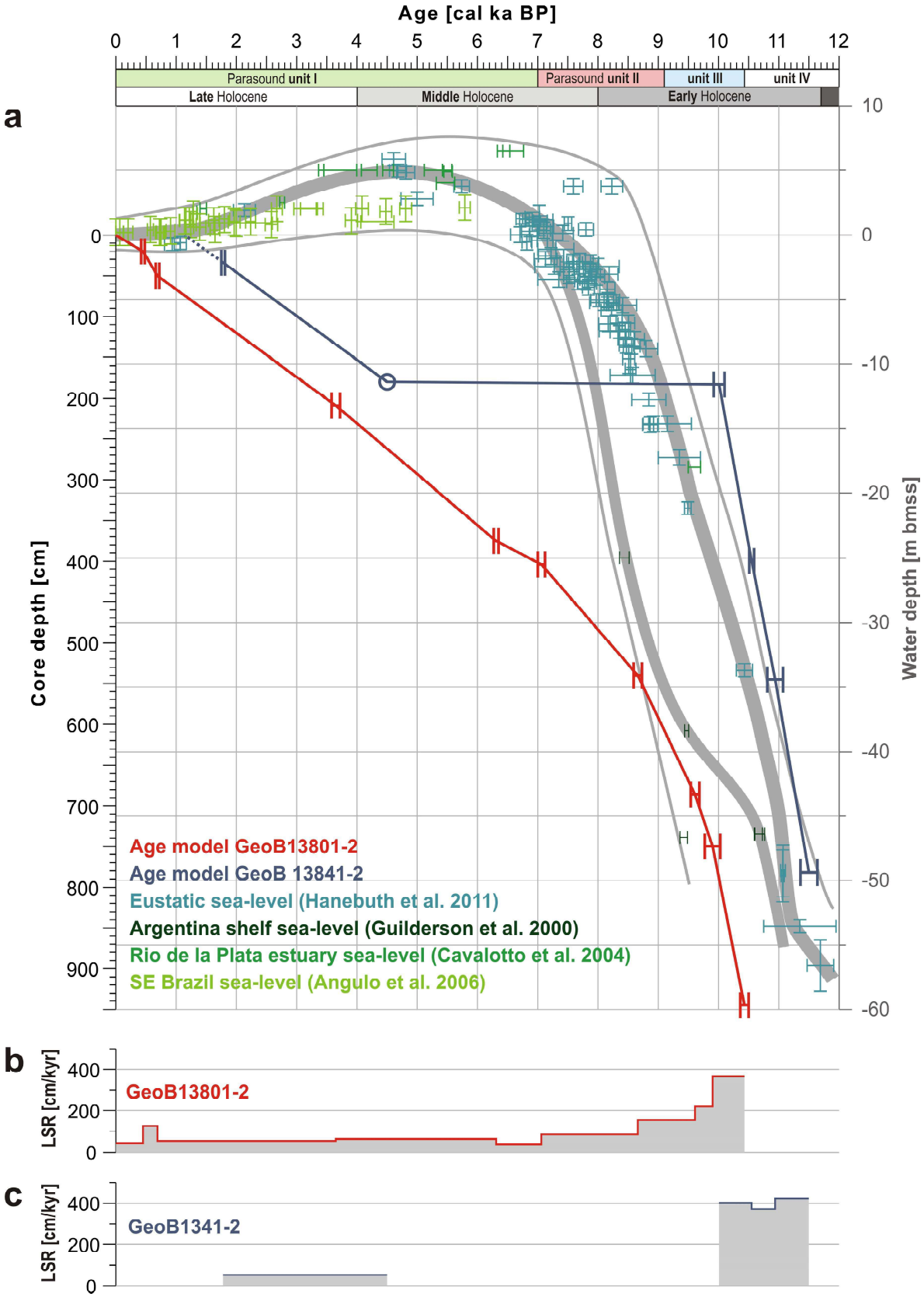
a
Age [cal ka BP]
0 1 2 3 4 5 6 7 8 9 10 11 12
Parasound unit I
Parasound unit II
unit III
unit IV
Late Holocene
Middle Holocene
Early Holocene
Core depth [cm]
Water depth [m bmss]
0 100 200 300 400 500 600 700 800 900
10 0 -10 -20 -30 -40 -50 -60
Age model GeoB13801-2
Age model GeoB 13841-2
Eustatic sea-level (Hanebuth et al. 2011)
Argentina shelf sea-level (Guilderson et al. 2000)
Rio de la Plata estuary sea-level (Cavalotto et al. 2004)
SE Brazil sea-level (Angulo et al. 2006)
b
LSR [cm/kyr]
400 200 0
GeoB13801-2
c
LSR [cm/kyr]
400 200 0
GeoB1341-2

◀ **Fig. 7.5:** (a) Depth - age models of GeoB13801-2 (*red* line) and GeoB13841-2 (*blue* line) along with Holocene relative sea-level reconstruction as a composite of regional data from Angulo et al. (2006 – Southeastern Brazil); Cavalotto et al. (2004 – La Plata estuary) and Guilderson et al. (2000 – Argentine shelf), as well as eustatic data from Hanebuth et al. (2011). All sea-level age points were recalibrated following the procedure described for the age model of the present cores; thin gray lines represent a simple graphic envelope around the sea-level data points. Regional data coverage regarding the regional sea level history off Southeast South American is good after ca. 7 ka BP, but for the Holocene period prior to 7 ka BP data coverage is very sparse. To fill the gap the eustatic sea-level data were added. Contrasting the middle and late Holocene, the early Holocene regional data points from the Argentine shelf diverge several meters from the eustatic data, suggesting significant regional effects on deglacial sea-level rise off Argentina e.g., due to subsidence. Albeit, a single data point from the Rio de la Plata estuary at ca. 9.55 cal ka PB correlates well with the eustatic data, underlining the need for an extension of the sea level data set off Uruguay. In the following the eustatic data are used as the minimum and the regional data as a maximum location of sea level below the modern mean sea-surface (bmss) at a given time for the early Holocene. (b and c) Linear sedimentation rates (LSR) for the two cores resulting from linear interpolation between the tie points shown in panel (a).

depth the slope angle decreases (~1.3°) forming the uppermost slope terrace. In this profile the terrace is 5.5 km wide and covered by up to 15 m of sediments exhibiting a well stratified acoustic facies (Fig. 7.3a).

From detailed visual core description and radiocarbon dating it emerged that Core 13801-2 is the only one of the three terrace cores with a continuous sedimentary sequence. Consequently, Core 13801-2 was the basis for litho- and chronostratigraphic correlation with the northerly Cores 13840-1 and 13841-2 (Fig. 7.4). The oldest terrace sediments are recovered by core GeoB13841-2 reaching back to 11.5 cal ka BP (Fig. 7.4). The earliest early Holocene sediments in Core 13841-2 are mainly of sandy silts with frequently occurring mm- to several cm-thick layers of silty fine sand to pure fine sands. Moreover, this interval is characterized by high abundances of biogenic carbonaceous shell fragments (mainly bivalves) and intact bivalves (*Yoldiella* genus). The record of early Holocene sedimentation ends within Core 13841-2 at 10.01 cal ka BP (Fig. 7.4). The early Holocene within Core 13801-2 is recorded from 10.43 – 8.0 cal ka BP (Fig. 7.4). Similar to Core 13841-2 the early Holocene lithology of Core 13801-2 is characterized by sandy silts frequently interrupted by fine sandy layers, which eventually occur as mm-thick laminations, and high abundance of biogenic shell fragments and articulated shells of *Yoldiella* bivalves (Fig. 7.4). The transition from early to middle Holocene in Core 13801-2 is characterized by an interval of predominantly silty sands (ca. 620 – 390 cm). Whereas the lithology of core Core 13841-2 suggest a hiatus from 10.01 cal ka BP until ca. 4.5 cal ka BP, including the sandy interval, those silty sands correlate via radiocarbon dating with the predominantly sandy interval at the base of Core 13840-1 from the northerly inner terrace (Fig. 7.4). Rather homogenous sandy silts with only two gradually bound intervals of sandier lithology (at 330 cm and 260 cm core depth) characterize the end of the middle and the late Holocene in Core 13801-2. Between ca. 3 to 0.7 cal ka BP the silty lithology gets slightly sandier before it gets finer again towards the modern top of the core (Fig. 7.4). The top of core GeoB13801-2 is assumed to be of modern age based on anthropogenic effects (*Suess* effect) observed in stable carbon isotopic ratios obtained from this core (Chapter eight). Both northerly cores show the same slight coarsening within their late Holocene sections, but miss the subsequent fining, suggesting non-modern core-top ages (Fig. 7.4). Moreover, a radiocarbon sample at 34 cm depth in Core 13841-2 dates to 1.78 cal ka BP, underlining a non-recent age at the core top.

Tracing the most prominent reflectors in the parasound profile crossing Core 13801-2 allows for the identification of four units, of which three via alignment with the litholog of Core 13801-2 can be related to the principal lithologies (Fig. 7.3c). The lower most Unit IV shows relatively weak reflection and internal reflectors are frequently disturbed. Moreover, the upper part of Unit IV is nearly transparent and has not been reached by coring. The overlying Unit III is characterized by strong and well stratified reflectors and corresponds to a predominately silty lithology with frequently occurring millimeter- to decimeter-thick fine sand layers in Core

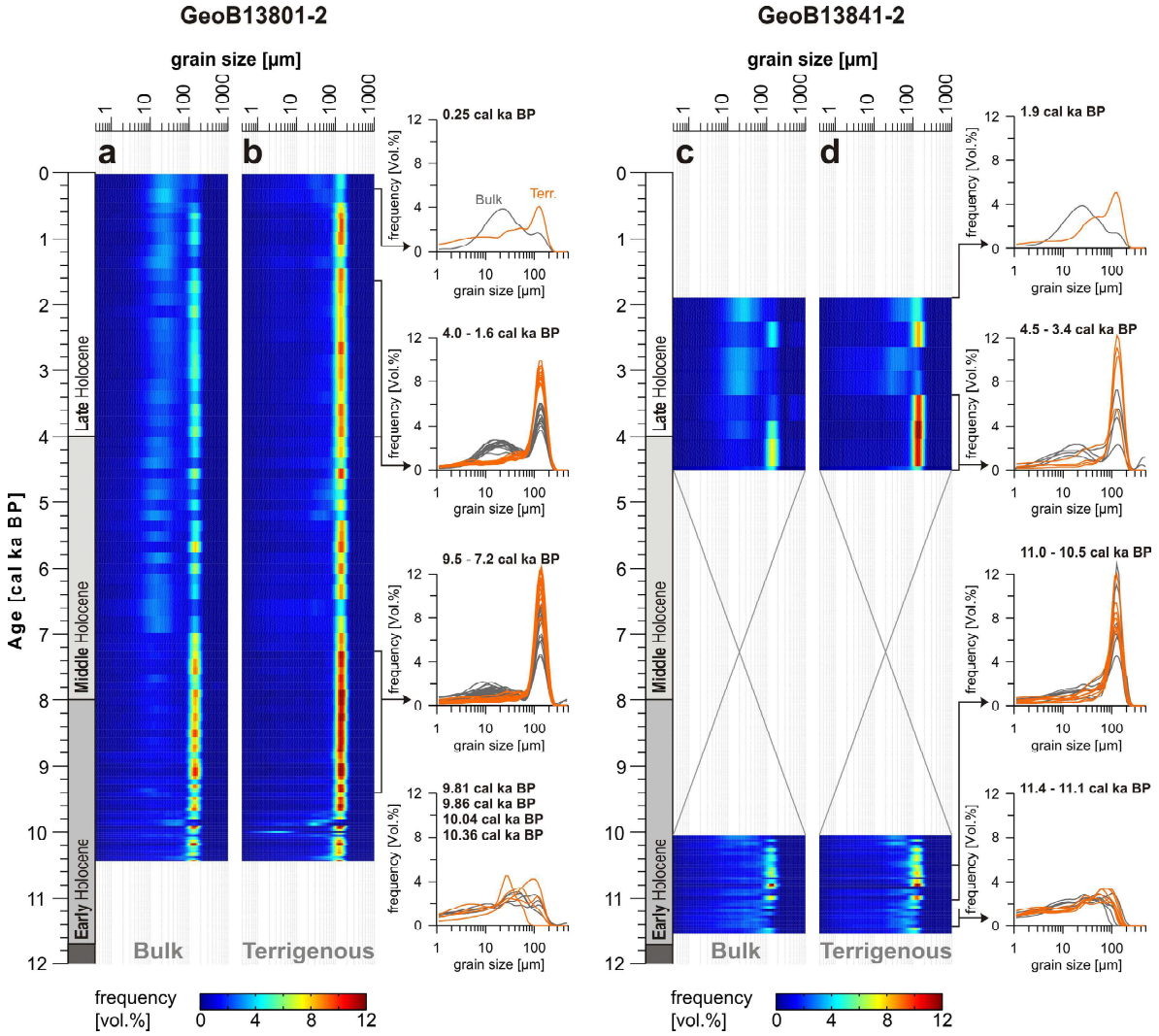

Fig. 7.6: Bulk and terrigenous down-core grain size distributions from core GeoB13801-2 (a and b) and GeoB13841-2 (c and d). A prominent 150 µm mode is dominating both, the bulk and terrigenous, grain size spectra of cores GeoB13801-2 and GeoB1341-2 during the early to late Holocene.

13801-2 (Figs. 7.3c and 7.4). Unit II is again characterized by weaker reflection and can be correlated to an interval of sandy lithology within core GeoB13801-2 (Figs. 7.3c and 7.4). The uppermost Unit I shows a series of internal reflectors, which might be related to more sandy intervals within the principally silty lithology (Figs. 7.3c and 7.4).

We constructed depth-age models for Cores 13801-2 and 13841-2 (Fig. 7.5a). The depth-age model of Core 13801-2 is based on the nine radiocarbon dates represented in Table 7.2 and Fig. 7.4. For Core 13841-2 additional to the five radiocarbon dates represented in Table 2 and Fig. 4, one age tie point (encircled in Fig. 7.5a) is obtained from the litho- and chronostratigraphic correlation. Both Cores, 13841-2 and 13801-2, show linear sedimentation rates (LSR) of up to ca. 400 cm/kyr until ca. 10 cal ka BP (Fig. 7.5b and c). Whereas the time interval 10 – 4.5 cal ka BP is missing in GeoB13841-2, core GeoB13801-2 shows gradually decreasing LSR down to ca. 50 cm/kyr until ca. 7 cal ka BP (Fig. 7.5b). Apart from a short time interval between 0.45 – 0.7 cal ka BP in Core 13801-2, both cores, 13801-2 and 13841-2, show a late Holocene LSR of ca. 50 cm/kyr (Fig. 7.5b and c).

The grain size distributions of Core 13801-2 are dominated by a distinct terrigenous fine sand mode at 150 µm throughout the Holocene (Fig. 7.6a and b). Only within the early Holocene

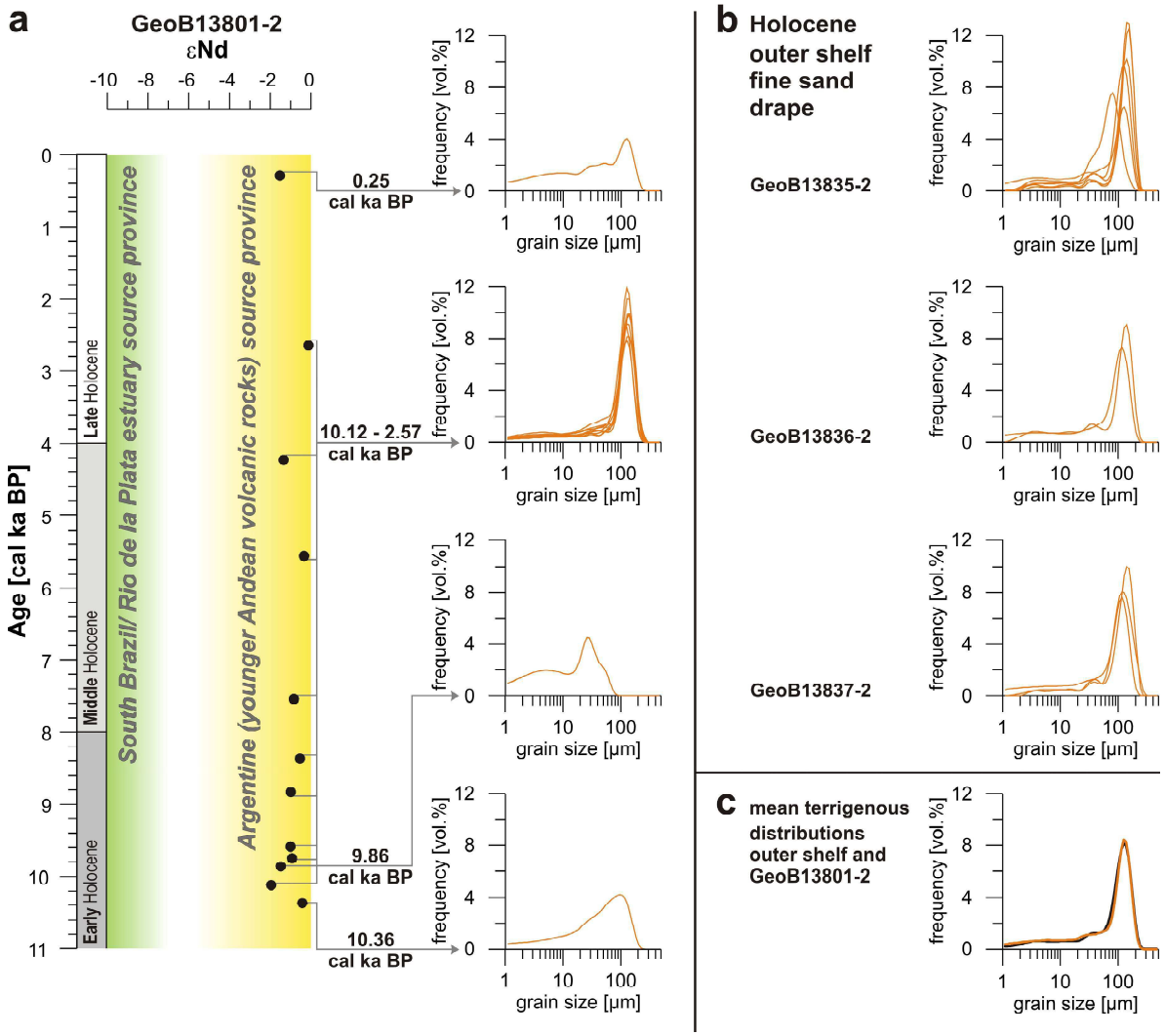

Fig. 7.7: (a) GeoB13801-2 εNd values are clearly within the range of an Argentine/ Patagonian source province after de Mahiques et al. (2008). To the right hand-side of the εNd values the terrigenous grain size spectra of the corresponding grain size samples are represented. (b) Terrigenous grain size spectra of the outer shelf sand drape samples. A comparison (c) of the mean grain size distribution of all outer shelf samples (*black* line) shown in (b) with the mean terrigenous grain size distribution of GeoB13801-2 (*orange* line) identifies the outer shelf sand drape as a potential direct source for the 150 µm sand mode.

lithology four samples (lowermost spectra plots of Fig. 7.6a and b) show a significant variation from this otherwise stable pattern. Between 9.5 to 7.2 cal ka BP the 150 µm terrigenous fine sand mode is dominant but with a very subordinate 10 µm mode in the bulk distribution. This interval corresponds to the mainly silty lithology interval at the early to middle Holocene transition (Fig. 7.6a, b and Fig. 7.5). After ca. 7 cal ka BP and for the rest of the middle and late Holocene a biogenic 15 – 20 µm mode is established in the bulk grain size distribution (Fig. 7.6a and b). Moreover, after 7 cal ka BP the terrigenous 150 µm mode material is eventually reduced, typically co-occurring with a higher amount of the 15-20 µm biogenic mode, such that the 150 µm peak nearly disappears in the bulk distributions (e.g. at 0.25 cal ka BP; Fig. 7.6a and b). The grain size distribution of Core 13841-2 generally shows similar trends. With a terrigenous 150 µm mode dominating the distributions throughout the Holocene, being most prominent in the early Holocene samples, and an additional biogenic approx. 20 µm mode appearing at the end of the middle and during the late Holocene (Fig. 7.6c and d). Grain size samples of Core 13841-2 older than 11 cal ka BP are similarly dominated by the terrigenous sediment component (no significant difference between bulk and terrigenous spectra). However their

distributions are less well sorted with a consequently less pronounced and finer terrigenous mode at 70 – 80 µm (lowermost spectra plot in Fig. 7.6c and d).

Holocene grain size distribution from the outer shelf Cores 13835-2, 13836-2 and 13837-2, are clearly dominated by the terrigenous sediment component (no significant change in the grain size spectra from bulk to terrigenous). Likewise the terrace cores they show a dominant terrigenous mode at 150 µm (Fig. 7.7b).

Neodymium isotopic analyses on the terrigenous fraction of GeoB13801-2 provide εNd values varying between -0,1 and -1,9 (Fig. 7.7a). Following the source area definition of de Mahiques et al. (2008) this gives a clear and constant Argentine/ Patagonian (younger Andean volcanic rocks) source province (εNd values of -4 – 0; de Mahiques et al., 2008) throughout the Holocene (Fig. 7.7a).

Discussion

Sedimentation on the terrace: contouritic versus direct shelf sediment export

The morpho-sedimentary configuration of the Southeast South American margin is dominated by the presence of a large contourite depositional system, characterized amongst others by several contourite terraces (Hernández-Molina et al., 2009). Although the centre of contouritic deposition on the Argentine/Uruguayan margin has previously been described to be situated between ca. 1100 and 1500 m water depth (Hernández-Molina et al., 2009; Violante et al., 2010), the constantly dominating presence of a well sorted terrigenous 150 µm fine sand component might suggest a contouritic deposition process for the uppermost slope terrace too. From the upper slope (200 – 600 m water depth) of the Campos Basin (off Southeastern Brazil) a sand-rich slope-plastered sheet drift was described as the result of shelf sand spill-over processes interacting with the western boundary Brazil Current (Viana, 2002; Viana and Faugères, 1998). In this case the conditioning factors for sand accumulations at the upper slope appear to be (1) a convex upper slope morphology; (2) sandy sediments available at the shelf edge; (3) off-shelf transport of shelf sands by shelf-edge currents; and (4) the presence of a strong slope current (Viana and Faugères, 1998).

The second and third point are given as well for the uppermost slope terrace off Uruguay: siliciclastic sands widely cover the outer shelf up to 35°S (Martins et al., 2003) and Subantarctic shelf water (SASW) as well as Subtropical shelf water (STSW) circulating fast enough on the outer shelf to enable off-shelf sand transport (Gwilliam, 1996; Piola et al., 2008). In contrast the first point of a convex upper slope morphology is not given around 36°S. Here the outer shelf- upper slope isobaths run rather straight NE – SW (cf. Fig. 7.1) precluding a slope current acceleration – deceleration comparable to the Campos Basin situation. The fourth conditioning factor in the case of the Campos Basin – the presence of a strong slope current – is in fact the point which gives the upper slope sand deposits the contouritic (= contour current controlled deposit) component by controlling the deposition. Off Uruguay/Argentina in contrast, 36°S is the latitude where under present-day oceanographic conditions the Brazil current (as STSW) collides with the northward flowing SASW over the outer shelf and uppermost slope (e.g., Piola et al., 2008). It has been suggested that both water masses are advected offshore here (Matano et al., 2010), hampering a contouritic influence on the terrace sediments but being a potentially effective process for off-shelf sand transport.

To distinguish current-controlled from hemipelagic or down-slope depositional processes on the basis of sedimentological data the sortable silt (terrigenous 10 – 63 µm fraction) mean size versus the relative sortable silt content (within the terrigenous <63 µm fraction) has been shown

useful (Bender et al., 2012; McCave and Hall, 2006). The cross-plot from the grain size data of GeoB13801-2 shows a low correlation coefficient of 0.02 (Fig. 7.8). Under current-controlled deposition sortable silt mean grain size and content should have a significantly higher correlation coefficient reflecting current sorting processes (McCave and Hall, 2006). However, it has to be noted that the sortable silt proxy has been established from deep sea settings and might be less liable in settings with generally >50% sand in the terrigenous fraction.

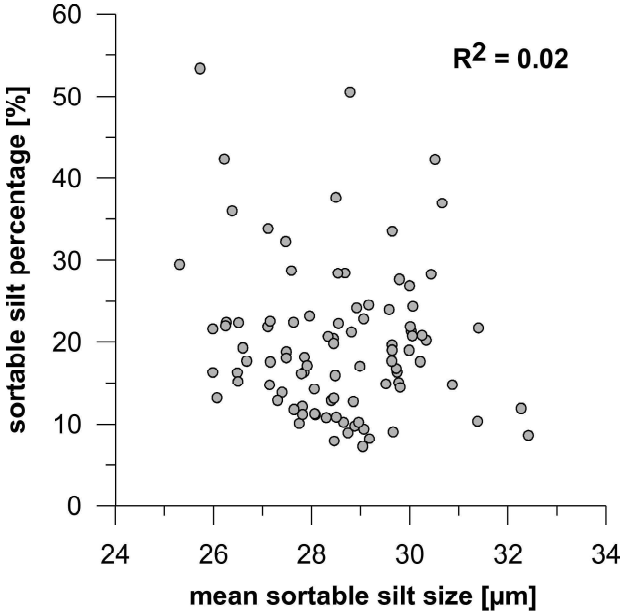

Fig. 7.8: Mean sortable silt (10 – 63 µm) size versus the sortable silt percentage of core GeoB13801-2 having a very low correlation coefficient rejecting a current-related depositional process for the terrace sediments?

The combined findings of i) very low correlation between sortable silt mean size and sortable silt content, and ii) no fining in the grain size distributions in any current direction (N – S), which would indicate current sorting, support the hypothesis that sedimentation on the terrace is not contouritic. Moreover, the fact that samples from the outer shelf sand drape (13835-2; 13836-2; 13837-2) give virtually the same grain size compared to those of the terrace indicates that the terrace is primarily built-up by rather direct off-shelf export of those sediments (Fig. 7.7c). This hypothesis is further underlined by the terrigenous sediments εNd signature on the terrace indicating a very constant Argentine (shelf) source (Fig. 7.7a). The outer shelf sands are part of a mid-outer shelf siliciclastic sand tongue extending from the Argentine shelf towards the Northeast up to 35°S (Martins et al., 2003, Brazeiro et al., 2003). Those sands are likely transported northwards by the relatively fast flowing outer shelf SASW (up to 30 cm/s; Gwilliam, 1996). Furthermore, εNd analyses from the Uruguayan outer shelf cores confirmed an Argentine shelf source for the outer shelf sands as well (Lantzsch et al., subm.).

Holocene shelf sediment export

Considering that the sediment supply to the terrace is primarily via direct shelf sediment input, it is straight forward to suggest a strong control of deglacial sea-level rise on terrace sediment input. The correlation of LSRs, Parasound and lithologic units with the stages of Holocene sea-level rise support this hypothesis (Fig. 7.5). Early Holocene high sedimentation rates of up to 400 cm/kyr reflect the massive reworking of shoreface transgression across the outer to middle shelf region (Fig. 7.5c). At ca. 10 cal ka BP a critical point appears to be crossed by transgressive reworking, reflected by a ca. 5.5 ka long hiatus in Core 13841-2 and decreasing LSR within Core 13801-2 (Fig. 7.5). By that time sea level was located between 30 – 45 m bmss (Fig. 7.5a). In fact, -30 m to -45 m water depth is close to the depth of the upper rim of the NE–SW extending La Plata palaeo-valley on the Uruguayan shelf. The changing circulation patterns on the shelf resulting from the gradual flooding of this palaeo-valley led to reduced mud dispersal out of the La Plata palaeo-estuary and apparently hindered sediment accumulation on the outer terrace after 10 cal ka BP until ca. 4.5 cal ka BP. This change is reflected by significant reduction of the silt mode (Fig. 7.6a and b) leading to the pronounced sandy lithology between 9.2 – 7 cal ka BP in Core 13801-2

(Figs. 7.4 and 7.5). Those silts are now preferentially deposited within the palaeo-valley. The complete flooding of the La Plata palaeo-channel by ca. 7 cal ka BP, and the subsequent approach of modern sea-level conditions invoked a re-organization in fine fraction distribution on the shelf and export off the shelf (Fig. 7.5a). This clear change in shelf sediment export is reflected by the additional appearance of a ca. 20 µm mode resulting in an again generally more silty lithology (Parasound Unit I) after ca. 7 cal ka BP (Fig. 7.6a). Scanning electron microscopy (SEM) showed that the observed 20 µm mode is composed of aggregates of clay-sized terrigenous minerals presumably bound by chemically weak carbonate (Figs. 7.6a, b and 7.9). Argentine loess, a frequently appearing sediment component in the region, can be excluded since the aggregates disintegrate during chemical treatment (pers. comm R. Violante).

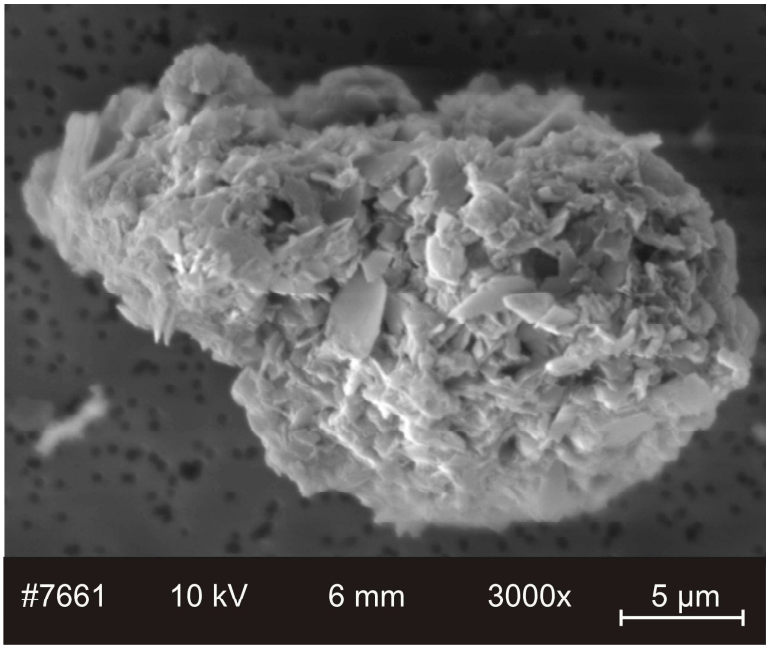

Fig. 7.9: Scanning electron microscope image of a 20 µm mode aggregate form the bulk faction of Core GeoB13801-2 at 6.5 cal ka BP (= 380 cm core depth).

Moreover, by 7 ka BP the modern frequency of warm El Niño Southern Oscillation (ENSO) events initiated (Moy et al., 2002). Under modern conditions warm ENSO events result in enhanced precipitation over Southeast South America, causing increased La Plata discharge (Garreaud et al., 2009). However, the synchronously prevailing northeasterly winds hamper the norheastward coastal extension and the La Plata discharge plume is advected offshore (Garreaud et al., 2009; Piola et al., 2005). Due to the coincidence of appearance of this faction on the terrace with the onset of modern ENSO frequency as well as modern sea-level conditions we suggest a fluviatile origin for the 20 µm mode.

The reinstating sedimentation at the location of Core 13841-2 at ca. 4.5 cal ka BP suggests an extension of the sediment deposition towards the outer terrace. This expansion coincides with the maximum of regional sea-level height, ca. 2 – 5 m above the modern mean surface (Angulo et al., 2006; Cavallotto et al., 2004; Fig. 7.5a). Noteworthy, whereas Core 13801-2 has a recent core top, Cores 13840-1 and 13841-2 are missing the past ca. 1.2 ka BP. The end of sedimentation at the northerly section of the terrace indicates a newly reorganization in shelf sediment export at ca. 1.2 cal ka BP.

Interaction with slope water masses and preservation potential of the terrace strata

The uppermost slope terrace is vertically centred at the present-day water mass boundary of the shelf waters with underlying South Atlantic central water (SACW) (ca. 250 m water depth; Piola and Matano, 2001; Figs. 7.2 and 7.3). It has recently been suggested, that the significant turbulent energy patterns at vertical water mass boundaries (e.g. internal tides and waves) are an effective mechanism for the formation of terrace structures at continental margins

on geologic time-scales. This hypothesis is based on persistent contouritic flow patterns and strong water mass contrasts leading to distinct water mass interfaces. As discussed above the presented core data do not support the hyposthesis of contouritic conditions at the uppermost slope terrace during the Holocene. Moreover, temperature and salinity profiles (Antonov et al., 2010; Locarnini et al., 2010) suggest that the discussed water mass boundary is very gradual. During the Holocene this water mass boundary apparently does not have a significant control on the above discussed depositional patterns of the uppermost slope terrace. After all, the hypothesized mechanism might be a plausible explanation for the initial creation of the terrace in the geologic past.

The relatively young age of the terrace deposits raises the question of preservation potential of the terrace sedimentary strata. Considering the minimum and maximum LSRs on the terrace (50 cm/kyr for the late Holocene; 400 cm/kyr for the early Holocene) indicates that the deglacial as well as last glacial maximum strata are either very condensed or largely missing on the terrace. It further suggests that large amounts of sediments are either by-passed or eroded during past sea-level lowstands by significantly stronger slope currents. Consequently the terrace strata have low preservation potential in the long-term geologic record.

Conclusions

A ca. 20-km long and 5.5-km wide terrace at the uppermost slope off Uruguay is covered by up to 15 m thick, acoustically stratified sediments. In contrast to the common morphosedimentary configuration of the Southeast South American ocean margin the terrace strata are built-up by direct off-shelf sediment export plausibly related to the off-shelf advection of shelf waters resulting from the confluence of SASW and STSW.

Holocene shelf sediment export dynamics appear to be primarily controlled by transgression across the shelf:

- Rapid early Holocene sea-level rise results in maximum sedimentation rates of ca. 400 cm/ kyr and preferential deposition on the outer terrace due to strong reworking on the outer and middle shelf.

- By 10.0 ka BP the initial flooding of the La Plata palaeo-valley results in the deflection of the fine sediment fraction on the shelf and the main depocentre shifts towards the middle of the terrace.

- The reorganization of circulation and sedimentary patterns on the shelf induced by the La Plata palaeo-valley flooding leads to the deposition of predominantly sandy sediments on the terrace between 9.2 – 7.0 ka BP.

- At ca. 7.0 ka BP the approach of modern sea-level stabilizes sedimentation rates at ca. 50 cm/ kyr and the synchonous onset of modern El Niño Southern Oscillation possibly enables a new fluvial influence on the terrace sedimentation.

Evidently the terrace sedimentary strata have low preservation potential on long geologic time scales. However they enable the high temporal resolution study of Holocene shelf sediment export and may even be suitable for very high resolution paleoceanographic studies of this key western boundary current region.

Acknowledgements

This study was funded through the DFG Graduate College "Proxies in Earth History (EUROPROX)" and MARUM DFG-Research Center/Cluster of Excellence "The Ocean in the Earth System". The work of TH was funded through DFG-Heisenberg scholarship HA4314/4-1. We wish to thank Benedict Preu for professional processing and image production from the raw Parasound data. We further wish to thank Anna Lipke, whose B.Sc. thesis initially showed us the scientific potential of the uppermost slope terrace sediments; Cristiano Chiessi for making Neodymium analyses in the labs of USP Geosciences department possible; and Hendrik Lantzsch for providing rough age determination of the outer shelf cores.

References

Angulo, R.J., Lessa, G.C., de Souza, M.C., 2006. A critical review of mid- to late-Holocene sea-level fluctuations on the eastern Brazilian coastline. Quat. Sci. Rev. 25, 486-506, doi: 10.1016/j.quascirev.2005.03.008.

Antonov, J.I., Seidov, D., Boyer, T.P., Locarnini, R.A., Mishonov, A.V., Garcia, H.E., Baranova, O.K., Zweng, M.M., Johnson, D.R., 2010. World Ocean Atlas 2009, Volume 2: Salinity. U.S. Government Printing Office, Washington, D.C., p. 184.

Bender, V.B., Hanebuth, T.J.J., Mena, A., Baumann, K.-H., Francés, G., von Dobeneck, T., 2012. Control of sediment supply, palaeoceanography and morphology on late Quaternary sediment dynamics at the Galician continental slope. Geo-Marine Letters 32, 313-335, doi: 10.1007/s00367-012-0282-2.

Brazeiro, A., Acha, M., Mianzan, H., Gómez, M., Fernandez, V., 2003. Áreas prioritarias para la conservación y manejo de la integridad biológica del Río de la Plata y su Frente Marítimo. Jornadas Nacionales de Ciencias del Mar. XIII Coloquio Argentino de Oceanografía Mar del Plata.

Campos, E.J.D., Mulkherjee, S., Piola, A.R., de Carvalho, F.M.S., 2008. A note on a mineralogical analysis of the sediments associated with the Plata River and Patos Lagoon outflows. Cont. Shelf Res. 28, 1687-1691, doi: 10.1016/j.csr.2008.03.014.

Cavallotto, J.L., Violante, R.A., Parker, G., 2004. Sea-level fluctuations during the last 8600 years in the de la Plata river (Argentina). Quat. Int. 114, 155-165, doi: 10.1016/s1040-6182(03)00050-8.

de Mahiques, M.M., Tassinari, C.C.G., Marcolini, S., Violante, R.A., Figueira, R.C.L., da Silveira, I.C.A., Burone, L., de Mello e Sousa, S.H., 2008. Nd and Pb isotope signatures on the Southeastern South American upper margin: Implications for sediment transport and source rocks. Mar. Geol. 250, 51-63, doi: 10.1016/j.margeo.2007.11.007.

Folk, R.L., 1968. The petrology of sedimentary rocks. Hemphill Publishing Company, Austin, Texas, p. 170.

Garreaud, R.D., Vuille, M., Compagnucci, R., Marengo, J., 2009. Present-day South American climate. Palaeogeogr. Palaeoclimat. Palaeoecol. 281, 180-195, doi: 10.1016/j.palaeo.2007.10.032.

Guilderson, T.P., Burckle, L., Hemming, S., Peltier, W.R., 2000. Late Pleistocene sea level variations derived from the Argentine Shelf. Geochem. Geophy. Geosy. 1, 1055, doi: 10.1029/2000gc000098.

Gwilliam, C.S., 1996. Modelling the global ocean circulation on the T3D, in: Ecer, A., Periaux, J., Satdfuka, N., Taylor, S. (Eds.), Parallel Computational Fluid Dynamics. Elsevier, Amsterdam, pp. 33-40.

Hamilton, P.J., O'Nions, R.K., Bridgwater, D., Nutman, A., 1983. Sm-Nd studies of Archaean metasediments and metavolcanics from West Greenland and their implications for the Earth's early history. Earth Planet. Sci. Lett. 62, 263-272, doi: 10.1016/0012-821x(83)90089-4.

Hanebuth, T.J.J., Voris, H.K., Yokoyama, Y., Saito, Y., Okuno, J., 2011. Formation and fate of sedimentary depocentres on Southeast Asia's Sunda Shelf over the past sea-level cycle and biogeographic implications. Earth-Sci. Rev. 104, 92-110, doi: 10.1016/j.earscirev.2010.09.006.

Hernández-Molina, F.J., Paterlini, M., Violante, R., Marshall, P., de Isasi, M., Somoza, L., Rebesco, M., 2009. Contourite depositional system on the Argentine Slope: An exceptional record of the influence of Antarctic water masses. Geology 37, 507-510, doi: 10.1130/g25578a.1.

Locarnini, R.A., Mishonov, A.V., Antonov, J.I., Boyer, T.P., Garcia, H.E., Baranova, O.K., Zweng, M.M., Johnson, D.R., 2010. World Ocean Atlas 2009, Volume 1: Temperature. U.S. Government Printing Office, Washington, D.C., p. 184.

Martins, L.R., Martins, I.R., Urien, C.M., 2003. Aspectos sedimentares da plataforma continental na área de Influência do Rio de La Plata. Gravel 1, 68-80.

Matano, R.P., Palma, E.D., Piola, A.R., 2010. The influence of the Brazil and Malvinas Currents on the Southwestern Atlantic Shelf circulation. Ocean Sci. 6, 983-995, doi: 10.5194/os-6-983-2010.

McCave, I.N., Hall, I.R., 2006. Size sorting in marine muds: Processes, pitfalls, and prospects for paleoflow-speed proxies. Geochem. Geophy. Geosy. 7, 1-37, doi: 10.1029/2006GC001284.

Miller, M.C., McCave, I.N., Komar, P.D., 1977. Threshold of sediment motion under unidirectional currents. Sedimentology 24, 507-527.

Möller, O.O., Piola, A.R., Freitas, A.C., Campos, E.J.D., 2008. The effects of river discharge and seasonal winds on the shelf off southeastern South America. Cont. Shelf Res. 28, 1607-1624, doi: 10.1016/j.csr.2008.03.012.

Moy, C.M., Seltzer, G.O., Rodbell, D.T., Anderson, D.M., 2002. Variability of El Niño/Southern Oscillation activity at millennial timescales during the Holocene epoch. Nature 420, 162-165, doi: 10.1038/nature01194.

Peterson, R.G., Stramma, L., 1991. Upper-level circulation in the South Atlantic Ocean. Prog. Oceanogr. 26, 1-73, doi: 10.1016/0079-6611(91)90006-8.

Piola, A.R., Campos, E.J.D., Möller, O.O., Charo, M., Martinez, C., 2000. Subtropical Shelf Front off eastern South America. J. Geophys. Res. - Oceans 105, 6565-6578.

Piola, A.R., Matano, R.P., 2001. Brazil and Falkland (Malvinas) Currents, in: Steele, J.H., Thorpe, S.A., Turekian, K.K. (Eds.), Ocean Currents: A Derivative of the Encyclopedia of Ocean Sciences. Academic Press, Elsevier Ltd., London, Burlington, San Diego, pp. 35-43.

Piola, A.R., Matano, R.P., Palma, E.D., Möller, O.O., Campos, E.J.D., 2005. The influence of the Plata River discharge on the western South Atlantic shelf. Geophys. Res. Lett. 32, 4, doi: 10.1029/2004gl021638.

Piola, A.R., Möller, O.O., Guerrero, R.A., Campos, E.J.D., 2008. Variability of the subtropical shelf front off eastern South America: Winter 2003 and summer 2004. Cont. Shelf Res. 28, 1639-1648, doi: 10.1016/j.csr.2008.03.013.

Reimer, P.J., Baillie, M.G.L., Bard, E., Bayliss, A., Beck, J.W., Blackwell, P.G., Ramsey, C.B., Buck, C.E., Burr, G.S., Edwards, R.L., Friedrich, M., Grootes, P.M., Guilderson, T.P., Hajdas, I., Heaton, T.J., Hogg, A.G., Hughen, K.A., Kaiser, K.F., Kromer, B., McCormac, F.G.,

Manning, S.W., Reimer, R.W., Richards, D.A., Southon, J.R., Talamo, S., Turney, C.S.M., van der Plicht, J., Weyhenmeye, C.E., 2009. Intcal09 and Marine09 radiocarbon age calibration curves, 0-50,000 years cal BP. Radiocarbon 51, 1111-1150.

Sato, K., Tassinari, C.C.G., Kawashita, K., Petronilho, L., 1995. O Método Geocronológico Sm-Nd No IGc-USP e Suas Aplicações. An. Acad. Bras. Ciênc. 67, 313-336.

Stramma, L., England, M., 1999. On the water masses and mean circulation of the South Atlantic Ocean. J. Geophys. Res. - Oceans 104, 20863-20883, doi: 10.1029/1999JC900139.

Stuiver, M., Reimer, P.J., 1993. Extended 14C data-base and revised Calib 3.0 14C age calibration program. Radiocarbon 35, 215-230

Urien, C.M., Ewing, M., 1974. Recent sediments and environments of Southern Brazil, Uruguay, Buenos Aires, and Rio Negro continental shelf, in: Burk, C.A., Drake, C.L. (Eds.), The Geology of Continental Margins. Springer, Berlin, Heidelberg, New York, pp. 157-177.

Viana, A.R., 2002. Seismic expression of shallow- to deep-water contourites along the south-eastern Brazilian margin. Mar. Geophys. Res. 22, 509-521.

Viana, A.R., Faugères, J.-C., 1998. Upper slope sand deposites: The example of Campos Basin, a latest Pleistocene--Holocene record of the interaction between alongslope and downslope currents, in: Stoker, M.S., Evans, D., Cramp, A. (Eds.), Geological processes on continental margins: Sedimentation, mass-wasting and stability. Geological Society, London, Special Publications, pp. 287-316.

Violante, R.A., Paterlini, C.M., Costa, I.P., Hernández-Molina, F.J., Segovia, L.M., Cavallotto, J.L., Marcolini, S., Bozzano, G., Laprida, C., García Chapori, N., Bickert, T., Spieß, V., 2010. Sismoestratigrafia y evolución geomorfológica del talud continental adyacente al litoral del este bonaerense, Argentina. Lat. Am. J. Sedimentol. Basin Anal. 17, 33-62.

8. Palaeoclimatic forcing of Holocene Subtropical Shelf Front shifts off Southeast South America

Vera B. Bender [a, b], Cristiano M. Chiessi [c], Till J. J. Hanebuth [b]

[a] *MARUM – Center for Marine Environmental Sciences, University of Bremen, Leobener Strasse, 28359 Bremen, Germany.*

[b] *Faculty of Geosciences, University of Bremen, Klagenfurter Strasse, 28359 Bremen, Germany.*

[c] *Escola de Artes, Ciências e Humanidades, Universidade de São Paulo, Rua Arlindo Béttio 1000, 03828-000 São Paulo, SP, Brazil.*

To be submitted to Paleoceanography

Abstract

Over the Uruguayan shelf and uppermost slope the coalescence of northward flowing subantarctic shelf water and southward flowing subtropical shelf water forms a distinct thermohaline front termed the Subtropical Shelf Front (STSF). Running in SW direction across the shelf from the coastal waters off Patos Lagoon towards the shelf break at ca. 36°S, the STSF represents the shelf-ward extension of the Brazil-Malvinas Confluence zone. We reconstructed relative latitudinal STSF shifts during the Holocene based on palaeoceanographic (benthic foraminifera $\delta^{18}O$ and $\delta^{13}C$) and sedimentologic (e.g. TOC, $CaCO_3$, grain-size composition, εNd) proxies from a new high-accumulation sediment record located at the continental uppermost slope (250 m modern water depth). The presented results add direct evidence for (1) a southward STSF displacement (<3° latitude) at the beginning of the early Holocene (>9.4 cal ka BP) plausibly linked to a more southerly position of the Southern westerlies in combination with modified shelf water circulation due to lowered sea-level; (2) from ca. 9.4 cal ka BP onwards a gradual STSF northward migration primarily forced by the northward migration of the Southern westerlies; (3) a relatively stable position of the front between 7.2 – 4.0 cal ka BP; (4) slightly higher variability in the $\delta^{18}O$ record after 4.0 cal ka BP might be linked to the intensification of El Niño Southern Oscillation; and (5) a northward migration of the STSF during the past ca. 200-years possibly linked to anthropogenic influence.

Introduction

The Holocene evolution of the western South Atlantic is poorly understood due to the lack of high temporal resolution records [*Leduc et al.*, 2010; *Wanner et al.*, 2011]. Under modern conditions the western South Atlantic is one of the most energetic regions of the world's oceans dominated by the encounter of the poleward-flowing Brazil current (BC) and the equatorward-flowing Malvinas current (MC) (Fig. 8.1), forming the Brazil-Malvinas Confluence (BMC) over most of the continental slope [*Peterson and Stramma*, 1991; *Stramma and England*, 1999]. On the shelf and uppermost slope cold, relatively fresh and eutrophic Subantarctic Shelf Water (SASW) and warm, salty and relatively oligotrophic Subtropical Shelf Water (STSW) collide in a similar way forming a strong barotropic front, the Subtropical Shelf Front (STSF; Figs. 8.1 and 8.2) [*Piola et al.*, 2008; *Piola et al.*, 2000]. The density-compensated thermohaline nature of the STSF makes it a key component in the cross-shelf offshore transport of water masses in the western South Atlantic [*Matano et al.*, 2010]. Though the STSF appears to be the northward shallow-water extension of the BMC, the processes controlling its latitudinal location are still under discussion [e.g., *Matano et al.*, 2010]. In this context, it is suggested that the cross-shelf scale of the pressure gradient enforced by the MC as well as the northernmost extension of the MC itself play a major role in controlling the latitudinal re-location of the STSF [*Matano et al.*, 2010; *Palma et al.*, 2008].

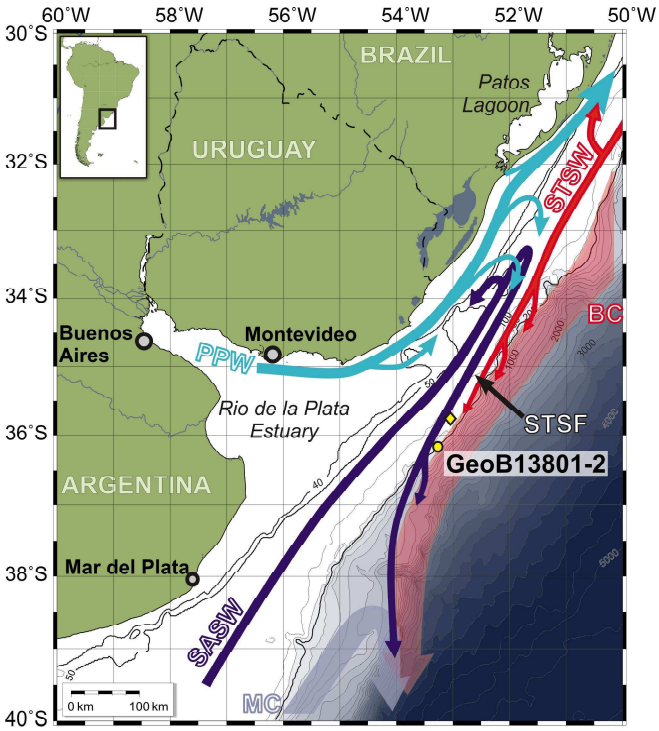

Fig. 8.1: Location of sediment core GeoB13801-2 at the SE South America continental margin. Oceanographic features are redrawn after *Piola et al.* [2008] summarizing the mean winter circulation patterns; BC: Brazil Current; MC: Malvinas Current; PPW: Plata Plume Water; SASW: Subantarctic Shelf Water; STSF: Subtropical Shelf Front; STSW: Subtropical Shelf Water. The yellow diamond marks the location of fine sands draping the outer shelfand sampled for grain-size distribution comparison

Below the surface mixed layer, the STSF location experiences no significant seasonality [*Möller et al.*, 2008; *Piola et al.*, 2008]. Due to the strong temperature, salinity and preformed nutrient content differences between the SASW and the STSW the use of oxygen and carbon isotopic composition in benthic foraminifera represent appropriate tools to identify changes in the dominantly influencing shelf water mass and thus latitudinal shifts of the front.

Both water masses present at the STSF furthermore have sediment transportation potential; SASW and STSW circulating with up to 30 cm/s and up to 20 cm/s over the outer shelf off SE South America, respectively [*de Mahiques et al.*, 2008; *Gwilliam*, 1996].

Along the southeastern South American continental margin the Neodymium isotopic signatures (εNd) of the bulk siliciclastic sediment component have been shown to relate to distinct source provinces (i.e. Patagonia – Argentine shelf; Rio de la Plata estuary and Southeastern Brazil) and a reliable proxy for terrigenous sediment dynamics [*de Mahiques et al.*, 2008].

This study presents the first high temporal resolution (200 – 20 years sample spacing) paleoceanographic (benthic stable oxygen and carbon isotopes) record in combination with sedimentologic data (total organic carbon (TOC) content, calcium carbonate ($CaCO_3$) content, grain-size composition, εNd) from the western South Atlantic covering the most of the Holocene. With this multi-proxy approach we aim to identify lateral shifts in the shelf current and front regimes off Uruguay with respect to the different Southern Hemisphere climate forcing mechanisms over this time period.

Regional setting

The study site is located at the uppermost slope off Uruguay that is largely dominated by shelf oceanographic processes (Fig. 8.1). The inner shelf circulation off Uruguay is strongly influenced by the La Plata river discharge (~23,000 m^3/s) which, together with the Patos Lagoon outflow (~1750 m^3/s), forms the distinctly buoyant, low-salinity (<26 psu) Plata Plume Water (PPW; Fig. 8.1) [*Piola et al.*, 2008; *Piola et al.*, 2000]. The PPW is commonly northward directed and recognized as far north as 25°S [*Piola et al.*, 2000]. The maximum PPW northward penetration is primarily controlled by the pronounced seasonality of the along-shore wind stress. During austral winter with southwesterly winds the PPW shows its northernmost penetration, while during austral summer under northeasterly winds the PPW retracts to the south and is rather advected offshore [*Möller et al.*, 2008; *Piola et al.*, 2005]. There is strong evidence that PPW distribution also responds to El Niño Southern Oscillation (ENSO) variability through changes in the interannual wind patterns [*Piola et al.*, 2005]. During El Niño events, although positive precipitation anomalies over the drainage basin lead to increased La Plata river outflow, the regional atmospheric circulation resembles the austral summer situation and PPW is confined to higher latitudes [*Piola et al.*, 2005].

Subsurface circulation below 50 m modern water depth on the shelf off Uruguay is dominated by the southward-flowing, oligotrophic, warm (>16°C) and saline (>34.8 psu) Subtropical Shelf Water (STSW) and the northward-flowing, eutrophic, relatively cold (<11°C) and fresh (<34 psu) Subantarctic Shelf Water (SASW) [*Brandini et al.*, 2000; *Piola et al.*, 2008; *Piola et al.*, 2000] (Figs. 8.1 and 8.2). The encounter of STSW and SASW forms a distinctly steep

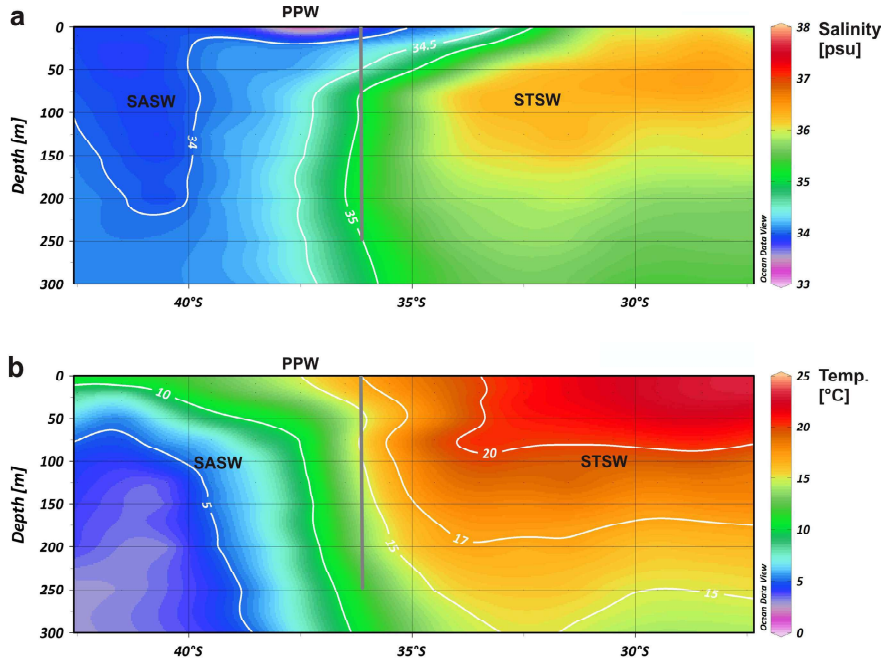

Fig. 8.2: Latitudinal transects of annual (**a**) salinity [*Antonov et al.*, 2010] and (**b**) temperature [*Locarnini et al.*, 2010] along the outer shelf /uppermost slope from ca. 42°S to 32°S. For water masses abbreviations see Fig. 8.1. Vertical gray line indicates the location of sediment core GeoB13801-2 below the Subtropical Shelf Front.

thermohaline transition termed the Subtropical Shelf Front (STSF) [*Piola et al.*, 2000]. The STSF runs southwestward from the 50 m isobath at 32°S towards the shelf break around 36°S (Fig. 8.1) [*Piola et al.*, 2000]. At the surface the position of the STSF shows minor seasonal variation (southward displacement during austral winter), however, at the subsurface in the middle and outer shelf the STSF can be considered stable throughout the year (s. Fig. 1 in the supplementary information to this article) [*Möller et al.*, 2008; *Piola et al.*, 2008].

Due to its density-compensated thermohaline structure the STSF favors offshore advection of the colliding shelf water masses, making the STSF a critical component in cross-shelf water transport in the western South Atlantic [*Matano et al.*, 2010; *Piola et al.*, 2008]. Numerical simulations indicate that the barotropic pressure gradient enforced by the MC on the shelf circulation plays a major role in determining the latitudinal STSF location [*Palma et al.*, 2008]. The northward effect of this barotropic pressure gradient is mainly determined by shelf width. Under present-day shelf morphology (shelf width of ca. 160 km at 37°S) this leads to a northernmost penetration of SASW approx. 600 km northeast of the MC northernmost penetration [*pers. comm. A. Piola*].

Material and methods

The studied gravity core GeoB13801-2 (36°08.49'S; 53°17.96'W) was retrieved at 241 m water depth during cruise M78/3a with the German *R/V Meteor* in May / June 2009 (Fig. 8.1). The core was collected from a small terrace at the uppermost continental slope off Uruguay. Total core recovery was 950 cm of mainly silty fine sands.

The age model of GeoB13801-2 (Fig. 8.3) is based on nine accelerator mass spectrometer radiocarbon (AMS ^{14}C) dates performed at the Poznan Radio-carbon Laboratory (Poland). For radiocarbon dating different types of marine carbonate were hand-picked from the >250 µm fraction (Table 8.1). The ages were converted into 1-sigma calibrated ages using the Marine09 calibration data set [*Reimer et al.*, 2009] and the Calib 6.1.1 software [*Stuiver and Reimer*, 1993]. All dates reported below are in calibrated thousands of years before present (cal ka BP).

Total carbon (TC) and total organic carbon (TOC) were quantified using the LECO CS-200 system located at the Faculty of Geosciences, University of Bremen. Carbonate ($CaCO_3$) content was calculated from the difference of TC and TOC employing the standard equation $CaCO_3$ [wt.%] = (TC – TOC) * 8,333.

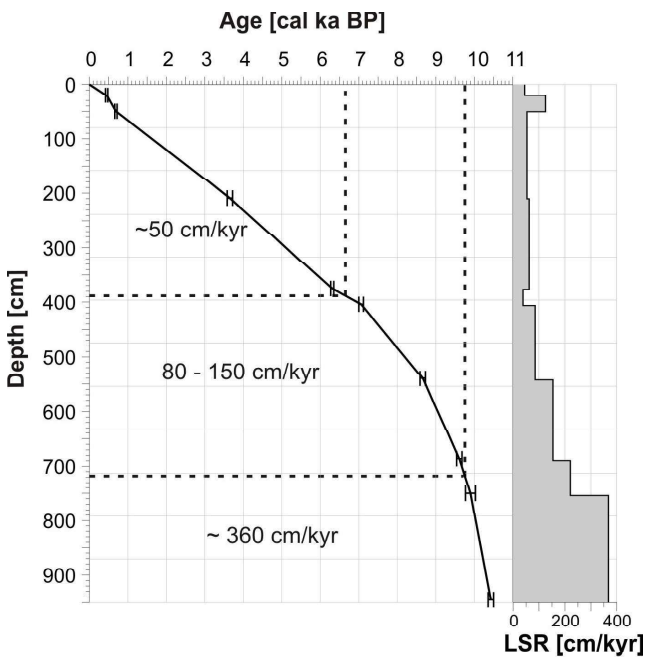

Fig. 8.3: Depth - age model of sediment core GeoB13801-2. Corresponding linear sedimentation rates (LSR) are shown on the right-hand side of the main panel and averaged for lithologically similar units within the main panel.

Table 8.1: GeoB13801-2 radiocarbon dates and calibrated ages.

Lab No.	Core depth [cm]	Material	^{14}C ages [^{14}C yr BP]	1σ calibrated age range [cal yr BP]	Calibrated age (intercept) [cal kyr BP]
Poz-42421	20	Bulk foraminifera 250 - 1000 µm	800 ± 30	420 - 479	0.45 ± 0.03
Poz-42425	50	Bulk foraminifera 250 - 1000 µm	1155 ± 30	665 - 723	0.69 ± 0.03
Poz-42422	209	*Uvigerina bifurcata*	3730 ± 50	3572 - 3720	3.65 ± 0.07
Poz-42423	375	Bulk biogen. carbonate 250 - 1000 µm	5890 ± 40	6265 - 6353	6.31 ± 0.04
Poz-42424	404	Bulk biogen. carbonate 250 - 1000 µm	6535 ± 35	6998 - 7118	7.06 ± 0.06
Poz-35195	540	*Uvigerina bifurcata*	8180 ± 40	8589 - 8733	8.66 ± 0.07
Poz-42426	686	*Uvigerina bifurcata*	8970 ± 50	9539 - 9688	9.61 ± 0.07
Poz-42427	750	Bulk foraminifera 125 - 1000 µm	9130 ± 60	9771 - 10032	9.90 ± 0.13
Poz-35197	945	Fresh bivalves of *Yoldiella* genus	9560 ± 50	10366 - 10503	10.43 ± 0.07

Calcium and Titanium relative concentrations were obtained utilizing the AVAATECH X-ray fluorescence core scanner of MARUM, University of Bremen and are given in counts per second (cps).

Grain size distributions from 2000 to 0.4 to µm were analyzed by means of a Coulter Laser Particle Sizer LS200 at the grain size laboratory of MARUM, University of Bremen. Prior to the analyses of terrigenous grain size distributions samples were digested in successive steps with 35% H_2O_2, 10% HCl and 6% NaOH to remove organic carbon, biogenic carbonate and opal, respectively. Sand (2000 – 63 µm), silt (63 – 4 µm) and clay (<4 µm) content were calculated from the cumulative grain size distributions (bulk and terrigenous).

Stable oxygen and carbon isotopic analyses were performed on about 40 specimens of 125 – 150 µm sized benthic foraminifera *Cibicides mckannai* using a Finnigan MAT 252 mass spectrometer at the stable isotopes laboratory of MARUM, University of Bremen. We used *C. mckannai* since it was the only species of foraminifer genera (benthic and planktic) typically used for paleoceanographic purposes, that was present throughout the entire record. Long-term laboratory analytical standard deviation is <0.07‰ and <0.05‰ for $\delta^{18}O$ and $\delta^{13}C$, respectively. All values are given as ‰ deviations from the Vienna Pee Dee belemnite (VPDB) (calibrated by NBS 19 and IAEA 66 standards). The $\delta^{18}O$ data set is additionally corrected for continental ice volume (i.e., sea level) effects based on *Lambeck and Chappell* [2001] and *Schrag et al.* [2002], in the following denoted as ice-volume-corrected $\delta^{18}O$ ($\delta^{18}O_{ivc}$).

For ordination of the samples a principal components analysis (PCA) was performed using the Multivariate Statistical Package (MVSP) Version 3.2 [*Kovach*, 2010] on the standardized data of calcium carbonate content, TOC content, bulk and terrigenous clay, silt and sand content, bulk and terrigenous mean grain size, as well as $\delta^{18}O_{ivc}$ and $\delta^{13}C$.

Samples from the different lithologies in GeoB13801-2 were analyzed for their Neodymium (Nd) isotopic composition at the Geochronological Research Center of the University of São Paulo. Sample preparation followed the standard analytical procedure given by *Sato et al.* [1995], including calcium carbonate removal, HF-HNO_3 dissolution and HCl cation exchange, finally using a Teflon powder column to separate the rare earth elements. Analyses were performed on a multicollector Finnigan MAT262 mass spectrometer. Obtained Nd ratios were normalized to a $^{146}Nd/^{144}Nd$ ratio of 0.7219, and εNd values were calculated following the equation given by *Hamilton et al.* [1983].

Results

Age model

We consider our core top to be of modern age, since we attribute the 0.8 ‰ decrease in the upper most samples of our $\delta^{13}C$ record (see below) to the oceanic *Suess effect*. This effect ascribes the observed historical decrease of $\delta^{13}C$ to the oceanic uptake of isotopically light CO_2 by the industrial burning of fossil fuels [*Suess*, 1955].

All radiocarbon dates gave reliable and consecutive results with a basal sample dating back to 10.5 cal ka BP (Table 8.1). From the detailed lithologic core description no obvious hiati were recognizable, consequently we linearly interpolated ages between all dated levels given in Table 8.1. The resulting depth – age model shows a high but strongly varying sedimentation rate, decreasing from about 360 cm/kyr between 10.5 – 9.9 cal ka BP down to about 50 cm/kyr from 7.0 cal ka BP until the present.

Sediment composition parameters

The lithology of core GeoB13801-2 is generally dominated by a very constant terrigenous fine sandy grain-size, originating from a proximal outer shelf sand drape and making-up between 60 to 80 wt.% of the total terrigenous fraction (Figs. 8.4 and 8.5a). The siliciclastic nature of core GeoB13801-2 is reflected by the bulk clay and silt content closely following the variations of the terrigenous clay and silt fractions (Fig. 8.5a, c and d). Variations within this otherwise conservative lithologic regime of GeoB13801-2 can be described in four successive phases (Fig. 8.5):

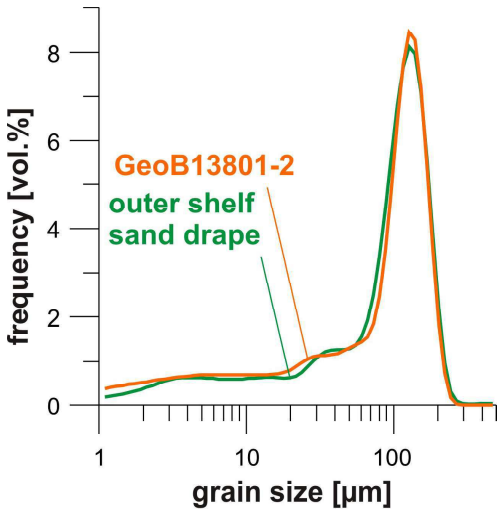

Fig. 8.4: Mean terrigenous grain size distribution of GeoB13801-2 (orange) and from the outer shelf sand drape (green) indicating direct off-shelf supply of terrigenous sediments from the outer shelf sand drape towards the uppermost slope terrace.

From 10.4 to 8.8 cal ka BP we observe high variability in all sediment compositional parameters and temporarily extraordinary high terrigenous clay (max. 67 vol.% at 9.99 cal ka BP) and/or silt (max. 72 vol.% at 9.85 cal ka BP) content occur (Fig. 8.5a–e). Bulk TOC content is low at ca. 1 wt.%, and bulk carbonate content is high at ca. 10 wt.% (Fig. 8.5b and e).

Between 8.8 to 7.2 cal ka BP sediment composition is very stable, with terrigenous clay and silt as low as 20%, bulk carbonate content at ca. 8 wt.% and bulk silt content at ca. 35% (Fig. 8.5a, c and e). A very slight increasing trend in TOC content from 0.5 wt.% towards ca. 1 wt.% within this phase is visible and mirrored by the bulk clay content (from 6% to 9%; Fig. 8.5b and d).

After 7.2 cal ka BP until 4.0 cal ka BP variability in the sediment compositional parameters is again strengthening. Terrigenous clay and silt, as well as TOC and carbonate content increase, synchronously reach a first maximum at ca. 6.4 cal ka BP of 65% (terr. clay and silt together), 3.2 wt.% (TOC) and 15 wt.% (carbonate) (Fig. 8.5a, b and e). A second maximum at ca. 5.2 cal ka BP is most pronounced in the carbonate content (up to ca. 18 wt.%) and Ca/Ti ratio (Fig. 8.5e and f).

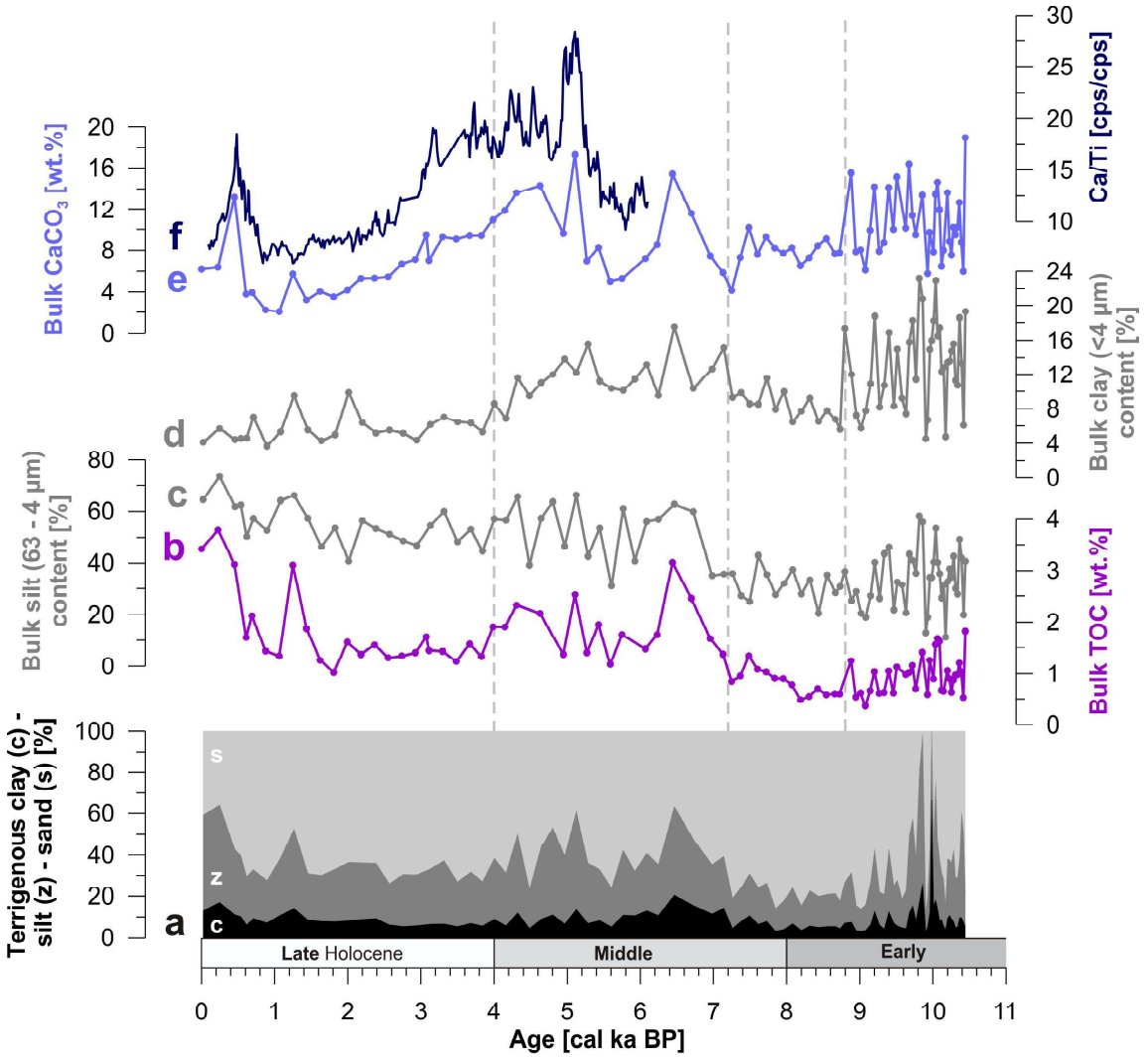

Fig. 8.5: GeoB13801-2 temporal variation of (a) cumulative terrigenous clay (c) – silt (z) – sand (s) relationship, (b) bulk TOC, (c) bulk silt content, (d) bulk clay content, (e) bulk carbonate content, and (f) calcium/ titanium ratio (≈ marine/ terrigenous input).

After 4.0 cal ka BP the sediment compositional records stabilize again with a ca. 400-years positive excursions in all parameters centred at 1.2 cal ka BP. Terrigenous clay, silt and bulk TOC content are, besides this 1.2 cal ka BP positive excursion, constantly varying around 30% (terr. clay and silt together) and 1.25 wt.% (TOC), and only increase up to 60% and 3.8 wt.%, respectively, for the most recent 500 years (Fig. 8.5a and b). In contrast carbonate content (mirrored by Ca/Ti ratio) pursues a decreasing trend from ca. 4.0 cal ka BP until ca. 0.8 cal ka BP from ca. 10 wt.% carbonate down to 2 wt.% (Fig. 8.5e), and shows another ca. 400-years positive peak of up to 13 wt.% carbonate at 0.6 cal ka BP, before decreasing down to ca. 6 wt.% at the top of the record (Fig. 8.5e).

Stable isotopic composition

Stable oxygen isotopes

Between 10.4 to 10.0 cal ka BP $\delta^{18}O_{ivc}$ values show the highest variability throughout the record ranging from 0.3‰ to 1.63‰ (Fig. 8.6a). From ca. 10 until 9.4 cal ka BP $\delta^{18}O_{ivc}$ values stabilize at ca. 1.8‰, followed by an abrupt decrease to 1.2‰ at 9.33 cal ka BP. After 9.3 cal ka BP $\delta^{18}O_{ivc}$

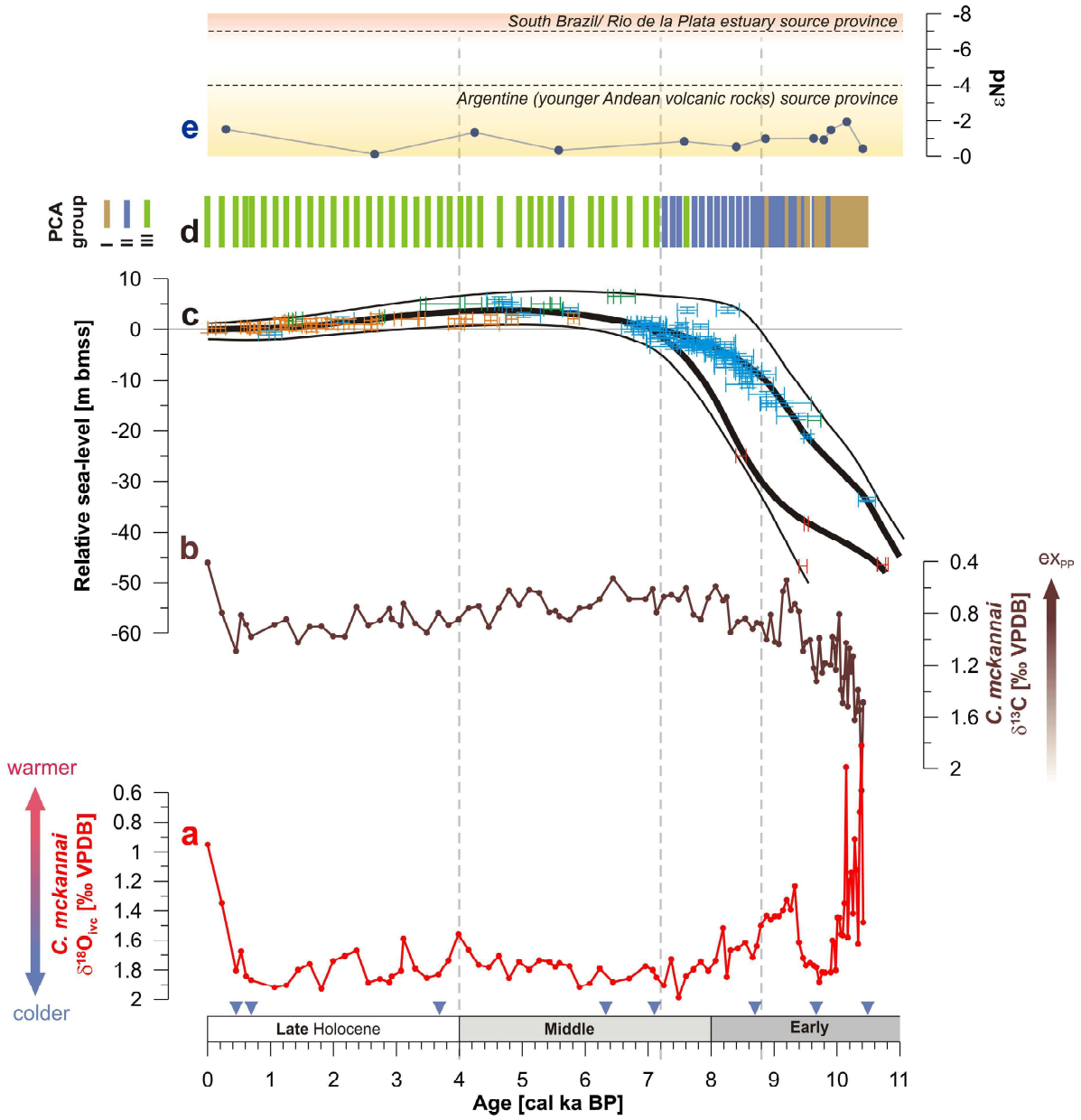

Fig. 8.6: GeoB13801-2 (a, b) *Cibicides mckannai* stable oxygen ($\delta^{18}O_{ivc}$ - ice volume corrected) and carbon ($\delta^{13}C$; ex_{PP}: export primary productivity). c) relative sea-level as composite of regional data from *Angulo et al.* [2006] (Santa Catarina data set South of 28°S), *Cavallotto et al.* [2004], and *Guilderson et al.* [2000], as well as eustatic data from *Hanebuth et al.* [2011]; all sea-level age points were recalibrated following the procedure described for the age model of GeoB13801-2; thin black lines demark a graphic envelope around all sea-level data points. d) temporal occurrence of the three PCA groups (Fig. 8.7). e) GeoB13801-2 εNd and published source provinces εNd [*de Mahiques et al.*, 2008]. Blue triangles demark AMS^{14}C dated levels, and vertical dashed lines mark important dates discussed in the text.

values gradually increase again reaching 1.8‰ at about 7.2 cal ka BP. After 7.2 until ca. 0.2 cal ka BP $\delta^{18}O_{ivc}$ values vary around 1.8‰. The most-recent 200 years are characterized by a remarkably abrupt fall down to 0.95‰. We interpret the GeoB13801-2 benthic *C. mckannai* $\delta^{18}O_{ivc}$ values as an indicator for relative bottom water temperature change, whereby lighter values correspond to an increased influence of relatively warm STSW and heavier values indicating a stronger influence of relatively cold SASW (see supplementary information - at the end of this chapter - for more detail).

Stable carbon isotopes

During the early Holocene, $\delta^{13}C$ values decrease from 2.17‰ at 10.4 cal ka BP down to ca. 0.7‰ at 8 cal ka BP, with the highest variability found throughout the record between 10.4 to 10 cal ka BP (Fig. 8.6b). Between ca. 8 to 0.2 cal ka BP $\delta^{13}C$ values slightly increase from ca. 0.7‰ to 0.9‰. Likewise the $\delta^{18}O_{ivc}$ record, $\delta^{13}C$ values show a strong decrease during the most recent ca. 200 years reaching 0.4‰. We interpret our benthic *C. mckannai* $\delta^{13}C$ record as a relative export productivity proxy, with low isotopic ratios indicating increased surface water export productivity, and vice versa (s. supplementary information - at the end of this chapter - for more detail).

Neodymium isotopic composition

Calculated εNd values vary between -0.1 to -1.9 throughout the core (Fig. 8.6e). According to the end-member characterization of *de Mahiques et al.* [2008] these values are typical for the influence of the southern, i.e. Argentine / Patagonian source province (εNd values of -4 to 0; younger Andean volcanic rocks).

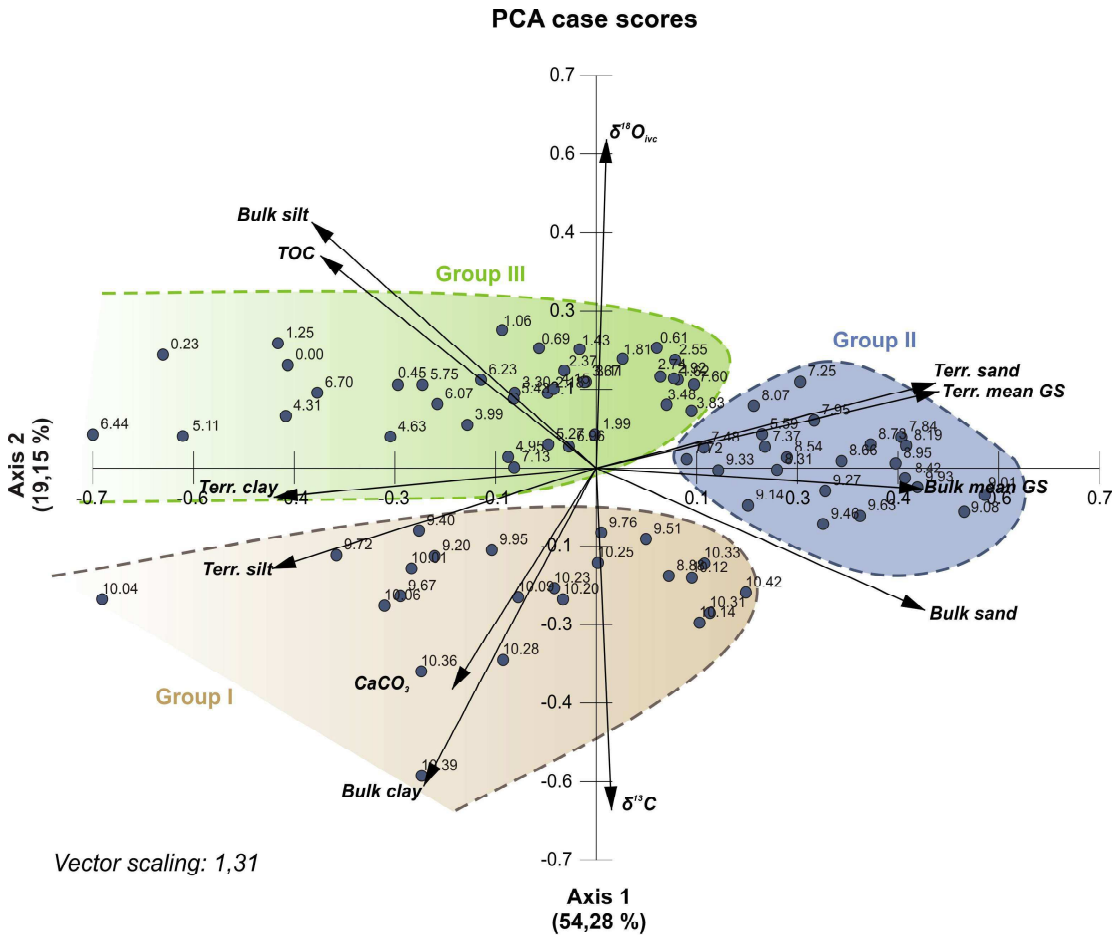

Fig. 8.7: PCA ordination diagram of all samples based on the selected variables carbonate content ($CaCO_3$), total organic carbon content (TOC), bulk and terrigenous clay content (bulk clay; terr. clay), bulk and terrigenous silt content (bulk silt; terr. silt), bulk and terrigenous sand content (bulk sand; terr. sand), bulk and terrigenous mean grain size (bulk mean GS; terr. mean GS), ice volume corrected *Cibicides mckannai* stable oxygen isotopic ratio ($\delta^{18}O_{ivc}$) and Cibicides mckannai stable carbon isotopic ratio ($\delta^{13}C$). Samples are labeled by their inferred age in cal ka BP. Three main sample groups can be identified, denominated as Groups I – III.

Principal component analysis (PCA)

A PCA ordination of the sedimentological parameters carbonate content, TOC content, bulk and terrigenous clay/silt/sand content, bulk and terrigenous mean grain sizes, together with $\delta^{18}O_{ivc}$ and $\delta^{13}C$ values allowed for the distinction of two principal components explaining 73.4% of the total variance (Fig. 8.7). Moreover, three sample clusters are identified; termed Groups I – III. Group I is positively correlating with terrigenous silt, bulk clay, calcium carbonate content, and $\delta^{13}C$ (Fig. 8.7). The temporal occurrence of Group I is restricted to the time interval prior to 8.8 cal ka BP (Fig. 8.6d). Group II is marked by a positive correlation of terrigenous sand content and mean grain sizes (bulk and terrigenous), having its main occurrence between 8.8 to 7.2 cal ka BP, a single occurrence at 5.5 cal ka BP (Figs. 8.7 and 8.6d). Group III is positively correlated with TOC, bulk silt and terrigenous clay content, and dominantly occurs after 7.2 cal ka BP (Figs. 8.7 and 8.6d).

Discussion

Early Holocene trends

The GeoB13801-2 $\delta^{18}O_{ivc}$ record shows a transition from relatively warm bottom water towards colder waters from 10.4 until ca. 7.2 cal ka BP (Fig. 8.6a). This warm to cold bottom water transition implies an early Holocene northward migration of the STSF that crossed the latitude of 36°S around 7.2 cal ka BP. Comparison to estimation of predicted calcite $\delta^{18}O$ ($\delta^{18}O_{pc}$) at the modern water depth of GeoB13801-2 show that the very low $\delta^{18}O_{ivc}$ values recorded prior to 10 cal ka BP (ca. 0.5‰) are indeed values that are predicted for STSW 3° north of GeoB13801-2 (0.5‰ at modern GeoB13801-2 water depth; 0.35‰ at approx. early Holocene GeoB13801-2 water depth, s. supplementary information). Moreover, the same calculation indicates that the high $\delta^{18}O_{ivc}$ values after 7.2 cal ka BP (1.5 – 2.0‰; Fig. 8.6a) are very close to SASW $\delta^{18}O_{pc}$ values approx. 1° South of the STSF (2.2 ‰ at modern water depth of Geob13801-2; s. supplementary information).

Two factors have acted simultaneously producing a northward migration of the STSF: i) sea-level rise, and ii) a northward migration of the northern boundary of the Southern Westerly Winds (SWW).

Under modern conditions the latitudinal location of the STSF is related to the northward effect of the barotropic pressure gradient imposed by the MC on the shelf circulation, which controls the northernmost penetration of SASW [*Matano et al.*, 2010; *Palma et al.*, 2008]. The MC pressure gradient forcing is mainly determined by the shelf width. By 10.4 cal ka BP sea level was located around the 50 m isobaths (-50 m below mean sea sea-level, Fig. 8.6c) reducing the shelf north of 37°S to half of its modern width (cf. Figs. 8.1). Consequently the cross-shelf scale of the MC barotropic pressure gradient forcing on shelf circulation was significantly reduced, resulting in a reduced northward penetration of SASW, presumably causing a more southerly location of the STSF. As sea level rose, the width of the shelf gradually increased what may have caused a more northward penetration of SASW and pushed the STSF northward. The northward migration of the STSF at 36°S stabilizes by 7.2 cal ka BP, synchronous to sea-level reaching -5 m of the modern sea-level (Fig. 8.6). If sea-level rise and the STSF northward migration are directly linked, GeoB13801-2 $\delta^{18}O_{ivc}$ and sea level height should develop parallel to each other. Apart from an abrupt colder period between 10.0 to 9.4 cal ka BP (see below), $\delta^{18}O_{ivc}$ values show a linear trend towards bottom water cooling (Fig. 8.6a). Regional sea-level data for the

period prior to ca. 6.5 cal ka BP is sparse (Fig. 8.6c). Moreover, compared to the middle and late Holocene, early Holocene regional data [*Guilderson et al.*, 2000] diverge significantly from the eustatic curve [*Hanebuth et al.,* 2011] (Fig. 8.6c). The sparse data coverage and divergence from the higher resolution eustatic data hampers the identification of robust regional trends in early Holocene sea level rise. However, early and middle Holocene sea-level rise exerted an overall strong control on shelf configuration as well as surface water export productivity, which is expressed in the sediment compositional data and $\delta^{13}C$ values: the high lithologic variability PCA Group I and low export productivity correlate with the time of presumably strong sea-level induced reworking on the outer to middle shelf (>-50 m to approx. -35 m; *Guilderson et al.*, 2000) until 8.8 cal ka BP; rather stable lithology PCA Group II and increasing export productivity occur during times of decelerating sea-level rise and the approach of modern sea level on the SE South American shelf (8.8 – 7.2 cal ka BP: -35 m to ca. -5 m; *Guilderson et al.*, 2000; *Hanebuth et al.*, 2011); whereas the main occurrence of PCA Group III and relatively high productivity correlates well with the stabilizing sea-level conditions after 7.2 cal ka BP (between -5 m to +6.5m; *Cavallotto et al.*, 2004; *Hanebuth et al.*, 2011; Fig. 8.6b, c and d). The approach of modern sea-level height and consequently modern shelf circulation patterns by approx. 8.8 cal ka BP is not explicitly paralleled by the $\delta^{18}O_{ivc}$ record (Fig. 8.6a, c and d). We consequently suggest that sea-level migration over the shelf during early Holocene had an influence on the southward displacement of the STSF through altering the shelf width, but apparently it did not exert a dominant control on the fronts' more southerly location and subsequent northward migration.

The second mechanism determining the latitudinal position of the STSF is the latitude of northernmost MC penetration along the middle slope. Numerical modeling showed that a northward shift of the Southern Westerly Wind system (SWW) would cause an enhanced inflow of Antarctic Intermediate Water into the western South Atlantic and consequently enhanced northward penetration of the MC [*Sijp and England*, 2008]. A more poleward location of the SWW would in turn cause a retraction of the MC and consequently a southward displacement of the STSF [*Biastoch et al.*, 2009; *Sijp and England*, 2008]. Multi-proxy reconstructions of the SWW northern boundary and strength indicate a poleward confinement during late glacial to early Holocene, followed by an approx. 10° northward migration of its northern boundary between 8.5 to 5.5 cal ka BP [e.g. *Hebbeln et al.*, 2002; *Kaiser et al.*, 2008; *Lamy et al.*, 2010; *Mohtadi and Hebbeln*, 2004]. The northward migration of the STSF presented in this study starts ca. 1000-years earlier (at ca. 9.5 cal ka BP; Fig. 8.8) than the hypothesized SWW northward migration, and stabilizes at 36°S already by 7.2 cal ka BP (Figs. 8.6a and 8.8). The earlier initiation might be linked to the regional sea-level effect discussed above. Whereas the earlier stabilization by 7.2 cal ka BP could be either i) the point in time when the STSF crosses 36°S and any further variations are not documented by our record; or ii) indeed the time of maximum Holocene STSF northward displacement. Besides enhancing intermediate water the inflow through the Drake Passage, a northward shift of the SWW has a wide impact on the whole Southern Ocean circulation via its influence on the Antarctic Circumpolar Current (ACC) [*Biastoch et al.*, 2009; *Sijp and England*, 2008; *White and Peterson*, 1996]. The latitudinal location of ACC is strongly linked to the latitude of maximum wind stress of the SWW [*Sijp and England*, 2008]. Contrasting the SWW, the ACC northward shift is geographically confined by the Drake Passage, thus, the oceanographic effect might come to a halt before the atmospheric wind system reaches its maximum northern position. The fact that after 7.2 cal ka BP GeoB13801-2 $\delta^{18}O_{ivc}$ values do not further increase and stay closely below $\delta^{18}O_{pc}$ values estimated for modern SASW 1°S suggests that the maximum Holocene northward STSF displacement was reached close to 36°S by this time.

Between 10.0 to 9.4 cal ka BP $\delta^{18}O_{ivc}$ values seem to indicate an abrupt and significant northward STSF shift in the range of 2°- 3° latitude (Fig. 8.6a, and supplementary information). Following the above hypothesis that shifts of the northern SWW boundary primarily force STSF shifts,

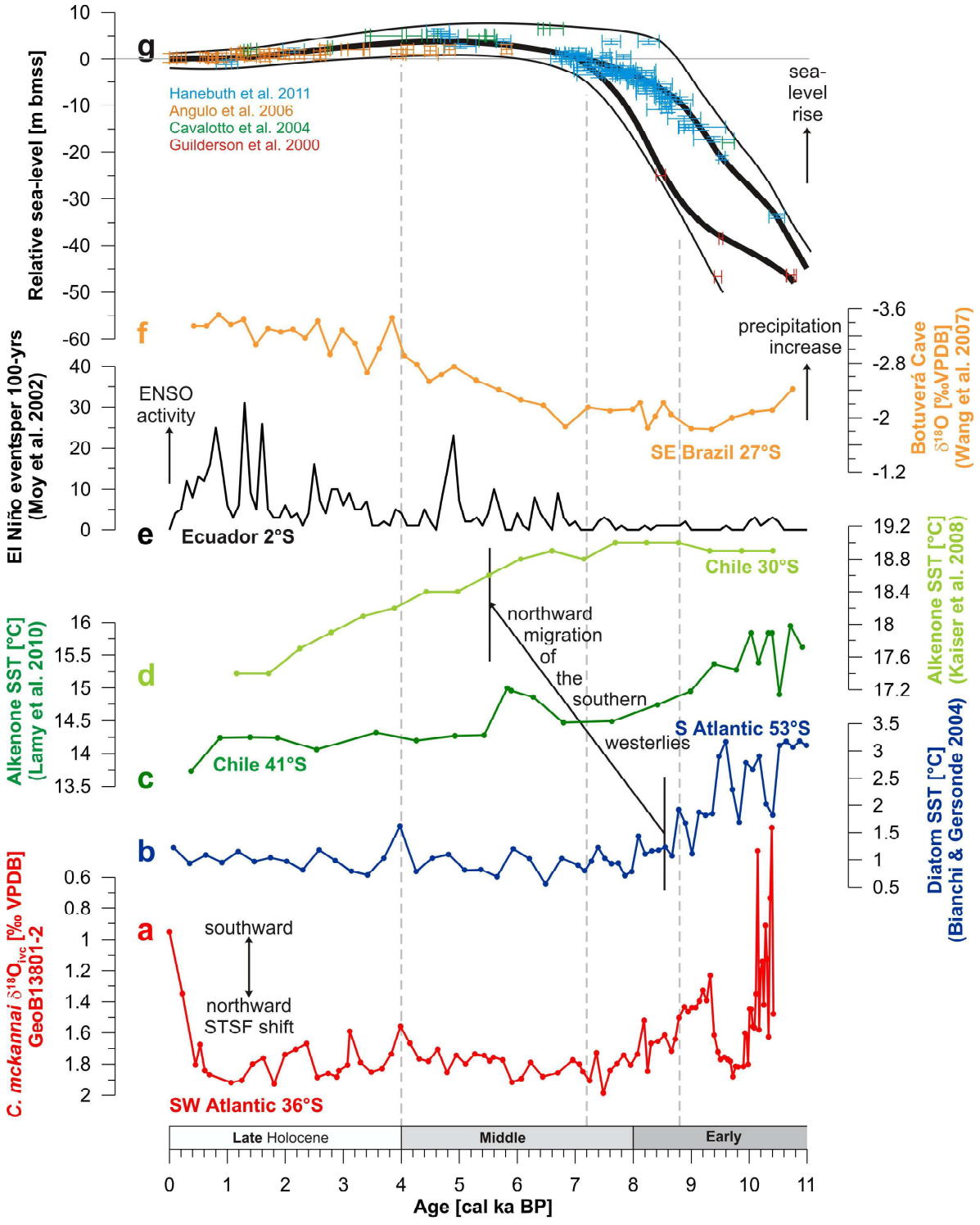

Fig. 8.8: (a) GeoB13801-2 C. mckannai $\delta^{18}O_{ivc}$ together with selected paleoclimatic proxy records from around the South American continent, (b) Diatom-based sea-surface temperature (SST) reconstructions from the South Atlantic [*Bianchi and Gersonde*, 2004]; (c) Alkenone-based SST from offshore Chile (41°S) [*Lamy et al.*, 2010]; (d) Alkenone-based SST from offshore Chile (30°S) [*Kaiser et al.*, 2008]; (c – d) reflecting the northward migration and expansion of the Southern westerlies discussed in detail by *Lamy et al.* [2010]; (e) frequency of warm ENSO events in numbers per 100-years [*Moy et al.*, 2002]; (f) speleothem $\delta^{18}O$ from SE Brazil (27°S) reflecting precipitation [*Wang et al.*, 2007]; as well as (g) combined (s. Fig. 8.6 for details) Holocene sea-level.

this millennial-scale northward STSF shift implies a contemporary northward migration of the SWW. From the SWW migration proxy records compiled by *Lamy et al.* [2010] no temporally correlating excursion is apparent which might by due to its focus on orbital time-scales. Though only extending back to 7.7 cal ka BP, *Lamy et al.* [2001] show millennial-scale variability on the iron input offshore Chile at 41°S linked to the northern boundary variability of the SWW. A pollen record from 41°S indicates maximum SWW influence at ca. 9.5 cal ka BP, suggesting an increased northern SWW influence [*Moreno et al.*, 2010]. Thus millennial-scale variability on the northern boundary of the SWW, similar to those suggested for the middle to late Holocene by *Lamy et al.* [2001] plausibly occurred also in the early Holocene. Since other South to Equatorial Atlantic paleoceanographic records are either lacking temporal resolution in the Holocene or do not show any comparable abrupt 10.0 to 9.4 cal ka BP excursion, we cannot further test this hypothesis yet.

Middle to late Holocene trends

The approach of modern sea level height by 7.2 cal ka BP lead to a general change in the sediment composition (occurrence of PCA Group III) and possibly favored increased export primary productivity (Fig. 8.6b and c).

Following a relatively stable phase between 7.2 to 4.0 cal ka BP, we find slightly increased variability in the $\delta^{18}O_{ivc}$ of GeoB13801-2 (± 0.3‰ $\delta^{18}O_{ivc}$) suggesting a less stable STSF position close to 36°S, as well as a more silty sediment composition during the late Holocene indicating a slight modification of the shelf sediment input dynamics (Figs. 8.5 and 8.6a). A change in the global climatic forcing mechanisms from external (solar insolation) to internal (oceanic-atmospheric coupling/ ENSO for South America) at ca. 5 cal ka BP has been suggested by *Debret et al.* [2009]. Within the present-day South American atmospheric circulation system warm ENSO (El Niño) events lead to reduced precipitation over the South American tropics and warmer than normal temperatures over the tropical and subtropical latitudes. These precipitation and temperature anomalies cause enhanced precipitation over southeastern South America and central Chile during warm ENSO (El Niño) events [*Garreaud et al.*, 2009]. The modern ENSO pattern started by 7 cal ka BP, and by ca 4 cal ka BP the frequency of warm (El Niño) ENSO events significantly increased [*Moy et al.*, 2002]. This enhanced El Niño frequency after 4.0 cal ka BP is recorded

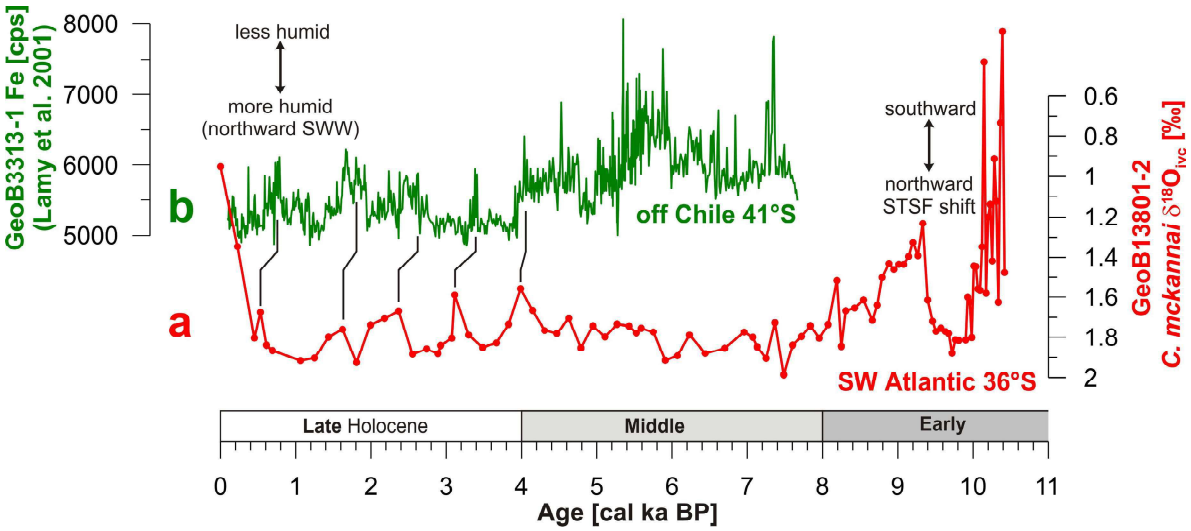

Fig. 8.9: Correlation of late Holocene GeoB13801-2 *C. mckannai* $\delta^{18}O_{ivc}$ (a) millennial scale variability with rainfall variability over central Chile recorded by iron intensity from GeoB3313-1 (41°S; b) [*Lamy et al.*, 2001].

across the South American continent, e.g. by enhanced precipitation recorded in a speleothem $\delta^{18}O$ record from Southeast Brazil (Botuverá Cave, 27°S; Fig. 8.8) and increased variability in a speleothem $\delta^{18}O$ record from Peru (del Tigre Perdido cave, 5°S) [*van Breukelen et al.*, 2008]. On the Uruguayan – SE Brazilian shelf under present-day conditions increased precipitation over Southeast South America during El Niño events leads to enhanced La Plata river outflow, however the principally Northeasterly winds during El Niño prevent the northeastward extension of PPW and the plume is advected offshore [*Möller et al.*, 2008; *Piola et al.*, 2008]. The dynamic effect of this PPW offshore advection on the STSF is still largely unknown, however the considerably less saline PPW compared to SASW ($\Delta S > 6$ psu) plausibly has little direct effect on sub-surface waters. Offshore Chile (41°S) millennial-scale positive excursions of iron influx have been linked with less humidity onshore due to more southerly located SWW [*Lamy et al.*, 2001]. Moreover a general shift in the correlation/ anticorrelation of this SWW latitudinal location variability with Antarctic ice-core data after 4.0 cal ka BP is plausibly related due to the onset of modern ENSO states [*Lamy et al.*, 2001]. We suggest that ENSO climatic forcing causing this millennial-scale variability of the late Holocene northern SWW boundary leads to equivalent variability in the STSF latitudinal location (Fig. 8.9).

Pre-industrial and modern trends (the most recent 200 years)

The very light $\delta^{13}C$ values of the most recent 200 years in the record of GeoB13801-2 are attributed to the *Suess effect* [*Suess*, 1955], implying an anthropogenic influence on this time slice of the record. Similar anthropogenic influences on marine proxy records have been observed elsewhere [e.g., *McGregor et al.*, 2007; *Mulitza et al.*, 2010]. In an analog way, we suggest that the very low GeoB13801-2 $\delta^{18}O_{ivc}$ values indicating a recent southward shift of the STSF are linked to anthropogenic climate forcing. A post-industrial southward migration of the SWW linked to anthropogenic forcing has recently been suggested by a few oceanographers [*Lumpkin and Garzoli*, 2011; *Toggweiler and Russell*, 2008]. A poleward migration of the SWW leads to a better alignment of SWW with the Antarctic Circumpolar Current, causing an increase in Agulhas leakage and a subsequent strengthening and more southward location of the South Atlantic subtropical gyre [*Biastoch et al.*, 2009; *Sijp and England*, 2008]. The data of this study supports the idea of significant changes in oceanic circulation, at least for the South Atlantic, due to a post-industrial southward shift of the SWW. The fact that within the record of GeoB13801-2 those most recent very light $\delta^{18}O_{ivc}$ values only compare to the time interval 10.4 to 10 cal ka BP should not only alarm paleoclimatologists.

A paleoceanographically independent siliciclastic sediment source

Despite a southward displacement of the STSF and corresponding STSW influence during the early, as discussed above, GeoB13801-2 εNd signatures show an unambiguous and constant Argentine/Patagonian (younger Andean volcanic rocks) source province for the terrigenous sediments deposited throughout the Holocene. Holocene terrigenous sedimentation at the location of GeoB13801-2 is dominated by a very constant ~150 µm fine sand component (cf. Fig. 8.4 and 8.5). Siliciclastic sands, extending from the Argentine shelf, widely cover the Uruguayan outer shelf up to 34°S [*Brazeiro et al.*, 2003; *Martins et al.*, 2003] and appears to be of late Glacial to Holocene age (M78/3 unpublished preliminary cruise results). We sampled this sandy drape at ca. 35°50'S (12 samples in total, from different depths of three sediment cores; Fig. 8.1). The grain size analyses from these samples provide virtually an identical average terrigenous grain-size distributions compared to those of GeoB13801-2 (Fig. 8.4), suggesting that the uppermost slope terrace sediments are directly fed from the outer shelf fine sand deposits. Since these Uruguayan outer shelf sands are part of a sand tongue extending from the Argentine shelf northwards [*Brazeiro et al.*, 2003; *Martins et al.*, 2003]. In contrast *de*

Mahiques et al. [2008] showed that STSW/ BC under modern conditions are not transporting significant amounts of sediments further South than 27°S, though STSW reaches as far South as 36°S. These shelf sands are obviously transported by the SASW over long distances and at ca. 36°S, where SASW collides with STSW and both shelf water masses are advected off-shore, exported over the shelf break [*Matano et al.*, 2010]. Consequently, an Argentine/Patagonian source province for the Uruguayan outer shelf sand drape, as well as for the uppermost slope sediments, is very plausible. Moreover, the siliciclastic input is relatively independent from the latitude of the STSF.

Conclusions

Paleoceanographic analysis of a high-accumulation rate sediment record from the uppermost slope off Uruguay (36°S) adds novel and direct evidence for latitudinal shifts of the STSF during the Holocene related to different climatic mechanisms:

1. Southward displacement of the STSF during the early Holocene was most probably linked to a more southerly position of the SWW and to the narrower continental shelf due to a ca. 50 m lowered sea-level.

2. The subsequent northward shift of the STSF was primarily forced by the northward migration of the SWW until ca. 7.2 cal ka BP.

3. Though still bathed by relatively cold waters, slightly higher variability after 4.0 cal ka BP was potentially linked to the intensification of ENSO.

4. The recent southward migration of the STSF during the most-recent 200-years BP is probably an effect of the anthropogenic influence on global climate.

The combined findings indicate that the Holocene paleoceanographic changes over the Uruguayan shelf and uppermost slope is strongly linked to Southern Hemisphere atmospheric and oceanic circulation. However, the detailed regional linkage of millennial-scale variability is still widely unclear and, especially in the case of El Niño Southern Oscillation effects on the Subtropical shelf front location, deserves detailed attention in the future.

Acknowledgements

This study was funded through the DFG Graduate College "Proxies in Earth History (EUROPROX)" and MARUM – Center for Marine Environmental Science/DFG Cluster of Excellence "The Ocean in the Earth System". Bastian Steinborn is thanked for his support in picking *C. mckannai*. The SESA meeting group and especially Renata H. Nagai is thanked for fruitful discussions.

References

Angulo, R. J., G. C. Lessa, and M. C. de Souza (2006), A critical review of mid- to late-Holocene sea-level fluctuations on the eastern Brazilian coastline, *Quat. Sci. Rev., 25*(5-6), 486-506, doi: 10.1016/j.quascirev.2005.03.008.

Antonov, J. I., D. Seidov, T. P. Boyer, R. A. Locarnini, A. V. Mishonov, H. E. Garcia, O. K. Baranova, M. M. Zweng, and D. R. Johnson (2010), *World Ocean Atlas 2009, Volume 2: Salinity,* 184 pp., U.S. Government Printing Office, Washington, D.C.

Bianchi, C., and R. Gersonde (2004), Climate evolution at the last deglaciation: the role of the Southern Ocean, *Earth Planet. Sci. Lett., 228*(3-4), 407-424, doi: 10.1016/j.epsl.2004.10.003.

Biastoch, A., C. W. Boning, F. U. Schwarzkopf, and J. R. E. Lutjeharms (2009), Increase in Agulhas leakage due to poleward shift of Southern Hemisphere westerlies, *Nature, 462*(7272), 495-499, doi: 10.1038/Nature08519.

Brandini, F. P., D. Boltovskoy, A. Piola, S. Kocmur, R. Röttgers, P. Cesar Abreu, and R. Mendes Lopes (2000), Multiannual trends in fronts and distribution of nutrients and chlorophyll in the southwestern Atlantic (30–62°S), *Deep-Sea Res. Pt. I - Oceanogr. Res.*

Pap., 47(6), 1015-1033, doi: 10.1016/s0967-0637(99)00075-8.
Brazeiro, A., M. Acha, H. Mianzan, M. Gómez, and V. Fernandez (2003), Áreas prioritarias para la conservación y manejo de la integridad biológica del Río de la Plata y su Frente Marítimo, *Jornadas Nacionales de Ciencias del Mar. XIII Coloquio Argentino de Oceanografía, Mar del Plata*.
Cavallotto, J. L., R. A. Violante, and G. Parker (2004), Sea-level fluctuations during the last 8600 years in the de la Plata river (Argentina), *Quat. Int., 114*(1), 155-165, doi: 10.1016/s1040-6182(03)00050-8.
de Mahiques, M. M., C. C. G. Tassinari, S. Marcolini, R. A. Violante, R. C. L. Figueira, I. C. A. da Silveira, L. Burone, and S. H. de Mello e Sousa (2008), Nd and Pb isotope signatures on the Southeastern South American upper margin: Implications for sediment transport and source rocks, *Mar. Geol., 250*(1-2), 51-63, doi: 10.1016/j.margeo.2007.11.007.
Debret, M., D. Sebag, X. Crosta, N. Massei, J. R. Petit, E. Chapron, and V. Bout-Roumazeilles (2009), Evidence from wavelet analysis for a mid-Holocene transition in global climate forcing, *Quat. Sci. Rev., 28*(25-26), 2675-2688, doi: 10.1016/j.quascirev.2009.06.005.
Garreaud, R. D., M. Vuille, R. Compagnucci, and J. Marengo (2009), Present-day South American climate, *Palaeogeogr. Palaeoclimat. Palaeoecol., 281*(3-4), 180-195, doi: 10.1016/j.palaeo.2007.10.032.
Guilderson, T. P., L. Burckle, S. Hemming, and W. R. Peltier (2000), Late Pleistocene sea level variations derived from the Argentine Shelf, *Geochem. Geophy. Geosy., 1*(12), 1055, doi: 10.1029/2000gc000098.
Gwilliam, C. S. (1996), Modelling the global ocean circulation on the T3D, in *Parallel Computational Fluid Dynamics*, edited by A. Ecer, J. Periaux, N. Satdfuka and S. Taylor, pp. 33-40, Elsevier, Amsterdam.
Hamilton, P. J., R. K. O'Nions, D. Bridgwater, and A. Nutman (1983), Sm-Nd studies of Archaean metasediments and metavolcanics from West Greenland and their implications for the Earth's early history, *Earth Planet. Sci. Lett., 62*(2), 263-272, doi: 10.1016/0012-821x(83)90089-4.
Hanebuth, T. J. J., H. K. Voris, Y. Yokoyama, Y. Saito, and J. Okuno (2011), Formation and fate of sedimentary depocentres on Southeast Asia's Sunda Shelf over the past sea-level cycle and biogeographic implications, *Earth-Sci. Rev., 104*(1-3), 92-110, doi: 10.1016/j.earscirev.2010.09.006.
Hebbeln, D., M. Marchant, and G. Wefer (2002), Paleoproductivity in the southern Peru-Chile Current through the last 33 000 yr, *Mar. Geol., 186*(3-4), 487-504, doi: 10.1016/S0025-3227(02)00331-6.
Kaiser, J., E. Schefuß, F. Lamy, M. Mohtadi, and D. Hebbeln (2008), Glacial to Holocene changes in sea surface temperature and coastal vegetation in north central Chile: high versus low latitude forcing, *Quat. Sci. Rev., 27*(21-22), 2064-2075, doi: 10.1016/j.quascirev.2008.08.025.
Kovach, W. L. (2010), A Multivariate Statistical Package for Windows, ver. 3.2, edited, Kovach Computing Services, Pentraeth, Wales.
Lambeck, K., and J. Chappell (2001), Sea level change through the last glacial cycle, *Science, 292*(5517), 679-686.
Lamy, F., D. Hebbeln, U. Rohl, and G. Wefer (2001), Holocene rainfall variability in southern Chile: a marine record of latitudinal shifts of the Southern Westerlies, *Earth Planet. Sci. Lett., 185*(3-4), 369-382, doi: 10.1016/S0012-821X(00)00381-2.
Lamy, F., R. Kilian, H. W. Arz, J. P. Francois, J. Kaiser, M. Prange, and T. Steinke (2010), Holocene changes in the position and intensity of the southern westerly wind belt, *Nat. Geosci., 3*(10), 695-699, doi: 10.1038/ngeo959.
Leduc, G., R. Schneider, J. H. Kim, and G. Lohmann (2010), Holocene and Eemian sea surface temperature trends as revealed by alkenone and Mg/Ca paleothermometry, *Quat. Sci. Rev., 29*(7-8), 989-1004, doi: 10.1016/j.quascirev.2010.01.004.
Locarnini, R. A., A. V. Mishonov, J. I. Antonov, T. P. Boyer, H. E. Garcia, O. K. Baranova, M. M. Zweng, and D. R. Johnson (2010), *World Ocean Atlas 2009, Volume 1: Temperature*, 184 pp., U.S. Government Printing Office, Washington, D.C.
Lumpkin, R., and S. Garzoli (2011), Interannual to decadal changes in the western South Atlantic's surface circulation, *J. Geophys. Res. - Oceans, 116*, C01014, doi: 10.1029/2010jc006285.
Martins, L. R., I. R. Martins, and C. M. Urien (2003), Aspectos sedimentares da plataforma continental na área de Influência do Rio de La Plata, *Gravel, 1*, 68-80.
Matano, R. P., E. D. Palma, and A. R. Piola (2010), The influence of the Brazil and Malvinas Currents on the Southwestern Atlantic Shelf circulation, *Ocean Sci., 6*, 983-995, doi: 10.5194/os-6-983-2010.
McGregor, H. V., M. Dima, H. W. Fischer, and S. Mulitza (2007), Rapid 20th-century increase in coastal upwelling off northwest Africa, *Science, 315*(5812), 637-639, doi: 10.1126/science.1134839.
Mohtadi, M., and D. Hebbeln (2004), Mechanisms and variations of the paleoproductivity off northern Chile (24 degrees S-33 degrees S) during the last 40,000 years, *Paleoceanography, 19*(2), Pa2023, doi: 10.1029/2004pa001003.
Möller, O. O., A. R. Piola, A. C. Freitas, and E. J. D. Campos (2008), The effects of river discharge and seasonal winds on the shelf off southeastern South America, *Cont. Shelf Res., 28*(13), 1607-1624, doi: 10.1016/j.csr.2008.03.012.
Moreno, P. I., J. P. Francois, C. M. Moy, and R. Villa-Martinez (2010), Covariability of the Southern Westerlies and atmospheric CO(2) during the Holocene, *Geology, 38*(8), 727-730, doi: 10.1130/G30962.1.
Moy, C. M., G. O. Seltzer, D. T. Rodbell, and D. M. Anderson (2002), Variability of El Niño/Southern Oscillation activity at millennial timescales during the Holocene epoch, *Nature, 420*(6912), 162-165, doi: 10.1038/nature01194.
Mulitza, S., et al. (2010), Increase in African dust flux at the onset of commercial agriculture in the Sahel region, *Nature, 466*(7303), 226-228, doi: 10.1038/Nature09213.
Palma, E. D., R. P. Matano, and A. R. Piola (2008), A numerical study of the Southwestern Atlantic Shelf circulation: Stratified ocean response to local and offshore forcing, *J. Geophys. Res. - Oceans, 113*, C11010, doi: 10.1029/2007jc004720.
Peterson, R. G., and L. Stramma (1991), Upper-level circulation in the South Atlantic Ocean, *Prog. Oceanogr., 26*(1), 1-73, doi: 10.1016/0079-6611(91)90006-8.
Piola, A. R., O. O. Möller, R. A. Guerrero, and E. J. D. Campos (2008), Variability of the subtropical shelf front off eastern South America: Winter 2003 and summer 2004, *Cont. Shelf Res., 28*(13), 1639-1648, doi: 10.1016/j.csr.2008.03.013.
Piola, A. R., E. J. D. Campos, O. O. Möller, M. Charo, and C. Martinez (2000), Subtropical Shelf Front off eastern South America, *J. Geophys. Res. - Oceans, 105*(C3), 6565-6578
Piola, A. R., R. P. Matano, E. D. Palma, O. O. Möller, and E. J. D. Campos (2005), The influence of the Plata River discharge on the western South Atlantic shelf, *Geophys. Res. Lett., 32*(1), 4, doi: 10.1029/2004gl021638.
Reimer, P. J., et al. (2009), Intcal09 and Marine09 Radiocarbon Age Calibration Curves, 0-50,000 Years Cal Bp, *Radiocarbon, 51*(4), 1111-1150.
Sato, K., C. C. G. Tassinari, K. Kawashita, and L. Petronilho (1995), O Método Geocronológico Sm-Nd No IGc-USP e Suas Aplicações, *An. Acad. Bras. Ciênc., 67*(3), 313-336

Schrag, D. P., J. F. Adkins, K. McIntyre, J. L. Alexander, D. A. Hodell, C. D. Charles, and J. F. McManus (2002), The oxygen isotopic composition of seawater during the Last Glacial Maximum, *Quat. Sci. Rev., 21*(1-3), 331-342

Sijp, W. P., and M. H. England (2008), The effect of a northward shift in the southern hemisphere westerlies on the global ocean, *Prog. Oceanogr., 79*(1), 1-19, doi: 10.1016/j.pocean.2008.07.002.

Stramma, L., and M. England (1999), On the water masses and mean circulation of the South Atlantic Ocean, *J. Geophys. Res. - Oceans, 104*(C9), 20863-20883

Stuiver, M., and P. J. Reimer (1993), Extended 14C Data-Base and Revised Calib 3.0 14C Age Calibration Program, *Radiocarbon, 35*(1), 215-230.

Suess, H. E. (1955), Radiocarbon concentration in modern wood, *Science, 122*(3166), 415-417, doi: 10.1126/science.122.3166.415-a.

Toggweiler, J. R., and J. Russell (2008), Ocean circulation in a warming climate, *Nature, 451*(7176), 286-288, doi: 10.1038/Nature06590.

van Breukelen, M. R., H. B. Vonhof, J. C. Hellstrom, W. C. G. Wester, and D. Kroon (2008), Fossil dripwater in stalagmites reveals Holocene temperature and rainfall variation in Amazonia, *Earth Planet. Sci. Lett., 275*(1-2), 54-60, doi: 10.1016/j.epsl.2008.07.060.

Wang, X. F., A. S. Auler, R. L. Edwards, H. Cheng, E. Ito, Y. J. Wang, X. G. Kong, and M. Solheid (2007), Millennial-scale precipitation changes in southern Brazil over the past 90,000 years, *Geophys. Res. Lett., 34*(23), doi: 10.1029/2007gl031149.

Wanner, H., O. Solomina, M. Grosjean, S. P. Ritz, and M. Jetel (2011), Structure and origin of Holocene cold events, *Quat. Sci. Rev., 30*(21-22), 3109-3123, doi: 10.1016/j.quascirev.2011.07.010.

White, W. B., and R. G. Peterson (1996), An Antarctic circumpolar wave in surface pressure, wind, temperature and sea-ice extent, *Nature, 380*(6576), 699-702, doi: 10.1038/380699a0.

Supplementary information

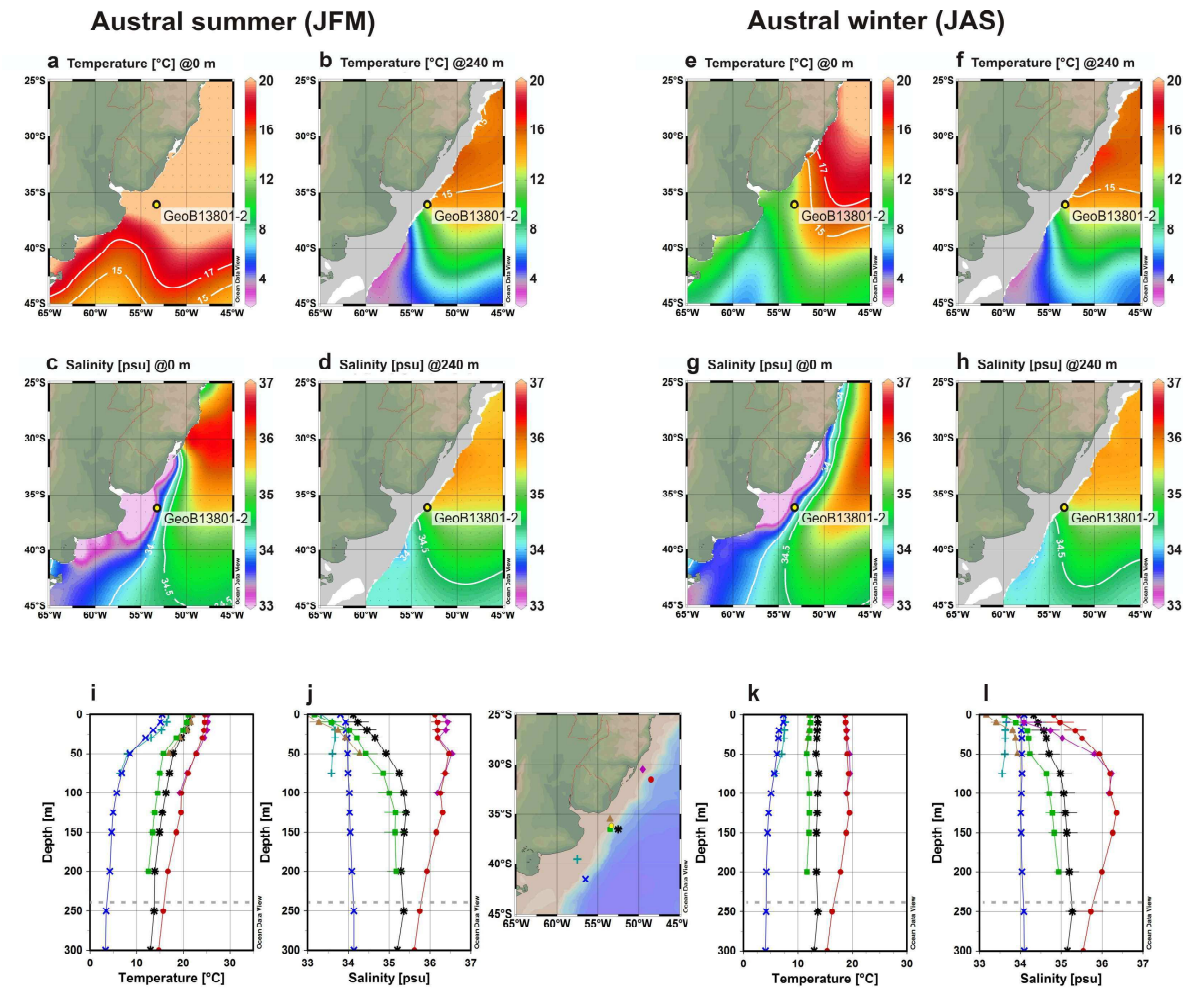

SI Fig. 1: Isosurface maps of temperature [*Locarnini et al.*, 2010] and salinity [*Antonov et al.*, 2010] at the surface (0 m water depth) and 240 m water depth (water depth of sediment core GeoB13801-2) during austral summer (January – March) (a – d) and austral winter (July – September) (e – h); as well as individual temperature and salinity profiles (i – j: austral summer; k – l: austral winter) of selected stations representing characteristics of the different shelf / upper slope water masses. *Blue* and *cyan*: Subantarctic Shelf Water / Malvinas Current; *red* and *magenta*: Subtropical Shelf Water / Brazil Current; *brown*: Plata Plume Water; *black* and *green*: mixture of Subantarctic and Subtropical Shelf Water within the Subtropical Shelf Front. The grey dashed line in i – l demarks the modern water depth at the location of GeoB13801-2. Note that the temperature and salinity patterns in the sub-surface waters (below ca. 100 m water depth) are stable throughout the year.

Interpretation of GeoB13801-2 stable isotopes record

Oxygen isotopes record

Oxygen isotopic composition ($\delta^{18}O$, wherein δ refers to the sample $^{18}O/^{16}O$ ratio compared to a given standard) of foraminiferal calcite is principally determined by isotopic composition of the sea water and water temperature during shell calcification [e.g., *Emiliani*, 1955; *McCrea*, 1950; *Rohling and Cooke*, 2003; *Shackleton*, 1967; *Shackleton and Opdyke*, 1973]. Consequently, the $\delta^{18}O$ of benthic foraminifer tests is a widely used proxy for bottom water temperature [e.g. , *Arz et al.*, 1999; *Chiessi et al.*, 2008; *Duplessy et al.*, 2005; *Malone et al.*, 2004; *Thornalley et al.*, 2010; *Waelbroeck et al.*, 2002].

On millennial time-scales $\delta^{18}O$ of the sea water is globally influenced by the waxing and waning of the large polar ice sheets. Through applying the correction equation proposed by *Schrag et al.* [2002] based on the sea-level data of *Lambeck and Chapell* [2001], the GeoB13801-2 benthic *C. mckannai* $\delta^{18}O_{ivc}$ record acknowledges this ice-volume/sea-level effect on the isotopic composition of ambient sea-water. Moreover, fresh water input, precipitation and evaporation effects alter water mass specific $\delta^{18}O$ composition significantly [e.g., *Rohling and Cooke*, 2003]. Due to its tropical origin STSW should consequently have a much heavier oxygen isotopic signature than SASW. In contrast, the temperature dependent $\delta^{18}O$ fractionation during shell calcification acts in the opposite direction (presence of relatively warm STSW would lead to lighter $\delta^{18}O$ foraminiferal values). Thus, for the interpretation of GeoB13801-2 *C. mckannai* $\delta^{18}O_{ivc}$ record it is of eminent importance to determine in which direction the two shelf water masses influence the $\delta^{18}O$ calcite signal.

For this reason we calculated the predicted $\delta^{18}O$ of calcite ($\delta^{18}O_{pc}$) at four different stations along the western South Atlantic ocean margin by solving the paleotemperture equation of *Shackleton* [1974] (SI Fig. 2). $\delta^{18}O$ of sea water ($\delta^{18}O_{sw}$) profiles for those four stations were extracted from the global gridded data set of *LeGrande and Schmidt* [2006]. The stations respective annual temperature profiles were taken from the World Ocean Atlas [*Locarnini et al.*, 2010]. Though the paleotemparture equation of *Shackleton* [1974] is based on a different benthic foraminifera genus (uvigerinids), we prefer to use this equation unaltered due to the following reasons: 1) to the best of our knowledge there exists no paleotemperature equation for the species we used (*Cibicides mckannai*); 2) to the best of our knowledge no *Cibicides* spp. paleotemperature equation exists for the western South Atlantic; 3) though *Fontanier et al.* [2006] proposed a +0.5‰ correction factor between *U. peregrina* and *Cibicidoides pachydermus*, we did not felt comfortable with employing this correction, since a) the same study also showed significant intrageneric variability and b) this correction factor has been established from the Bay of Biscay,

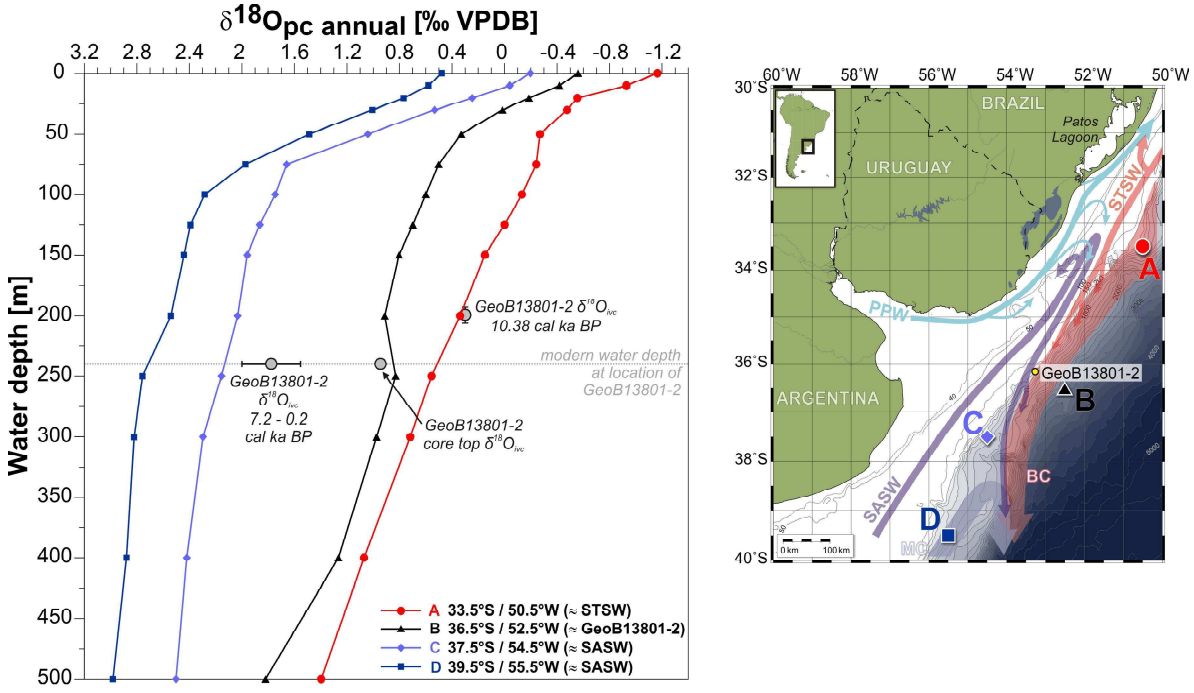

SI Fig. 2: Predicted $\delta^{18}O$ of calcite based on annual temperature profiles ($\delta^{18}O_{pc\ annual}$) from the western South Atlantic compared to $\delta^{18}O_{ivc}$ values from GeoB13801-2 (*gray* dots). Note that the $\delta^{18}O_{pc\ annual}$ of station A (3° north of GeoB13801-2) at the modern water depth of GeoB13801-2 is much closer to the value of station B (≈ GeoB13801-2), than station C, which is only 1° south of GeoB13801-2.

which in many respects is a very different oceanographic setting compared to the western South Atlantic. Moreover, we find that at the station B (≈ GeoB13801-2 location) at the modern water depth of GeoB13801-2, the $\delta^{18}O_{pc}$ annual value of approx. 0.87‰ fits well with the top most value in the GeoB13801-2 *C. mckannai* $\delta^{18}O_{ivc}$ record of approx. 0.95‰ (SI Fig. 2 and manuscript Fig. 8.5a). The calculated $\delta^{18}O_{pc}$ annual profiles also show that the station A, under the influence of STSW, is up to 2.3‰ lighter than those under the influence of SASW (stations C and D; SI Fig. 2). Consequently we interpret the GeoB13801-2 benthic *C. mckannai* $\delta^{18}O_{ivc}$ record in the way that lighter values correspond to an increased influence of STSW and heavier values indicating a relative shift towards stronger SASW influence.

Carbon isotopes record

The interpretation of the stable carbon isotopic ratio ($\delta^{13}C$) as paleoceanographic proxy is more challenging, since a number of factors have influence on the carbon isotopic composition of the ambient sea water (photosynthesis – respiration effects, isotopic fractionation during air-sea exchange, remineralization effects in deeper-waters) and its imprint in benthic foraminifer carbonate tests (species-specific metabolic effects and microhabitat - porewater gradient effects) [e.g., *Belanger et al.*, 1981; *Grossman*, 1987; *McCorkle et al.*, 1990; *Woodruff et al.*, 1980; see also review by *Rohling and Cooke*, 2003]. $\delta^{13}C$ ratios of benthic foraminifera have, nevertheless, been widely used in paleoceanography as a proxy for paleoproductivity and deep-ocean water-mass configuration [e.g., *Bickert and Mackensen*, 2004; *Curry and Oppo*, 2005; *Curry et al.*, 1988; *Duplessy et al.*, 1984; *Mackensen et al.*, 2001; *Zahn et al.*, 1986].

The benthic foraminifera genus *Cibicides* in general, as well as the epifaunal suspension feeder *Cibicides mckannai* in particular, have been shown to secret calcite reliably close to the $\delta^{13}C$ signature of the ambient sea water dissolved inorganic carbon ($\delta^{13}C_{DIC}$) [*Belanger et al.*, 1981; *Graham et al.*, 1981; *Hill et al.*, 2003; *Woodruff et al.*, 1980; *Zahn et al.*, 1986]. However, it has

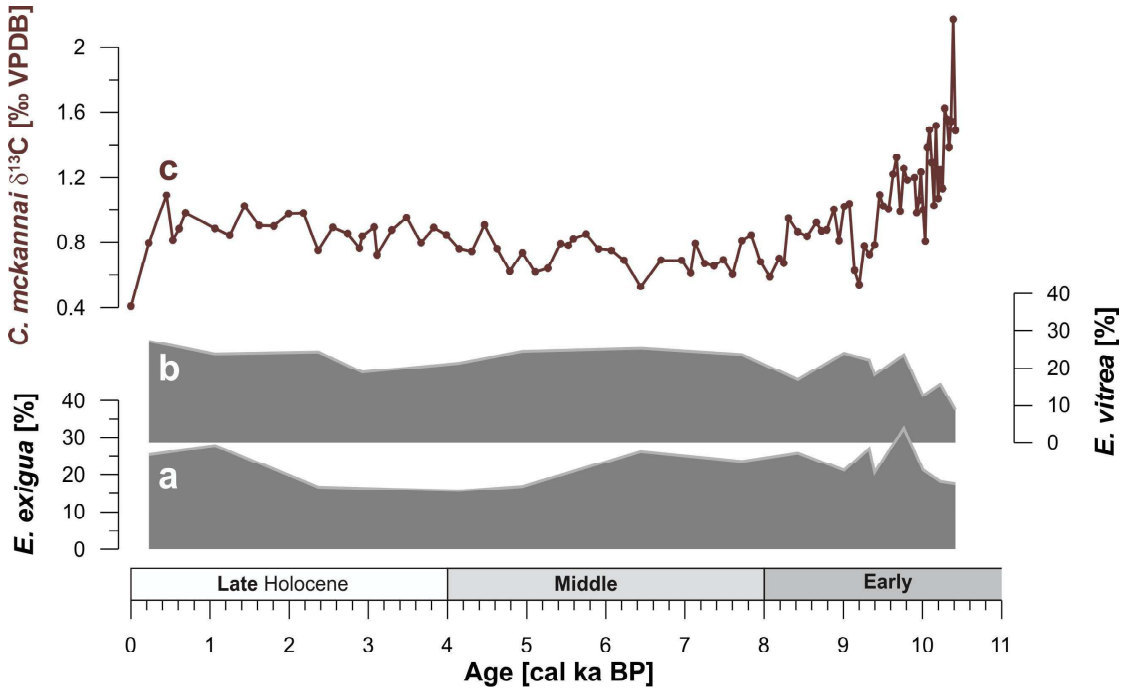

SI Fig. 3: Abundance of *Epistominella exigua* (a) and *Epistominella vitrea* (b; both given in percentage of total assemblage), as well as the $\delta^{13}C$ of *Cibicides mckannai* shells obtained from GeoB13801-2.

been shown that the $\delta^{13}C$ of epibenthic *Cibicides* might be significantly depleted in ^{13}C beneath high productivity areas. This effect is due to the formation of phytodetritus layers at the seafloor and subsequent microbial respiration of the organic matter therein, and frequently referred to as the *phytodetritus* or *Mackensen effect* [*Mackensen et al.*, 1993]. Though the benthic foraminifer assemblage of GeoB13801-2 points towards significant influence of seasonally high phytodetritus input by the frequent occurrence of *E. exigua* this signal is remarkably constant throughout the record (SI Fig. 3). We therefore consider potential internal variations due to the *Mackensen effect* as negligible, and interpret the GeoB13801-2 *C. mckannai* $\delta^{13}C$ record as a relative export productivity proxy, with low isotopic ratios indicating increased surface water export productivity, and vice versa (e.g. *Wefer et al.*, 1999).

References

Antonov, J. I., D. Seidov, T. P. Boyer, R. A. Locarnini, A. V. Mishonov, H. E. Garcia, O. K. Baranova, M. M. Zweng, and D. R. Johnson (2010), *World Ocean Atlas 2009, Volume 2: Salinity*, 184 pp., U.S. Government Printing Office, Washington, D.C.

Arz, H. W., J. Pätzold, and G. Wefer (1999), The deglacial history of the western tropical Atlantic as inferred from high resolution stable isotope records off northeastern Brazil, *Earth Planet. Sci. Lett., 167*(1-2), 105-117

Belanger, P. E., W. B. Curry, and R. K. Matthews (1981), Core-Top Evaluation of Benthic Foraminiferal Isotopic-Ratios for Paleo-Oceanographic Interpretations, *Palaeogeogr. Palaeoclimat. Palaeoecol., 33*(1-3), 205-220, doi: 10.1016/0031-0182(81)90039-0.

Bickert, T., and A. Mackensen (2004), Last glacial to Holocene changes in South Atlantic deep water circulation, in *The South Atlantic in the Late Quaternary*, edited by G. Wefer, S. Mulitza and V. Ratmeyer, pp. 599-620, Springer, Berlin.

Chiessi, C. M., S. Mulitza, A. Paul, J. Pätzold, J. Groeneveld, and G. Wefer (2008), South Atlantic interocean exchange as the trigger for the Bølling warm event, *Geology, 36*(12), 919-922, doi: 10.1130/g24979a.1.

Curry, W. B., and D. W. Oppo (2005), Glacial water mass geometry and the distribution of $\delta^{13}C$ of ΣCO_2 in the western Atlantic Ocean, *Paleoceanography, 20*(1), Pa1017, doi: 10.1029/2004pa001021.

Curry, W. B., J. C. Duplessy, L. D. Labeyrie, and N. J. Shackleton (1988), Changes in the distribution of $\delta^{13}C$ of deep water ΣCO_2 between the last glaciation and the Holocene, *Paleoceanography, 3*(3), 317-341, doi: 10.1029/PA003i003p00317.

Duplessy, J. C., N. J. Shackleton, R. K. Matthews, W. Prell, W. F. Ruddiman, M. Caralp, and C. H. Hendy (1984), ^{13}C record of benthic foraminifera in the last interglacial ocean - Implications for the carbon-cycle and the global deep-water circulation, *Quat. Res., 21*(2), 225-243, doi: 10.1016/0033-5894(84)90099-1.

Duplessy, J. C., E. Cortijo, E. Ivanova, T. Khusid, L. Labeyrie, M. Levitan, I. Murdmaa, and M. Paterne (2005), Paleoceanography of the Barents Sea during the Holocene, *Paleoceanography, 20*(4), Pa4004, doi: 10.1029/2004pa001116.

Emiliani, C. (1955), Pleistocene temperatures, *Journal of Geology, 63*(6), 538-578

Fontanier, C., A. Mackensen, F. J. Jorissen, P. Anschutz, L. Licari, and C. Griveaud (2006), Stable oxygen and carbon isotopes of live benthic foraminifera from the Bay of Biscay: Microhabitat impact and seasonal variability, *Mar. Micropaleontol., 58*(3), 159-183, doi: 10.1016/j.marmicro.2005.09.004.

Graham, D. W., B. H. Corliss, M. L. Bender, and L. D. Keigwin (1981), Carbon and oxygen isotopic disequilibria of recent deep-sea benthic foraminifera, *Mar. Micropaleontol., 6*(5-6), 483-497, doi: 10.1016/0377-8398(81)90018-9.

Grossman, E. L. (1987), Stable isotopes in modern benthic foraminifera - A study of vital effect, *J. Foraminifer. Res., 17*(1), 48-61.

Hill, T. M., J. P. Kennett, and H. J. Spero (2003), Foraminifera as indicators of methane-rich environments: A study of modern methane seeps in Santa Barbara Channel, California, *Mar. Micropaleontol., 49*(1-2), 123-138, doi: 10.1016/S0377-8398(03)00032-X.

Lambeck, K., and J. Chappell (2001), Sea level change through the last glacial cycle, *Science, 292*(5517), 679-686, doi: 10.1126/science.1059549.

LeGrande, A. N., and G. A. Schmidt (2006), Global gridded data set of the oxygen isotopic composition in seawater, *Geophys. Res. Lett., 33*(12), L12604, doi: 10.1029/2006gl026011.

Locarnini, R. A., A. V. Mishonov, J. I. Antonov, T. P. Boyer, H. E. Garcia, O. K. Baranova, M. M. Zweng, and D. R. Johnson (2010), *World Ocean Atlas 2009, Volume 1: Temperature*, 184 pp., U.S. Government Printing Office, Washington, D.C.

Mackensen, A., M. Rudolph, and G. Kuhn (2001), Late Pleistocene deep-water circulation in the subantarctic eastern Atlantic, *Global Planet. Change, 30*(3-4), 197-229, doi: 10.1016/S0921-8181(01)00102-3.

Mackensen, A., H. W. Hubberten, T. Bickert, G. Fischer, and D. K. Futterer (1993), The $\delta^{13}C$ in benthic foraminiferal tests of *Fontbotia wuellerstorfi* (Schwager) relative to the $\delta^{13}C$ of dissolved inorganic carbon in Southern-Ocean deep-water - Implications for glacial ocean circulation models, *Paleoceanography, 8*(5), 587-610, doi: 10.1029/93PA01291.

Malone, M. J., J. B. Martin, J. Schönfeld, U. S. Ninnemann, D. Nürnburg, and T. S. White (2004), The oxygen isotopic composition and temperature of Southern Ocean bottom waters during the last glacial maximum, *Earth Planet. Sci. Lett., 222*(1), 275-283, doi: 10.1016/j.epsl.2004.02.027.

McCorkle, D. C., L. D. Keigwin, B. H. Corliss, and S. R. Emerson (1990), The influence of of microhabitats on the carbon isotopic composition of deep-sea benthic foraminifera, *Paleoceanography, 5*(2), 161-185, doi: 10.1029/PA005i002p00161.

McCrea, J. M. (1950), On the isotopic chemistry of carbonates and a paleotemperature scale, *J Chem Phys, 18*(6), 849-857, doi: 10.1063/1.1747785

Rohling, E., and S. Cooke (2003), Stable oxygen and carbon isotopes in foraminiferal carbonate shells, in *Modern Foraminifera*, edited by B. Sen Gupta, pp. 239-258, Springer Netherlands.

Schrag, D. P., J. F. Adkins, K. McIntyre, J. L. Alexander, D. A. Hodell, C. D. Charles, and J. F. McManus (2002), The oxygen isotopic composition of seawater during the Last Glacial Maximum, *Quat. Sci. Rev., 21*(1-3), 331-342, doi: 10.1016/S0277-3791(01)00110-X.

Shackleton, N. J. (1967), Oxygen isotope analyses and pleistocene temperatures re-assessed, *Nature, 215*(5096), 15, doi: 10.1038/215015a0.

Shackleton, N. J. (1974), Attainment of isotopic equilibrium between ocean water and the benthonic foraminifera genus *Uvigerina*:

Isotopic changes in the ocean during the last glacial, *Colloque International du CNRS*, 219, 203–209

Shackleton, N. J., and N. D. Opdyke (1973), Oxygen isotope and palaeomagnetic stratigraphy of equatorial Pacific core V28-238: Oxygen isotope temperatures and ice volumes on a 105 year and 106 year scale, *Quat. Res., 3*(1), 39-55, doi: 10.1016/0033-5894(73)90052-5.

Thornalley, D. J. R., H. Elderfield, and I. N. McCave (2010), Intermediate and deep water paleoceanography of the northern North Atlantic over the past 21,000 years, *Paleoceanography, 25*, Pa1211, doi: 10.1029/2009pa001833.

Waelbroeck, C., L. Labeyrie, E. Michel, J. C. Duplessy, J. F. McManus, K. Lambeck, E. Balbon, and M. Labracherie (2002), Sea-level and deep water temperature changes derived from benthic foraminifera isotopic records, *Quat. Sci. Rev., 21*(1–3), 295-305, doi: 10.1016/s0277-3791(01)00101-9.

Wefer, G., W. H. Berger, J. Bijma, and G. Fischer (1999), Clues to ocean history: A brief overview of proxies, in *Use of Proxies in Paleoceanography: Examples from the South Atlantic*, edited by G. Fischer and G. Wefer, pp. 1-68, Springer-Verlag, Berlin Heidelberg.

Woodruff, F., S. M. Savin, and R. G. Douglas (1980), Biological fractionation of oxygen and carbon isotopes by recent benthic foraminifera, *Mar. Micropaleontol., 5*(1), 3-11, doi: 10.1016/0377-8398(80)90003-1.

Zahn, R., K. Winn, and M. Sarnthein (1986), Benthic foraminiferal $\delta^{13}C$ and accumulation rates of organic carbon: *Uvigerina peregrina* group and *Cibicidoides wuellerstorfi*, *Paleoceanography, 1*(1), 27-42, doi: 10.1029/PA001i001p00027.

9. Conclusions and future perspectives

In the literature palaeoceanographic and sedimentary systems are commonly studied separately. Moreover, slope records are frequently used for palaeoceanographic reconstructions without acknowledging the interaction of sedimentary and oceanographic process affecting those records. Only the combined use of proxy methods from both fields of science, allows for an integrated understanding of the full richness of processes influencing shelf and slope deposits. Towards such an integrated understanding this thesis combined sedimentologic and palaeoceanographic slope records for the reconstruction of shelf dynamics and sediment export, as well as their effect on slope sedimentary patterns.

Chapters 4 and 5 (co-authored papers) show in detail the late Pleistocene to Holocene sedimentary evolution of the NW Iberian shelf system as well as the late Holocene spatio-temporal evolution of fine-grained depocentres. In chapter 4 it has been shown that large amounts of fine sands were deposited on the NW Iberian shelf during the last sea-level rise and that the modern sea-level highstand is characterized by the deposition of muddy sediments on the mid-shelf. Chapter 5 reveals the time-transgressive late Holocene evolution of those muddy deposits, and elucidates that fluvial input of fine grained sediments onto the shelf and subsequent mud-depocentre formation only started after the sedimentary (re-)fill of the NW Iberian estuaries during early to middle Holocene sea-level rise. In summary, chapters 4 and 5 built the basis enabling a better understanding of deglacial to Holocene sedimentary patterns found on the NW Iberian slope (chapter 6).

In chapter 6 latest Quaternary sedimentary patterns on the NW Iberian slope are interpreted in a palaeoclimatic context. The detailed knowledge of the shelf sedimentary patterns enabled the differentiation of local shelf export signals from over-regional palaeoceanographic signals. Sediment grain-size compositions evidently reflect palaeoclimatic effects. On the one hand, through variations in the thermohaline circulation and consequently deep - intermediate water mass circulation strength at the slope (e.g. intensification during warm phases like the Bølling/Allerød). On the other hand, through sea-level rise induced massive fine sand reworking on the shelf. Moreover, from this study it emerges that palaeoceanographic changes (initiation of a strong outer shelf current) were necessary to foster fine sand export.

In chapter 7 a second external shelf archive is introduced, an uppermost slope terrace off Southeast South America. The combined findings of this chapter show that the terrace is an effective and direct recorder of shelf sediment export. Throughout the Holocene these sedimentary dynamics are primarily controlled by the deglacial transgression but also show an independent palaeoclimatic component after approx. 7 ka BP. Moreover, the findings of this study point to the capability of the terrace records for high-resolution palaeoclimatic studies due to high sedimentation rates (min. ca. 50 cm/kyr).

In chapter 8, one of the terrace cores is employed for the high-resolution reconstruction of Holocene subtropical shelf front shifts. The latitudinal location of this front, a critical boundary for water mass as well as sediment transport along the Southeast South American shelf, is primarily controlled by Holocene palaeoclimatic variations (northward migration and extension of the Southern Westerlies; middle to late Holocene evolution of the El Niño Southern Oscillation). Moreover, for the most recent 200 years an anthropogenic forcing is suggested.

In summary, this thesis has shown that shelf sedimentary export signals can be recognized as far down-slope as the lower slope, although this requires integrated knowledge of the local shelf-slope sedimentary history. The detailed knowledge of local margin morphology has

further been shown as a crucial component. At the uppermost slope small morphologic steps might act as excellent off-shelf transport archives and slope incisions (e.g. gully or canyon structures) can act as efficient sediment conduits. At the middle to lower slope morphologic highs potentially deflect sediment transporting contour currents, causing deposition on the stoss-side of the obstacle. Finally, two different types of slope records have been proven to be qualified external records of sedimentary and palaeoceanographic shelf dynamics and export archives. At the Southeast South American continental margin an uppermost slope terrace has been shown as reliable and direct archive for shelf dynamics. Off NW Iberia middle to lower sedimentary patterns could in parts be linked with the last deglacial to Holocene history of sediment dynamics on the shelf. The combined use of sedimentologic and palaeoceanographic methods in this thesis emphasizes the potential of this integral approach. Moreover, the central findigs of this study underline the importance of slope records as external archives for shelf sedimentary and oceanographic dynamics as well as for understanding the sedimentary shelf-slope linkage, a topic that surely deserves future scientific interest.

In this context it is worth noting, that massive sand deposits are preserved on the outer NW Iberian shelf, and a series of shelf edge gullies have been detected during the most recent MARUM expedition to the NW Iberian continental margin (Fig. 9.1). Despite the fact, that gullies play an important role in the evolution of continental margins over long time periods (Field et al. 1999), these interesting features are generally only starting to receive the befitting scientific interest. Contrasting larger commonly erosive canyon-head regions, gullies frequently show small terraces often trapping sediments, a feature we also observed in the NW Iberian gullies. Those sediments (likewise the records from the Uruguayan uppermost slope terrace) can be used for high temporal resolution climatic reconstructions (e.g. Mulitza et al. 2010). Thus, besides their potential role for shelf sediment export, further key scientific questions in studying these interesting gully structures could be:

- How do shelf edge gullies form and what is necessary to nourish them?
- Does their formation process differ depending on the climate zone (key study areas: Mauretania (sub-tropical; strong chemical weathering onshore); NW Iberia (temperate; non-glaciated coast); Barents sea (sub-polar; glaciated coast)?
- Do gullies have phases of preferential activity, like it is known from larger canyon systems?

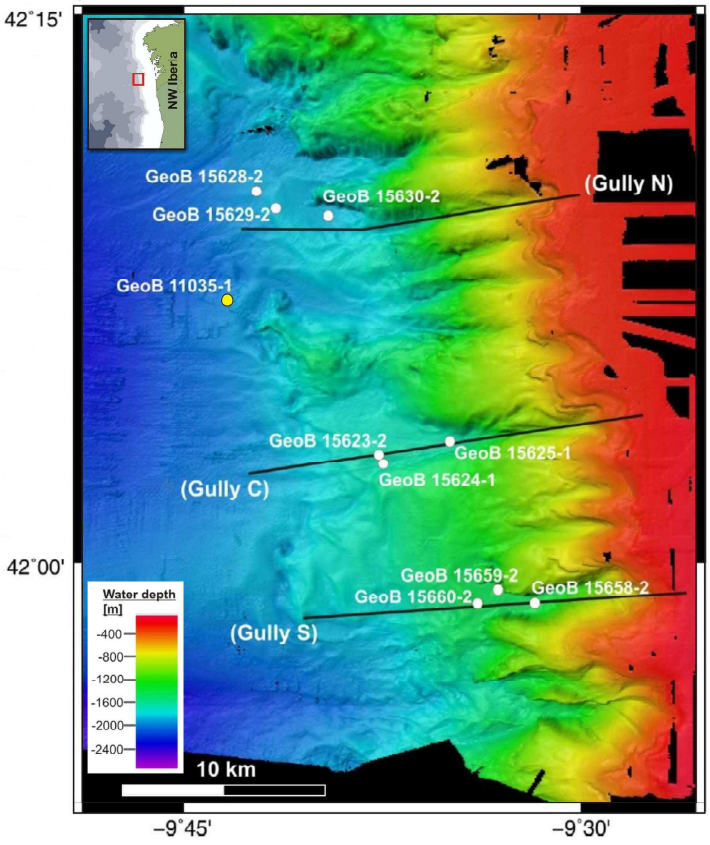

Fig. 9.1: Close-up of the multi-beam bathymetry recorded during *R/V Meteor* expedition M84/4 (May 2011) off NW Iberia showing a series of shelf edge gullies, of which the larger ones have been sampled by gravity coring (white dots). Also shown: location of GeoB11035-1 (yellow dot; Bender et al. 2012).

- Are they directly connected to shelf export routes?
- How do gullies interact with oceanographic elements, such as slope currents, water mass boundaries, internal waves, and sea level variations?

Finally, two further data sets comprising scientifically interesting palaeoclimatic implications exist from sediment core GeoB13801-2 (uppermost slope terrace off Uruguay). In March 2012 the core has been scanned in 1 cm resolution (ca. 20 years/ cm!) for elemental concentrations (XRF core scanner). Correlation of this record with equivalent very high-resolution data (1 mm scanning resolution) from the Uruguayan middle shelf mud-belt indicates a direct genetic linkage of the two depocentres, and a strong connection to the middle to late Holocene evolution of El Niño Southern Oscillation frequency over Southeast South America. The publication of these results in a co-author manuscript (PI on the mud-belt data: Till Hanebuth) is intended. Additionally, over the past 1.5 years I created a well detailed data set of benthic foraminifera assemblages from the same core (GeoB13801-2). Preliminary interpretation of these results indicate interesting implications for the palaeoenvironmental use (e.g., sea-level influence, Plata plume water influence) of benthic foraminifera assemblages at the uppermost slope offshore the La Plata estuary (s. Appendix). Though, the interpretation of this data set needs some further processing, I see a substantial scientific value for the benthic foraminifera community, and plan to promote publication of this dataset.

References

Bender VB, Hanebuth TJJ, Mena A, Baumann K-H, Francés G, von Dobeneck T (2012) Control of sediment supply, palaeoceanography and morphology on late Quaternary sediment dynamics at the Galician continental slope. Geo-Marine Letters 32:313-335. doi:10.1007/s00367-012-0282-2

Field ME, Gardner JV, Prior DB (1999) Geometry and significance of stacked gullies on the northern California slope. Mar Geol 154:271-286

Mulitza S, Heslop D, Pittauerova D, Fischer HW, Meyer I, Stuut JB, Zabel M, Mollenhauer G, Collins JA, Kuhnert H, Schulz M (2010) Increase in African dust flux at the onset of commercial agriculture in the Sahel region. Nature 466:226-228. doi:10.1038/Nature09213

Appendix: Results of benthic foraminifera assemblage analysis from core GeoB13801-2: Palaeoceanographic implications from benthic foraminifera assemblages in a high shelf sediment export region?

The strongly increased use of benthic foraminiferal tests in geochemical proxy methods (e.g., stable isotopes, Mg/Ca, Sr/Ca) significantly fostered benthic foraminiferal ecology studies (e.g., Gooday 1988; Jorissen et al. 1992; Alve and Bernhard 1995; Ernst and van der Zwaan 2004). Those ecological studies led to the cognition, that the faunal composition of benthic foraminifer communities is controlled by a limited number of environmental parameters. At small spatial scale the most important environmental parameters controlling the depth at which species live in the sediment (their microhabitats), are quality and quantity of organic flux (≈food) as well as pore-water oxygen profiles (e.g., review by Gooday 2003). As a consequence, benthic foraminiferal assemblages have become a widely used tool in the construction of benthic ecosystem oxygenation, surface export productivity and deep-sea water mass characteristics (e.g., Gupta 1997; Baas et al. 1998; Martins et al. 2007; Zarriess and Mackensen 2010).

Material and Methods

GeoB13801-2 (36°08'29''S; 53°17'10''W) was retrieved during expedition M78/3a with German *R/V Meteor* in May/ June 2009 from 241 m water depth at the uppermost slope off Uruguay (cf. Fig. 7.1). The age model of core GeoB13801-2 is explained in detail in chapter seven.

Benthic foraminifera assemblage investigation was done on the >63 µm fraction. Though time consuming, it has been shown that small-size fractions (125/ 150 to 63 µm) may contain highly informative species which otherwise are completely overlooked (Schröder et al. 1987; e.g. Duchemin et al. 2007). Further, opportunistic phytodetritus-exploiting species, as they might be expected in front of a large fluvial system like the La Plata river, frequently have small tests only adequately represented by using the >63 µm fraction (Gooday 1988; Gooday 1993; Smart et al. 1994). After separation of the mud fraction (<63 µm) by wet sieving, samples for benthic foraminifera assemblage investigation were split with a micro-splitter depending on sample size between 8-10 times. This has been done in order to obtain a representative split containing a minimum of 300 benthic foraminifera specimens for assemblage counting. Generic assignments follow those of Löblich and Tappan (1988), the Catalogue of Foraminifera (Ellis and Messina 1940) and to a minor degree Boltovskoy et al. (1980).

Four benthic indices were calculated from the complete benthic foraminifera faunal data set:

The Benthic Foraminifera High Productivity index (BFHP), originally described by Martins et al. (2007), is computed through the quantification of specimens of species related to high and sustained flux of metabolizable organic matter, such as *Bolivina* spp. and *Bulimina* spp. amongst others. We modified the procedure of Martins et al. (2007) by also including taxa related to high phytodetritus input, such as *Epistominella exigua* (refer to the end of this chapter for a complete list of used taxa).

The Benthic Foraminifera Oxygen Index (BFOI) reflects alterations in dissolved oxygen concentration at the sediment/ water interface based on an empirical relation between oxic (O) and dysoxic (D) indicator species; BFOI = (O/(O+D))x100 (Kaiho 1994) (refer to the end of this chapter for list of used taxa).

Two further ecological indices were calculated; benthic foraminifera diversity was evaluated by calculating the Shannon-Wiener index H('S) = $\sum$ pi • lnpi, wherein pi is the proportion of each species in the respective sample S; and infaunal/epifaunal ratio was calculated to describe the dominating microhabitat preferences of each sample (refer to the end of this chapter for list of used taxa and respective microhabitual preferences).

Multivariate statistical analyses were performed using the Multivariate Statistical Package (MVSP) Version 3.2 of Kovach Computing Services (Kovach 2010).

Hierarchical R-mode and Q-mode cluster analyses were carried out using the Morisita-Horn quantitative similarity coefficient and the Unweighted Pair-Group Method Using Arithmetic Averages (UPGMA) for clustering. Prior to statistical analyses rare species occurring at percentages less than 2% in all samples as well as fragmented specimens were removed from the faunal data set to reduce noise. Further, to obtain a more normal distribution the remaining total faunal data set of 21 species was transformed using the log10(x+1) transformation.

Results

Benthic foraminifera assemblage investigation of core GeoB13801-2 resulted in the identification of 94 benthic foraminifera species. Of those 94 species, 73 species occur only rarely with less than 2 % in all samples, and three species are clearly dominating the assemblage in all samples; *Epistominella exigua*, *Epistominella vitrea* and *Cibicides mckannai*.

R-mode cluster analysis of the 21 most abundant species revealed five main assemblages, which were denominated after the respective governing species: *E. vitrea* (A1), *B. pseudoaffinis*

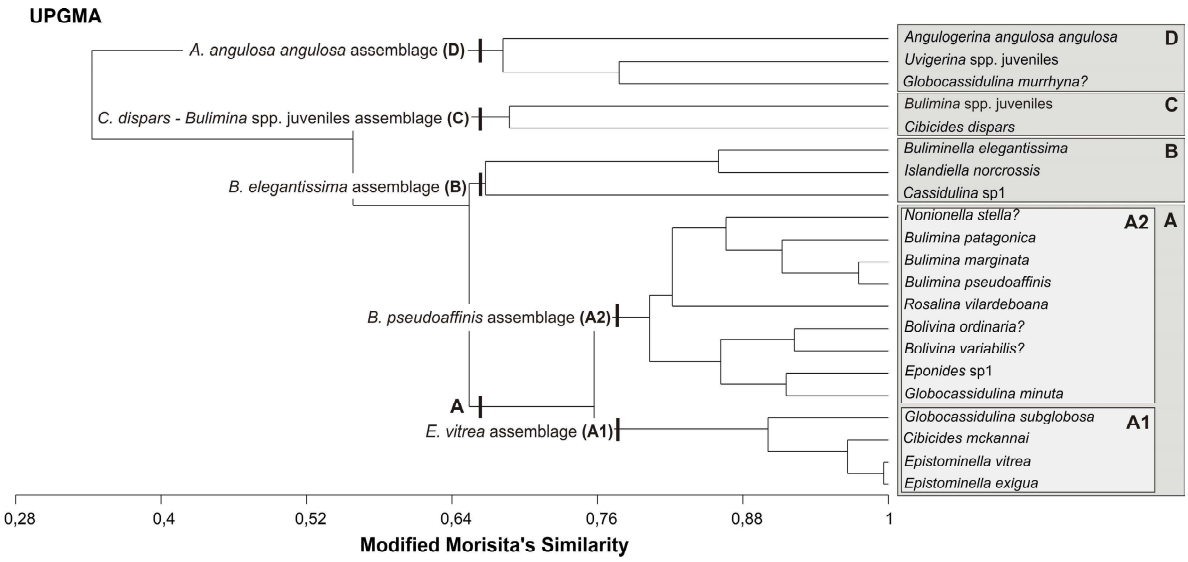

Fig. A.1: Dendrogram of R-mode clustering on the 21 most abundant species, by means of the Morisita-Horn quantitative similarity coefficient and the unweighted pair-group method using arithmetic averages (UPGMA) for clustering.

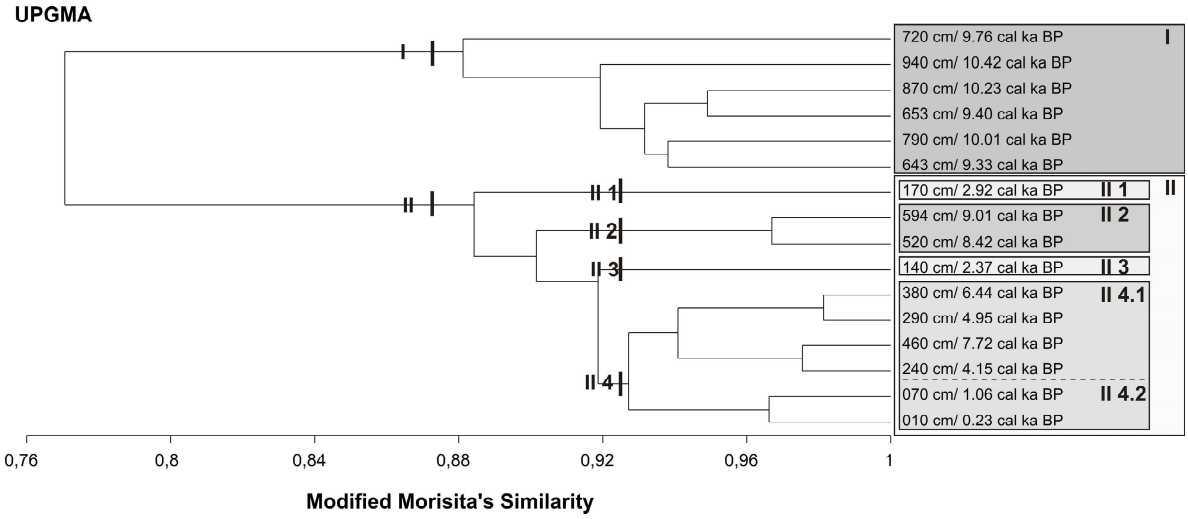

Fig. A.2: Dendrogram resulting from the Q-mode clustering of the most abundant species on samples, using the same analysis set-up as for R-mode cluster analysis (cf. Fig. A.1).

(A2), *B. elegantissima* (B), *C. dispars – Bulimina* spp. juveniles (C), and *A. angulosa angulosa* (D) assemblage (Fig. A.1). Clustering according to samples (Q-mode) gave two main groups (Benthic Foraminifera Assemblage Zones – BFAZ I and II), wherein BFAZ II further splits in four sub-groups (BFAZ II 1 – II 4; Fig. 2) and BFAZ II 1 and II 3 only consist of one sample each (Figs. A.2 and A.3).

The *E. vitrea* (A1) assemblage is composed by *G. subglobosa*, *E. exigua*, *E. vitrea*, and *C. mckannai* (Fig. A.1). Those four species occur in relative high numbers throughout the entire core (note different scaling in Fig. 3 for species of this assemblage). Whereas *E. exigua* and *E. vitrea* generally dominate the total assemblage, *C. mckannai* is slightly reduced in BFAZ I (>9.3 cal ka BP), while *G. subglobosa* occurrence is slightly enhanced within this assemblage zone (Fig. A.3).

The *B. pseudoaffinis* (A2) assemblage is composed by *N. stella?*, *B. patagonica*, *B. marginata*, *B. pseudoaffinis*, *R. vilardeboana*, *B. ordinaria?*, *B. variabilis?*, *Eponides* sp1, and *G. minuta* (Fig. A.1). This assemblage is characterized by main occurrences in BFAZ I, gradual decreases in BFAZ II 2 (9.3 to 8.1 cal ka BP), and subordinate reoccurrences at different time intervals thereafter (Fig. A.3).

The *B. elegantissima* (B) assemblage is composed of *B. elegantissima*, *I. norcrossi* and *Cassidulina* sp1 (Fig. A.1). This assemblage mainly occurs prior to 8,8 cal ka BP, basically correlating with BFAZ I (Fig. A.3).

The *C. dispars* – *Bulimina* spp. juveniles (C) assemblage is composed of only these two species (Fig. A.1). Their main occurrence in the early Holocene section of the core and very low and sporadic re-occurrence in the late Holocene section appear to be their grouping factor (Fig. A.3).

The *A. angulosa angulosa* (D) assemblage is composed of *A. angulosa angulosa*, *Uvigerina* spp. juveniles and *G. murrhyna*? (Fig. A.1). The species of this assemblage gradually increase from the middle Holocene onwards and have their main occurrences in the late Holocene (Figs. A.3). Apart from the dominant species of assemblage A1, this assemblage D characterizes BFAZ II 4.1 and II 4.2 (Fig. A.3).

The strong difference between BFAZ I and II is also apparent from the results of benthic foraminifer faunal indices (Fig. A.4). BFAZ I (prior to 9.3 cal ka BP) is characterized by highest BFHP values,

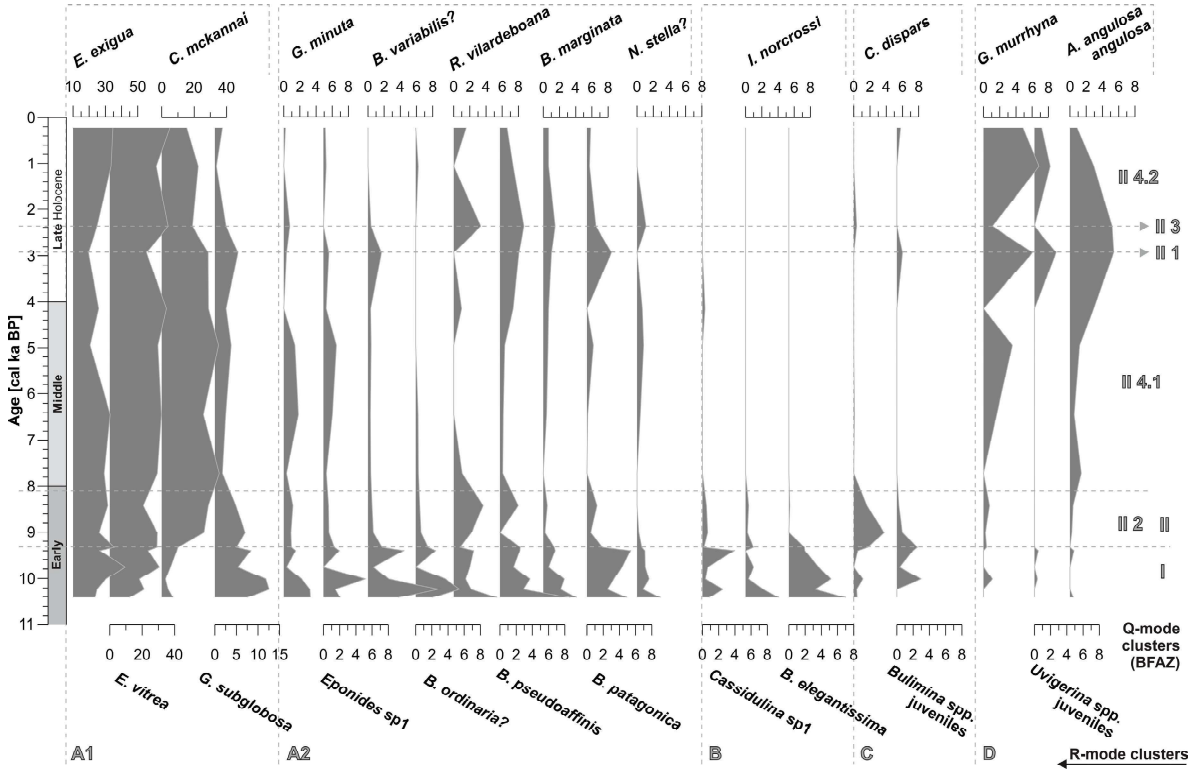

Fig. A.3: The 21 most abundant species grouped according to their R-mode clusters. Dashed grey lines indicate the R-mode as well as Q-mode clustering groups based on Figs. A.1 and A.2.

a high infaunal / epifaunal index, slightly higher diversity and significantly reduced BFOI values (Fig. A.4). At ca. 9.3 cal ka BP BFHP, infaunal / epifaunal index and diversity sharply decrease, while BFOI sharply increases for the rest of the Holocene (BFAZ II; Fig. A.4). The transition between main BFAZ I and II correlates well with the that of principal component analysis (PCA) group I and II of GeoB13801-2 sediment compositional parameters presented in chapter seven (Fig. A.4). From the benthic assemblage analysis a transitional character emerges for BFAZ II 2 (Fig. A.3), moreover this zone roughly correlates with the temporal occurrence of PCA group II (Figs. A.4). BFAZ II 4.1 and II 4.2 principally correlate with PCA group III (Fig. A.4).

Interpretation and discussion

The most drastic changes in the assemblage correlate with the transition from PCA group I to II at ca. 9.3 cal ka BP. PCA group I (prior to 9.3 cal ka BP) is characterized by strong lithologic variability, high bulk and terrigenous clay contents, high terrigenous clay contents, relatively low TOC content, high carbon isotopic ratios and is associated with the fast preceding early Holocene sea-level transgression. Together this indicates relatively low productivity conditions (cf. chapter seven), thus lower food availability for the benthic foraminifer community prior to 9.3 cal ka BP. This interpretation is corroborated by the occurrence of B. elegantissima during this time interval, a species that is known for its occurrence in transitional environments and preferential diet on refractory (low quality) organic matter (Murray 2006; Burone et al. 2011), potentially supplied through sea-level transgressive reworking. In contrast, the BFHP indicates higher surface productivity prior to 9.3 cal ka BP (Fig. A.4). In this context it has to noted that the BFHP index has been established and only been applied on shallow water shelf environments so far (Martins et al. 2007; Nagai et al. 2009). Moreover, the BFHP index is mainly based on infaunal living species (cf. appended lists; Martins et al. 2007). The close correlation

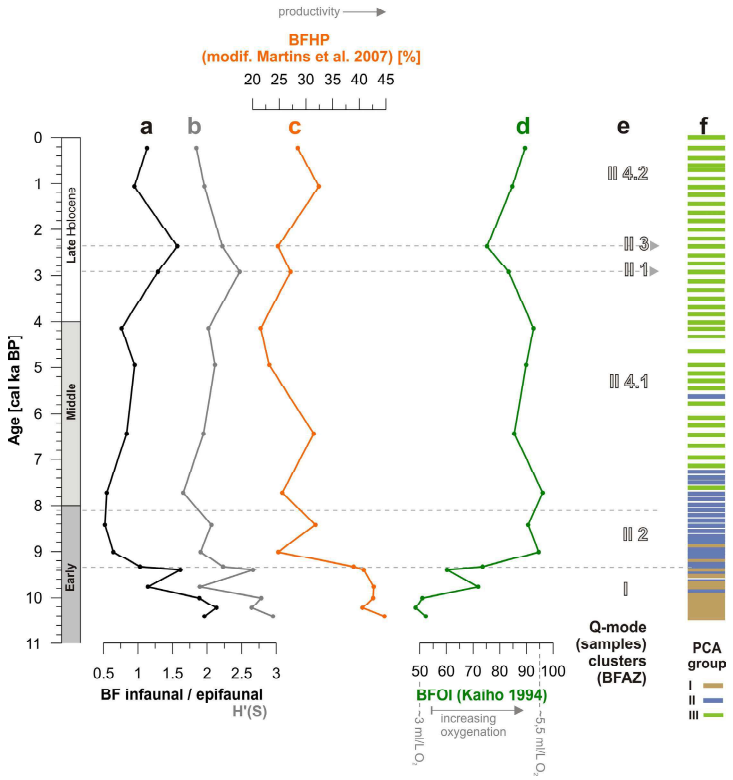

Fig. A.4: GeoB13801-2 (a) Benthic Foraminifera (BF) infaunal / epifaunal ratio, (b) Shannon-Wiener diversity index (H'(S)), (c) Benthic Foraminifera High Productivity Index (BFHP), (d) Benthic Foraminifera Oxygen Index (BFOI), along with (e) Q-mode clusters and (f) temporal occurrence of the three principal component analysis (PCA) groups of GeoB13801-2 sediment compositional data shown in chapter seven (Paleoclimatic forcing of Holocene Subtropical Shelf Front shifts off Southeast South America). Horizontal dashed lines correspond to the Benthic Foraminifera Assemblage Zones (BFAZ) resulting from Q-mode cluster analysis.

of infaunal / epifaunal index and BFHP index (Fig. A.4) indicates that the microhabitual preferences of the species present in core GeoB13801-2 excerpts a strong control on the results of BFHP calculations at this core location. Besides food availability and pore-water oxygen levels, the substratum plays a significant role for benthic foraminifer faunal composition (e.g. most epifaunal species prefer coarse or hard substrates to attach to). A clear change in lithology is observed in core GeoB13801-2 from PCA group I to group II towards higher sand content. This lithologic coarsening might be the reason for a shift towards more epifaunal lifestyle of the benthic foraminifer community at ca. 9.3 cal ka BP and additionally enabled better pore-water ventilation as indicated by increasing BFOI (Fig. A.4). Consequently the BFHP index at this uppermost slope, high siliciclastic sediment input location appears to be of limited use and environmental interpretations should rather be drawn from the individual assemblage composition.

Throughout the Holocene the total assemblage is strongly dominated by the occurrence of *E. exigua* and *E. vitrea*. Both are opportunistic species and especially *E. exigua* is well known for its ability to grow and reproduce rapidly in presence of phytodetritus but still has a large tolerance to varying organic flux (Gooday 1993; Smart et al. 1994; Altenbach et al. 1999). Apparently the surface productivity of phytodetritus pulsed by the near-by Plata plume water had a significant influence on benthic foraminifer community structure throughout the Holocene.

A contradiction to the conclusions drawn from the multi-proxy data set presented in chapter seven arises from the occurrence of *I. norcossi* prior to ca. 8.0 cal ka BP (Fig. A.3). Stable oxygen isotopic ratios indicate the presence of rather warm waters (subtropical shelf water) at the location of GeoB13801-2 for this time interval. However, the *Islandiella* genus is known to prefer rather cold water (<10° C; Murray 2006) and on the SE Brazilian shelf it has been found only under upwelling of relatively cold and fresh South Atlantic Central Water (Burone et al. 2011). There is no sound explanation yet for this apparent contradiction.

Besides the assemblage change at ca. 9.3 cal ka BP, which appears to be linked to lithology and sea-level effects, between ca. 2.5 to 3 cal ka BP abundant occurrence of *A. angulosa angulosa* and reoccurrence of *R. vilardeboana*, *B. pseudoaffinis*, *B. patagonica* and *B. marginata* indicate another slight environmental change. Whereas the ecology and microhabitual preferences of *A. angulosa angulosa*, *R. vilardeboana*, *B. pseudoaffinis* and *B. patagonica* are principally unknown, *B. margianta* is described in the literature a deep-infaunal living opportunist able to respond to high food availability (Jorissen et al. 1992; Murray 2003). Noteworthy this reoccurrence correlates with a lithologic change towards increased silt and clay contents in the late Holocene, which might be associated with the increasing frequency of El Niño events potentially leading to more frequent off-shore advection of the Plata plume water (cf. chapter seven).

Lists of species included in indices calculations

Species used for calculation of BFHP

Bolivina spp. (Sen Gupta and Machain-Castillo 1993; Schmiedl et al. 1997 (based on *B. ex gr. dilatata*); Martins et al. 2007); *Brizalina* spp. (Sen Gupta and Machain-Castillo 1993; Martins et al. 2007); *Bulimina marginata* & *Bulimina aculeate* (Mackensen et al. 1990); *Bulimina* spp. (Martins et al. 2007); *Cassidulina* spp. (based on *C. laevigata*; Corliss and Van Weering 1993; Gooday and Hughes 2002; Gross 2002; Duchemin et al. 2008; Alve 2010) and *C. carinata* (Fontanier et al. 2003; Murray 2003; Duchemin et al. 2008); *Epistominella exigua* (Gooday 1988; Gooday 1993; Gooday 1994; Smart et al. 1994; Schmiedl et al. 1997; Fontanier et al. 2003; Ernst and van der Zwaan 2004; Fontanier et al. 2005; Smart 2008); *Fursenkoina* spp. (Alve 1994; Martins et al. 2007); *Nonionella iridea* (e.g. Gooday 1986; Mackensen et al. 1990; Gooday and Hughes 2002; Gross 2002; Murray 2003; Duchemin et al. 2008; Alve 2010); *Nonionella* spp (Martins et al. 2007); *Uvigerina mediterranea* (Koho et al. 2008); *Uvigerina peregrina* (e.g. De Rijk et al. 1999; Altenbach et al. 2003);.

Species used for calculation of BFOI

Oxic indicators

Cibicides spp. (Jorissen 1987; Kaiho 1994; Altenbach et al. 2003); *Globocassidulina subglobosa* (Lutze and Coulbourn 1984; Kaiho 1994; Schmiedl et al. 1997); *Hanzawaia* spp. (based on H. concentric; Schönfeld 1997; Altenbach et al. 2003); *Pyrgo depressa* (based on *Pyrgo murrhina*; Kaiho 1994; Abu-Zied et al. 2008); *Rosalina* spp. (based on *R. bradyi*; Abu-Zied et al. 2008); *Triloculina* spp. (Kaiho 1994).

Dysoxic indicators

Bulimina pseudoaffinis (unornamented, thin wall; Kaiho 1994), *Bulimina marginata* (Jorissen 1987; Rohling et al. 1993; Alve and Bernhard 1995); *Bolivina* spp. (Kaiho 1994; de Stigter et al. 1998, *B. spathulata*, *B. dilatata*); *Brizalina* spp. (Douglas and Heitman 1979); *Cassidulina* spp. (Sen Gupta and Machain-Castillo 1993); *Fursenkoina* spp. (Douglas and Heitman 1979; Kaiho 1994 (*F. complanata*, *F. rotundata*); Alve and Bernhard 1995 (*Stainforthia fusiformis*)); *Globobulimina* spp. (e.g. Sen Gupta and Machain-Castillo 1993; Kaiho 1994; De Rijk et al. 1999).

Species used for calculation of infaunal / epifaunal ratio

Infaunal species

Amphicoryna spp. (Fontanier et al. 2003 (*A. scalaris*)); *Angulogerina* spp. (Corliss and Chen 1988 (*T. angulosa*; tapered & cylindrical morphotype); de Stigter et al. 1998 (*T. angulosa*)); *Bolivina* spp. (Corliss and Chen 1988 (*Bolivina* cf. *B. robusta*; flattened tapered morphotype); de Stigter et al. 1998 (*B. spathulata*, *B. dilatata*); Murray 2006 (genus)); *Brizalina* spp. (Corliss and Chen 1988 (*B. difformis*; flattened tapered morphytype); Murray 2006 (genus); Bubenshchikova et al. 2008(for *B. subspinescens*, *B. pacifica*));*Buccella* spp. (Murray 2006 (genus); Bubenshchikova et al. 2008); *Bulimina* spp. (Corliss and Chen 1988 (tapered & cylindrical morphotype); Murray 2006 (genus)); *Bulimina marginata* (Corliss and Chen 1988; Fontanier et al. 2002; Murray 2003; Murray 2006); *Bulimina aculeata* (Fontanier et al., 2002; Murray, 2006); *Buliminella elegantissima* (Bubenshchikova et al., 2008 (*B. tenuata*); Murray, 2006); *Cassidulina* spp. (Corliss and Chen 1988 (*C. laevigata*, *C. obtusa*, *C. reniforme*; flattened ovoid morphotype); de Stigter et al. 1998 (*C. laevigata*); Murray 2006 (genus)); *Cassidulinoides* spp. (de Stigter et al. 1998 (*C. bradyi*)); *Elphidium* spp. (Corliss and Chen, 1988 (*Elphidium* spp.; rounded planispiral morphotype); Murray, 2006 (genus)); *Elphidium excavatum*? (Alve and Murray, 1999; Corliss and Chen, 1988; Murray, 2006); *Epistominella vitrea* (Jorissen et al. 1992; Murray 2006); *Fissurina* spp. (Corliss and Chen 1988 (*Fissurina* spp., *F. laevigata*, *F. lucida*, *F. semimarginata*; flattened ovoid morphotype)); *Fursenkoina* spp. (Corliss and Chen 1988 (*F. schreibersiana*; tapered & cylindrical morphotype); Murray 2006 (genus); Bubenshchikova et al. 2008 (for *F. apertura*)); *Globobulimina turgida*? (Corliss 1985 (*G. affinis*); Corliss 1991 (*G. affinis*); Kaiho 1994 (genus); Gooday and Rathburn 1999 (genus); Kaiho 1999 (genus); Murray 2006 (genus); Koho et al. 2011); *Globocassidulina* spp. (Corliss and Chen 1988 (spherical morphotype); Murray 2006 (genus)); *Globocassidulina subglobosa* (Corliss and Chen 1988); *Globulina* spp. (Corliss and Chen 1988 (genus: spherical morphotype enhanced; Živkovic and Babić 2003)); *Islandiella* spp. (Corliss and Chen, 1988 (*I. helenae*/*norcossi*; flattened ovoid morphotype); Murray, 2006 (genus)); *Islandiella norcrossi* (Corliss and Chen 1988; Bubenshchikova et al. 2008); *Lagena* spp. (Haynes 1981 (genus); Corliss and Chen 1988 (*L. apiopleura*, sperical morphotype); Murray 2006 (genus)); *Nonion* sp. (Corliss and Chen, 1988 (*N. labradoricum*, rounded planispiral morphotype); Murray, 2006 (genus)); *Nonionella* spp. (Corliss and Chen, 1988 (*N. auricola*; rounded planispiral morphotype); Murray, 2006 (genus)); *Nonionella iridea*? (Murray 2006); *Nonionella stella*? (Bernhard et al. 1997; Murray 2006); *Nonionellina* sp. (Bubenshchikova et al., 2008 (for *N. labradorica*); Murray, 2006 (genus)); *Pseudononion* spp. (Corliss and Chen 1988 (rounded planispiral morphogroup)); *Oolina* spp. (Corliss and Chen 1988 (genus: spherical morphotype enhanced Živkovic and Babić 2003)); *Trifarina* sp1 *earlandi*? (Corliss and Chen 1988 (*T. angulosa*, *T. fluens*; tapered & cylindrical morphotype); de Stigter et al. 1998 (*T. angulosa*); Murray 2006 (genus)); *Uvigerina* spp. (Corliss and Chen 1988 (tapered & cylindrical morphotype); Murray 2006 (genus); Bubenshchikova et al. 2008); *Uvigerina peregrina* (Corliss and Chen 1988; Altenbach and Sarnthein 1989; Altenbach et al. 1999; Fontanier et al. 2002; Fontanier et al. 2006; Murray 2006); *Uvigerina mediterranea* (de Stigter et al. 1998; Altenbach et al. 1999; Fontanier et al. 2006; Murray 2006); *Valvulineria rugosa* (Bubenshchikova et al. 2008 (for *V. glabra*, *V. sadonica*)).

Epifaunal species

Cibicides spp. (Corliss and Chen, 1988 (*C. lobatulus*, *C. refulgens*, *C. wuellerstorfi*, plano-convex trochospiral morphotype); Murray, 2006 (genus)); *Discorbinella bertheloti* (Corliss and Chen 1988); *Epistominella exigua* (Altenbach et al., 1999; Corliss and Chen, 1988; Gooday, 1993; Murray, 2006; Schönfeld, 1997; Smart et al., 1994); *Eponides* spp. (Corliss and Chen, 1988 (*E.*

tumidulus; biconvex trochospiral morphotype); Murray, 2006 (genus)); *Hanzawaia* spp. (Corliss and Chen, 1988 (*H. concentrica*; plano-convex trochospiral morphotype); Murray, 2006 (genus)); *Lenticulina* spp. (Corliss and Chen, 1988 (*Lenticulina* spp.; biconvex trochospiral morphotype); Murray, 2006 (genus)); *Pyrgo depressa* (Corliss and Chen, 1988 (*P. murrhina*, *P. williamsoni*; milioline morphotype); Murray, 2006 (genus)); *Rosalina* spp. (Murray 2006 (genus)); *Triloculina* sp (Corliss and Chen, 1988 (*T. frigida*; milioline morphotype); Murray, 2006 (genus)).

References

Abu-Zied RH, Rohling EJ, Jorissen FJ, Fontanier C, Casford JSL, Cooke S (2008) Benthic foraminiferal response to changes in bottom-water oxygenation and organic carbon flux in the eastern Mediterranean during LGM to recent times. Marine Micropaleontology 67:46-68. doi:10.1016/j.marmicro.2007.08.006

Altenbach AV, Lutze GF, Schiebel R, Schönfeld J (2003) Impact of interrelated and interdependent ecological controls on benthic foraminifera: An example from the Gulf of Guinea. Palaeogeography Palaeoclimatology Palaeoecology 197:213-238. doi:10.1016/S0031-0782(03)00463-2

Altenbach AV, Pflaumann U, Schiebel R, Thies A, Timm S, Trauth M (1999) Scaling percentages and distributional patterns of benthic foraminifera with flux rates of organic carbon. Journal of Foraminiferal Research 29:173-185

Altenbach AV, Sarnthein M (1989) Productivity record in benthic foraminifera. In: Berger WH, Smetacek VS, Wefer G (eds) Productivity of the Ocean: Present and Past. John Wiley & Sons Ltd, Chichester, pp 255-269

Alve E (1994) Opportunistic features of the foraminifer *Stainforthia fusiformis* (Williamson): Evidence from Frierfjord, Norway. Journal of Micropalaeontology 13:24-24. doi:10.1144/jm.13.1.24

Alve E (2010) Benthic foraminiferal responses to absence of fresh phytodetritus: A two-year experiment. Marine Micropaleontology 76:67-75. doi:10.1016/j.marmicro.2010.05.003

Alve E, Bernhard JM (1995) Vertical migratory response of benthic foraminifera to controlled oxygen concentrations in an experimental mesocosm. Marine Ecology-Progress Series 116:137-151

Baas JH, Schönfeld J, Zahn R (1998) Mid-depth oxygen drawdown during Heinrich events: Evidence from benthic foraminiferal community structure, trace-fossil tiering, and benthic δ13C at the Portuguese Margin. Marine Geology 152:25-55. doi:10.1016/S0025-3227(98)00063-2

Bernhard JM, Sen Gupta BK, Borne PF (1997) Benthic foraminiferal proxy to estimate dysoxic bottom-water oxygen concentrations: Santa Barbara basin, US Pacific continental margin. Journal of Foraminiferal Research 27:301-310

Boltovskoy E, Giussani G, Watanabe S, Wright R (1980) Atlas of Benthic Shelf Foraminifera of the Southwest Atlantic. Dr. W. Junk by Publishers The Hague, 147 p

Bubenshchikova N, Nürnberg D, Lembke-Jene L, Pavlova G (2008) Living benthic foraminifera of the Okhotsk Sea: Faunal composition, standing stocks and microhabitats. Marine Micropaleontology 69:314-333. doi:10.1016/j.marmicro.2008.09.002

Burone L, de Mello e Sousa S, de Mahiques M, Valente P, Ciotti A, Yamashita C (2011) Benthic foraminiferal distribution on the southeastern Brazilian shelf and upper slope. Marine Biology 158:159-179. doi:10.1007/s00227-010-1549-7

Corliss BH (1985) Microhabitats of benthic foraminifera within deep-sea sediments. Nature 314:435-438. doi:10.1038/314435a0

Corliss BH (1991) Morphology and microhabitat preferences of benthic foraminifera from the Northwest Atlantic ocean. Marine Micropaleontology 17:195-236. doi:10.1016/0377-8398(91)90014-W

Corliss BH, Chen C (1988) Morphotype patterns of Norwegian Sea deep-sea benthic foraminifera and ecological implications. Geology 16:716-719. doi:10.1130/0091-7613(1988)016<0716:mponsd>2.3.co;2

Corliss BH, Van Weering TCE (1993) Living (stained) benthic foraminifera within surficial sediments of the Skagerrak. Marine Geology 111:323-335. doi:10.1016/0025-3227(93)90138-L

De Rijk S, Troelstra SR, Rohling EJ (1999) Benthic foraminiferal distribution in the Mediterranean Sea. Journal of Foraminiferal Research 29:93-103

de Stigter HC, Jorissen FJ, van der Zwaan GJ (1998) Bathymetric distribution and microhabitat partitioning of live (Rose Bengal stained) benthic foraminifera along a shelf to bathyal transect in the southern Adriatic Sea. Journal of Foraminiferal Research 28:40-65

Douglas RG, Heitman HL (1979) Slope and basin benthic foraminifera of the California borderland. In: Doyle LJ, Pilkey OH (eds) Geology of Continental Slopes. Society of Economic Paleontologists and Mineralogists Special Publications, pp 231-246

Duchemin G, Fontanier C, Jorissen FJ, Barras C, Griveaud C (2007) Living small-sized (63-150 µm) foraminifera from mid-shelf to mid-slope environments in the Bay of Biscay. Journal of Foraminiferal Research 37:12-32

Duchemin G, Jorissen FJ, Le Loc'h F, Andrieux-Loyer F, Hily C, Thouzeau G (2008) Seasonal variability of living benthic foraminifera from the outer continental shelf of the Bay of Biscay. Journal of Sea Research 59:297-319. doi:10.1016/j.seares.2008.03.006

Ellis BF, Messina A (1940) Catalogue of Foraminifera (with supplements). In. American Museum of Natural History and Micropaleontology Project, New York

Ernst S, van der Zwaan B (2004) Effects of experimentally induced raised levels of organic flux and oxygen depletion on a continental slope benthic foraminiferal community. Deep-Sea Research Part I: Oceanographic Research Papers 51:1709-1739. doi:10.1016/j.dsr.2004.06.003

Fontanier C, Jorissen FJ, Chaillou G, Anschutz P, Gremare A, Griveaud C (2005) Live foraminiferal faunas from a 2800 m deep lower canyon station from the Bay of Biscay: Faunal response to focusing of refractory organic matter. Deep-Sea Research Part I: Oceanographic Research Papers 52:1189-1227. doi:10.1016/j.dsr.2005.01.006

Fontanier C, Jorissen FJ, Chaillou G, David C, Anschutz P, Lafon V (2003) Seasonal and interannual variability of benthic foraminiferal faunas at 550 m depth in the Bay of Biscay. Deep-Sea Research Part I: Oceanographic Research Papers 50:457-494. doi:10.1016/s0967-0637(02)00167-x

Fontanier C, Jorissen FJ, Licari L, Alexandre A, Anschutz P, Carbonel P (2002) Live benthic foraminiferal faunas from the Bay of Biscay: Faunal density, composition, and microhabitats. Deep-Sea Research Part I: Oceanographic Research Papers 49:751-785. doi:10.1016/S0967-0637(01)00078-4

Fontanier C, Mackensen A, Jorissen FJ, Anschutz P, Licari L, Griveaud C (2006) Stable oxygen and carbon isotopes of live benthic foraminifera from the Bay of Biscay: Microhabitat impact and seasonal variability. Marine Micropaleontology 58:159-183. doi:10.1016/j.marmicro.2005.09.004

Gooday AJ (1986) Meiofaunal foraminiferans from the bathyal Porcupine-Seabight (Northeast Atlantic): Size structure, standing stock, taxonomic composition, species-diversity and vertical-distribution in the sediment. Deep-Sea Research Part I: Oceanographic Research Papers 33:1345-1355. doi:10.1016/0198-0149(86)90040-3

Gooday AJ (1988) A response by benthic foraminifera to the deposition of phytodetritus in the deep-sea. Nature 332:70-73. doi:10.1038/332070a0

Gooday AJ (1993) Deep-sea benthic foraminiferal species which exploit phytodetritus - Characteristic features and controls on distribution. Marine Micropaleontology 22:187-205. doi:10.1016/0377-8398(93)90043-W

Gooday AJ (1994) The biology of deep-sea foraminifera: A review of some advances and their applications in paleoceanography. Palaios 9:14-31

Gooday AJ (2003) Benthic foraminifera (protista) as tools in deep-water palaeoceanography: Environmental influences on faunal characteristics. Advances in Marine Biology 46:1-90. doi:10.1016/S0065-2881(03)46002-1

Gooday AJ, Hughes JA (2002) Foraminifera associated with phytodetritus deposits at a bathyal site in the northern Rockall Trough (NE Atlantic): seasonal contrasts and a comparison of stained and dead assemblages. Marine Micropaleontology 46:83-110

Gooday AJ, Rathburn AE (1999) Temporal variability in living deep-sea benthic foraminifera: A review. Earth-Science Reviews 46:187-212

Gross O (2002) Sediment interactions of foraminifera: Implications for food degradation and bioturbation processes. Journal of Foraminiferal Research 32:414-424

Gupta AK (1997) Paleoceanographic and paleoclimatic history of the Somali Basin during the Pliocene-Pleistocene: Multivariate analyses of benthic foraminifera from DSDP Site 241 (Leg 25). Journal of Foraminiferal Research 27:196-208

Haynes JR (1981) Foraminifera. John Wiley & Sons, Ltd, New York, 433 p

Jorissen FJ (1987) The distribution of benthic foraminifera in the Adriatic Sea. Marine Micropaleontology 12:21-48. doi:10.1016/0377-8398(87)90012-0

Jorissen FJ, Barmawidjaja DM, Puskaric S, Vanderzwaan GJ (1992) Vertical distribution of benthic foraminifera in northern Adriatic Sea: The relation with organic flux. Marine Micropaleontology 19:131-146. doi:10.1016/0377-8398(92)90025-f

Kaiho K (1994) Benthic foraminiferal dissolved-oxygen index and dissolved-oxygen levels in the modern ocean. Geology 22:719-722. doi:10.1130/0091-7613(1994)022<0719:BFDOIA>2.3.CO;2

Kaiho K (1999) Effect of organic carbon flux and dissolved oxygen on the benthic foraminiferal oxygen index (BFOI). Marine Micropaleontology 37:67-76. doi:10.1016/S0377-8398(99)00008-0

Koho KA, Garcia R, de Stigter HC, Epping E, Koning E, Kouwenhoven TJ, van Der Zwaan GJ (2008) Sedimentary labile organic carbon and pore water redox control on species distribution of benthic foraminifera: A case study from Lisbon-Setubal Canyon (southern Portugal). Progress In Oceanography 79:55-82. doi:10.1016/j.pocean.2008.07.004

Koho KA, Pina-Ochoa E, Geslin E, Risgaard-Petersen N (2011) Vertical migration, nitrate uptake and denitrification: Survival mechanisms of foraminifers (Globobulimina turgida) under low oxygen conditions. Fems Microbiology Ecology 75:273-283. doi:10.1111/j.1574-6941.2010.01010.x

Kovach WL (2010) A Multivariate Statistical Package for Windows, ver. 3.2. In. Kovach Computing Services, Pentraeth, Wales.

Löblich AR, Tappan H (1988) Foraminiferal genera and their classification. Van Nostrand Reinhold & Macmillan, New York, London, Melbourne, Agincourt, 970 p

Lutze GF, Coulbourn WT (1984) Recent benthic foraminifera from the continental-margin of Northwest Africa - Community structure and distribution. Marine Micropaleontology 8:361-401. doi:10.1016/0377-8398(84)90002-1

Mackensen A, Grobe H, Kuhn G, Fütterer DK (1990) Benthic foraminifereal assemblages from the eastern Weddel Sea 68 and 73°S: Distribution, ecology and fossilization potential. Marine Micropaleontology 16:241-283. doi:10.1016/0377-8398(90)90006-8

Martins V, Dubert J, Jouanneau JM, Weber O, da Silva EF, Patinha C, Dias JMA, Rocha F (2007) A multiproxy approach of the Holocene evolution of shelf-slope circulation on the NW Iberian continental shelf. Marine Geology 239:1-18. doi:10.1016/j.margeo.2006.11.001

Murray JW (2003) Foraminiferal assemblage formation in depositional sinks on the continental shelf west of Scotland. Journal of Foraminiferal Research 33:101-121

Murray JW (2006) Ecology and Application of Benthic Foraminifera. Cambridge University Press, Cambridge, 426 p

Nagai RH, Sousa SHM, Burone L, Mahiques MM (2009) Paleoproductivity changes during the Holocene in the inner shelf of Cabo Frio, southeastern Brazilian continental margin: Benthic foraminifera and sedimentological proxies. Quaternary International 206:62-71. doi:10.1016/j.quaint.2008.10.014

Rohling EJ, Destigter HC, Vergnaudgrazzini C, Zaalberg R (1993) Temporary repopulation by low-oxygen tolerant benthic foraminifera within an Upper Pliocene sapropel: Evidence for the role of oxygen depletion in the formation of sapropels. Marine Micropaleontology 22:207-219. doi:10.1016/0377-8398(93)90044-x

Schmiedl G, Mackensen A, Müller PJ (1997) Recent benthic foraminifera from the eastern South Atlantic Ocean: Dependence on food supply and water masses. Marine Micropaleontology 32:249-287. doi:10.1016/s0377-8398(97)00023-6

Schönfeld J (1997) The impact of the Mediterranean Outflow Water (MOW) on benthic foraminiferal assemblages and surface sediments at the southern Portuguese continental margin. Marine Micropaleontology 29:211-236. doi:10.1016/S0377-8398(96)00050-3

Schröder CJ, Scott DB, Medioli FS (1987) Can smaller benthic foraminifera be ignored in paleoenvironmental analyses. Journal of Foraminiferal Research 17:101-105

Sen Gupta BK, Machain-Castillo ML (1993) Benthic foraminifera in oxygen-poor habitats. Marine Micropaleontology 20:183-201. doi:10.1016/0377-8398(93)90032-s

Smart CW (2008) Abyssal NE Atlantic benthic foraminifera during the last 15 kyr: Relation to variations in seasonality of productivity. Marine Micropaleontology 69:193-209. doi:10.1016/j.marmicro.2008.07.007

Smart CW, King SC, Gooday AJ, Murray JW, Thomas E (1994) A benthic foraminiferal proxy of pulsed organic-matter paleofluxes. Marine Micropaleontology 23:89-99. doi:10.1016/0377-8398(94)90002-7

Zarriess M, Mackensen A (2010) The tropical rainbelt and productivity changes off northwest Africa: A 31,000-year high-resolution record. Marine Micropaleontology 76:76-91. doi:10.1016/j.marmicro.2010.06.001

Acknowledgments

First of all, I wish to thank Prof. Tilo von Dobeneck for giving me the opportunity to conduct this PhD project. Although I was never able to fully warm my heart for environmental magnetism, you always supported my studies and gave me so valuable scientific advice more than once! I feel honoured and wish to thank Prof. Michel de Mahiques for agreeing on being the second reviewer of my thesis.

Special thanks go to PD Dr. Till Hanebuth, who has been my scientific mentor for more than six years now. We sometimes may have different idealistic attitudes, however I learned so much from you and I am grateful for your support!

At the University of Bremen I thank the *AG Marine Geophysics*: Martina Braun, Liane Brück, Heike Piero, Christian Hilgenfeldt, Dr. Thomas Frederichs, Dr. Hendrik Müller, Benjamin Baasch, Lucia Korff, Firoz Badesab, Dr. Cletus Itambi, Sebastian Razik, and last but not least my 2.5-year *Büromitinsassin* Dr. Janna Just! – though I am still most comfortable with MagSus as the only environmental magnetic parameter in my studies you always considered me an integral part of your working group, thank you! Moreover, for manifold scientific and technical support I thank my dear colleagues: Dr. Hendrik Lantzsch, Dr. Kalle Baumann, Dr. Käthe Stolz, Brit Kockisch, Ferdinand Oberle, Benedict Preu, Dr. Tilmann Schwenk, Dr. Inka Meyer, Dr. Torsten Bickert, Marion Castex, Bastian Steinborn, Alex Petrovic, and Dr. Solveig -$C_8H_{10}N_4O_2$ – Caffeine- Bühring.

I thank Prof. Helmut Willems as chair of the International Graduate College EUROPROX – Proxies in Earth History, as well as all other EUROPRX members for the inspiring discussions during our coffee & science meetings!

Being a EUROPROXy made me stay abroad for some time during my PhD studies, and so I owe many *thank-you's* to several people outside of Bremen:

At the Universidade de Vigo I thank Prof. Guillermo Francés and Anxo Mena for the enduring well co-operation, as well as Prof. Daniel Rey and Dr. Belén Rubio for taking me onto BIO HESPERÍDES expedition MARBANGA.

Mud, mud, mud.... give me mud ☺
Snapshot taken after all scientific samples were carefully and safely recovered, documented and stored!!!

I thank Dr. Cristiano Chiessi, especially for inviting me to Universidade de São Paulo (Brazil) and introducing me to the following people, whom I also owe many thanks: Dr. Silvia Helena de Mello e Sousa, Renata Hanae Nagai (*...the non-linear response of the climatic system to solar insolation changes...?* ☺), Cintia Yamashita and all the lovely girls from Silvias Lab, Dr. Wânia Duleba, and Jana del Favero.

At Servicio de Hidrografía Naval in Buenos Aires (Argentina) I owe thanks to Prof. Roberto Violante and his team, especially Dr. Graziella Bozzano for their kind hospitality; and Prof. Alberto Piola for expert advice when working within an oceanographers nightmare!

This thesis wouldn't have been possible without the big love and big hearts that surround me, inspire, motivate, sometimes drive me crazy, but always believe in me: My parents Petra & Matthias Ritschel, Klaus Bender & Ursel Neubauer; the rest of my family – Kwesch's, Bender's, Hahn's – you all know you're part of this; my best friends: Hanna Lührs and Anne Timm – I promise to care and call more often in the future! A very special thank-you goes to - Ein ganz besonderer Dank gilt *meiner (90-jährigen!) Omitante*, Diakonieschwester i.R. Elsbeth Bender! And last but not least I am more than grateful to my dearest Matthias Wilhelm - let's go and find our *places, strange and quiet*...!

This thesis is dedicated
to my beloved grandfather
Reinhold Bender
(*17.12.1919 – †24.02.2012)

Out of the night that covers me,

Black as the Pit from pole to pole,

I thank whatever gods may be

For my unconquerable soul.

[...]

It matters not how strait the gate,

How charged with punishments the scroll.

I am the master of my fate:

I am the captain of my soul.

(Invictus – William Ernest Henley)